

https://dspace.org/

The effects of cancer drugs and copper complexes on pancreatic cancer haem oxygenase-1 and cell survival

Jhetam, Zakeeya

2024
University of the Witwatersrand, Johannesburg
https://hdl.handle.net/10539/47077

Jhetam, Zakeeya . (2024). The effects of cancer drugs and copper complexes on pancreatic cancer haem oxygenase-1 and cell survival [Master`s dissertation, University of the Witwatersrand, Johannesburg]. WIReDSpace.

Downloaded from a DSpace repository. https://dspace.org/



UNIVERSITY OF THE
WITWATERSRAND,
JOHANNESBURG

The effects of cancer drugs and copper complexes on pancreatic cancer haem oxygenase-1 and cell survival

Zakeeya Jhetam

A dissertation submitted to the Faculty of Health Sciences, University of the Witwatersrand, in fulfilment of the requirements for the degree of Master of Sciences in Medicine

Johannesburg, 2024

Declaration

I, Zakeeya Jhetam, declare that this dissertation is my own, unaided work. It is being submitted for the degree of Master of Science at the University of the Witwatersrand, Johannesburg. It has not been submitted before for any degree or examination at this or any other University.



Zakeeya Jhetam

Signed on this …17th.. day of …August….2024

Dedication

I proudly dedicate this dissertation to my Mom and Dad and my sister for their undying love and support.

"It is not permitted for the sun to catch up to the moon, nor can the night outstrip the day: Each (just) swims along in (its own) orbit (according to Law)."
Quran (36:40)

Abstract

Pancreatic ductal adenocarcinoma (PDAC) is the most common type of pancreatic malignancy. PDAC is one of the deadliest cancers, with a 5 year survival rate of only 3.2 % when diagnosed at an advanced stage. Approximately 75-80 % of PDAC cases are diagnosed at a late/inoperable stage where palliative chemotherapy is the only treatment option available. Current treatment options are met with numerous challenges. Despite the advances and success in targeted therapy and immune checkpoint blockade in various solid tumours, PDAC is unresponsive to these treatments. The stress-response protein, HMOX1, has been implicated in treatment failure of chemotherapy in numerous cancer-types. There is a need for novel therapeutic approaches in the treatment of PDAC and the reasons for treatment failure of chemotherapy for pancreatic cancer cells requires urgent attention. Copper complexes as anticancer agents have shown promising cytotoxicity against numerous cancers, and appear to cause cell death by inducing apoptosis. The ligands to which copper are complexed play a major role in the specificity and mode of cell death of the complexes. The ligands that were evaluated in this study had previously shown anti-cancer activity, and allow the binding of the complexes to DNA. This study evaluated three different classes of copper complexes for their anti-cancer activity on AsPC-1 and MIA PaCa-2 pancreatic cancer cells. A copper-phenanthroline-theophylline complex (AD3), a copper 8-aminoquinolone naphthyl complex (OM), and two copper isoindoline complexes (L1Cu and L6Cu) were cytotoxically active in both the AsPC-1 and MIA PaCa-2 cell lines. The complexes had clinically relevant IC_{50} values of below 5 μM and were significantly more active than the positive control, doxorubicin.

Preliminary investigations on the effect of the copper complexes on the morphology of the cells indicated the absence of necrotic cell death, while features of apoptosis, such as membrane blebbing and chromatin condensation were observed. The copper complexes caused statistically significant formation of reactive oxygen species (ROS), in both cell lines. The copper complexes caused the binding of annexin-V in both cell lines and provided evidence for apoptosis. Apoptotic cell death was confirmed by the activation of caspase-3/7, with copper complexes causing between 16 % and 67 % caspase-3/7 activation in AsPC-1 cells while >88% of MIA PaCa-2 treated cells had active caspase-3/7. The loss of mitochondrial membrane potential was seen in 100 % of treated cells in both cell lines with the activation of caspase-9 confirming activation of the intrinsic apoptotic pathway.

The copper complexes increased the expression of HMOX1 in both cell lines, as seen in immunofluorescence and western blot studies. AD3 was the strongest inducer of HMOX1 whilst L1Cu caused the smallest increase in HMOX1 expression. The inhibition of HMOX1 by a small-molecule inhibitor, OB24 HCl, significantly decreased the IC_{50} values of the copper complexes, indicating that HMOX1-inhibition sensitized the cells to the cytotoxic effect of the copper complexes. At the concentration used, OB24 HCl had no effect on cell viability. The data suggested that HMOX1-inhibition may be a viable therapeutic consideration in PDAC. Taken together, the data from this study supports the further pre-clinical investigation of copper complexes as cancer treatments together with an in depth investigation on HMOX1.

Acknowledgements

In the name of Allah, the Most Gracious, the Most Merciful

In embarking upon this academic journey, I have been supported by a multitude of individuals who have been indispensable throughout the course of my journey. It is with heartfelt gratitude that I extend my appreciation to each and every one of them.

- To my supervisor, Dr Leonie Harmse, I am incredibly grateful to have had you as my supervisor. Your unrelenting guidance and belief in my potential and capabilities has allowed me to expand not only my knowledge and skills, but my confidence in my abilities, too. Your insightful feedback and constructive criticism has shaped my research and writing, pushing me to achieve my best. It has been a privilege to learn from your expertise. Thank you for your patience and understanding throughout this degree, you have been an integral part of my academic endeavour.
- To my co-supervisor, Dr Marietha Nel, thank you for your insight and invaluable feedback.
- To my dear friends: Karina and Niyanta, thank you for sharing this journey with me. Our shared laughter has made this experience joyful. Your presence has been a strength during challenging times. Thank you for being a source of laughter and comfort throughout this journey. I know I have gained life-long friends in you.
- To my dear sister, Farha, my best friend and biggest cheerleader. Thank you for being there for me in all my ups and down. This would not have been possible without you.
- To my Mum and Dad, thank you for all your hard work and sacrifices that allowed me to pursue my dreams. Dad, thank you for all that you do for me, I have appreciated all the little things. Mum, your strength has been an inspiration to me. Your love and patience has created a safe space for me to always believe in myself.
- Lastly, my success is only due to Allah, the Most High, who continues to envelop me in His blessings and mercy.

Research outputs

1. Bert Myburgh Research Forum, Department of Surgery, Wits University. Oral Presentation, "Copper complexes induce intrinsic apoptosis in pancreatic cancer cell lines, and induce the expression of haem oxygenase-1."
Winner: Second Prize, Best presentation

2. 2023 School of Clinical Medicine, Wits University. Poster Presentation, "Copper complexes cause apoptosis and increase expression of the stress response protein, haem oxygenase-1 in pancreatic cancer cell line.
Winner: Second prize in the category of: Poster: MSc/ Medical Scientist/ Researcher/ Lecturer.

3. 2023 South African Society for Basic and Clinical Pharmacology, 56th Conference, Rhodes University. Poster Presentation, "Copper complexes cause apoptosis and increase expression of the stress response protein, haem oxygenase-1 in pancreatic cancer cell lines."

4. 2022 Faculty of Health Sciences Research Day, Wits University. Poster Presentation, "Copper complexes inhibit pancreatic cancer cell survival."

Manuscripts in preparation

Copper complexes induce the expression of haem oxygenase -1 and cause apoptotic cell death in pancreatic cancer cells.

Table of contents

Declaration ii

Dedication iii

Abstract iv

Acknowledgements vi

Research outputs vii

Table of contents viii

List of Figures xiv

List of Tables xvii

Abbreviations, acronyms and symbols xix

Units of Measure xxii

CHAPTER ONE: Introduction 1

1.1 Pancreatic cancer statistics 1

1.2 Types of PC tumours 2

1.3 Features of PDAC 2

1.4 Tumourigenesis of PDAC 2

1.4.1 Metastasis 3

1.4.2 Molecular signature of PDAC 4

1.4.2.1 *KRAS* 4

1.4.2.2 *CDKN2A* 4

1.4.2.3 *TP53* 5

1.4.2.4 *SMAD4/DPC4* 5

1.5 Signs and symptoms of PDAC 6

1.6 Serological biomarkers for the detection of PDAC 6

1.7 Treatment of PDAC 6

1.7.1 Treatment of resectable disease 6

1.7.2 Treatment of borderline resectable disease 7

1.7.3 Treatment of unresectable/metastatic disease 7

1.7.4 Treatment resistance/failure in PDAC 10

1.8 Haem oxygenase-1 11

1.8.1 HMOX1 in cancer cells 12

1.8.2 HMOX1 inhibitors 14

1.9 Types of cell death 14
1.9.1 Necrosis 15
1.9.2 Secondary necrosis 15
1.9.3 Apoptosis 15
1.9.3.1 Extrinsic pathway 15
1.9.3.2 Intrinsic pathway 16
1.9.3.3 Execution phase of apoptosis 16
1.9.3.4 Evasion of apoptosis by cancer cells 17
1.9.4 Necroptosis 18
1.9.5 Autophagy 18
1.9.6 Ferroptosis 19
1.9.7 Pyroptosis 19
1.9.8 Cuproptosis 19
1.10 Copper complexes and their potential anti-cancer activity 19
1.11 Pancreatic cancer cell lines 22
1.11.1 AsPC-1 22
1.11.2 MIA PaCa-2 22
1.12 Rationale of the study 22
1.13 Aim and Objectives 23

CHAPTER TWO: Methods 24

2.1 Cell culture 24
2.1.1 Cell culture reagents 24
2.1.2 Cell culture maintenance and subculture 25
2.1.3 Cryopreservation 25
2.2 Determining viability of cells: Trypan Blue dead cell exclusion assay 25
2.3 Test compounds 26
2.4 MTT cell viability assay 28
2.5 Cell morphology 30
2.6 Measurement of reactive oxygen species 31
2.7 Evaluation of apoptosis 31
2.7.1 Annexin-V 32
2.7.2 JC-1 assay 33

2.7.3 Caspase-9 34
2.7.4 Caspase-3/7 35
2.8 Immunofluorescence 35
2.9 Western blot 38

CHAPTER THREE: Results 43

3.1 The effect of the copper complexes and their ligands on the cell viability of AsPC-1 and MIA PaCa-2 cells 43
3.1.1 Identification of active copper complexes against AsPC-1 and MIA PaCa-2 cell lines 43
3.1.2 Selection of a cancer drug to use as a positive control 45
3.1.3 Determination of the IC_{50} values of active compounds 45
3.2 Effects of the copper complexes and doxorubicin on cell morphology of AsPC-1 and MIA PaCa-2 cells 48
3.2.1 Effects of the copper complexes and doxorubicin on the cell morphology of AsPC-1 cells 48
3.2.2 Effects of the copper complexes and doxorubicin on the cell morphology of MIA PaCa-2 cells 49
3.3 Translocation of phosphatidylserine to the surface of AsPC-1 and MIA PaCa-2 cells 52
3.3.1 The effect of copper complexes and doxorubicin on annexin-V binding in AsPC-1 cells 52
3.3.2 The effect of copper complexes and doxorubicin on annexin-V binding in MIA PaCa-2 cells 55
3.3.3 Summary of the effects of copper complexes on annexin-V-binding 55
3.4 Evaluation of the ability of the copper complexes to induce ROS formation 57
3.4.1 The effects of the copper complexes on ROS formation in AsPC-1 cells 57
3.4.2 The effects of the copper complexes on ROS formation in MIA PaCa-2 cells 57
3.4.3 Summary of the effects of the copper complexes on ROS formation 59
3.5 Evaluation of the effect of the copper complexes on mitochondrial membrane potential 61
3.5.1 The effect of the copper complexes on mitochondrial membrane potential in AsPC-1 cells 61

3.5.2 The effect of the copper complexes on mitochondrial membrane potential in MIA PaCa-2 cells 63
3.5.3 Summary of the effects of the copper complexes on mitochondrial membrane potential 63
3.6 The effect of the copper complexes on caspase-9 activity 63
3.6.1 The effect of the copper complexes on caspase-9 activity in AsPC-1 cells 65
3.6.2 The effect of the copper complexes on caspase-9 activity in MIA PaCa-2 cells 65
3.6.3 Summary of the effects of the copper complex on caspase-9 activity 68
3.7 The effect of the copper complexes on caspase-3/7 activation 68
3.7.1 The effect of the copper complexes on caspase-3/7 activity in AsPC-1 cells 68
3.7.2 The effect of the copper complexes on caspase-3/7 activity in MIA PaCa-2 cells 70
3.7.3 Summary of the effects of the copper complexes on caspase-3/7 activity 70
3.8 The effect of the copper complexes on HMOX1 expression 72
3.8.1 The effect of the copper complexes on HMOX1 expression in AsPC-1 cells 72
3.8.1.1 Immunofluorescence studies investigating the effect of the copper complexes on HMOX1 expression in AsPC-1 cells 72
3.8.1.2 Western blot studies investigating the effect of the copper complexes on HMOX1 expression in AsPC-1 cells 75
3.8.2 The effect of the copper complexes on HMOX1 expression in MIA PaCa-2 cells 75
3.8.2.1 Immunofluorescence studies investigating the effect of the copper complexes on HMOX1 expression in MIA PaCa-2 cells 75
3.8.2.2 Western blot studies investigating the effect of the copper complexes on HMOX1 expression in MIA PaCa-2 cells 79
3.9 The effect of HMOX1 inhibition on the IC_{50} values of copper complexes in AsPC-1 and MIA PaCa-2 cells 80
3.9.1 The effect of OB24 HCl on the cell viability of AsPC-1 and MIA PaCA-2 cell line 81
3.9.2 The effect of the combination of OB24 HCl and the copper complexes

on the cell viability of AsPC-1 and MIA PaCa-2 cells 82

CHAPTER FOUR: Discussion 84

4.1 Introduction 84

4.2 The cytotoxic effects of the copper complexes on AsPC-1 and MIA PaCa-2 cells 84

4.3 The effects of the copper complexes on the morphology of AsPC-1 and MIA PaCa-2 cells 88

4.4 The effect of the copper complexes on phosphatidylserine exposure in AsPC-1 and MIA PaCa-2 cells 89

4.5 The effect of the copper complexes on the formation of reactive oxygen species in AsPC-1 and MIA PaCa-2 cells 91

4.6 The effect of the copper complexes on mitochondrial membrane potential of AsPC-1 and MIA PaCa-2 cells 93

4.7 The effect of the copper complexes on caspase-3/7 activation in AsPC-1 and MIA PaCa-2 cells 94

4.8 The effect of the copper complexes on caspase-9 activation in AsPC-1 and MIA PaCa-2 cells 95

4.9 The effect of the copper complexes on HMOX1 expression as evaluated by immunofluorescence and western blot studies 97

4.10 The effect of HMOX1 inhibition on the cytotoxicity of the copper complexes in AsPC-1 and MIA PaCa-2 cells 99

4.11 Comparisons of the effects of the copper complexes on cell-death-assay-findings and HMOX1-expression between cell lines 100

CHAPTER FIVE: Conclusion 102

5.1 The copper complexes inhibited the growth of AsPC-1 and MIA PaCa-2 cell lines at low micromolar IC_{50} values 102

5.2 The copper complexes caused the formation of ROS 102

5.3 The copper complexes activate the intrinsic apoptotic pathway 102

5.4 The copper complexes induce the expression of HMOX1 103

5.5 The effect of HMOX1-inhibition on the cytotoxicity of the copper complexes 104

5.6 Limitations 104
5.7 Future considerations 104
5.8 Conclusion 105
References 106
Appendix 129

List of Figures

CHAPTER ONE: Introduction

Figure 1.1. PDAC progression model 3

Figure 1.2 Extrinsic and Intrinsic Apoptotic pathways 17

CHAPTER THREE: Results

Figure 3.1 The effect of the copper complexes and their ligands on cell viability of AsPC-1 (A) and MIA PaCa-2 (B) cells 44

Figure 3.2 The effect of DMSO and ethanol on the cell viability of AsPC-1 and MIA PaCa-2 cells 45

Figure 3.3 The effect of gemcitabine and doxorubicin on the cell viability of AsPC-1 and MIA PaCa-2 cells 46

Figure 3.4 Representative sigmoidal log dose response curves of active copper complexes and doxorubicin in AsPC-1 cells (A and B) and MIA PaCa-2 cells (C and D) 47

Figure 3.5 Representative photomicrographs showing morphological changes in AsPC-1 cells after a 24 hour treatment with copper complexes 50

Figure 3.6 Representative photomicrographs showing morphological changes in MIA PaCa-2 cells after a 24 hour treatment with copper complexes 51

Figure 3.7 Representative photomicrographs (A) and a bar graph (B) of annexin-V binding and PI staining of AsPC-1 cells after a 24 hour treatment with copper complexes 54

Figure 3.8 Representative photomicrographs (A) and a bar graph (B) of annexin-V binding and PI staining of MIA PaCa-2 cells after a 24 h treatment with copper complexes 56

Figure 3.9 Representative photomicrographs (A) and a bar graph (B) of ROS formation in AsPC-1 cells after 6 hour treatment with copper complexes 58

Figure 3.10 Representative photomicrographs (A) and a bar graph (B) of ROS formation in MIA PaCa-2 cells after 6 hour treatment with copper complexes 60
Figure 3.11 Representative photomicrographs (A) and a bar graph (B) showing the effects of the copper complexes on mitochondrial membrane potential in AsPC-1 cells after 18 h treatment 62
Figure 3.12 Representative photomicrographs (A) and a bar graph (B) showing the effects of the copper complexes on mitochondrial membrane potential in MIA PaCa-2 cells after 18 h treatment 64
Figure 3.13 Representative photomicrographs (A) and a bar graph (B) showing the effects of the copper complexes on caspase-9 activation in AsPC-1 cells after a 48 h treatment period 66
Figure 3.14 Representative photomicrographs (A) and a bar graph (B) showing the effects of the copper complexes on caspase-9 activation in MIA PaCa-2 cells after a 48 h treatment period 67
Figure 3.15 Representative photomicrographs (A) and a bar graph (B) showing the effects of the copper complexes on caspase-3/7 activation in AsPC-1 cells after a 48 h treatment period 69
Figure 3.16 Representative photomicrographs (A) and a bar graph (B) showing the effects of the copper complexes on caspase-3/7 activation in MIA PaCa-2 cells after a 48 h treatment period 71
Figure 3.17 Representative photomicrographs of immunofluorescence showing the effects of the copper complexes on HMOX1 expression in AsPC-1 cells after 18 h 74
Figure 3.18 Immunoblot of HMOX1 (A) and a graph (B) of the pixel densities of HMOX1 bands in AsPC-1 cells 76
Figure 3.19 Representative photomicrographs of immunofluorescence showing the effects of the copper complexes on HMOX1 expression in MIA PaCa-2 cells after 18 h treatment 78

Figure 3.20 Immunoblot of HMOX1 (A) and a graph (B) of the pixel densities of HMOX1 bands in MIA PaCa-2 cells 80

Figure 3.21 Graph (A) showing cell viability (%) of AsPC-1 and MIA PaCa-2 cells treated with OB24 HCl only and structure of OB24 HCl (B) 81

List of Tables

CHAPTER ONE: Introduction

Table 1.1. Five year relative survival rates of PC based on stages 1

Table 1.2. The number of new cases of PC recorded according to race in South Africa 2

Table 1.3 Mechanism of action and adverse effects of drugs used in the treatment of PDAC 9

CHAPTER TWO: Methods

Table 2.1 Molecular structures of copper complexes and their ligands. 27

Table 2.2 SDS-PAGE gel. Table showing the constituents of the SDS-PAGE gel 38

Table 2.3 Buffer recipes. Table showing the constituents of the buffers used in the Western blot assay 39

CHAPTER THREE: Results

Table 3.1 IC_{50} values of the copper complexes and doxorubicin against AsPC-1 and MIA PaCa-2 cells after a 48 hour treatment period 47

Table 3.2 The effect of the copper complexes on the cell morphology of AsPC-1 and MIA PaCa-2 cells 52

Table 3.3 The mean fluorescence intensity and nuclear localization of HMOX1 in AsPC-1 cells after treatment with copper complexes and doxorubicin for 18 hours 73

Table 3.4 The mean fluorescence intensity and nuclear localization of HMOX1 in MIA PaCa-2 cells after treatment with copper complexes and doxorubicin for 18 hours 77

Table 3.5 The IC_{50} values of copper complexes alone and in combination with 20 μM of a HMOX1 inhibitor, OB24 HCl, in AsPC-1 cells 82

Table 3.6 The IC_{50} values of copper complexes alone and in combination

with 20 μM of a HMOX1 inhibitor, OB24 HCl, in MIA PaCa-2 cells 82

CHAPTER FOUR: Discussion

Table 4.1 IC_{50} values of copper complexes from various studies, using the MTT assay 87

Table 4.2 Summary of the effect of the copper complexes on caspase-3/7 and caspase-9 activation (%) in AsPC-1 and MIA PaCa-2 cells 96

Abbreviations, acronyms and symbols

5-FU	5-fluorouracil
ANOVA	Analysis of variants
AO	Acridine orange
Apaf-1	Apoptotic protease activating factor-1
APS	Ammonium persulfate
ATCC	American Type Culture Collection
Bak	Bcl-2 antagonist killer 1
Bax	Bcl-2-associated X protein
Bcl-2	B-cell lymphoma-2
Bcl-x	B-cell lymphoma-extra-large protein
BH	Bcl-2 homology domain
Bid	BH3-interacting domain death agonist
BRCA-1/2	Breast cancer gene-1/2
CA125	Cancer antigen 125
CA19-9	Carbohydrate antigen 19-9
CAD	Caspase-activated DNase
Cas9	CRISPR-associated proteins
CDK	Cyclin-dependent kinase
CDKN2A	Cyclin dependent kinase inhibitor 2A
CEA	Carcinoembryonic antigen
CO	Carbon monoxide
CO_2	Carbon dioxide
CRISPR	Clustered regularly interspaced short palindromic repeats
Cu	Copper
DCFDA	2',7'-Dichlorodihydrofluorescein diacetate
ddH_2O	Double distilled water
DIABLO	Direct inhibitor of Apoptosis-binding protein with low PI
DISC	Death-inducing signalling complex
DMEM	Dulbecco's Modified Eagle Medium
DMSO	Dimethylsulfoxide

DNA	Deoxyribonucleic acid
DTT	Dithiothreitol
EDTA	Ethylenediaminetetraacetic acid
EMT	Epithelial-to-Mesenchymal Transitioning
EtOH	Ethanol
FADD	Fas-associated death domain
FAMMM	Familial Atypical Multiple Mole Melanoma
FBS	Foetal bovine serum
FITC	Fluorescein-5-isothiocyanate
FMK	Fluoremethyl ketone
FOLFIRINOX	5-Fluorouracil/leucovorin/irinotecan/oxaliplatin
G1 phase	Gap 1 phase
GDP	Guanosine diphosphate
GTP	Guanosine triphosphate
GTPase	Guanosine triphosphatase
HCl	Hydrochloride
HMOX1	Haem oxygenase-1
HO	Hoechst 33342
HRP	Horseradish peroxidase
HtrA2	High temperature requirement protein A2
IAPs	Inhibitors of apoptosis proteins
IC_{50}	Half maximal inhibitory concentration
IC_{80}	80% inhibitory concentration
IC_{99}	99% inhibitory concentration
IL-8	Interleukin-8
JC-1	1,1',3,3'-Tetraethyl-5,5',6,6'-tetrachloroimidacarbocyanine iodide
KCl	Potassium chloride
KH_2PO_4	Potassium dihydrogen phosphate
KRAS	Kirsten rat sarcoma virus
LOH	Loss of Heterozygosity
MAPK	Mitogen-activated protein kinase
MCL1	Myeloid cell leukaemia-1
MMP	Mitochondrial membrane potential
MOA	Mechanism of action

MOMP	Mitochondrial outer membrane permeability
MPTP	Mitochondrial permeability transition pore
MTS	(3-(4,5-dimethylthiazol-2-yl)-5-(3-carboxymethoxyphenyl)-2-(4-sulfophenyl)-2H-tetrazolium)
MTT	(3-(4,5-Dimethylthiazol-2-yl)-2,5-Diphenyltetrazolium Bromide)
Na_2HPO_4	Disodium phosphate
Nab-paclitaxel	Nano-albumin-bound paclitaxel
NaCl	Sodium chloride
NF-κB	Nuclear factor kappa B
NTRK	Neurotrophic receptor tyrosine kinase
PALB-2	Partner and localizer of BRCA-2
PanIN	Pancreatic intraepithelial neoplasm
PARP	Poly-ADP ribose polymerase
PBS	Phosphate buffered saline
PC	Pancreatic cancer
PCC	Pearson's correlation coefficient
PD-1	Programmed cell death protein-1
PDAC	Pancreatic ductal adenocarcinoma
PI	Propidium iodide
PNET	Pancreatic neuroendocrine tumours
Puma	p53 upregulated modulator of apoptosis
PVDF	Polyvinylidene difluoride
RNA	Ribonucleic acid
ROS	Reactive oxygen species
RPMI	Roswell Park Memorial Institute
S phase	Synthesis phase
SDS	Sodium dodecyl-sulfate
SDS-PAGE	Sodium dodecyl-sulfate polyacrylamide gel electrophoresis
SMAC	Second mitochondria-derived activator of caspase
SMAD4/DPC4	Suppressor of mothers against decapentaplegic family ember 4/Deleted in Pancreatic Cancer-4
TBST	Tris-buffered-saline-Tween
TEMED	Tetramethylethylenediamine
TGF-β	Transforming growth factor beta

TNF-R	Tumour necrosis factor-receptor
TNF-α	Tumour necrosis factor alpha
TP53	Tumour protein p53
TRADD	TNF receptor-associated death domain
TRK	Tropomyosin receptor kinase
VEGF	Vascular endothelial growth factor
VEGFR	Vascular endothelial growth factor receptor
WHO	World Health Organization
XIAP	X-linked inhibitor of apoptosis
Zn	Zinc
α	Alpha
β	Beta
κ	Kappa
λ	Lambda

Units of measure

%	Percentage
× *g*	Gravity force
g/mol	Grams per mole
AU	Arbitrary Units
Da	Dalton
h	Hour
mL	Millilitre
mM	Millimolar
nM	Nanomolar
nm	Nanometer
°C	Degrees Celsius
kDa	kiloDalton
L	Litre
M	Molar
mg	Milligrams
rpm	Rotations per unit
V	Voltage
v/v	Volume per volume

w/v	Weight per volume
µg	Micrograms
µl	Microlitre
µM	Micromolar
cm^3	Cubic centimetre

Chapter I: Introduction

1.1 Pancreatic cancer statistics

According to GLOBOCAN 2022, the International Agency for Research on Cancer reported an estimated 510 992 new cases of pancreatic cancer (PC) worldwide in 2022 (WHO, 2022). PC is ranked as the seventh leading cause of cancer-related deaths worldwide, with 467 409 deaths in 2022 (WHO, 2022). PC remains one of the deadliest cancers, with a mortality/incidence ratio of 91 % (WHO, 2022) and a 5 year survival rate of 12.5 % for all stages combined (American Cancer Society, 2023). Advanced disease at diagnosis is associated with a poor survival rate (Table 1.1). The poor prognosis of PC is partly due to the late presentation of symptoms, causing patients to be diagnosed at a later, inoperable stage (De La Cruz *et al*., 2014).

Table 1.1 Five year relative survival rates of PC based on stages (National Cancer Institute, 2023)

Stage	Frequency of diagnosis (%)	5 year relative survival rate (%)
Localized	13	44.3
Regional	29	16.2
Distant	51	3.2
Unknown	7	10.5

The incidence of PC in Africa is 3.7 % of the total global cases (WHO, 2022). In South Africa, the National Cancer Registry recorded 248 female and 254 male diagnoses of PC in 2020, contributing to approximately 0.7% of all cancer cases in the country (NICD, 2020). PC was more prevalent among the white population than the black population (NICD, 2020) (Table 1.2), which is contrary to global trends that show a higher incidence among black populations compared to white populations (Yadav and Lowenfels, 2013). Coloured populations had the third highest number of new cases, followed by the Asian population group (Table 1.2). According to the latest Stats SA Census data, the white population makes up 7.3 % of the total population of South Africa (Census, 2022). White South Africans have the highest incidence of PC cases in South Africa, while accounting for one of the smallest racial groups. The majority of all cases occurred in individuals over the age of 50 (NICD, 2020).

Table 1.2 The number of new cases of PC recorded according to race in South Africa (NICD, 2020)

	Black	White	Coloured	Asian
2019	124	238	58	16
2018	120	217	67	17
Total	**244**	**455**	**125**	**33**

1.2 Types of PC tumours

PCs can be divided into exocrine and endocrine tumours. The most common type of PC, pancreatic ductal adenocarcinoma (PDAC), is an exocrine tumour which originates in the epithelial lining of the pancreatic duct (Pai and Spalding, 2015). Less common are tumours of the endocrine tissue which are termed pancreatic neuroendocrine tumours (PNET) (Rawla *et al*., 2019). PNETs, also known as Islet cell tumours, account for less than 2 % of PC cases (National Cancer Institute, 2022). Because PDAC is typically diagnosed at a late/inoperable stage (stage III or IV), it has a poor prognosis compared to PNETs (Rawla *et al*., 2019). When diagnosed at stage IV, PDAC has a 5-year survival rate of 3 % (American Cancer Society, 2024) compared to the 23 % of PNETs (American Cancer Society, 2023).

1.3 Features of PDAC

The main precursor lesion to invasive PDAC is pancreatic intraepithelial neoplasm (PanIN). High grade PanINs, also known as "carcinoma *in situ*", have a high frequency for developing into invasive PDAC and warrants evaluation and surgical intervention (Pittman *et al*., 2017; McCarthy *et al*., 2001). Approximately two thirds of PDACs are found in the head of the pancreas, while the remainder are found in the body or tail, at a frequency of 15 % each (Luchini *et al*., 2020). Lifestyle risk factors for PDAC include smoking, excessive alcohol consumption, obesity, high consumption of dietary saturated fats, diabetes mellitus and chronic pancreatitis (McGuigan *et al*., 2018). Inherited syndromes that increase a patient's pancreatic cancer risk include Peutz-Jeghers syndrome, Familial Atypical Multiple Mole Melanoma (FAMMM), Lynch syndrome, Hereditary Breast And Ovarian Cancer Syndrome and hereditary pancreatitis (McGuigan *et al*., 2018).

1.4 Tumourigenesis of PDAC

The progression model for PDAC begins with the most common precursor lesion, PanIN. *KRAS* activation is an initiating event in the development of low grade PanINs. Loss of *CDKN2A/*p16 function then occurs. Loss of *TP53* and *SMAD4/DPC4* subsequently occur in

high grade PanIN lesions, promoting invasion and metastasis of pancreatic tumour cells (Figure 1.1) (Iacobuzio-Donahue *et al*., 2012).

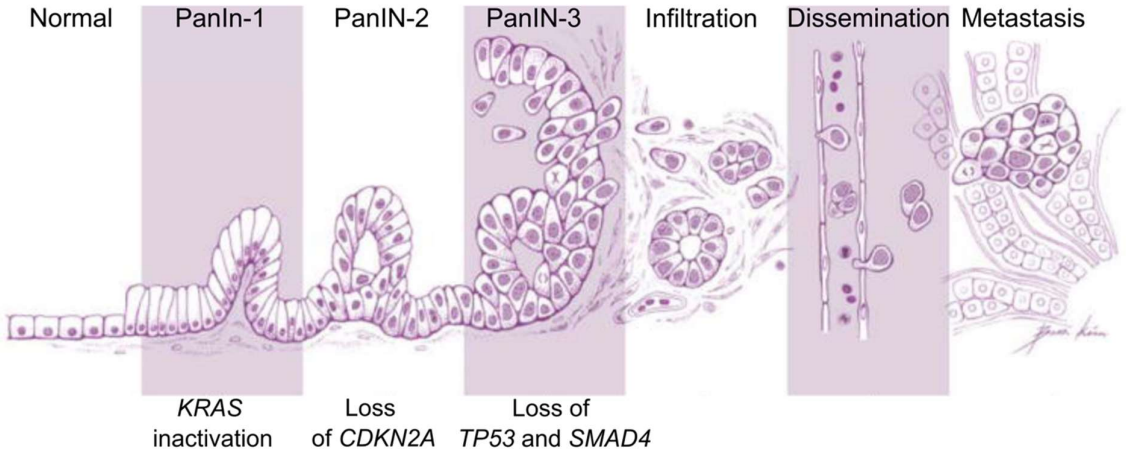


Figure 1.1 PDAC progression model. Progression model depicting the mutations that drive PDAC tumorigenesis. Legend: PanIn: Pancreatic intraepithelial neoplasm; *KRAS*: Kirsten rat sarcoma virus; *CDKN2A*: Cyclin dependent kinase inhibitor 2A; *TP53*: Tumour suppressor protein 53; *SMAD4*: Supressor of mothers against decapentaplegic family member 4. Reproduced from Iacobuzio-Donahue *et al*., (2012).

1.4.1 Metastasis

The process of cancer metastasis begins when carcinoma cells lose their cell-cell and cell-extracellular matrix connections through the loss of adhesion molecules, promoting detachment of epithelial cells from the basement membrane and hence, invasion into the surrounding stroma (Keleg *et al*., 2003). The loss of epithelial characteristics and development of motile characteristics of the cancer cell represents the process of epithelial-to-mesenchymal transitioning (EMT). Thereafter, the mobilized tumour cells extravasate into the blood and lymphatic system (Das and Batra, 2015). Circulating tumour cells then enter the parenchyma of distant organ sites and re-establish colonies of neoplasms (Tuveson and Neoptolemos, 2012).

The liver is the most common site of metastasis of a primary pancreatic tumour, followed by the lungs and peritoneum (diSibio and French, 2008). Other less common sites of metastasis include the adrenal gland, bone and gall bladder (diSibio and French, 2008).

In PDAC, mutations associated with tumour progression and promotion of metastasis occur in *KRAS*, *CDKN2A*, *TP53* and *SMAD4/DPC4* (Tuveson and Neoptolemos, 2012). A Loss of

Heterozygosity (LOH) mutation in *KRAS* promotes migration and motility of tumour cells resulting in metastasis in mice and human tumours (Qiu *et al*., 2011). SMAD4-inactivation is present in metastatic disease but not locally advanced disease, suggesting a correlation between SMAD4 loss and PDAC metastasis (Iacabuzio-Donahue *et al*., 2009). In genetically engineered mouse models with mutant *KRAS* and deletion of the Ink4A/Arf locus (encodes for the tumour suppressor protein, p16), micrometastasis to the liver and the lungs were seen (Mazur and Siveke, 2012).

1.4.2 Molecular signature of PDAC

1.4.2.1 *KRAS*

The *KRAS* proto-oncogene encodes for a small GTPase protein, KRAS. Embedded in the inner membrane of the cell, KRAS is a kinase involved in the mitogen-activated protein kinase (MAPK) growth signaling pathway (Waters and Der, 2018). When activated by the binding of growth factor ligands to their respective receptor tyrosine kinases, KRAS triggers downstream kinases and molecules that amplify signaling for the activation of transcription factors. Subsequently, the nucleus receives signals to enter into cell division, promoting growth and proliferation of the cell (Waters and Der, 2018). KRAS exists between its inactive, GDP-bound state and active, GTP-bound state. After converting GTP to GDP, KRAS is inactivated and stops relaying growth signals to the nucleus (Waters and Der, 2018). Mutant KRAS protein is permanently locked in its activated state, continually conferring growth signals to the nucleus irrespective of the presence or absence of extracellular stimuli. In this way, mutated *KRAS* is an oncogenic driver for tumourigenesis (Waters and Der, 2018) and promotes proliferation, cell survival, angiogenesis and invasion of the tumour (Podolsky *et al*., 2016). *KRAS* mutations are found in 95 % of PDAC cases (Iacobuzio-Donahue *et al*., 2012). The point mutation in *KRAS* is an early event involved in the formation of PDAC, present in 92 % of low grade PanINs, the major precursor lesion to PDAC (Kanda *et al*., 2012). In a PDAC mouse model, *KRAS* activation exhibited an aggressive phenotype, conferring a growth advantage and promoting metastasis of the tumour (Qiu *et al*., 2011).

1.4.2.2 *CDKN2A*

The *CDKN2A* gene is a tumour suppressor gene that encodes for the protein p16 which is a cyclin-dependent kinase inhibitor that impedes the progression of the cell cycle from G1 to S phase (Serrano *et al*., 1983). This prevents abnormal cell growth and a loss of p16 promotes tumour development and proliferation of neoplastic cells (Schutte *et al*., 1997). Mutations in

the *CDKN2A* gene, rendering p16 inactive, is present in approximately 98% of PDACs (Schutte *et al*., 1997). Inactivation of p16 occurs early on in the transformation of normal cells into invasive carcinoma (Iacobuzio-Donahue, 2011). In PDAC mice models, biallelic inactivation of *p16* combined with *KRAS* activation promoted tumour progression and metastases (Qiu et al., 2011).

1.4.2.3 *TP53*

The *TP53* gene encodes for the tumour-suppressor protein, p53. Termed the 'guardian of the genome', p53 prevents the replication of damaged or mutated DNA. DNA damage and oncogene expression activates p53 (Toufektchan and Toledo, 2018). It functions by stimulating the transcription of proteins involved in cell cycle arrest, DNA repair and apoptosis of damaged cells (Toufektchan and Toledo, 2018). Loss of function of p53 allows uncontrolled proliferation of damaged cells. Additionally, mutated p53 may promote the survival and progression of tumour cells (Muller and Vousden, 2014). Approximately 70% of PDAC cases have a mutation of the *TP53* gene, causing the formation of mutant p53 protein, which not only loses its tumour suppressive effects, but also gains oncogenic functions (Voutsadakis, 2021; Maddalena *et al*., 2021). According to the progression model of PDAC the loss of p53 occurs at a later stage and is present in high-grade PanIN lesions. In a mouse model, mutated T*P53* was found to promote tumour invasion and lymph node metastasis of pancreatic tumour cells (Hu *et al*., 2021). Gain-of-function mutant p53 caused decreased infiltration of immune $CD8^+$ T cells into mice pancreatic tumours and modulated the tumor microenvironment by increasing fibrosis of the surrounding tissue, indicating the immunosuppressive properties of gain-of-function p53 (Maddalena *et al*., 2021).

1.4.2.4 *SMAD4/DPC4*

The *SMAD4* gene is responsible for encoding the SMAD4 protein. SMAD4 is activated in response to transforming growth factor beta (TGF-β) signaling. The SMAD4/TGF-β pathway promotes cell cycle arrest, apoptosis and DNA repair (Hu *et al*., 2021). SMAD4 acts as a transcription factor and tumour suppressor protein and is inactivated in approximately 50% of PC cases (McCarthy and Chetty, 2018). The loss of tumour-suppressing properties of SMAD4 occurs in high grade PanIN lesions, thereby promoting invasion and metastasis of precursor lesions (Hu *et al*., 2021).

1.5 Signs and symptoms of PDAC

Early stages of PDAC are clinically asymptomatic (Schawkat *et al*., 2020). Non-specific symptoms such as abdominal pain, unexplained weight loss, nausea and vomiting, anorexia and weakness are the most common presentation of late stage PDAC (De La Cruz *et al*., 2014). Tumours situated in the head of the pancreas causing biliary tree obstruction present with abdominal pain, jaundice, pruritus, dark urine and acholic stools due to the prevention of bile secretions (De La Cruz *et al*., 2014). Early satiety and food intolerance are clinical manifestations specific to tumours of the body and tail of the pancreas (De La Cruz *et al*., 2014). Additionally, sudden onset of type 2 diabetes mellitus in a thin person over the age of 50 years that is unresponsive to treatment is suggestive of pancreatic cancer (De La Cruz *et al*., 2014).

1.6 Serological biomarkers for the detection of PDAC

Carbohydrate antigen 19-9 (CA19-9), carcinoembryonic antigen (CEA) and cancer antigen 125 (CA125) are widely used tumour markers for the detection of PC. The tumour markers display limited specificity for PC when used alone. Consequently, the use of a combination of serum biomarkers is employed as a screening measure to increase the sensitivity and specificity for PC detection (Wu *et al*., 2022). Additionally, these biomarkers are used as predictors for prognosis of disease following diagnosis (van Oosten *et al*., 2023).

1.7 Treatment of PDAC

The multidisciplinary approach to PDAC treatment depends on the stage of the tumour at diagnosis: resectable, borderline resectable, locally advanced or metastatic disease (unresectable). Resectable tumours are defined as tumours that have no contact with any major peripancreatic blood vessels. Borderline resectable tumours constitute tumours that have blood vessel abutment of less than or equal to 180°. Unresectable tumours demonstrate encasement of the blood vessel of greater than 180° (Toesca *et al*., 2018).

1.7.1 Treatment of resectable disease

Surgical resection followed by adjuvant chemotherapy is the standard of care applied to resectable disease (Kwaśniewska *et al*., 2023). Adjuvant chemotherapy refers to chemotherapy that is administered after resection of the tumour to decrease the risk for relapse. In the treatment of early stage PDAC, pancreatectomy remains the only potentially curable treatment option. However, the 5-year survival of patients who underwent resection is still only 24 % (Li

et al., 2022). Additionally, only 15-20 % of patients are eligible for surgical resection upon diagnosis (Principe *et al*., 2021). The options for adjuvant chemotherapy include a modified FOLFIRINOX (5-fluorouracil (5-FU)/folinic acid plus irinotecan and oxaliplatin) regimen or gemcitabine/capecitabine (Manrai *et al*., 2021). Neoptolemos *et al*. (2017) conducted a phase III, randomised clinical trial investigating the use of gemcitabine plus capecitabine vs gemcitabine monotherapy as adjuvant therapy for resected PDAC. The results indicated a median overall survival of 28.0 months in the gemcitabine plus capecitabine group *vs* 25.5 months in the gemcitabine-only group (Neoptolemos *et al*., 2017). A more recent multicentre, randomised phase III trial evaluated a modified FOLFIRINOX regimen against gemcitabine-monotherapy in adjuvant chemotherapy (Conroy *et al*., 2022). The median overall survival in the modified FOLFIRINOX group was 53.5 months compared to the 35.5 months in the gemcitabine group. The results from this trial prompted for the modified FOLFIRINOX regimen to be the standard of care in patients who undergo resection for PDAC (Conroy *et al*., 2022).

1.7.2 Treatment of borderline resectable disease

Borderline resectable disease refers to tumours that present as unresectable upon diagnosis, but have the potential for surgical resection after chemoradiation therapy (Toesca *et al*., 2018). Neoadjuvant chemotherapy serves to reduce the tumour size and involvement with peripancreatic blood vessels in order to increase the chances of tumour resection with negative margins (Toesca *et al*., 2018). There is a growing body of evidence in support of neoadjuvant chemotherapy (Smaglo, 2023). Currently, there are ongoing phase III clinical trials investigating the use of FOLFIRINOX in the pre-operative setting vs post-operatively. The results from a retrospective study supports the use of neoadjuvant chemotherapy which showed that patients who received chemotherapy before surgical resection remained disease-free for a minimum of 48 months (Shrestha *et al*., 2017).

1.7.3 Treatment of unresectable/metastatic disease

First-line therapy for patients with metastatic disease is determined according to the patient's ability to tolerate treatment. Combination chemotherapy regimens consisting of FOLFIRINOX or gemcitabine plus nano-albumin-bound (nab)-paclitaxel are currently the first-line treatment options in fit patients (Garajová *et al*., 2023). Patients who are unable to tolerate FOLFIRINOX are treated with gemcitabine monotherapy. Alternatively, treatment of gemcitabine in combination with capecitabine is offered (Garajová *et al*., 2023). For patients in advanced

stages of disease who are bed-bound, therapy is offered according to a case-by-case basis (Garajová *et al*., 2023).

A multicentre, randomised phase II-III clinical trial evaluated the efficacy of FOFIRINOX vs gemcitabine monotherapy (Conroy *et al*., 2011). The results indicated a median overall survival of 11.1 months in FOLFIRINOX-treated patients vs the 6.8 months in patients treated with gemcitabine. This trial was pivotal in the change of first-line therapy for metastatic PDAC from gemcitabine monotherapy to the FOLFIRINOX regimen. Despite the increase in adverse effects in the FOLFIRINOX group, including grade 3/4 neutropenia, febrile neutropenia, diarrhoea, sensory neuropathy, there was also an increase in the time it took to see a reduction in quality of life compared to the gemcitabine group (Conroy *et al*., 2011). In a retrospective study, Klein-Brill *et al*. (2022) compared the two first line therapies, FOLFIRINOX vs gemcitabine/(nab)-paclitaxel and found an increase in overall survival of 2 months in the FOLFIRINOX group. The FOLFIRINOX group was also associated with fewer posttreatment complications (Klein-Brill *et al*., 2022).

Patients who failed on first-line FOLFIRINOX therapy and are fit are treated with combination gemcitabine and nab-paclitaxel (Petrelli *et al*., 2023). Gemcitabine monotherapy is offered as second-line treatment in patients who are unable to tolerate more aggressive regimens (Principe *et al*., 2021). Second-line therapy additionally involves the use of 5-FU/folinic acid with nano-liposomal irinotecan in patients who have previously used gemcitabine-based therapy. The regimen was well tolerated and showed an increase of 1.9 months in median overall survival compared to 5-FU/folinic acid alone (Wang-Gillam *et al*., 2019).

PDAC patients with mutations in *BRCA-1/2* or *PALB-2* show increased sensitivity to a combination regimen of gemcitabine and cisplatin, which is used as first-line therapy in these patients (Principe *et al*., 2021). Additionally, *BRCA*-mutated patients benefit from the use of targeted immunotherapy, namely olaparib (PARP inhibitor), particularly those who did not progress on platinum-based therapy (Principe *et al*., 2021). An additional subset of PDAC patients that benefits from immunotherapy includes those deficient in DNA mismatch repair with high microsatellite instability. These patients respond well to pembrolizumab, an immune checkpoint inhibitor (Principe *et al*., 2021). The use of tropomyosin receptor kinase (TRK) inhibitors in patients with *NTRK* gene fusions further contributes to precision medicine

approaches (Principe *et al*., 2021). *NTRK* gene fusions are rare oncogenic drivers in PDAC which may be a potential target for therapy in these tumours (O'Reilly and Hechtman, 2019).

The mechanism of action and adverse effects of the chemotherapy drugs used in the treatment of all stages of PDAC are summarized in Table 1.3.

Table 1.3 Mechanism of action and adverse effects of drugs used in the treatment of PDAC (Wellstein and Sausville, 2023; Wellstein and Giaccone, 2023; Wellstein and Atkins, 2023)

Cancer drug	Mechanism of Action (MOA)	Adverse effects
5-FU	Incorporates into DNA and RNA Inhibits thymidylate synthase, preventing DNA-repair mechanisms Results in DNA-strand breakage	Anorexia, nausea, diarrhoea, mucosal ulceration, Myelosuppression: thrombocytopenia, anaemia Hand-foot syndrome (erythema, oedema, burning sensation)
Irinotecan	Prodrug Inhibits topoisomerase-I, preventing DNA replication, repair and transcription	Diarrhoea Myelosuppression: severe neutropenia, febrile neutropenia Nausea, vomiting, fatigue, mucositis Skin flushing, alopecia Cholinergic syndrome
Oxaliplatin	Binds to electron-rich regions in proteins and various sites on DNA, forming inter- and intra-strand crosslinks Inhibits DNA replication and transcription, leading to single- and double-stand breaks Causing the induction of apoptosis Additionally suppresses expression of thymidylate synthase - synergistic with 5-FU	Peripheral neuropathy Sensory neurotoxicities: dysesthesias, ataxia, numbness of extremities
Gemcitabine	Enters cells through nucleoside transporters Intracellularly converted to active di- and tri-phosphates Di-phosphate inhibits ribonucleoside diphosphate reductase, causing depletion in deoxyribonucleotide pool, preventing DNA synthesis	Myelosuppression Hepatotoxicity Flu-like syndrome, asthenia (weakness) Interstitial pneumonitis

	Tri-phosphate incorporates into DNA, causing strand termination that is resistant to repair	
Paclitaxel	Binds to β-tubulin of microtubules, causing their disassembly Causes mitotic arrest and induction of apoptosis	Neutropenia Peripheral and sensory neuropathy Myalgias Mucositis
Capecitabine	Prodrug of 5-FU. MOA as for 5-FU	Hand-foot syndrome (erythema, oedema, burning sensation)
Cisplatin	As for oxaliplatin	Nephrotoxicity Ototoxicity (tinnitus, hearing loss of high-frequencies) Nausea, vomiting Mild/moderate myelosuppression: leukopenia, thrombocytopenia, Anaemia
Olaparib	Poly-(ADP-ribose) Polymerase (PARP)-inhibitor, used only in BRCA-mutated patients. PARP normally repairs single-stranded breaks in DNA Without PARP, double-strand breaks accumulate during DNA replication. Cells with functional BRCA are able to repair double-stranded breaks. In tumour cells lacking functional BRCA, PARP-inhibitors prevent repair of DNA double-strand breakage, causing induction of apoptosis	Myelodysplastic syndrome, acute myelocytic leukaemia Pneumonitis Nausea, vomiting, loss of appetite Fatigue, myalgia and arthralgia Anaemia
Pembrolizumab	Antibody that blocks PD-1 allowing for restoration/maintenance of antitumour T cell response	Fatigue, cough, nausea, constipation, diarrhoea Pruritus, arthralgia, decreased appetite Immune-mediated inflammation: pneumonitis, colitis, hepatitis

1.7.4 Treatment resistance/failure in PDAC

Drug resistance of PDAC cells poses another obstacle in the treatment of the disease. Resistance of the tumour to chemotherapy is as a result of the desmoplastic, immunosuppressive tumour microenvironment and the poor vasculature surrounding the tumour which results in decreased delivery and perfusion of the drug into the tumour (Olive *et al*., 2009; Sofuni *et al*., 2005; Carapuça *et al*., 2016). The dense stroma in the tumour microenvironment prevents the infiltration of T and B lymphocytes, contributing to the immunosuppressive environment (Ene-Obong et al., 2013). Consequently, immune checkpoint

blockade and targeted therapy is ineffective in PDAC tumours, despite showing promising activity in various other solid tumours (Hecht *et al*., 2021; Tempero *et al*., 2021; Van Cutsem *et al*., 2020). There is, therefore, an urgent need for novel drug therapies in PDAC. Additionally, the factors contributing to treatment resistance in PDAC requires attention and resolution.

1.8 Haem oxygenase-1

Haem oxygenase-1 (HMOX1) is the inducible isoform of the enzyme which catalyses the breakdown of pro-oxidant, cytotoxic, free haem into biologically active carbon monoxide (CO), free ferrous iron and biliverdin, which is rapidly catabolized to bilirubin by the action of biliverdin reductase (Mascaró *et al*., 2021). HMOX1 is induced in response to cellular stresses such as ROS, ultraviolet irradiation, pro-inflammatory cytokines, hypoxia, ischemia, heavy metals and nitric oxide as well as other stimuli such as the presence of its substrate haem (Muchaa *et al*., 2019; Jun *et al*., 2018). HMOX1 is normally embedded in the membrane of the smooth endoplasmic reticulum. Most of the protein, including its active N terminus, resides in the cytoplasm. A shorter portion containing the C terminus resides in the lumen of the smooth endoplasmic reticulum (Yoshida and Sato, 1989). Additionally, HMOX1 localizes to other subcellular compartments including the mitochondria, vacuoles, caveolae in the plasma membrane and the nucleus. Translocation to the nucleus is possible through the truncation of the C terminus of the protein which is associated with loss of its enzymatic activity (Lin *et al*., 2007; Mascaró *et al*., 2021). The cytoprotective properties of HMOX1 include its ability to prevent against neuron damage, atherosclerosis, cardiovascular disease, cancer and inflammation (Lee *et al*., 2014). As a result of truncation and nuclear translocation of HMOX1, the protein is able to upregulate cytoprotective genes involved in hydrogen peroxide-induced oxidative stress (Lin *et al*., 2007). The transcription factor effects are independent of its enzymatic activity. Additionally, the by-products of the enzyme activity of HMOX1 (carbon monoxide, biliverdin, ferrous iron) contribute to its cytoprotective effects. Bilirubin demonstrated antioxidant effects against hydrogen peroxide-induced cytotoxicity as well as ROS-mediated cell injury in cultured cells (Ryter *et al*., 2006). Biliverdin reductase gene silencing causing decreased levels of bilirubin resulted in the accumulation of ROS and the promotion of apoptosis in HeLa cells and primary neuronal cells (Ryter *et al*., 2006). Ferrous iron is a pro-oxidant molecule that is rapidly sequestered by ferritin, an intracellular protein responsible for iron storage and homeostasis (Kim *et al*., 2011). Accumulation of ferritin in the cell in conjunction with HMOX1 expression is associated with cytoprotective properties in

cultured cells (Ryter *et al*., 2006). CO has shown anti-apoptotic effects in several studies. In mouse fibroblasts and endothelial cells, CO inhibited TNF-α induced apoptosis. In addition, anti-apoptotic effects were observed in ischemia/reperfusion injury after low dose treatment with CO (Ryter *et al*., 2006).

1.8.1 HMOX1 in cancer cells

HMOX1 exhibits contrasting protumour and antitumour effects in different types of cancer (Mascaró *et al*., 2021). In prostate cancer cells, the HMOX1 product, CO was shown to inhibit tumour growth and increased the sensitivity of tumour cells to chemotherapy by causing metabolic exhaustion. In addition, overexpression of HMOX1 in the cells further stimulated cell death in response to chemotherapy (Wegiel *et al*., 2013). In a *KRAS*-positive lung cancer mouse model, treatment with CO significantly inhibited tumour growth (Wegiel *et al*., 2013). Overexpression of HMOX1 in rat and human breast cancer cell lines caused anti-proliferative and pro-apoptotic effects (Hill *et al*., 2005). MCF-7 breast cancer cells overexpressing HMOX1 demonstrated a reduction in tumour invasion due to HMOX1 (Lin *et al*., 2008). In colorectal cancer patients, tumours expressing HMOX1 were associated with a longer median survival time. In addition, colorectal cancer cell lines demonstrated cell cycle arrest and apoptosis as a result of HMOX1, however, intact p53 tumour-suppressive properties was required (Andrés *et al*., 2014).

In contrast, overexpression of HMOX1 promotes protumour effects, allowing cancer cells to evade apoptosis, contributing to resistance of tumour cells to chemotherapy and radiation (Nuhn *et al*., 2009; Chau, 2015). Increased proliferation was observed in melanoma cells overexpressing HMOX1 while tumour-bearing mice displayed increased lung metastasis and induced the production of vascular endothelial growth factor (Was *et al*., 2006). In prostate cancer patients, nuclear HMOX1 correlated with disease progression (Sacca *et al*., 2007). Nuclear translocation of HMOX1 conferred resistance to chronic myeloid leukaemia cells to imatinib treatment (Tibullo *et al*., 2013).

In pancreatic cancer, mice with overexpressed HMOX1 demonstrated an increase in angiogenesis and endothelial cell survival and proliferation compared to mice without HMOX1 overexpression (Sunamura *et al*., 2003). Additionally, the HMOX1-mice developed lung metastases at a greater frequency than mice without overly expressed HMOX1 (85% vs 33% respectively) (Sunamura *et al*., 2003). Samples from PDAC patients revealed a 6-fold increase

in HMOX1 mRNA compared to normal pancreatic tissue, indicating that HMOX1 is overexpressed in pancreatic cancer (Berberat *et al*., 2005). Exposure of pancreatic cancer cells to chemotherapy and radiation increased the expression of HMOX1 in these cells, further contributing to treatment resistance (Berberat *et al*., 2005). In cultured pancreatic cancer cell lines, gene silencing of HMOX1 reduced cell proliferation and sensitized the cells to radiotherapy as well as gemcitabine treatment (Berberat *et al*., 2005). *In vitro* studies have shown that concurrent administration of gemcitabine with HMOX1 inhibitors increased the effectiveness of gemcitabine by sensitizing the pancreatic cancer cell lines to gemcitabine and promoting apoptosis (Abdalla *et al*., 2019). Further studies have shown that HMOX1 inhibitors arrested the cell cycle by inducing the cyclin-dependent kinase (CDK) inhibitor, p21 and inhibiting CDKs in thyroid cancer cells (Yang *et al*., 2018).

Increased expression of HMOX1 in the cells of the tumour microenvironment, such as tumour-associated macrophages, dendritic cells and tumour-infiltrating lymphocytes, contributes to the suppression of the immune response, allowing for the survival and proliferation of the tumour cells (Nitti *et al*., 2023). In a murine model of PDAC, inhibition of HMOX1 in tumour-associated macrophages resulted in a reduction in tumour growth (Arnold *et al*., 2014). Treatment of breast carcinoma-bearing mice with the HMOX1 inhibitor, zinc protoporphyrin, caused an increase in immune response to paclitaxel by increasing $CD8^+$ T cells (Kim *et al*., 2021). Using a murine fibrosarcoma model where HMOX1 was deleted in the tumour-associated macrophages, Consonni *et al*. (2021) observed a decrease in lung metastasis of the primary tumour. In a murine melanoma model, deletion of HMOX1 in the myeloid compartment (immune cells) caused a switch of M2 tumour-associated macrophages to their anti-tumour phenotype, M1 (Consonni *et al*., 2021). Additionally, the decrease in mesenchymal markers observed in the mice with HMOX1 deletion in the myeloid compartment, indicated the inhibition of epithelial-to-mesenchymal transition, decreasing the migratory capacity of the tumour cells (Consonni *et al*., 2021). In the same model, there was also an observed increase in tumour-infiltrating lymphocytes and a decrease in the immunosuppressive regulatory T cells, indicating enhancement of the immune response after deletion of HMOX1 in immune cells (Consonni *et al*., 2021). In both the fibrosarcoma and melanoma murine models, inhibition of HMOX1 by zinc protoporphyrin sensitized the tumours to anti-PD-1 immunotherapy (Consonni *et al*., 2021).

1.8.2 HMOX1 inhibitors

Mechanisms used to inhibit the activity of HMOX1 includes RNA interference, CRISPR/Cas9, pharmacological inhibition using metalloporphyrins or imidazole-based inhibitors (Podkalicka *et al*., 2018). RNA interference and CRISPR/Cas9 directly target the HMOX1 gene, resulting in downregulation or knockdown of the gene function (Podkalicka *et al*., 2018). *In vivo* and *in vitro* application of RNA interference (small interfering RNA/ short hairpin RNA) resulting in HMOX1-silencing was demonstrated in multiple studies (Sass et al., 2008; Kang et al., 2014; Kim et al., 2008; Wei et al., 2014). Studies using CRISPR/Cas9 to induce HMOX1 knockout/inhibition have also been demonstrated (Liu *et al*., 2019). Pharmacological inhibition of HMOX1 is achieved through the use of metalloporphyrins. Metalloporphyrins are potent, non-selective inhibitors of all isoforms of HMOX. While their HMOX1-inhibitory effects have been demonstrated in numerous *in vitro* and *in vivo* settings (Li *et al*., 2023; Cheng *et al*., 2016; Furfaro *et al*., 2022), their phototoxicity and high lipophilicity currently precludes their use in the clinical setting (Schulz *et al*., 2012). Additional pharmacological inhibitors include the imidazole-based inhibitors such as OB24 HCl, the inhibitor used in this study (Alaoui-Jamali *et al*., 2009). Imidazole-based inhibitors are highly potent and show selectivity towards HMOX1 (Podkalicka *et al*., 2018). There is limited information available regarding their safety profiles, pharmacokinetics and distribution in a clinical setting (Podkalicka *et al*., 2018).

1.9 Types of cell death

There are two broad types of cell death: accidental cell death and regulated cell death. Accidental cell death occurs when extreme disturbances in cellular homeostasis causes an immediate physical rupture of cellular components (Galluzzi and Myint, 2023). Necrosis is a form of accidental cell death. On the other hand, disruptions in cellular homeostasis leading to damage of cellular components trigger certain repair pathways that attempt to restore the function of the cell. The pathways include DNA-damage response pathways, the unfolded protein response and autophagy (Galluzzi and Myint, 2023). Should these pathways fail to repair the damaged cell, the pathways will activate mediated-cell death pathways to promote the demise of the cell in a process broadly termed regulated cell death. Regulated cell death occurs in normal physiological conditions as well as tissue injury and disease states (Ye *et al*., 2023). Regulated cell death includes extrinsic and intrinsic apoptosis, necroptosis, ferroptosis, pyroptosis, cuproptosis and autophagy (Tsvetkov *et al*., 2022; Galluzzi and Myint, 2023). This study presents evidence for apoptotic cell death. As such, apoptosis will be discussed in greater detail than the alternative modes of cell death.

1.9.1 Necrosis

Necrotic cell death is induced by external stimuli such as hypoxia, radiation, heat or chemical injury (D'arcy 2019). Necrosis involves the up-regulation of pro-inflammatory proteins such as nuclear factor kappa B (NF-κB). Necrotic cell death is associated with the swelling of the cell, cell membrane rupture and overflow of the contents of the cell into surrounding tissue. This results in the triggering of a cascade of inflammatory molecules causing damage to the surrounding tissue (D'Arcy, 2019). Consequently, necrosis is unwanted in the context of anti-cancer treatment due to its inflammatory effects and its contribution to tumour lysis syndrome (Woo *et al*., 2020).

1.9.2 Secondary necrosis

In vivo, apoptotic cells and their blebs are rapidly cleared by circulating phagocytes. This is often accompanied by the release of anti-inflammatory signals (Galluzzi and Kroemer, 2017). *In vitro*, there is an absence of circulating immune cells which precludes the removal of apoptotic cells by phagocytes. As a result, the floating apoptotic cells lose their structural integrity, swelling of the cells' organelles results in plasma membrane rupture and subsequently, the release of cytoplasmic contents (Galluzzi and Kroemer, 2017). This process is known as secondary necrosis.

1.9.3 Apoptosis

Apoptosis is a controlled form of cell death that is crucial in physiological processes. Unlike necrosis, apoptosis does not elicit an inflammatory response, and only the individual cell undergoing apoptosis is affected. Features of apoptosis include rounding-up of the cell, cell shrinkage (pyknosis), chromatin condensation, nuclear fragmentation and membrane blebbing (Kroemer 2008). A family of cysteine-aspartate proteases called caspases triggers the activation of apoptosis, although apoptosis can be carried out in a non-caspase-dependent manner. There are two types of apoptotic pathways namely, the extrinsic/death receptor pathway and the intrinsic/mitochondrial pathway (Haynes *et al*., 2023).

1.9.3.1 Extrinsic pathway

Following extracellular stress signals, the extrinsic pathway is initiated by the binding of extracellular-exposed death receptors with their respective protein family ligands (Figure 1.2). The death receptors belong to the tumour necrosis factor (TNF) receptor superfamily. The ligands include TNF-α and the Fas-ligand which bind to the TNF-receptor-1 and Fas receptors,

respectively (Haynes *et al*., 2023). The death receptors possess an intracellular protein-protein domain called the death domain which interacts with the death domains of other receptors. The binding of the ligands with their respective receptor results in the recruitment of adapter proteins (TRADD/FADD) which bind to their respective receptors. The adapter proteins then dimerize with pro-caspase 8, resulting in the formation of the death-inducing signalling complex (DISC) (Haynes *et al*., 2023). The formation of DISC results in the cleavage of pro-caspase 8 to caspase 8, thereby activating it. Subsequent activation of caspase-3 by caspase-8 occurs, thereby activating the execution phase of apoptosis. Additionally, the activation of caspase-8 triggers the activation of BH3-interacting domain death agonist (Bid) to tBid which, in turn, activates Bax (Haynes *et al*., 2023). Bax is a protein recruited in the intrinsic pathway and functions by creating pores in the mitochondrial membrane, thereby causing the release of cytochrome c from the mitochondria, and eventually activating caspase-3 downstream of the intrinsic pathway (Haynes *et al*., 2023).

1.9.3.2 Intrinsic pathway

The intrinsic pathway, also known as the mitochondrial pathway, is mediated by intracellular signals that are relayed to the mitochondria (Figure 1.2). Stimuli include irreparable DNA damage, endoplasmic reticulum stress, hypoxia and oxidative stress (Haynes *et al*., 2023). Following the occurrence of stimuli, pro-apoptotic members of the BH3-only family (Bax, Bak) are activated, resulting in the disruption of the mitochondrial outer membrane permeability (MOMP). Proteins normally confined to the mitochondria, namely cytochrome c, Smac/DIABLO and Omi/HtrA2 (a serine protease) enter the cytosol due to increased permeability of the mitochondrial membrane (Haynes *et al*., 2023). Smac/DIABLO and Omi/HtrA2 function by inhibiting anti-apoptotic proteins, IAPs (inhibitors of apoptosis proteins). Cytochrome c binds to apoptotic protease activating factor-1 (Apaf-1) resulting in the formation of an apoptosome. The apoptosome associates with pro-caspase-9, which subsequently causes its cleavage and activation. Active caspase-9 triggers the activation of downstream executioner caspases, such as caspase-3, caspase-6 and caspase-7 (Haynes *et al*., 2023).

1.9.3.3 Execution phase of apoptosis

Following the activation of the most important executioner caspase, caspase-3, the endonuclease caspase-activated DNase (CAD) is activated. In an inactive state, CAD is complexed to its inhibitor which is degraded by caspase-3, rendering CAD active. CAD cleaves

chromosomal DNA resulting in chromatin condensation. Additionally, caspase-3 promotes the reorganisation of the cytoskeleton and the fragmentation of the cell into apoptotic bodies. Finally, apoptotic cells are tagged for phagocytic uptake by the translocation of phosphatidylserine to its outer surface (Haynes *et al*., 2023).

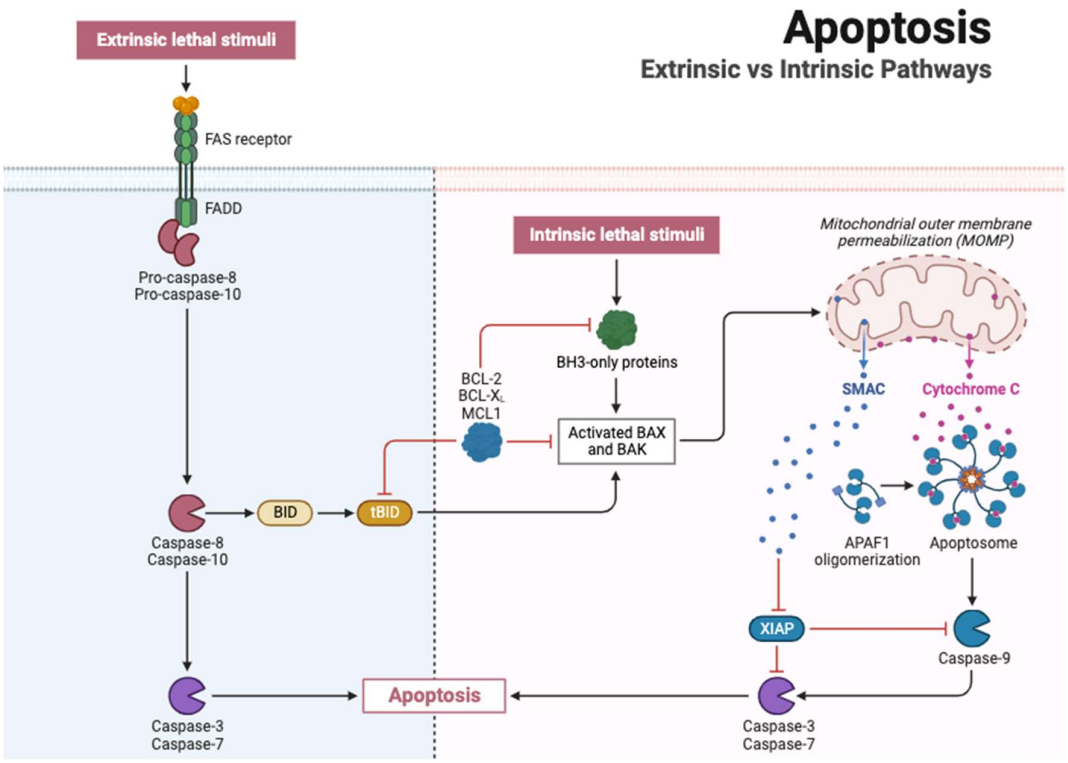


Figure 1.2 Extrinsic and Intrinsic Apoptotic pathways. Diagram depicting the extrinsic and intrinsic apoptotic pathways. Legend: FADD: Fas-associated death domain; BID: BH3-interacting domain death agonist; tBID: truncated Bid; Bcl-2: B-cell lymphoma-2; BCL-x: B-cell lymphoma-extra-large protein; MCL1: Myeloid cell leukaemia-1; Bax: Bcl-2-associated X protein Bak: Bcl-2 antagonist killer 1; SMAC: Second mitochondria-derived activator of caspase; APAF1: Apoptotic protease activating factor-1; XIAP: X-linked inhibitor of apoptosis. Modified from Wilson and Hunt, 2002; created with BioRender.com)

1.9.3.4 Evasion of apoptosis by cancer cells

One of the hallmarks of cancer is their ability to evade cell death by apoptosis, contributing to uncontrolled growth and proliferation; and resistance to chemo- and radiation therapy (Neophytou *et al*., 2021). Gene mutations resulting in the loss of pro-apoptotic proteins and the amplification of anti-apoptotic proteins enables cancer cells to evade apoptosis. Additionally, the loss of caspase functioning and compromised death receptor signalling allows cancer cells to evade apoptosis. Overexpression of the anti-apoptotic Bcl-2 protein occurs in numerous cancers and is associated with resistance to chemoradiation therapy (Weller *et al*., 1995; Geng

et al., 2013). Another mutation that is implicated in enabling cancer cells to evade apoptosis is the loss of function of p53. The role of wild type p53 is the upregulation of pro-apoptotic proteins such as Bid, Bax, Puma and noxa. The binding of p53 to the anti-apoptotic proteins (Bcl-2 and Bcl-x) inhibits their effects as inhibitors of apoptosis. Mutated p53 is the most common somatic mutation found in cancer (Bouaoun *et al*., 2016) and confers resistance of cancer cells to chemotherapy drugs such as gemcitabine, doxorubicin, cisplatin and cetuximab (Stahnke *et al*., 2001). Overexpression of inhibitors of apoptosis proteins (IAPs), such as XIAP and survivin, has been reported in numerous cancers is associated with poor prognosis and resistance to treatment (Tamm *et al*., 2004; Moussata *et al*., 2012). The IAPs inhibit caspase-activation, thereby preventing apoptosis. Overexpression of the IAP, c-IAP2, occurs during the early stages of malignant progression of PC (Esposito *et al*., 2007). Additionally, the tumour microenvironment plays a role in immune escape of the cancer cells, promoting survival and proliferation. The stroma surrounding the tumour consists of high levels of cancer associated fibroblasts that release various factors that result in activation of anti-apoptotic pathways, promote the epithelial-to-mesenchymal transitioning and increase the tumorigenic cancer stem cells (Neophytou *et al*., 2021).

1.9.4 Necroptosis

Necroptosis is a regulated form of cell death that is activated by TNF-α. It demonstrates all the features of necrosis such as membrane rupture, swelling of organelles, absence of nuclear fragmentation and the release of intracellular contents but occurs in a signal-mediated manner (Ye *et al*., 2023). Necroptosis is implicated in many disease conditions such as ischemia reperfusion injury (Linkermann *et al*., 2013), sepsis (Reilly *et al*., 2022) and neurodegenerative diseases (Yuan *et al*., 2019).

1.9.5 Autophagy

Autophagy refers to the process of conveying cytoplasmic constituents, including organelles, to the lysosome for the purpose of degradation. Under normal conditions, autophagy plays an important role in the homeostasis of amino acid levels in starvation; the development of the blastocyst before implantation; inhibition of tumour formation; anti-aging processes, elimination of microbes inside the cell and the regulation of the immune system (Levine and Kroemer, 2019). In certain cancers, such as PC, autophagy confers a survival advantage by allowing tumour cells to survive high metabolic demands of increased growth and

proliferation. In contrast, autophagy has exhibited tumour suppression effects in other cancers through the promotion of programmed cell death (Levine and Kroemer, 2019).

1.9.6 Ferroptosis

Ferroptosis is a form of cell death dependent on iron-induced ROS accumulation, that employs lipid peroxidation to induce cell death (Dixon *et al*., 2012). Certain cancers, *in vitro,* have been shown to be susceptible to cell death by induced ferroptosis (Yang et al., 2014).

1.9.7 Pyroptosis

Gasdermins are a family of proteins that mediate the inflammatory cell death pathway, pyroptosis. Gasdermins disrupt the integrity of the cell membrane through the formation of pores. This results in the release of pro-inflammatory cytokines into the extracellular space (Liu et al., 2021). Morphological features of pyroptosis include flattening of the cell, as the cytoplasmic contents of the cell are released into the extracellular space.

1.9.8 Cuproptosis

Cuprotosis is triggered by the accumulation of copper in the mitochondria, leading to lipoylation of mitochondrial enzymes involved in the tri-carboxylic acid cycle, which leads to proteotoxicity and death (Tsvetkov *et al*., 2022). Cells that utilise oxidative phosphorylation as their main source of energy are especially susceptible to death by cuproptosis. Certain cancers such as, melanoma, glioblastoma, cholangiocarcinoma, breast and leukaemic cancers rely mostly on oxidative phosphorylation (Porporato *et al*., 2018; Xie *et al*., 2023). Additionally, drug-resistant cancers exhibit a high dependency on mitochondrial metabolism as their energy source (Xie *et al*., 2023). Copper ionophores inducing copper-overload in cancer cells have been used to disrupt mitochondrial function and respiration, inducing cell death of cancer cells via cuproptosis (Tsvetkov *et al*., 2022)

1.10 Copper complexes and their potential anti-cancer activity

Copper is an essential element required for various physiological processes in the body. Copper functions in the activation of key enzymes such as cytochrome c oxidase, Cu-Zn superoxide dismutase, tyrosinase and dopamine β-hydroxylase (Kennelly, 2023). The enzymes are involved in mitochondrial respiration, protection of the cell against free radicals, the synthesis of melanin and the synthesis of epinephrine, respectively (Kennelly, 2023). In tumour cells, copper complexes were shown to promote the growth and metastases of tumours through their

ability to induce angiogenesis (Xie *et al*., 2009; McAuslan *et al*., 1980; Hu, 1998). Copper promoted the proliferation and migration of endothelial cells and was shown to stimulate the secretion of angiogenic factors such as vascular endothelial growth factor (VEGF) (Xie *et al*., 2009). As such, copper-reduction therapy is an attractive treatment strategy in the treatment of cancers. Copper-reduction therapy utilizing copper-chelators were shown to inhibit several angiogenic factors such as vascular endothelial growth factor (VEGF), interleukin-8 (IL-8) and matrix metalloproteinases in MDA-MB-231 breast cancer cells while also inhibiting the migration, invasion and tube formation of human umbilical vein endothelial cells (Zhou *et al*., 2019). In contrast, the anticancer activity of synthesized copper complexes have been shown extensively over the past four decades (Ji *et al*., 2023). A copper-phenanthroline complex inhibited the migratory abilities of SKOV-3 ovarian cancer cells and inhibited the expression of the metastasis-promoting protein, matrix metalloproteinase-2, indicating that the copper-phenanthroline complex inhibited metastasis (Shi *et al*., 2018). The same study demonstrated the ability of the copper-phenanthroline complex to inhibit angiogenesis by decreasing the expression of VEGF-R1, and preventing the formation of sprouting and tube formation in human umbilical vein endothelial cells (Shi *et al*., 2018). In a study conducted by Thathi *et al*. (2007), human hepatic and kidney carcinoma cells treated with a different copper/phenanthroline complex showed activation of caspase-3 and caspase-9, and demonstrated PARP-cleavage, indicating the induction of DNA damage and apoptosis. Recently, a synthesized copper-diketonate complex was cytotoxic against multiple human carcinoma cell lines, including pancreatic, with an IC_{50} value of 1.2 µM in the BxPC-3 pancreatic cancer cell line, after a 24 hour MTT assay (Pellei *et al* 2022). In the A549 lung carcinoma cell line, two copper isoquinolinyl aniline complexes were active at IC_{50} values of 3.1- and 6.4 µM, respectively (Gul *et al*., 2020). The complexes arrested the cell cycle of A549 cells, caused an increase in ROS formation, activated caspases -3, -8 and -9 and caused an increase in autophagy-related proteins, confirming the activation of both the intrinsic apoptotic pathway as well as autophagic cell death (Gul *et al*., 2020). Additionally, the same study demonstrated a reduction in tumour size in a xenograft lung cancer mouse model caused by the copper complexes (Gul *et al*., 2020). Another mechanism of action of copper complexes is through the activation of cuproptosis. A glucose-oxidase-engineered copper triazolate complex is an engineered molecule that is activated by the high glutathione levels in cancer cells, augments starvation in cancer cells, induces ROS and sensitizes mice bladder tumours to cuproptosis (Xu *et al*., 2022). A group of copper complexes, the Casiopeínas®, containing either a phenanthroline ligand or a bipyridyl ligand, demonstrated anti-cancer activity through

the production of ROS, caused mitochondrial membrane depolarization and activated caspase-3 in a paediatric metastatic neuroblastoma cell line (García-Ramos *et al*., 2017). Numerous other studies have reported the cytotoxicity of the Casiopeínas® in human cell cultures as well as in murine carcinoma models (Castillo-Rodríguez *et al*., 2021; Chavez-Gonzalez *et al*., 2017; Valdez-Camacho *et al*., 2020; Kachadourian *et al*., 2010). From this group of complexes, the Cas III-ia complex was selected for evaluation in phase I clinical trials due to its solubility in water and its lower toxicity profile compared to its more active counterparts (Masuri *et al*., 2022). A study by Rodrigues *et al*. (2023) highlighted the importance of the phenanthroline ligand in synthesized copper-diiminic hydroxybenzophenones, where an increase in cytotoxicity towards human hepatoma and colon carcinoma cell lines was observed in the complexes that contained a phenanthroline ligand. An additional mechanism of action of the anti-cancer activity of copper is through the inhibition of the proteasome. The proteasome is responsible for the degradation of damaged and misfolded proteins and plays a key role in the regulation of proteins in various cell processes (Peters *et al*., 1993). Disruption of ubiquitination of proteins mediated by the proteasome leads to the activation of apoptosis in tumour cells (An *et al*., 1998). Copper-indolecarboxylic acid/phenanthroline complexes inhibited the activity of the proteasome and induced apoptosis in MDA-MB-231 cells, in a dose-dependent manner (Zhang et al., 21016).

Another study on copper-indenoisoquinoline complexes demonstrated cytotoxic effects on five adenocarcinoma cell lines (cervix, breast, prostate and colorectal) at low μM IC_{50} values after a 72 h MTS assay (Molinaro *et al*., 2023). The complexes were able to inhibit topoisomerase I in a dose-dependent manner. Moreover, the complexes showed increased DNA-binding capabilities following the complexation with copper (II) as copper stabilized the aromatic ring before binding to DNA (Molinaro *et al*., 2023).

Studies evaluating the effect of copper-imidazo[1,2-a]pyridines were shown to induce apoptosis of HT-29 colorectal cancer cells (Harmse *et al*., 2019). The copper complexes decreased the levels of inhibitor of apoptosis proteins. Additionally, the compounds induced the expression of the stress-response protein, HMOX1, indicating the presence of cellular stress in the form of ROS which was confirmed by the DCFDA cellular ROS assay (Harmse *et al*., 2019). The same copper-imidazo[1,2-a]pyridines showed cytotoxic activity towards human colon carcinoma, breast carcinoma and leukaemic cell lines with IC_{50} values ranging from as low as 0.68 μM to 28 μM (Dam *et al*., 2018). A different study using the same copper-

imidazo[1,2-a]pyridines caused the activation of caspase-3 and caspase-9 in leukaemic cell lines, while an increase in the expression levels of pro-apoptotic proteins (Bax, Smac/DIABLO, HTRA2/Omi) was observed (Ismail et al., 2021). Gordon *et al*. (2022) evaluated the cytotoxic activity of the same copper-phenanthroline complex used in this study. Against neuroblastoma, lung, breast, colon and pancreatic carcinoma cell lines, the copper-phenanthroline complex had IC_{50} values of below 5 μM (Gordon *et al*., 2022).

1.11 Pancreatic cancer cell lines

1.11.1 AsPC-1

The AsPC-1 cell line was derived from nude mouse xenografts of cells established from a 62 year old white female patient with pancreatic ductal adenocarcinoma of the head of the pancreas. The patient developed metastases to various abdominal organs and presented with ascites. The epithelial cells were isolated from the patient's ascites and grown into primary tissue cultures (Chen *et al*., 1982). Nude mice were infected with the cells resulting in a tumour that displayed typical characteristics of pancreatic adenocarcinoma. The tumour produced abundant mucin and expressed CEA as well as human pancreas cancer associated antigen (Chen *et al*., 1982). The AsPC-1 cell line harbours mutations in *KRAS*, *TP53*, *CDKN2A/p16* and *SMAD4/DPC4* (Moore *et al*., 2001).

1.11.2 MIA PaCa-2

The MIA PaCa-2 epithelial cell line was derived from the primary tumour of a 65 year old white male patient with ductal adenocarcinoma (Yunis *et al*., 1977). The cell line did not express CEA (Yunis *et al*., 1977). The cell line exhibits mutations in *KRAS* and *TP53*, homozygous deletion in *CDKN2A/p16* genes but expresses wildtype *SMAD4/DPC4* (Moore *et al*., 2001).

1.12 Rationale of the study

The prognosis of patients with PDAC remains poor while the incidence is increasing. Current therapeutic approaches are not curative and serves to slow down the rate of tumour progression. Therefore, novel approaches to therapy are required. Copper complexes have previously shown promising activity against several cancer cell lines such as colorectal and leukaemic cell lines, therefore further studies are required on other cell lines, specifically pancreatic cancer cell lines.

Additionally, the role of HMOX1 in cancer demonstrates contrasting effects in different cancer types, necessitating the need for clarity and further studies. This study tested different classes of copper complexes on pancreatic cancer cell survival and HMOX1 expression as well as the role of HMOX1 expression on cell survival.

The two chosen cell lines represent the highly aggressive phenotype of PDAC. Additionally, the study uses cell lines established from the primary tumour as well as one from a metastatic site, ensuring a comprehensive representation of PDAC in a cell culture model.

1.13 Aim and Objectives

Aim:

To evaluate a few copper complexes of different classes of ligands on pancreatic cancer cell survival, determine the mechanism of cell death induced by the copper complexes and elucidate their effects on HMOX1.

Objectives:

(i) Evaluate the effects of copper complexes on pancreatic cell survival, using the MTT cell viability assay.
(ii) Determine the mechanism of cell death induced by copper complexes by evaluating cell morphology, mitochondrial membrane potential using the JC-1 assay, evaluating annexin-V-binding and by measuring caspase-3 and caspase-9 activity.
(iii) Determine the effect of the copper complexes on the formation of ROS.
(iv) Determine the effect of copper complexes on HMOX1 expression and its percentage of nuclear localization using immunofluorescence and western blotting.
(v) Determine the effect of HMOX-1 inhibition on the cytotoxicity of the copper complexes using the MTT cell viability assay.

Chapter II: Methods

2.1 Cell culture

AsPC-1 and MIA PaCa-2 cells were obtained from the American Type Culture Collection (Manassas, VA, USA). AsPC-1 cells were derived from the ascites of a patient with metastatic adenocarcinoma (Chen *et al*., 1982) while MIA PaCa-2 cells were derived from the tumour of a PDAC (Yunis et al., 1977). Cells were monitored daily using an Olympus CKX41 (Tokyo, Japan) inverted phase contrast microscope to observe the growth of cells and to ensure cultures were free from microbial contamination.

2.1.1 Cell culture reagents

Each cell line was maintained in medium specific to their requirements. AsPC-1 cells were cultured in Roswell Park Memorial Institute (RPMI) medium obtained from Sigma-Aldrich/Merck, SA) while MIA PaCa-2 cells were grown in a 50/50 (% v/v) solution of Dulbecco's Modified Eagle Medium (DMEM) and Ham's F-12 medium (Sigma-Aldrich/Merck, SA). Media was supplemented with 10% heat-inactivated foetal bovine serum (FBS) (Thermo Fisher, Life Technologies, SA), sodium pyruvate, non-essential amino acids and L-glutamine (Sigma-Aldrich/Merck, SA). Media was sterile filtered and stored at 4 °C. Before each use, media was warmed to 37 °C.

FBS was placed in a 56 °C water bath for 60 minutes to inactivate the complement system, then aliquoted into 50 mL centrifuge tubes and stored at -20 °C until required.

Phosphate buffered saline (PBS) was used for washing cell cultures prior to trypsinization, in order to remove cell debris and residual FBS which prevents the trypsinization of cells. PBS was composed of 1.37 mM NaCl, 0.27 mM KCl, 100 mM Na_2HPO_4 and 18 mM KH_2PO_4 (pH 7.2-7.4). After autoclaving, PBS was stored at room temperature.

Trypsin is a proteolytic enzyme that promotes the detachment of cells from the growth surface, allowing for resuspension during subculture. Trypsin is supplemented with ethylenediaminetetraacetic acid (EDTA). Both cell lines were adherent and required the use of trypsin in cell culture (Sigma-Aldrich/Merck, SA).

2.1.2 Cell culture maintenance and subculture

Cells were grown in sterile conditions in 75 cm^2 cell culture flasks (Greiner Bio-One) at 37 °C in a 5% CO_2, humidified incubator. Once cells reached 80% confluency, they were trypsinized as follows: after aspirating the media from the flask, cells were washed with sterile PBS three times. Four millilitres of trypsin were added to the flask and incubated at 37 °C for two to five minutes until the cell layer had detached. Thereafter, the cells were resuspended and four millilitres of media was added to the flask to deactivate the trypsin. Cell clusters were dissociated and evenly redistributed through repeatedly pipetting the cell suspension, after which approximately one millilitre of cell suspension was returned to the flask. Fresh media was added to the flask to a total volume of 20 mL. Media was replaced every two to three days until confluency was reached.

2.1.3 Cryopreservation

Cryopreservation utilizes low temperatures to halt the growth of cells and preserve their integrity until they are required. Cell culture stocks were made in freezing medium which was composed of each cell line's respective media, supplemented with 20 % FBS and 6% cell culture grade dimethylsulfoxide (DMSO) (Sigma-Aldrich/Merck, SA). The addition of DMSO served as a cryoprotective agent. After trypsinization, the cell suspension was placed in 15 mL centrifuge tubes and centrifuged (Thermo Fisher, Life Technologies Heraeus Megafuge 40, Rotor 75003607) at 1500 rpm for 5 minutes. Thereafter, the supernatant was discarded and the cell pellet resuspended in 15 mL of freezing media. After repeatedly pipetting the cell suspension to ensure even dispersion of cells, the cell suspension was aliquoted into 2 mL cryovials (Nest Biotech®, Whitehead Scientific SA). To prevent the formation of ice crystals which would disrupt their structural integrity, cells were frozen down slowly at a controlled rate of 1 °C/ minute. This was achieved by placing the cryovials in an insulation box which was constructed from a polystyrene box lined with cotton wool. This insulation box was placed in a -77 °C freezer for 72 hours. Thereafter, the cells were transferred to non-insulated boxes and stored in liquid nitrogen at -196 °C.

2.2 Determining viability of cells: Trypan Blue dead cell exclusion assay

Prior to plating of the cells for each experiment, viable cells were counted using trypan blue dye (Sigma-Aldrich/Merck, SA) in an exclusion assay. This assay is based on the principle that viable cells possess intact cell membranes, which prevents trypan blue dye from entering the

cells. Dead cells have a compromised cell membrane and allow entry of the dye into the cells, staining it blue (Strober, 2015).

Method

Following trypsinization of the cells, the cell suspension was placed in a 15 mL centrifuge tube and pipetted gently to ensure even distribution of the cells. Twenty five microliters each of the cell suspension and trypan blue dye (0.2% w/v) (Sigma-Aldrich/Merck, SA) was added to a microcentrifuge tube. Ten microliters of this mixture was placed under a thick glass coverslip on either side of a Neubauer hemocytometer. Cells were viewed and counted using a Nikon Optiphot light microscope at 100X magnification.at 100× magnification. The number of cells per millilitre was determined using the following equation:

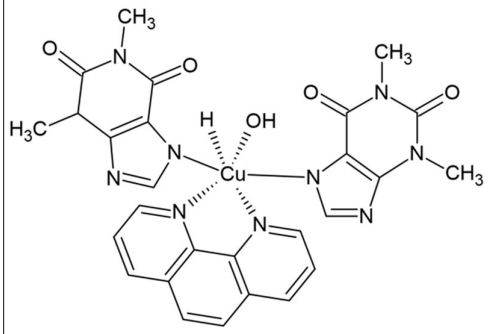
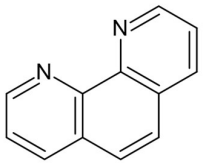
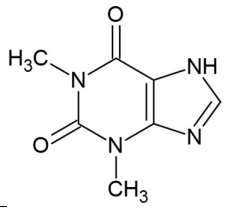
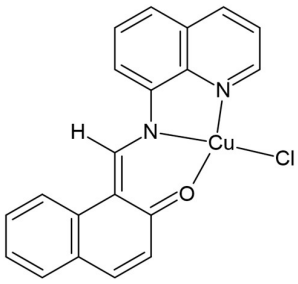
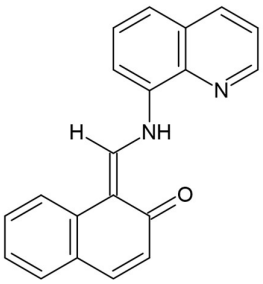
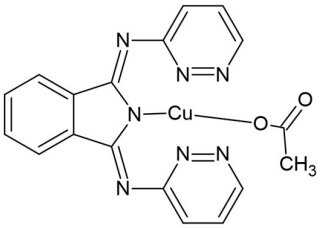
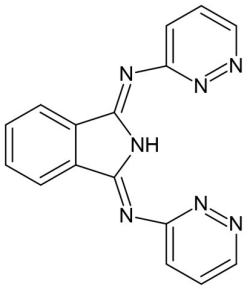
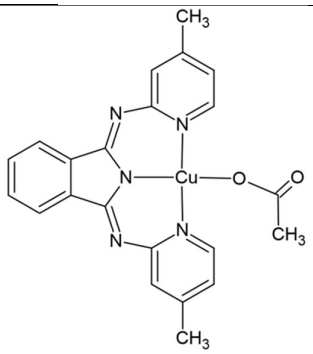
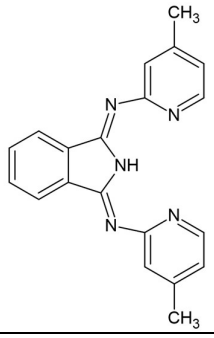
$$\frac{(Number\ of\ cells\ counted)(dilution\ factor)}{(Number\ of\ large\ squares\ counted)} \times 10^4$$

Using the cell count of the suspension, cells were seeded accordingly to attain the required number of cells/well for each experiment.

2.3 Test compounds

The compounds used in this study were synthesized by the University of the Witwatersrand, School of Chemistry as well as Department of Chemistry at the Nelson Mandela University. All compounds were assessed for purity and their structures verified via elemental analysis and X-ray crystallography. Their structures are shown in Table 2.1. All ligands and copper complexes used in this study were solubilized in 100 % cell culture-grade DMSO. The positive control, doxorubicin, was dissolved in 70 % cell-culture grade ethanol (BioUltra, Sigma-Aldrich/Merck, SA). Stock solutions of the compounds were prepared at concentrations of between 10-20 mM.

Table 2.1 Molecular structures of copper complexes and their ligands.

Compound Name	Copper complex	Copper-free ligand
AD3 Copper-phenanthroline-theophylline complex. Mw: 668.5 g/mol		Phenanthroline  Theophylline 
OM Copper 8-aminoquinolone naphthyl complex Mw: 396.33 g/mol		
L1Cu Aromatic copper isoindoline complex Mw: 422.88 g/mol		
L6Cu Aromatic copper isoindoline complex Mw: 448.96 g/mol		

2.4 MTT cell viability assay

The MTT (3-(4,5-dimethylthiazol-2-yl)-2,5-diphenyltetrazolium bromide) tetrazolium reduction assay is a quantitative colorimetric assay that measures cell viability and was used to determine the cytotoxic activity of the copper complexes and doxorubicin. In viable cells with active mitochondria, the mitochondrial enzyme, succinate dehydrogenase, cleaves the MTT dye and forms insoluble purple crystals (Mossman, 1983). The crystals are dissolved in an organic solvent (DMSO) and their absorbances measured to obtain percentage cell viability. MTT solution was prepared by adding 250 mg MTT powder into 50 mL PBS (5 mg/mL) which was sterile filtered and stored in the dark at 4 °C before use.

Method:

Cells were seeded in 96-well plates (Nest Biotech®, Whitehead Scientific SA) at a density of 12 000 cells/well for AsPC-1 cells and 8 000 cells/well for MIA PaCa-2 cells. Plates were incubated overnight at 37 °C in a 5 % CO_2, humidified incubator to allow the cells to adhere. Cells were treated with copper complexes and doxorubicin (in quadruplicate) at various concentration ranges (each data point in quadruplicate) and incubated for 48 hours. Four hours before the exposure time expired, 40 μL of MTT solution was added to each well and incubated for a further 4 hours. Thereafter, the plates were centrifuged at 503 $\times g$ for five minutes to ensure the crystals settled at the bottom of the wells. Media was aspirated and 200 μL of DMSO was added to each well to dissolve the crystals. The plates were shaken on an orbital plate shaker (Thermoshaker MRC) for 5 minutes at 1200 rpm to ensure the formazan crystals were dissolved. The abosrbance of each well was measured at a test and reference wavelength of 540 nm and 690 nm respectively using a Lab Systems Multiskan iEMS plate reader. The % cell viability was calculated using the following equation:

$$\frac{(absorbance\ of\ test\ compound) - (average\ absorbance\ of\ media\ only)}{(average\ absorbance\ of\ untreated\ control) - (average\ absorbance\ of\ media\ only)} \times 100$$

Three classes of copper complexes and their ligands were screened for their cytotoxic potential at concentrations of 50- and 5 μM, for 48 hours. The active compounds were tested at a range of concentrations between 0.05-20 μM while doxorubicin was tested at concentrations ranging between 0.05-300 μM (from 0 % growth inhibition to 100 % growth inhibition) to obtain the IC_{50} value for the compound. The IC_{50} value of a drug refers to the concentration of drug that causes 50% growth inhibition of the cells. The IC_{50} values of the copper complexes were

compared to the positive control doxorubicin, and to each other, to determine the statistical significance of their differences. A negative control of media only and an untreated control of cells only was included in all experiments. A vehicle control experiment testing the cytotoxicity of DMSO and ethanol was included to determine whether the solvents had cytotoxic activity on their own. The evaporation rate of the 70 % ethanol solvent in which doxorubicin was dissolved is minimal when stored correctly. Doxorubicin was used as a positive control. Ordinary one-way ANOVA followed by Dunnett's post hoc multiple comparisons test was used to evaluate the statistical significance of the differences in IC_{50} values. Significance criterion was set at $p < 0.05$ with a 95 % confidence interval. Statistical evaluations were performed, and sigmoidal dose response curves and IC_{50} values of the compounds were obtained using GraphPad Prism version 9.

Combination experiments using MTTs with a HMOX1-inhibitor, OB24 hydrochloride (OB24 HCl), were conducted to determine the effect of HMOX1 inhibition on the activity of the compounds and whether or not HMOX1 inhibition would render the cells more susceptible to the cytotoxic effects of the compounds. OB24 HCl was used at a constant concentration of 20 μM and added to each well containing the range of test compound concentrations. An equal volume of 50 μL each of OB24 HCl and the test compounds were added to each well, simultaneously.

Student's t test was used to evaluate the statistical significance of the differences in IC_{50} values obtained from treatment with copper complexes alone compared to IC_{50} values obtained from treatment with copper complexes and OB24 hydrochloride. Significance criterion was set at $p < 0.05$ with a 95 % confidence interval.

In subsequent experiments throughout this study, the copper complexes were evaluated at concentrations equivalent to their IC_{80} values. AsPC-1 cells were treated with AD3 at 6 μM, OM at 4 μM, and L1Cu and L6Cu at 2 μM. MIA PaCa-2 cells were treated with AD3 at 6 μM, OM at 5 μM, and L1Cu and L6Cu at 2 μM. Doxorubicin was used at a constant concentration of 5 μM.

2.5 Cell morphology

The effect of the copper complexes on the cell morphology of the cells was assessed utilizing the triple dye indicators, consisting of Hoechst 33342 (HO) (5 μg/mL) (Sigma-Aldrich/Merck, SA), propidium iodide (PI) (10 μg/mL) (Sigma-Aldrich/Merck, SA) and acridine orange (AO) (10 μg/mL) (Thermo Fisher, Life Technologies, SA) in PBS.

HO is a membrane permeant dye that stains the DNA of live and fixed cells by binding to the adenine-thymine regions of the minor groove of DNA (Chazotte, 2011). Healthy nuclei emit a uniform blue fluorescence while apoptotic nuclei emit a bright blue uneven fluorescence in which DNA appears condensed or fragmented. AO is a cell permeant dye that readily enters living cells (Bank, 1988). When bound to double stranded DNA, AO fluoresces bright green. When bound to single stranded DNA and RNA, AO fluoresces red. AO staining also allows for the visualization of lysosomes through the accumulation of this weakly basic dye inside the acidic granules, which fluoresce bright red (Darzynkiewicz *et al*., 1992). PI is unable to penetrate cells with intact membranse and is used to distinguish between viable and necrotic cells. Necrotic cells have a compromised cell membrane which allows for the entry of propidium iodide, staining the nucleus a birght red-orange (Dengler *et al*., 1995).

Method

Glass coverslips were soaked in 100 % analytical grade ethanol (Sigma-Aldrich/Merck, SA) for ten minutes and heat sterilized by removing each coverslip from the ethanol and flaming it. Sterile coverslips were gently placed into each well of a six-well plate (Sigma-Aldrich/Merck, SA). AsPC-1 and MIA PaCa-2 cells were seeded at a density of 200 000 cells/well and 50 000 cells/well respectively on glass coverslips in six-well plates and allowed to attach overnight. Cells were treated with copper complexes and doxorubicin for 24 hours. Following incubation, the copper complexes and doxorubicin were aspirated from each well and cells were washed with 2 mL PBS. One millitre of the vital dye stain solution was added to each well and incubated for 20 minutes in the dark, at room temperature. After the 20 minutes expired, the dye was removed and cells were washed with 2 mL PBS. Coverslips were mounted onto microscope slides (Lasec, SA) using Fluoromount Mounting Medium (Sigma-Aldrich/Merck, SA) and viewed using an Olympus BX41 epifluorescence microscope. AO was viewed using U-MNIB3 filter cube (Excitation: 480/20, Emission: 510/50); PI with U-MWIG2 (Excitation: 535/30, Emission: 580 long pass) and HO with U-MWU2 (Excitation: 365/10, Emission 420

long pass). Images were captured with an Olympus DP72 camera and analyzed with the Olympus CellSens Software package (Olympus, Tokyo, Japan). Experiments were repeated at least three times.

2.6 Measurement of reactive oxygen species

The Invitrogen™ CellRox® Deep Red Reagent (Thermo Fisher, Life Technologies, SA) was used to measure ROS activity. The assay is based on the utilization of the cell permeant dye which lacks fluorescence in its reduced state. Upon oxidation by ROS, the dye exhibits a bright red fluorescence with an absorption/emission maxima of approximately 644/655 nm.

Method

Cells were seeded on glass coverslips in a 6-well plate in 2 mL media per well and allowed to attach overnight at 37°C in a 5% CO_2, humidified incubator. Media was aspirated from the wells and washed with 2 mL PBS. The cells were incubated simultaneously with the copper complexes and doxorubicin in addition to the Deep Red reagent for 4, 6 and 18 hours at 37 °C. The CellRox® Deep Red reagent was used at a concentration of 2 μL/mL. A doxorubicin-only control that lacked Deep Red reagent was included to mitigate the effects of doxorubicin's innate fluorescence. Following the removal of the copper complexes and doxorubicin and Deep Red reagent, the cells were washed one time with PBS. The coverslips were mounted onto microscope slides. Slides were viewed with an Olympus BX41 epifluorescence microscope using the U- MWIG2 (Excitation: 535/30, Emission: 580 long pass). Images were captured with an Olympus DP72 camera and analyzed with the Olympus CellSens Software package. Experiments were repeated at least three times. Fluorescent intensities of individual images were measured using CellProfiler™ Image analysis software. Ordinary one-way ANOVA followed by Dunnett's post hoc multiple comparisons test was used to evaluate the statistical significance of the differences in ROS fluorescent intensities of treated cells compared to untreated cells. Significance criterion was set at $p < 0.05$ with a 95 % confidence interval.

2.7 Evaluation of apoptosis

Once necrosis was excluded as the cause of cell death, the compounds were evaluated for their ability to induce apoptosis via the annexin-V assay, JC-1 assay, caspase-3/7 and -9 assays. The data from the caspase-3/7 and caspase-9 assays determined whether the compounds induced apoptosis and whether it was via the intrinsic or extrinsic pathway. Caspase-3 is the executioner

caspase and is activated in both the intrinsic and extrinsic pathways. The presence of active caspase-9 in the cells indicates the activation of the intrinsic mitochondrial apoptotic pathway. The health of the mitochondria was assessed using the JC-1 assay, whereby depolarized mitochondria were visible as diffuse, smooth, green fluorescence. Mitochondrial depolarization was indicative of the activation of the intrinsic apoptotic pathway.

2.7.1 Annexin-V

The Annexin-V assay works on the principle that during early apoptosis, changes to the cell membrane occur, specifically, the translocation of phosphatidylserine from the inner surface of the cell membrane to the outer surface (Vermes *et al*., 1995). Annexin-V has a high affinity for phosphatidylserine. Binding of fluorescent-tagged annexin-V to phosphatidylserine can be used to detect phosphatidylserine exposure on the cell surface seen by the emission of green fluorescence on the cell membrane.

Method

The AlexaFluor® 488/Annexin-V Dead Cell Apoptosis kit (Thermo Fisher, Life Technologies, SA) was used to detect the presence of phosphatidylserine on the cell surface. The kit contained annexin-V conjugated to the green fluorescent dye AlexaFluor® 488; wash buffer; as well as PI dye. Cells were seeded on coverslips in six-well plates as described previously in 2 mL complete media (per well) and allowed to attach overnight. Cells were then treated with copper complexes and doxorubicin and incubated for 24 hours at 37 °C in a 5 % CO_2, humidified incubator. Subsequently, test compounds from each well were aspirated and cells washed with 2 mL PBS. The annexin-V detection reagent was prepared by adding Alexa Fluor® 488/annexin-V (5% v/v) and PI (2% v/v) to a solution containing one part buffer and four parts double distilled water (ddH_2O). Coverslips were mounted face down directly onto 30 µL of the reagent mixture on microscope slides. The slides were incubated in the dark at room temperature for 20 minutes and viewed using an Olympus BX41 epifluorescence microscope. The filter cube U-MNIB3 (Excitation: 480/20, Emission: 510/50) was used to view AlexaFluor® 488/Annexin-V while filter cube U-MWIG2 (Excitation: 535/30, Emission: 580 long pass) was used to view PI. Images were captured with an Olympus DP72 camera and analyzed with the Olympus CellSens Software package. Experiments were repeated at least three times and data was collated into a bar graph using GraphPad Prism version 9. ANOVA followed by Dunnett's post hoc multiple comparisons test was used to evaluate the significance

of the induction in annexin-V binding and PI staining between treated cells and the untreated control. Significance criterion was set at $p < 0.05$ with a 95 % confidence interval.

2.7.2 JC-1 assay

During apoptosis, an early occurrence is the disruption of active mitochondria. This includes the dissipation of the mitochondrial membrane potential (MMP) (Galluzzi *et al*., 2012) caused by the opening of the mitochondrial permeability transition pore (MPTP), which allows for ions and small molecules to pass through. The balance of ions and hence, the charge, on either side of the mitochondrial membrane disrupts the electron gradient across the membrane resulting in the decoupling of the respiratory chain and the release of cytochrome c into the cytosol which, in turn, triggers the release of caspases (Kroemer *et al*., 2007).

1,1',3,3'-Tetraethyl-5,5',6,6'-tetrachloroimidacarbocyanine iodide (JC-1) dye is a membrane permeant, cationic carbocyanine dye. At higher MMPs (healthy cells), JC-1 dye accumulates in the mitochondria as red fluorescent 'J-aggregates'. At lower MMPs (cells with disrupted mitochondrial activity) the dye exists in its monomer form and is visible as green fluorescence in the mitochondria (Reers *et al*., 1991). A decrease in the red/green fluorescence intensity ratio is indicative of mitochondrial depolarization.

Method

Cells were seeded on glass coverslips in six-well plates and allowed to attach overnight at 37 °C in a 5 % CO_2, humidified incubator. Cells were treated with copper complexes and doxorubicin for 18 hours and incubated at 37 °C. The treatment period of 18 hours was selected to evaluate the effect on MMP before the cells died. To prepare the reagent, 5 µL of JC-1 dye (Mitochondrial Membrane Potential Probe) (Thermo Fisher, Life Technologies, SA) was added to 5 mL warmed media. The mixture was gently pipetted to ensure even dissolution of the JC-1 dye and to disperse any crystals formed by the dye. The reagent mixture was centrifuged in a 15 mL tube at 1500 rpm for 5 minutes. Thereafter, the reagent mixture was passed through a 0.22 µm filter, to ensure the complete removal of JC-1 crystals.

The media from each well of the six-well plate was aspirated, and washed with 2 mL PBS. Five hundred microliters of the JC-1 reagent mixture was added to each well and incubated for 30 minutes at 37°C in the dark. After the incubation period, 500 µL PBS was dropped into each well to wash the dye off the coverslips. The coverslips were mounted onto microscope slides

and viewed using an Olympus BX41 epifluorescence microscope. The filter cubes used were U-MNIB3 (Excitation: 480/20, Emission: 510/50) and U-MWIG2 (Excitation: 535/30, Emission: 580 long pass). Images were captured with an Olympus DP72 camera and analyzed with the Olympus CellSens Software package. Experiments were repeated at least three times and data was collated into a bar graph using GraphPad Prism version 9. ANOVA followed by Dunnett's post hoc multiple comparisons test was used to evaluate the significance of the differences in JC-1 monomers and 'J-aggregate' formation between treated cells and the untreated control. Significance criterion was set at $p < 0.05$ with a 95 % confidence interval.

2.7.3 Caspase-9

An assay used to detect activated caspase-9 specifically was used. d. The assay comprises of the caspase-9 inhibitor, LEHD-FMK, conjugated to the fluorescent marker, fluorescein-5-isothiocyanate (FITC). FITC-LEHD-FMK is membrane permeable and irreversibly binds to activated caspase-9 in apoptotic cells.

Method

Cells were seeded on glass coverslips in six-well plates and allowed to attach overnight at 37°C in a 5% CO_2, humidified incubator. Cells were treated with the copper complexes and doxorubicin and incubated for 24-48 hours at 37 °C. Following aspiration of the test compounds, cells were washed once with 2 mL PBS. To prepare the reagent, three microliters of FITC-LEHD-FMK was added to 900 µL of wash buffer. One hundred and fifty microliters of the reagent was added to each coverslip and incubated for 60 minutes at 37°C. Thereafter, cells were washed with PBS and coverslips were mounted onto microscope slides. Slides were viewed using an Olympus BX41 epifluorescence microscope using the U-MNIB3 (Excitation: 480/20, Emission: 510/50) filter cube. Images were captured with an Olympus DP72 camera and analyzed with the Olympus CellSens Software package. Experiments were repeated at least three times and data was collated into a bar graph using GraphPad Prism version 9. ANOVA followed by Dunnett's post hoc multiple comparisons test was used to evaluate the significance of caspase-9 activation between treated cells and the untreated control. Significance criterion was set at $p < 0.05$ with a 95 % confidence interval.

2.7.4 Caspase-3/7

CellEvent™ Caspase-3/7 Green Detection Reagent (Thermo Fisher, Life Technologies) is a substrate for activated caspase -3 and -7. The reagent is comprised of a four amino acid peptide (DEVD) conjugated to a DNA-binding dye. In healthy cells, the substrate is non-fluorescent because the DEVD peptide prevents binding of the dye to DNA. In apoptotic cells that have active caspase -3 and -7, the DEVD peptide is cleaved allowing for the dye to bind to DNA, emitting a bright green fluorescence.

Method

Cells were seeded on glass coverslips in 6 well plates and allowed to attach overnight at 37°C in a 5% CO_2, humidified incubator. Cells were treated with the copper complexes and doxorubicin and incubated for 48 hours at 37°C. To prepare the reagent, a 5 μM solution of CellEvent™ Caspase-3/7 Green Detection Reagent was prepared in complete media. Following incubation, the test compounds were aspirated from the wells and washed with 2 mL PBS. One hundred microliters of the reagent was added to each coverslip and incubated for 45 minutes at 37°C in the dark. Coverslips were then mounted onto microscope slides and viewed with an Olympus BX41 epifluorescence microscope using the U-MNIB3 (Excitation: 480/20, Emission: 510/50) filter cube. Images were captured with an Olympus DP72 camera and analyzed with the Olympus CellSens Software package. Experiments were repeated at least three times and data was collated into a bar graph using GraphPad Prism version 9. ANOVA followed by Dunnett's post hoc multiple comparisons test was used to evaluate the significance of caspase-3/7 activation between treated cells and the untreated control. Significance criterion was set at $p < 0.05$ with a 95 % confidence interval.

2.8 Immunofluorescence

Immunofluorescence is an immunoassay that allows for the visualization of a target protein of a cell by fluorescence microscopy (Im *et al*., 2019). The primary antibody binds to the target antigen while the secondary antibody (a fluorophore) binds to the primary antibody, tagging it with a fluorescent probe. The protein of interest in this study was HMOX1.

Method:

Treatment and fixing of cells

Cells were seeded on coverslips in a six-well plate and allowed to attach overnight at 37°C in a 5 % CO_2, humidified incubator. Cells were treated with the copper complexes and doxorubicin and incubated for 18 hours. The treatment period of 18 hours was to evaluate HMOX1 expression before the cells had died. Following treatment, test compounds were aspirated and cells washed twice with 2 mL PBS and floating cells were harvested by centrifugation at 503 × *g*. Cells were fixed by adding 1.5 mL of a 3.7% formaldehyde solution to each well and incubated for 20 minutes at room temperature.

Blocking and permeabilization

Following fixing, the formaldehyde solution was aspirated and cells were washed twice with 2 mL PBS. Thereafter, a blocking and permeabilizing solution was prepared by combining 100 µL of 25% Triton X 100; 1 ml of 3 % human serum albumin; and PBS to a final volume of 10 mL. Triton X 100 is a nonionic surfactant and is used to permeabilize the cell membranes. Human serum albumin is a blocking agent which binds to and blocks non-specific binding sites, ensuring that antibodies bind solely to the target antigens. One and a half millilitres of the blocking/permeabilizing solution was added to each well and incubated for 10 minutes at room temperature. After removal of the permeabilization reagent from the wells, cells were washed twice with 2 mL PBS. One and a half millilitres of a blocking-only solution consisting of 0.3 % human serum albumin was added to each well and incubated for a further 45-60 minutes, after which the solution was aspirated and he coverslips washed three times with 2 mL PBS added to each well.

Preparing the primary antibody

The primary antibody of interest, anti-HMOX1 (Rabbit, polyclonal antibody) (PA5-27338; Thermo Fisher, Life Technologies, SA) was prepared in 0.5% HSA in a 1:200 dilution. Moistened filter paper was placed in the lid of a six-well plate, with squares of cut-out parafilm aligned onto the filter paper. Fifty microliters of the primary antibody was placed onto each parafilm. Each coverslip was lifted from the well (excess PBS dried off) and placed face down gently onto the drop of primary antibody. The lid was carefully placed into the container with wet tissue paper and incubated overnight at 4 °C.

Preparing the secondary antibody

An AlexaFluor 488 ® goat anti-Rabbit antibody (A32731; Thermo Fisher, Life Technologies, SA) was used as the secondary antibody which bound to anti-HMOX1 primary antibody and tagged it with a green fluorescence. The secondary antibody was diluted in a 1:800 ratio in 0.5% HSA. Following overnight incubation with the primary antibody, the coverslips were lifted gently off the parafilm and placed face-up into their respective wells which contained 2 mL PBS. The coverslips were lifted from the wells and placed face-up onto clean parafilm. Thereafter, 150 µL of secondary antibody was placed onto the cells, creating a cohesive bubble of reagent. The cells were incubated in this position in the dark at room temperature for 60 minutes. Coverslips were then lifted back up, allowing the secondary antibody to drip off the coverslip, and placed into their wells, cells-side up. Cells were washed once with 2 mL PBS. After aspirating the PBS, 1.5 mL HO (5 µg/ml) (Sigma-Aldrich/Merck, SA) stain was added to each well and incubated in the dark at room temperature for 20 minutes. Following the removal of HO, cells were washed with 2 mL PBS. Thereafter, coverslips were mounted onto microscope slides using Fluoromount™ (Sigma-Aldrich/Merck, SA) mounting media. Using clear nail polish, the sides of the coverslips were sealed to prevent drying out of the cells. The slides were then wrapped in foil to prevent photodegradation of the fluorescent signal and stored at 4°C. Slides were viewed with an Olympus BX41 epifluorescence microscope. The following filter cubes were used: U-MWU2 (Excitation: 365/10, Emission: 420 long pass) for Hoechst 33342; U-MNIB3 (Excitation: 480/20, Emission: 510/50) for AlexaFluor 488 ® /anti-HMOX1. Images were captured using an Olympus DP72 camera and analyzed with the Olympus CellSens Software package. Experiments were repeated at least three times. Fluorescent intensities of HMOX1 images were measured using CellProfiler™ Image analysis software. Ordinary one-way ANOVA followed by Dunnett's post hoc multiple comparisons test was used to evaluate the statistical significance of the differences in HMOX1 fluorescent intensities of treated cells compared to untreated cells. Significance criterion was set at $p < 0.05$ with a 95 % confidence interval. Colocalization analysis was performed using CellProfiler™ Image analysis software to determine the correlation (Pearson's correlation coefficient) between the HO signal and the HMOX1 signal. This analysis provided information on the subcellular location of HMOX1 within the cell. GraphPad Prism version 9 was used to perform statistical analysis.

2.9 Western blot

Western blot is used to identify and quantify proteins in a sample (Mahmood and Yang, 2012). The first stage is gel electrophoresis whereby the proteins in a sample are separated according to molecular weight. Thereafter, the separated proteins are transferred from the gel onto a polyvinylidene difluoride (PVDF) membrane. The membrane's non-specific binding sites are blocked and the membrane is probed with antibodies specific to the protein of interest. The bands are then visualized and quantified in relation to other samples.

Casting the SDS-PAGE gels

To cast the gels, the Bio-Rad Mini-PROTEAN® Short Plates (#1653308) and Mini-PROTEAN® Spacer Plates with 1.0 mm Integrated Spacers (#1653311) (Bio-Rad, SA) were used. The two glass plates were aligned, with the shorter plate in front, and placed into the casting frame. The casting frame was inserted into the casting apparatus and the clip was secured. Following the preparation of the resolving gel (APS and TEMED were added immediately prior to use) (Table 2.2), the gel mix was pipetted in between the glass plates to a volume that allowed for a gap of approximately 1 cm at the top of the resolving gel for the stacking gel. At the surface of the resolving gel, 100 % ethanol was pipetted in order to flatten out the surface of the gel, to prevent drying out of the gel and to remove bubbles formed at the meniscus of the unpolymerized gel. After the resolving gel polymerized (approximately an hour after casting), the ethanol was poured off. The stacking gel mixture was prepared (APS and TEMED was added immediately prior to use) (Table 2.2) and pipetted on top of the polymerized resolving gel. The combs were placed into the unpolymerized stacking gel layer. The sides of the comb were sealed with agarose. The stacking gel was allowed to polymerize for 2 hours. Thereafter, the casting frame was removed from the casting apparatus and stored in a container with tank buffer at 4 ℃ until use.

Table 2.2 SDS-PAGE gel. Table showing the constituents of the SDS-PAGE gel.

Resolving gel	**Stacking gel**
2.72 mL ddH2O	3.05 mL ddH2O
3.2 mL 30% acrylamide/bis	665 μL 30% acrylamide/bis
2 mL resolving gel buffer (1.5 M Tris-HCl, pH 8.8)	1.25 mL stacking gel buffer (0.5 M Tris-HCl, pH 6.8)
80 μL 10% sodium dodecyl-sulfate (SDS)	50 μL 10% SDS
50 μL 10% ammonium persulfate (APS)	25 μL 10% APS
5 μL Tetramethylethylenediamine (TEMED)	2.5 μL TEMED

Cell lysate preparation

Each sample lysate was prepared from cells grown in 75 cm^2 cell culture flasks. A total of six cell culture flasks were seeded (one for each of the following: untreated control, AD3, OM, L1Cu, L6Cu and doxorubicin). Once 80 % confluency was reached, each flask was trypsinized and the cell suspension transferred to a 50 mL centrifuge tube. A cell count was performed on the cell suspension. Subsequently, an equal number of cells was reseeded into each flask at a density of 8 000 000 cells per 75 cm^2 flask. The cells were allowed to attach overnight. Thereafter each flask was treated with the test compound at their respective IC_{80} values for 18 hours. An untreated flask and a doxorubicin control flask was included. Following the treatment period, cell culture flasks were placed on ice and a cell scraper was used to gently facilitate the detachment of the cells from the surface of the flask. The suspended cells were transferred to a 50 mL tube and centrifuged at 503 $\times g$ for 5 minutes. The supernatant was discarded and the cell pellet was resuspended in 1 mL RIPA lysis buffer (Table 2.3). One Roche protease inhibitor cocktail mini-tablet was added per 20 mL of buffer immediately prior to use. After ensuring complete dispersion of the cell pellet in the lysis buffer, the sample was passed through a 25-gauge needle to shear the DNA. Thereafter, the sample was transferred to a 2 mL microcentrifuge tube. The samples were incubated in the lysis buffer for one hour on a rocking platform at 4 ℃ to ensure complete breakdown of the various cell membranes (nuclear and external membrane) and release of its proteins. Subsequently, the microcentrifuge tubes were centrifuged at 14000 $\times g$ for 12 minutes in a Sorvall™ LYNX 4000 superseed centrifuge (Thermo Fisher, Life Technologies, SA). The protein lysate supernatant was transferred to fresh, labelled microcentrifuge tubes in 300 µL aliquots and stored at -70 ℃ until use. The Bradford assay was used to quantify the amount of protein present in each sample.

Table 2.3 Buffer recipes. Table showing the constituents of the buffers used in the Western blot assay

RIPA/lysis buffer	25 mM Tris base (pH 7.6) 150 mM NaCl 1% Triton X 100 1% sodium deoxycholate Roche protease inhibitor cocktail mini-tablet (1 per 20 mL)
5X Laemmli sample buffer	15 mL glycerol 1.5 g SDS 13.5 mL stacking gel buffer 1.15 g dithiothreitol (DTT)

	15 mg bromophenol blue
Tank buffer	30 g Tris 144 g glycine 10 g SDS
Transfer buffer	48 mM Tris 39 mM glycine 20% methanol
1X Tris-buffered-saline-Tween (TBST)	20 mM Tris 150 mM NaCl 0.1% Tween 20

Bradford assay

The Bio-Rad Protein Assay Kit II (Bio-Rad, SA) was used to perform the Bradford assay. When bound to proteins, the Bradford reagent (acidified Coomassie® Brilliant Blue G-250) undergoes a colour change, with the absorbance maximum changing from 470 nm to 595 nm (Kruger, 1994). A standard curve is generated from a series of dilutions of protein standards of known concentrations. Standardized bovine serum albumin (1 mg/mL) (Sigma-Aldrich/Merck, SA) was used as the protein standard. The quantity of protein in each sample was interpolated from the standard curve (Appendix A).

Samples were diluted in ddH_2O in a 1 in 10 dilution. In a 96-well plate, 5 µL of each 1 in 10 sample was added to each well in triplicate. Additionally, 5 µL of each concentration of bovine serum albumin standards (in-reaction concentrations of 0-1000 µg/mL) were added to each well in triplicate. Thereafter, 195 µL of Bradford reagent (diluted in a ratio of 1 part reagent: 4 parts ddH_2O) was added to each well. The absorbances were measured after 5 minutes at 595 nm using the Lab Systems Multiskan iEMS plate reader. The standard curve was generated using GraphPad Prism version 9. Protein concentrations of the samples were interpolated from the standard curve.

Gel electrophoresis

Following the quantification of the protein in each cell lysate, each sample was prepared in a 1:4 dilution of 5X Laemmli buffer (Table 2.3) to cell lysate. To prepare a concentration of 20 µg of protein in each sample, cell lysates were diluted in stacking gel buffer (Table 2.1). Samples were prepared in microcentrifuge tubes and kept on ice at all times. Samples were heated for 4 minutes in a water bath at 95 ℃ and immediately transferred to ice. Samples were

then centrifuged at 1400 rpm for 1 minute and placed back on ice. The Bio-Rad Mini-PROTEAN® Tetra vertical electrophoresis cell (Bio-Rad, SA) was used to run gel electrophoresis and separate the proteins in each sample according to size. The pre-cast gels were placed into the tank and tank buffer (Table 2.3) was poured into the inner chamber of the tank. An equal amount of sample (20 μL) was loaded into each well of the gel. Additionally, Precision Plus Protein™ WesternC™ molecular weight markers (Bio-Rad, SA) were loaded in the well of the first lane. Thereafter, tank buffer was poured into the outer chamber up to the required level and the apparatus was connected to the power supply. A voltage of 200 V was applied to the gel for approximately one hour until the bromophenol blue reached the end of the gel and the proteins were separated.

Blotting/membrane transfer

Following gel electrophoresis, the separated proteins in the gel were transferred onto a PVDF membrane using the wet transfer method. The Bio-Rad Mini Trans-Blot® Cell (Bio-Rad, SA) was used to transfer the proteins. A "transfer sandwich" was constructed consisting of a pre-soaked foam pad, pre-soaked filter paper, the gel, PVDF membrane, pre-soaked filter paper and foam pad. The foam pads and filter paper were soaked in transfer buffer (Table 2.3) prior to use. The "sandwich" was placed in the gel holder cassette and subsequently assembled into the tank in the correct orientation, ensuring that current flowed in a gel-towards-membrane direction. Cold transfer buffer was filled to the required level and the apparatus was connected to the power supply. A voltage of 100 V was applied to the cell for 1 hour.

Blocking the membrane

Following the transfer of the proteins from the gel onto the PVDF membrane, the membrane was carefully removed from the "transfer sandwich" using forceps. Non-specific binding sites on the membrane were blocked by the incubation of the membrane in 10 mL Invitrogen™ Membrane Blocking Solution (Thermo Fisher, Life Technologies, SA) for one hour at room temperature.

Antibody staining of the membrane

The primary anti-HMOX1 antibody (rabbit, polyclonal antibody) (PA5-27338; Thermo Fisher, Life Technologies, SA, Johannesburg, SA) was prepared in a 1 in 2000 dilution in Invitrogen™ Membrane Blocking Solution (Thermo Fisher, Life Technologies, SA). Beta-actin was used as

a loading control to confirm that equal amount of protein was added to each lane. Actin Antibody (H-300): sc-10731 (Santa Cruz Biotechnology, Inc) was added to the primary antibody solution at a concentration of 1 in 1000. Following blocking, the membrane was washed once in 1X TBST (Table 2.3) and incubated in 10 mL of primary antibody solution overnight on a rocking platform at 4 ℃. The following morning, the primary antibody solution was aspirated and the membrane washed 3 times while on a rocking platform for 10 minutes each in 20 mL 1X TBST. Thereafter, the membrane was incubated in 10 ml secondary antibody solution for one hour on a rocking platform at room temperature. The secondary antibody, Pierce® Goat Anti-Rabbit IgG, (H + L), horseradish peroxidase (HRP) conjugated (#31460, Thermo Fisher, Life Technologies, SA), was prepared in Membrane Blocking Solution at a concentration of 1 in 10 000. In addition, StrepTactin-HRP (Bio-Rad, SA) was added to the solution at a concentration of 1 in 10 000 as a probe to detect the molecular weight markers.

Visualizing the protein bands

Detection of the protein bands was made possible through a chemiluminescent reaction. HRP, which was conjugated to the secondary antibody, catalyses the reaction to generate a chemiluminescent signal in the presence of a substrate. The substrate used was the Pierce™ ECL Western Blotting Substrate (Thermo Fisher, Life Technologies, SA). The substrate was prepared by combining equal volumes of reagent A and B (according to the manufacturer's instructions). The membrane was incubated in the substrate for 5 minutes. Thereafter, the membrane was enclosed between two layers of acetate film and viewed using the Bio-Rad ChemiDoc™ MP imaging system. The blot was analysed using Bio-Rad Image Lab software. Ordinary one-way ANOVA followed by Dunnett's post hoc multiple comparisons test was used to evaluate the statistical significance of the differences in HMOX1 pixel densities induced by the copper complexes and doxorubicin compared to the untreated cells. Significance criterion was set at $p < 0.05$ with a 95 % confidence interval. Experiments were repeated at least three times. Pixel densities of the bands were collated into a bar graph. Statistical analysis was performed and bar graphs constructed using GraphPad Prism version 9.

CHAPTER III: RESULTS

This study evaluated the cytotoxic activity of three classes of copper complexes, namely, a copper-phenanthroline-theophylline complex (AD); a copper-8-aminoquinolonenaphthyl complex (OM); and copper-isoindoline complexes (LCu); and the respective copper-free ligand of each complex against the AsPC-1 and MIA PaCa-2 cell lines. The OM and LCu compounds were synthesized by the School of Chemistry, University of the Witwatersrand, Johannesburg. The AD copper complex was synthesized and supplied by the Department of Chemistry, Nelson Mandela University, Gqeberha. The compounds were prepared at stock concentrations of between 10-20 mM in DMSO or ethanol and stored at room temperature. While it is not the norm for the complexes to be stored at room temperature, the copper complexes were susceptible to degradation after undergoing repeated freeze-thaw cycles when stored at 4 ºC and -20 ºC, when DMSO becomes solid.

3.1 The effect of the copper complexes and their ligands on the cell viability of AsPC-1 and MIA PaCa-2 cells

3.1.1 Identification of active copper complexes against AsPC-1 and MIA PaCa-2 cell lines

Two copper-isoindoline complexes (L1Cu and L6Cu) and their respective ligands (L1 and L6) were tested at concentrations of 50 µM and 5 µM using the MTT cell viability assay as described in Section 2.4. The results are shown in Figure 3.2. The compounds that had less than 1 % cell viability at 50 µM and less than 50 % cell viability at 5 µM were selected for further investigation. None of the copper-free ligands showed any meaningful activity and were not investigated further. Amongst the LCu copper complexes, L1Cu and L6Cu met the criteria for activity against both cell lines (Fig. 3.1).

The copper complexes AD3 and OM efficiently inhibited the growth of several other cancer cell lines with IC_{50} values in the low micromolar range and were therefore included in this study (Gordon *et al*., 2022; Rooplal, 2023). Initial evaluation of AD3 and OM confirmed their cytotoxic activity against both AsPC-1 and MIA PaCa-2 cell lines (Fig. 3.1). Phenanthroline and theophylline form part of the structure of AD3 and were poorly active against both cell lines (Fig. 3.2). Similarly, the copper-free ligand of OM was poorly active (Fig. 3.1). Vehicle control cell viability assays were performed to determine the effect of DMSO and ethanol on the viability of the cells (Fig. 3.2). The results confirmed the absence of cytotoxic effects of the solvents on their own (Fig. 3.2).

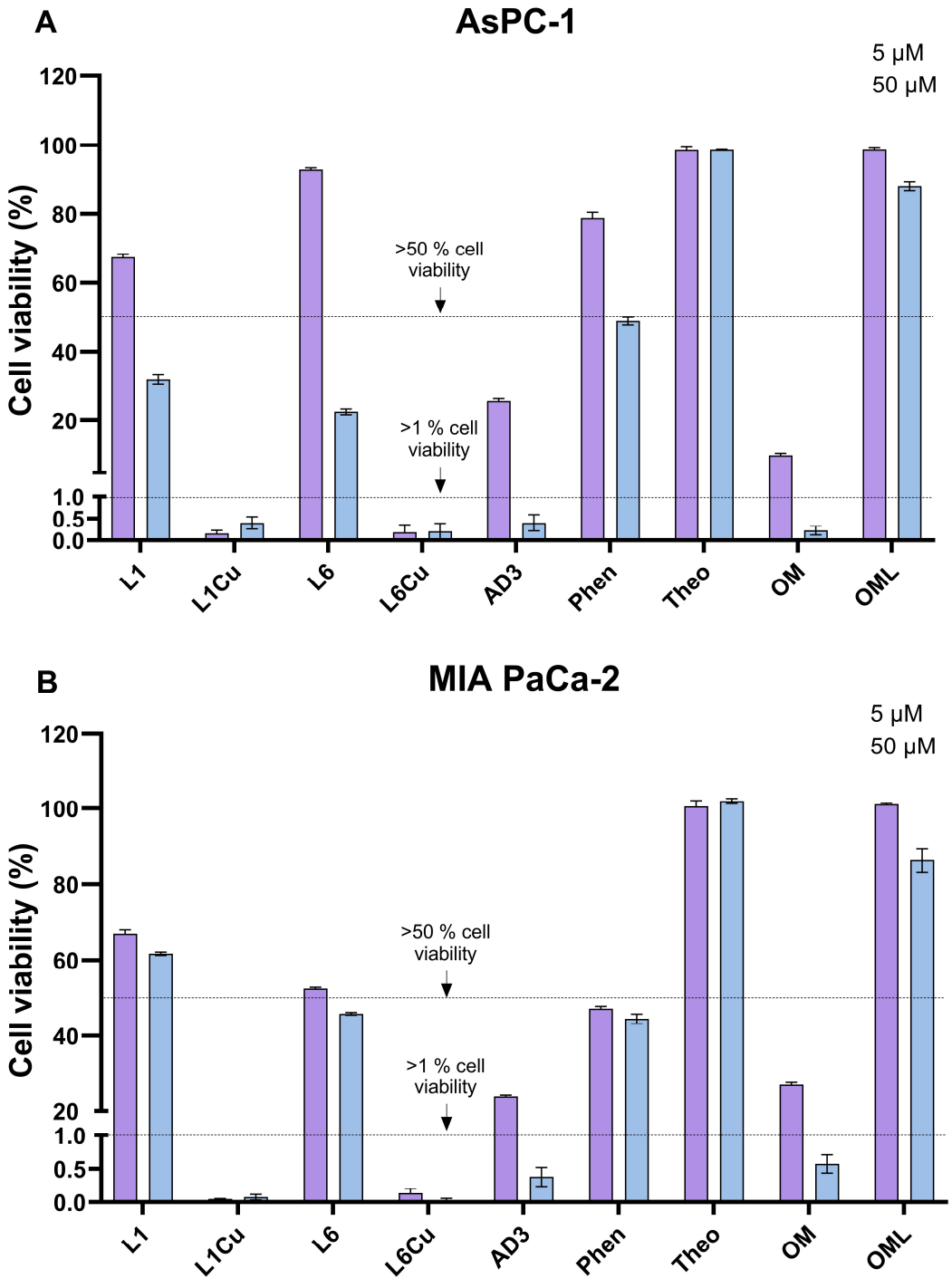


Figure 3.1 The effect of the copper complexes and their ligands on cell viability of AsPC-1 (A) and MIA PaCa-2 (B) cells. AsPC-1 and MIA PaCa-2 cells were treated with the copper complexes and their ligands at concentrations of 50 µM and 5 µM for 48 h and cell viability was measured with the MTT assay. Each bar represents the mean of at least four replicate values. Error bars represent the standard error of the mean (SEM). (Phen: phenanthroline; Theo: theophylline; OML: OM-ligand)

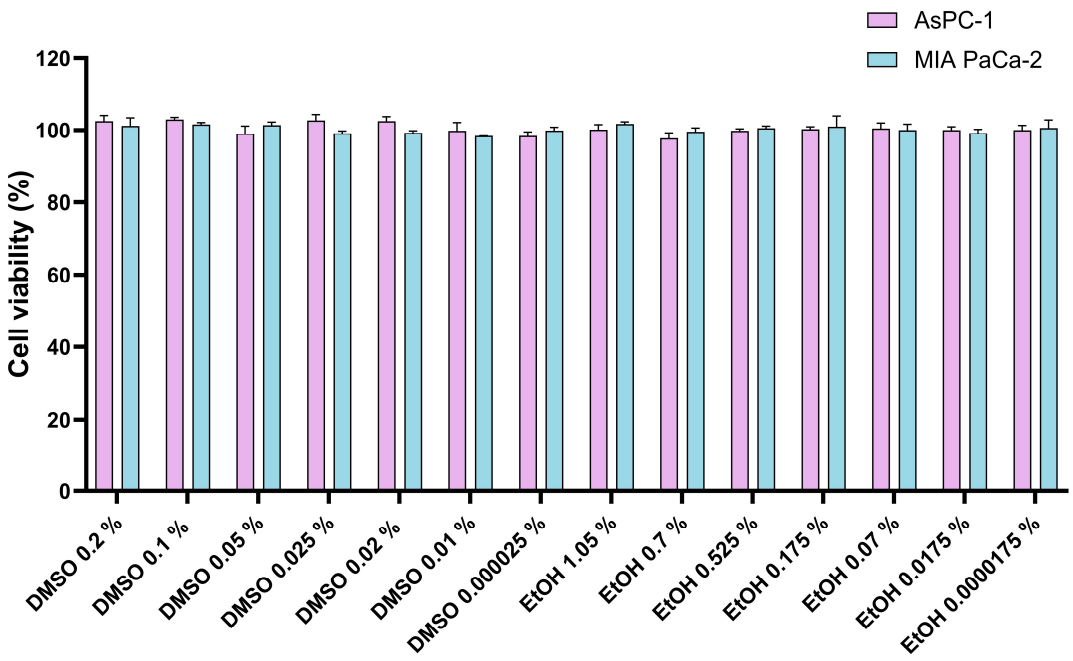


Figure 3.2 The effect of DMSO and ethanol on the cell viability of AsPC-1 and MIA PaCa-2 cells. AsPC-1 and MIA PaCa-2 cells were treated with DMSO and ethanol at various concentrations for 48 h and cell viability was measured with the MTT assay. Each bar represents the mean of at least four replicate values and experiments were repeated at least twice. Error bars represent the standard error of the mean (SEM). (DMSO: dimethyl sulfoxide; EtOH: ethanol).

3.1.2 Selection of a cancer drug to use as a positive control

Gemcitabine is a nucleoside analog used clinically to treat PDAC, while doxorubicin is used in-house and has consistently proven to be active against various cell lines. In order to select a positive control, gemcitabine and doxorubicin were tested against the AsPC-1 and MIA PaCa-2 cell lines to determine their anti-cancer activity using a 48 hour MTT assay as described above. Gemcitabine and doxorubicin were tested at concentrations of 50 µM and 5 µM. The results are shown in Figure 3.3. Gemcitabine showed poor activity against both cell lines at 50 µM and 5 µM compared with doxorubicin (Fig. 3.3). Therefore, doxorubicin was chosen as a positive control for this study.

3.1.3 Determination of the IC_{50} values of active compounds

The four copper complexes selected for further investigations were AD3, OM, L1Cu and L6Cu Doxorubicin was selected as a positive control. To determine their IC_{50} values, the copper complexes were treated with a concentration range of between 0.005 µM and 40 µM and

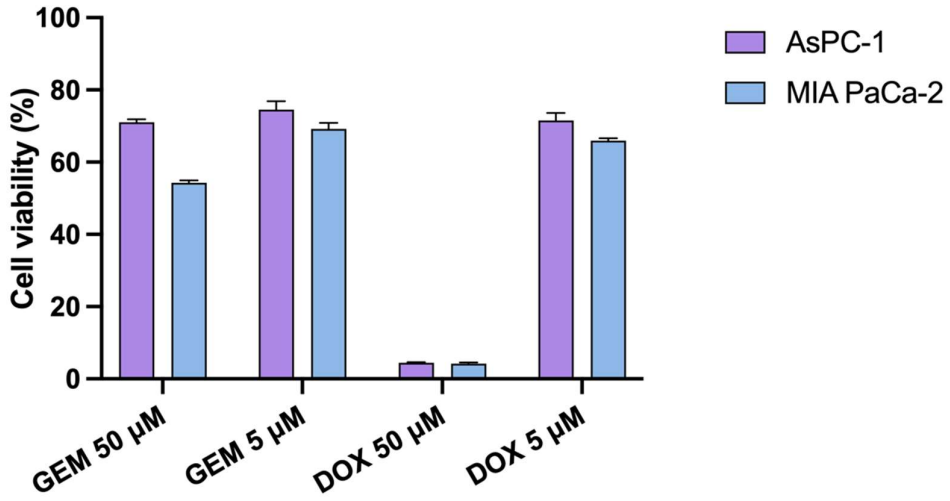


Figure 3.3 The effect of gemcitabine and doxorubicin on the cell viability of AsPC-1 and MIA PaCa-2 cells. AsPC-1 and MIA PaCa-2 cells were treated with gemcitabine and doxorubicin at concentrations of 50 µM and 5 µM for 48 h using the MTT cell viability assay. Each bar represents the mean and error bars represent the SEM of at least four replicate values. (GEM: gemcitabine; DOX: doxorubicin).

doxorubicin was tested at a concentration range between 0.005 µM and 300 µM. The high concentration of 300 µM was to ensure absolute growth inhibition of the cells treated with doxorubicin which was not achieved at lower concentrations. Dose response curves were generated and the half maximal inhibitory (IC_{50}) concentrations for each complex and doxorubicin were obtained using GraphPad Prism software version 9. Representative dose response curves are shown in Figure 3.4. Each data point was obtained in quadruplicate and experiments were repeated at least four times.

The IC_{50} values of the compounds are summarized in Table 3.1 and represent the average of at least four independent experiments. All four copper complexes had IC_{50} values below 5 µM in both cell lines. The IC_{50} values for the copper complexes ranged between 1.27 µM and 3.10 µM against AsPC-1 and between 1.08 µM and 4.04 µM in MIA PaCa-2 cells. In both cell lines, the IC_{50} values for the complexes were lower than those of doxorubicin, which had IC_{50} values of 6.64 ± 0.11 µM and 12.07 ± 0.61 µM in AsPC-1 and MIA PaCa-2 cells, respectively. One-way ANOVA followed by Dunnett's post hoc test showed very highly significant differences ($p < 0.0001$) in the IC_{50} values of the complexes compared to doxorubicin, indicating that all four copper complexes were significantly more active than doxorubicin in both cell lines (Table 3.1). The IC_{50} values of the copper complexes and doxorubicin were in a similar range across cell lines, with the exception of doxorubicin. Doxorubicin showed a close to 100 % increase in

its IC_{50} value between AsPC-1 to MIA PaCa-2 cells, indicating an increased sensitivity of AsPC-1 cells to doxorubicin.

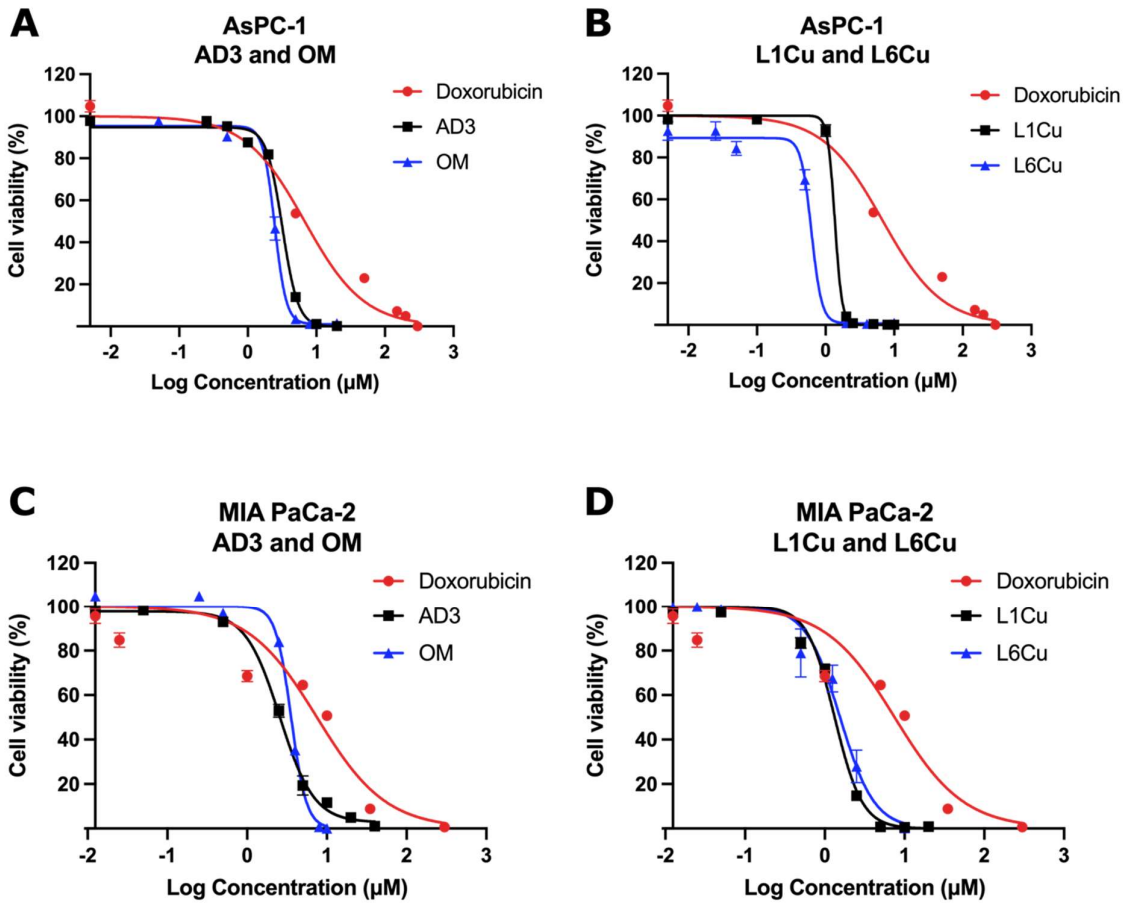


Figure 3.4 Representative sigmoidal log dose response curves of active copper complexes and doxorubicin in AsPC-1 cells (A and B) and MIA PaCa-2 cells (C and D). AsPC-1 and MIA PaCa-2 cells were treated with AD3, OM, L1Cu, L6Cu at concentrations ranging from 0.005 μM to 40 μM and doxorubicin was treated at concentrations ranging between 0.005 μM and 300 μM for 48 h using the MTT cell viability assay. Data points were collected in quadruplicate. Error bars represent the standard deviation. Sigmoidal dose response curves were generated using GraphPad Prism version 9. Experiments were repeated at least four times.

Table 3.1 IC_{50} values of the copper complexes and doxorubicin against AsPC-1 and MIA PaCa-2 cells after a 48 hour treatment period.

	AsPC-1		MIA PaCa-2	
Copper complexes	**IC_{50} (μM)**	**p value**	**IC_{50} (μM)**	**p value**
AD3	3.15 ± 0.07	<0.0001	4.04 ± 0.07	<0.0001
OM	2.75 ± 0.14	<0.0001	3.62 ± 0.08	<0.0001
L1Cu	1.41 ± 0.33	<0.0001	1.08 ± 0.15	<0.0001
L6Cu	1.27 ± 0.22	<0.0001	1.39 ± 0.16	<0.0001

Doxorubicin	6.64 ± 0.11	n/a	12.07 ± 0.61	n/a

IC_{50} values ± SEM of four independent experiments. Copper complexes compared to doxorubicin using ANOVA followed by Dunnett's post hoc multiple comparisons test. Significance criterion was set at $p < 0.05$. Legend: n/a= not applicable.

In clinical practice, patients are treated with the cancer drugs at their IC_{99} concentration in order to ensure 100 % kill of the tumour cells (Swinney, 2011). Therefore, the copper complexes were used at their IC_{80} concentrations (concentrations that resulted in 80% decrease in cell viability) for the rest of this study. Doxorubicin possesses an innate red fluorescence that can interfere with the assays based on immunofluorescence detection. In order to decrease this effect, doxorubicin was used at a constant concentration of 5 μM and not at its IC_{80} value. The maximum excitation and emission wavelength of doxorubicin is 470 nm and 560 nm, respectively (Kauffman *et al*., 2016).

3.2 Effects of the copper complexes and doxorubicin on cell morphology of AsPC-1 and MIA PaCa-2 cells

Fluorescent indicators were used to determine the effect of the copper complexes and doxorubicin on the cell morphology as described in Section 2.5.1. Following a 24 hour treatment period with the copper complexes and doxorubicin, notable morphological changes were observed in the cells. Experiments indicated that cells detached from the growth surface after a 30 hour treatment, therefore effects of the complexes on cell morphology and cell death mechanisms were assessed after a 24 hour treatment period. An untreated control was included. Cells were viewed with an Olympus BX41 microscope and images were captured with an Olympus DP72 camera. The results shown in Figures 3.5 and 3.6 represent the AsPC-1 and MIA PaCa-2 cell lines, respectively and were confirmed with three independent experiments. The effects of the copper complexes in both cell lines are summarized in Table 3.2.

3.2.1 Effects of the copper complexes and doxorubicin on the cell morphology of AsPC-1 cells

Untreated cells remained attached to the growth surface and had intact cell membranes while the nucleus of each cell was visible as oval-shaped and fluoresced with a homogenous HO signal (Fig. 3.5, panels a and b). The reason for the observed difference in intensities of the HO signal between cells in the control may be explained by the cells being over-confluent and growing on different plains of the coverslip, causing some cells to be out of focus (Fig. 3.5, panel b). Endosomes were present in untreated cells, depicted by green punctate fluorescence

in the AO stain (Fig. 3.5, panel c). Phase contrast images of treated cells are shown in Fig. 3.5, panels d, g, j, m and p and membrane blebbing was seen in AD3-, OM-, and doxorubicin-treated cells (Fig. 3.5, panels d, g and p). HO staining of the nuclei of treated cells showed ring condensation in all the cells (Fig. 3.5, panels e, h, k, n and q). Additionally, necklace condensation was seen in cells treated with L1Cu and L6Cu (Fig. 3.5, panels h, k and n). Ring condensation, necklace condensation and chromatin compaction are all stages of chromatin condensation (Tone` *et al*., 2007). The lack of orange/red-fluorescing nuclei in the merged PI/AO images indicated the absence of PI entering and binding to the nuclei and hence, overt necrosis was not seen in any of the cells, with the exception of an isolated yellow nucleus seen in doxorubicin-treated cells which was likely due to secondary necrosis (Fig. 3.5, panels c, f, i, l, o and r). The accumulation of non-nuclear orange-red vesicles in AD3-, L6Cu- and doxorubicin- treated cells indicated the formation of lysosomes and were possibly an indicator for early autophagy (Fig. 3.5, panels f, o and r). Additionally, green vesicles representing endosomes were seen in all copper complex-treated cells (Fig. 3.5, panels f, i, l, and o).

3.2.2 Effects of the copper complexes and doxorubicin on the cell morphology of MIA PaCa-2 cells

Phase contrast images of untreated MIA PaCa-2 cells showed spindle-shaped cells with fibrils connecting the cells to each other (Fig. 3.6, panel a) and oval-shaped nuclei that fluoresced uniformly blue as seen in HO-stained nuclei (Fig. 3.6, panel b). AO stained the untreated cells green and the lack of PI staining confirmed the absence of necrotic cells (Fig. 3.6, panel c). In the phase contrast image of AD3-treated cells, rounding up and detachment of the cells from the growth surface (floating cells were harvested for viewing) was observed (Fig. 3.6, panel d). Large vacuoles were observed in the cytoplasm of AD3- and OM-treated cells and the cells treated with OM, L1Cu, L6Cu and doxorubicin were rounded up but still attached to the growth surface (Fig. 3.6, panels d, g, j, m and p). In the HO-stained images, kidney-shaped nuclei were seen in AD3-treated cells, as well as chromatin compaction of the nuclei (Fig. 3.6, panel e). Chromatin compaction and ring condensation was observed in OM-, L1Cu- and L6Cu-treated cells, while the nuclei of doxorubicin-treated cells demonstrated ring condensation (Fig. 3.6, panels h, k, n and q). The HO stain in doxorubicin-treated cells was affected by the action of doxorubicin to compete with HO 33342 for binding to the minor groove in DNA, resulting in a diminished HO fluorescence (Ijäs *et al*., 2021; Chazotte, 2011) (Fig. 3.6, panel q). The nuclei of some L6Cu-treated cells showed increased fluorescence intensity suggesting the formation

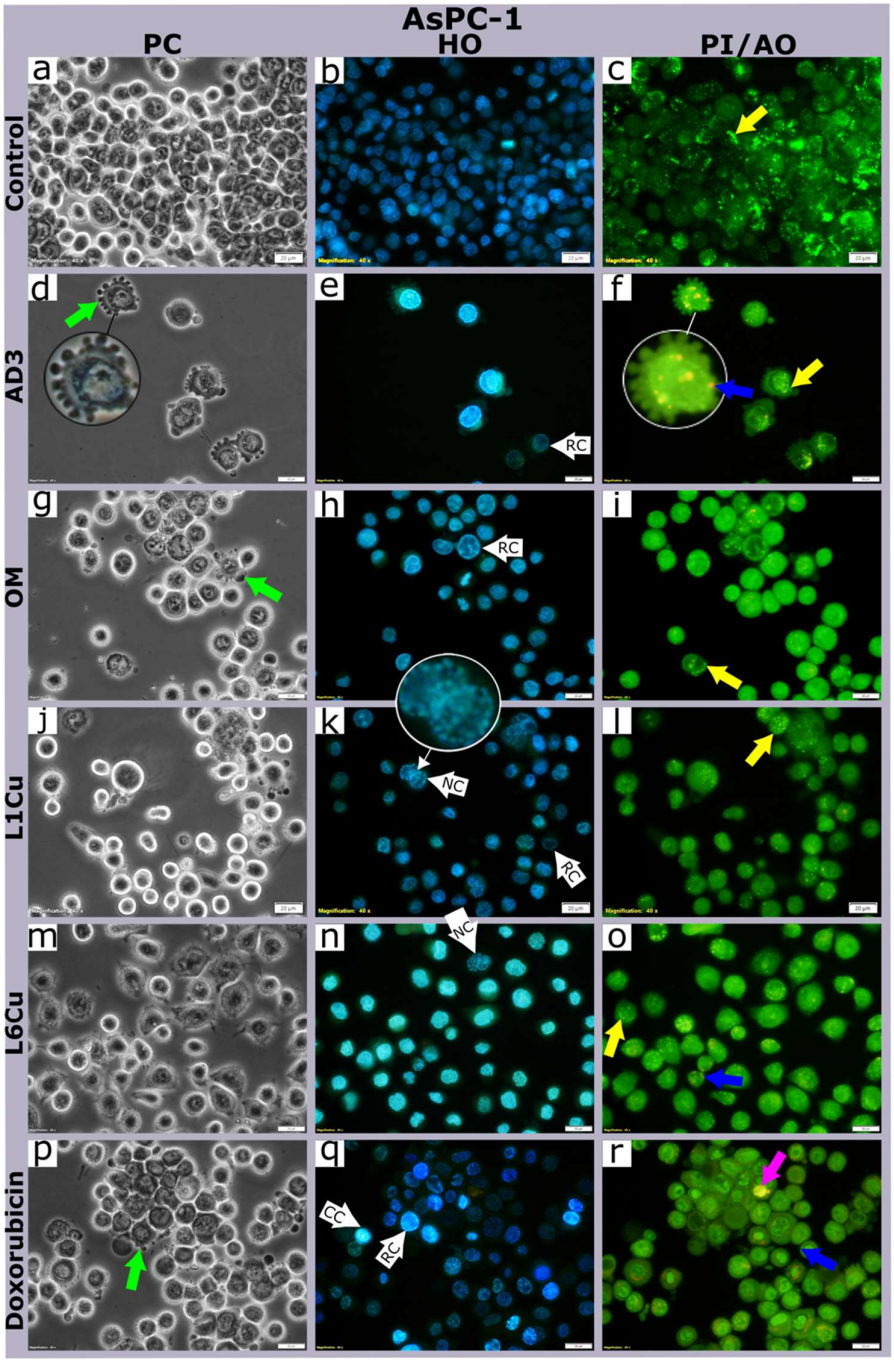


Figure 3.5 Representative photomicrographs showing morphological changes in AsPC-1 cells after a 24 hour treatment with copper complexes. A, panel a-c: untreated cells. A, panel d-f: AD3 (6 µM). A, panel g-i: OM (4 µM). A, panel j-l: L1Cu (2 µM). A, panel m-o: L6Cu (2 µM). A, panel p-r: doxorubicin (5 µM). Cells viewed with Olympus BX41 microscope. Images captured with Olympus DP72 camera. Magnification: 400X, scale bar: 20 µm. Each photomicrograph is representative of three independent experiments (n = 3). Legend: Red arrow = vacuoles. Green arrow = blebbing. Blue arrow = lysosomes. Yellow arrow = endosomes. Pink arrow = secondary necrotic cell. White arrow = chromatin condensation. CC = chromatin compaction. RC = ring condensation. NC = necklace condensation. PC = phase contrast. HO = Hoechst 33342. PI = propidium iodide. AO = acridine orange.

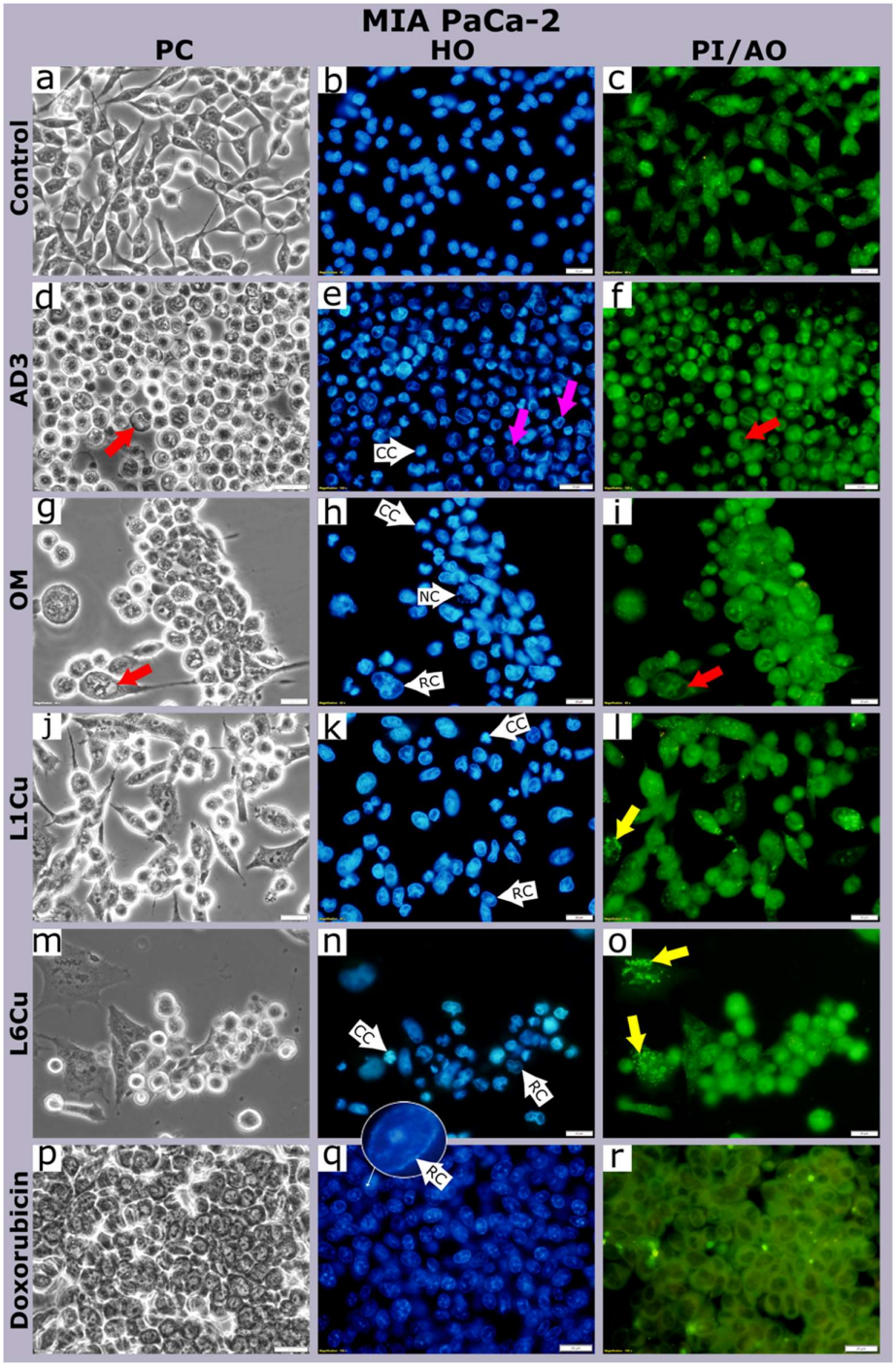


Figure 3.6 Representative photomicrographs showing morphological changes in MIA PaCa-2 cells after a 24 hour treatment with copper complexes. A, panel a-c: untreated cells. A, panel d-f: AD3 (6 µM). A, panel g-i: OM (5 µM). A, panel j-l: L1Cu (2 µM). A, panel m-o: L6Cu (2 µM). A, panel p-r: doxorubicin (5 µM). Cells viewed with Olympus BX41 microscope. Images captured with Olympus DP72 camera. Magnification: 400X, scale bar: 20 µm. Each photomicrograph is representative of three independent experiments (n = 3). Legend: Red arrow = vacuoles. Pink arrow = kidney-shaped nuclei. Yellow arrow = endosomes. White arrow = chromatin condensation. CC = chromatin compaction. RC = ring condensation. NC = necklace condensation. PC = phase contrast. HO = Hoechst 33342. PI = propidium iodide. AO = acridine orange.

of cytoplasmic vacuoles which cannot be observed by phase contrast when the cells are rounded up (Fig. 3.6, panel n). The absence of PI staining of the nuclei in PI/AO merged images confirmed that none of the cells were necrotic (Figure 3.6, panels f, i, l, o, r). Punctate green fluorescence was seen in the AO images of L1Cu- and L6Cu-treated cells, indicating the presence of endosomes (Fig. 3.6, panels l and o).

Table 3.2 The effect of the copper complexes on the cell morphology of AsPC-1 and MIA PaCa-2 cells.

	AD3		OM		L1Cu		L6Cu	
Apoptotic feature	**AsPC-1**	**MIA PaCa-2**	**AsPC-1**	**MIA PaCa-2**	**AsPC-1**	**MIA PaCa-2**	**AsPC-1**	**MIA PaCa-2**
Necrosis								
Ring condensation	✓	✓	✓	✓	✓	✓		✓
Necklace condensation				✓	✓		✓	
Chromatin compaction		✓	✓	✓		✓	✓	✓
Membrane blebbing	✓		✓					
Lysosomes	✓							
Endosomes	✓		✓		✓	✓	✓	✓
Vacuoles		✓		✓		✓		✓

3.3 Translocation of phosphatidylserine to the surface of AsPC-1 and MIA PaCa-2 cells

Since membrane blebbing and changes to nuclei suggesting apoptosis were observed in cell morphology studies, apoptosis as a mechanism of cell death was investigated. The annexin-V assay was used to determine if the copper complexes induced the translocation of phosphatidylserine to the outer surface of the cell membrane (as described in Section 2.7.1). Cells were treated with the copper complexes for 24 hours at concentrations equivalent to their IC_{80} values. Doxorubicin was used as a positive control at 5 µM and untreated cells were included. Cells were viewed with an Olympus BX41 microscope and images were captured with an Olympus DP72 camera. The results of the annexin-V assay in AsPC-1 and MIA PaCa-2 cells are shown in Figures 3.7 and 3.8, respectively.

3.3.1 The effect of copper complexes and doxorubicin on annexin-V binding in AsPC-1 cells

Phase contrast images showed a normal morphology of the untreated cells and no fluorescence signal was observed, indicating the absence of apoptotic/necrotic cells (Fig. 3.7 A, panels a and b). Membrane blebbing was observed in phase contrast images of AD3-, OM-, L1Cu- and L6Cu-treated cells and doxorubicin treated cells remained attached to the growth surface (Fig.

3.7 A, panels c, e, g, i and k). Annexin-V-binding was present in all treated cells (Fig. 3.7 A, panels d, f, h, j and l; Fig. 3.7 B). None of the treated cells showed PI staining, confirming the absence of necrotic cell death (Fig. 3.7 A, panels d, f, h and j). The cell membranes of doxorubicin-treated cells were intact, therefore, the orange-red fluorescence that was visible in the nuclei of doxorubicin-treated cells (Fig. 3.7 A, panel l) was likely due to the innate red fluorescent nature of doxorubicin and its ability to intercalate with DNA (Chen *et al*., 2012). Doxorubicin was significantly more effective than the copper complexes at inducing annexin-V binding due to phosphatidylserine exposure on the outer leaflet of the cell membrane (Fig. 3.7 B). L6Cu-treated cells had strong annexin-V binding in the cells that were beginning to detach from the growth surface (rounded cells), with 76.8 % of the cells demonstrating annexin-V-binding (Fig. 3.7 A, panel j; Fig. 3.7 B). Annexin-V-binding was observed in 50.5 % and 46.4 % of OM- and AD3-treated cells, respectively (Fig. 3.7 B). L1Cu was the least efficient effector of annexin-V binding, with 28.5 % of cells showing annexin-V-binding (Fig. 3.7 B).

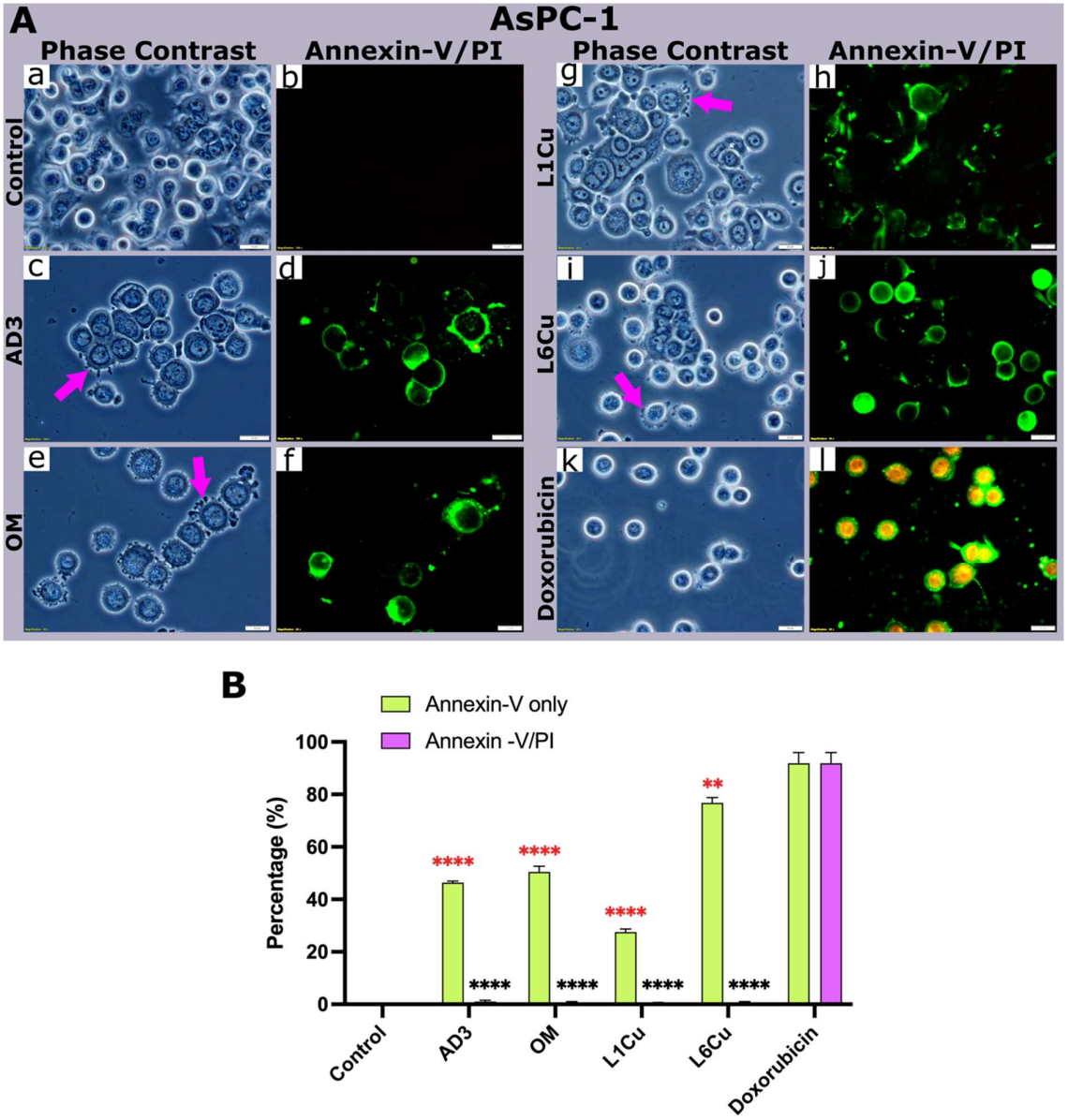


Figure 3.7 Representative photomicrographs (A) and a bar graph (B) of annexin-V binding and PI staining of AsPC-1 cells after a 24 hour treatment with copper complexes. A, panel a-b: untreated cells. A, panel c-d: AD3 (6 µM). A, panel e-f: OM (4 µM). A, panel g-h: L1Cu (2 µM). A, panel i-j: L6Cu (2 µM). A, panel k-l: doxorubicin (5 µM). Cells viewed with Olympus BX41 microscope. Green fluorescence indicates annexin-V-binding. Images captured with Olympus DP72 camera. Magnification: 400X, scale bar: 20 µm. Each photomicrograph is representative of at least three independent experiments (n = 3). Each bar represents mean from at least three independent experiments. Error bars represent SEM. Legend: Pink arrow = blebbing. PI = propidium iodide. Copper complexes compared to doxorubicin using ANOVA ($p < 0.05$) followed by Dunnett's post hoc multiple comparisons test. Fig. 3.7 B: red text represents statistical comparison of annexin-V-only; black text represents statistical comparison of annexin-V/PI. P values: not significant (ns): $p > 0.05$. * = $p \leq 0.05$. ** = $p \leq 0.01$. *** = $p \leq 0.001$. **** = $p \leq 0.0001$.

3.3.2 The effect of copper complexes and doxorubicin on annexin-V binding in MIA PaCa-2 cells

Untreated MIA PaCa-2 cells had their normal morphology and did not show annexin-V-binding or PI binding to the nucleus, indicating healthy cells (Fig 3.8 A, panels a and b). Phase contrast images of treated cells showed rounded cells detaching from the growth surface (Fig. 3.8 A, panels c, e, g, i and k). All the copper complexes and doxorubicin caused an increase in green fluorescence indicating the binding of annexin-V to phosphatidylserine on the cell surface (Fig. 3.8 A, panels d, f, h, j and l; Fig. 3.8 B). PI staining was observed in cells treated with AD3, OM, L1Cu and L6Cu indicating late apoptosis or secondary necrosis (Fig. 3.8 A, panels d, f, h, j). Late apoptosis/secondary necrosis was most prevalent in AD3- and OM-treated cells (Fig. 3.8 A, panels d and f). AD3-treated cells had a percentage of 26.4 % of cells that showed annexin-V-only binding while 46.9 % of cells had both annexin-V and PI staining (Fig. 3.8 B). In OM-treated cells, 32.5 % of cells showed annexin-V-binding while 21.4 % had both annexin-V and PI (Fig. 3.8 B). In L1Cu-treated cells, attached cells showed a faint green signal while rounded cells indicated both annexin-V-only-binding and annexin-V/PI binding (Fig. 3.8 A, panel h). Annexin-V-binding was observed in 20.1 % of L1Cu-treated cells while 3.7 % of cells showed the presence of both annexin-V and PI (Fig. 3.8 B). L6Cu-treated cells showed annexin-V-only-binding in 60.1 % of the cells as well as annexin-V/PI in 24.4 % (Fig. 3.8 A, panel j; Fig 3.8 B). Annexin-V-binding was observed in 30.8 % of cells treated with the positive control, doxorubicin (Fig. 3.8 A , panel l; Fig 3.8 B). The orange/red fluorescence of doxorubicin was also visible in the nuclei of MIA PaCa-2 cells and was likely not due to PI staining since the membranes appeared to be intact (Fig. 3.8, panels k and l). Only L6Cu was significantly more effective than doxorubicin at causing annexin-V-binding, with a p value of 0.009 (***) (Fig. 3.8 B).

3.3.3 Summary of the effects of copper complexes on annexin-V-binding

In summary, all four copper complexes induced phosphatidylserine exposure in both cell lines, with L6Cu being the strongest inducer and L1Cu being the least potent inducer of phosphatidylserine exposure. AsPC-1 cells did not show the presence of late apoptosis/secondary necrosis, while MIA PaCa-2 cells showed cells undergoing late apoptosis/secondary necrosis.

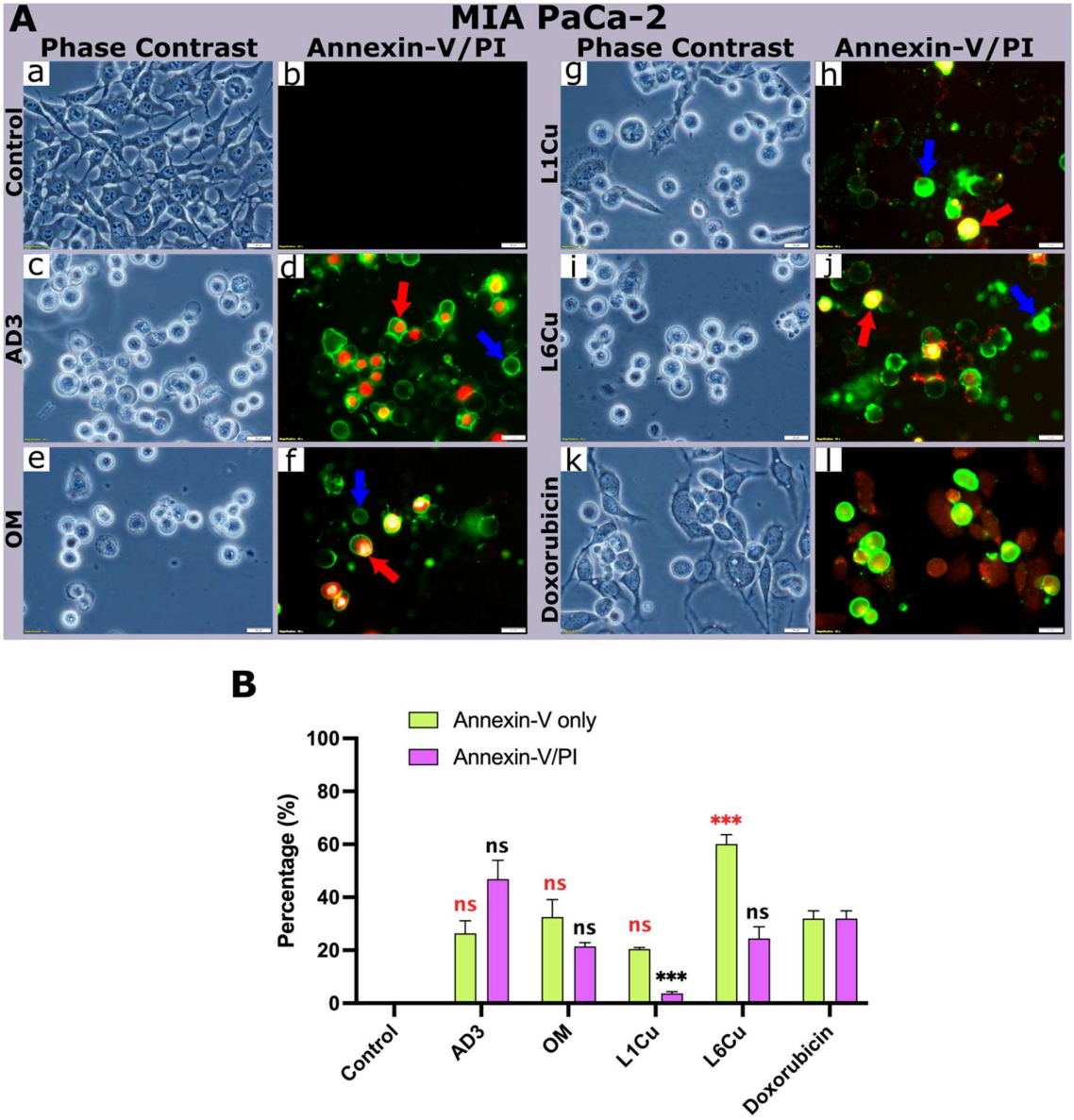


Figure 3.8 Representative photomicrographs (A) and a bar graph (B) of annexin-V binding and PI staining of MIA PaCa-2 cells after a 24 h treatment with copper complexes. A, panel a-b: untreated cells. A, panel c-d: AD3 (6 µM). A, panel e-f: OM (5 µM). A, panel g-h: L1Cu (2 µM). A, panel i-j: L6Cu (2 µM). A, panel k-l: doxorubicin (5 µM). Cells viewed with Olympus BX41 microscope. Green fluorescence= annexin-V-binding. Red fluorescence= propidium iodide-binding to nucleus. Images captured with Olympus DP72 camera. Magnification: 400X, scale bar: 20 µm. Each photomicrograph is representative of at least three independent experiments (n = 3). Each bar represents mean from at least three independent experiments. Error bars represent SEM. Legend: Blue arrow = early apoptotic cell. Red arrow = late apoptotic/secondary necrotic cell. PI = propidium iodide. Copper complexes compared to doxorubicin using ANOVA ($p < 0.05$) followed by Dunnett's post hoc multiple comparisons test. Fig. 3.8 B: red text represents statistical comparison of annexin-V-only; black text represents statistical comparison of annexin-V/PI. P values: not significant (ns): $p > 0.05$. * = $p \leq 0.05$. ** = $p \leq 0.01$. *** = $p \leq 0.001$. **** = $p \leq 0.0001$.

3.4 Evaluation of the ability of the copper complexes to induce ROS formation

The copper complexes were evaluated for their ability to induce oxidative stress by measuring the formation of ROS using the CellRox® Deep Red reagent. The cells were incubated with the copper complexes and doxorubicin and the CellRox® reagent for four, six and 18 hours and viewed with an Olympus BX41 microscope as described in Section 2.5.3. Images were captured using an Olympus DP72 camera. The copper complexes were tested at concentrations equivalent to their IC_{80} values and doxorubicin was used as a positive control at 5 μM and were compared to untreated cells. Given that the CellRox® reagent indicates the presence of ROS with red fluorescence, an additional doxorubicin control without CellRox® reagent was included to mitigate doxorubicin's innate red fluorescence. The results are shown in Figure 3.9 and 3.10 for AsPC-1 and MIA PaCa-2, respectively.

3.4.1 The effects of the copper complexes on ROS formation in AsPC-1 cells

ROS formation was induced by the copper complexes after a six hour treatment period (Figure 3.9). The copper complexes did not induce the formation of ROS at four and 18 hours (data not shown). After a six hour treatment period, untreated AsPC-1 cells had normal morphology and fluoresced with a low intensity signal, indicating low baseline levels of ROS (Fig. 3.9, panels a and b). Membrane blebbing was observed in the phase contrast images of all treated cells (Fig. 3.9, panels c, e, g, i, k). Compared to untreated cells, L1Cu caused a non-significant increase in ROS fluorescent signal (Fig. 3.9 A, panel h, Fig. 3.9 B) while AD3, OM and L6Cu (Fig 3.9 A, panels d, f and j; Fig. 3.9 B) caused highly significant increases in ROS formation. Doxorubicin-treated cells that were exposed to the CellRox® reagent (Fig. 3.9 A, panel l; Fig. 3.9 B) fluoresced with a bright red signal and had a statistically significant increase in red fluorescence compared to the doxorubicin-treated cells without CellRox® reagent exposure (Fig. 3.9 A, panel n; Fig. 3.9 B), suggesting that doxorubicin induced ROS formation.

3.4.2 The effects of the copper complexes on ROS formation in MIA PaCa-2 cells

Similar to AsPC-1 cells, the complexes induced ROS after a six hour treatment period (Fig. 3.10) but ROS was not observed at treatment periods of four hours and 18 hour (data not shown). At six hours, untreated MIA PaCa-2 cells displayed their normal, polygonal-shaped morphology with the complete absence of a fluorescence signal, indicating the absence of ROS in untreated MIA PaCa-2 cells (Fig. 3.10 A, panels a and b). Phase contrast images of treated cells showed elongated cells in AD3-, and L6Cu- treated cells whilst rounded-up cells were seen in OM-treated cells (Fig. 3.10 A, panels c, e, i). L1Cu showed both elongated and rounded

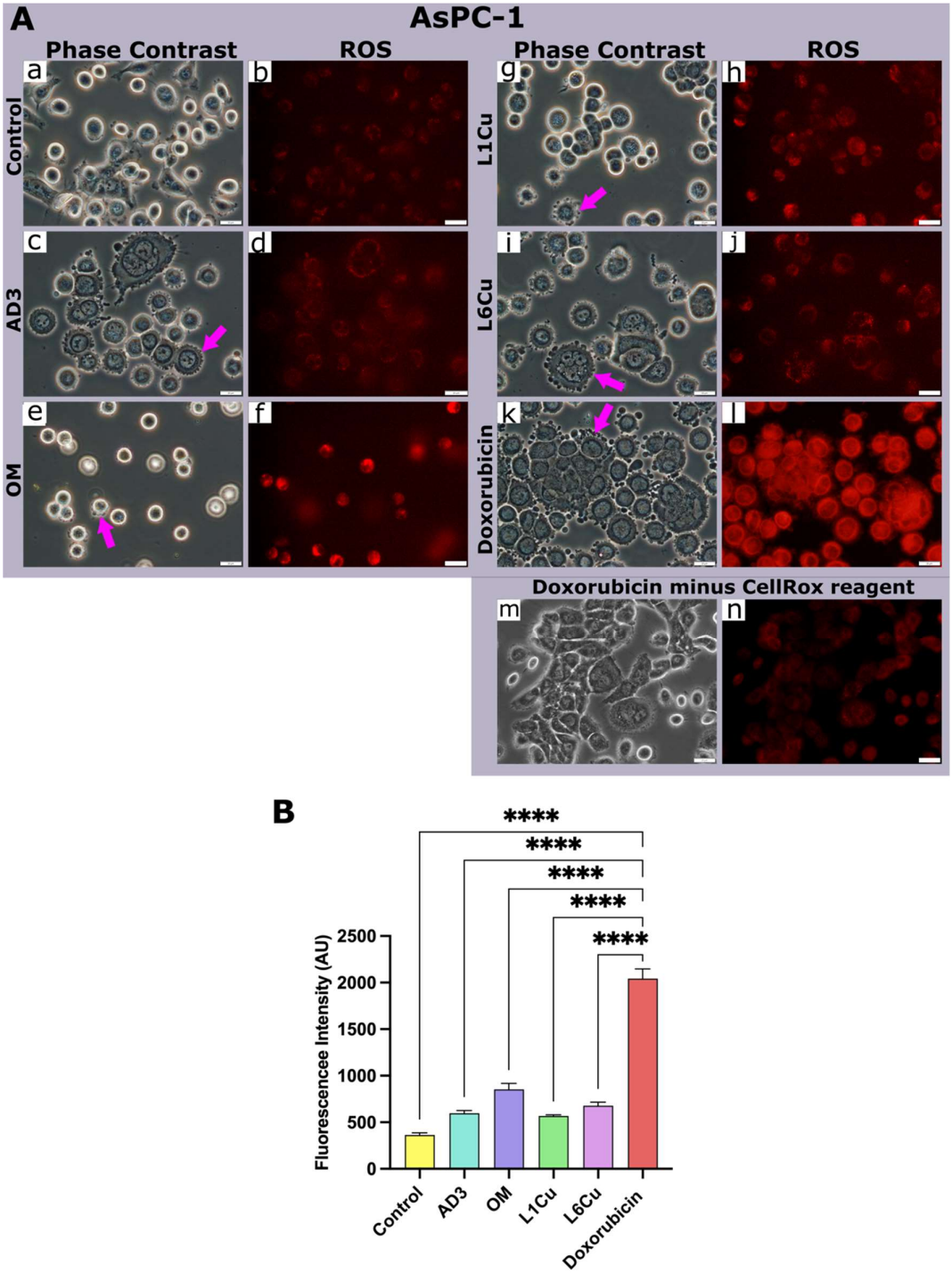


Figure 3.9 Representative photomicrographs (A) and a bar graph (B) of ROS formation in AsPC-1 cells after 6 hour treatment with copper complexes. A, panel a-b: untreated cells. A, panel c-d: AD3 (6 µM). A, panel e-f: OM (4 µM). A, panel g-h: L1Cu (2 µM). A, panel i-j: L6Cu (2 µM). A, panel k-l: doxorubicin (5 µM). A, panel m-n: doxorubicin-only control lacking CellRox® reagent. Cells viewed with Olympus BX41 microscope. Images captured with Olympus DP72 camera. Magnification: 400X, scale bar: 20 µm. Fluorescence intensities were measured using CellProfiler™. Legend: Pink arrow = blebbing. ROS = reactive oxygen species (indicated by red fluorescence). AU = arbitrary units. Each photomicrograph is representative of at least three independent experiments (n = 3). Copper

complexes compared to doxorubicin using ANOVA ($p < 0.05$) followed by Dunnett's post hoc multiple comparisons test. P values: not significant (ns): $p > 0.05$. * = $p \leq 0.05$. ** = $p \leq 0.01$. *** = $p \leq 0.001$. **** = $p \leq 0.0001$.

cells (Fig. 3.10 A, panel g). All the copper complexes induced an increase in red fluorescence intensity after a six hour treatment period (Fig. 3.10 A, panels d, f, h, j; Fig. 3.10 B), indicating the formation of ROS. The phase contrast images of doxorubicin-treated cells are shown in Fig. 3.10 A (panels k and m). Compared to the CellRox®-negative doxorubicin control (Fig. 3.10 A, panel n), doxorubicin-treated cells with CellRox® reagent showed intense red fluorescence (Fig. 3.10 A, panel l; Fig. 3.10 B) indicating that doxorubicin caused the formation of ROS. Doxorubicin was more effective than the copper complexes at inducing ROS formation (Fig. 3.10 B).

3.4.3 Summary of the effects of the copper complexes on ROS formation

In AsPC-1 cells, low levels of ROS were present in untreated cells and the copper complexes increased the ROS signal. In MIA PaCa-2 cells, ROS was absent from untreated cells and the complexes induced a high intensity ROS signal in treated cells. The results suggested that the copper complexes induced ROS more potently in MIA PaCa-2 cells than in AsPC-1 cells, reiterating the fact that MIA PaCa-2 cells showed increased sensitivity to the copper complexes. The results from the ROS assay suggested that the copper complexes likely stimulated the initiation of the intrinsic/mitochondrial apoptotic pathway through ROS-induction. Further apoptotic assays were performed to confirm the mechanism of cell death caused by the complexes.

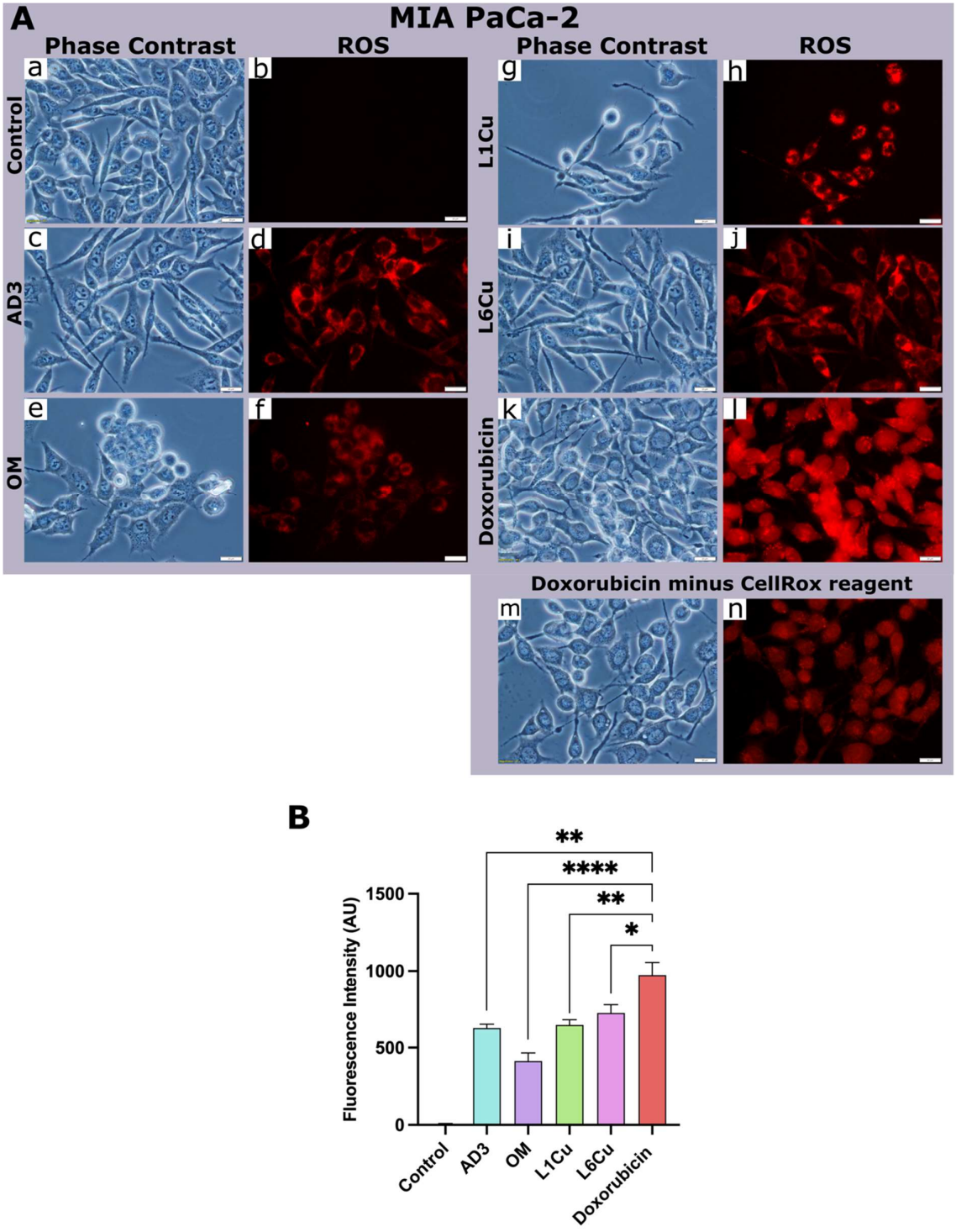


Figure 3.10 Representative photomicrographs (A) and a bar graph (B) of ROS formation in MIA PaCa-2 cells after 6 hour treatment with copper complexes. A, panel a-b: untreated cells. A, panel c-d: AD3 (6 µM). A, panel e-f: OM (5 µM). A, panel g-h: L1Cu (2 µM). A, panel i-j: L6Cu (2 µM). A, panel k-l: doxorubicin (5 µM). A, panel m-n: doxorubicin-only control lacking CellRox® reagent. Cells viewed with an Olympus BX41 microscope. Images captured with Olympus DP72 camera. Magnification: 400X, scale bar: 20 µm. Fluorescence intensities measured using CellProfiler™. Each photomicrograph is representative of at least three independent experiments (n = 3). Legend: ROS = reactive oxygen

species (indicated by red fluorescence). AU = arbitrary units. Copper complexes compared to doxorubicin using ANOVA ($p < 0.05$) followed by Dunnett's post hoc multiple comparisons test. P values: not significant (ns): $p > 0.05$. * = $p \leq 0.05$. ** = $p \leq 0.01$. *** = $p \leq 0.001$. **** = $p \leq 0.0001$.

3.5 Evaluation of the effect of the copper complexes on mitochondrial membrane potential

In the cell, the mitochondria are the main source of ROS production. Following the detection of ROS formation in treated cells, the status of the mitochondria was evaluated using the membrane permeant reagent, JC-1, as described in Section 2.5.2.4. The loss of MMP is a feature of the intrinsic apoptotic pathway (Redza-Dutordoir and Averill-Bates, 2016). Cells were treated with the copper complexes at concentrations equivalent to their IC_{80} concentrations and with doxorubicin at 5 μM for 18 hours. The results for AsPC-1 and MIA PaCa-2, are shown in Figure 3.11 and 3.12, respectively.

3.5.1 The effect of the copper complexes on mitochondrial membrane potential in AsPC-1 cells

Untreated cells showed punctate orange/red fluorescing 'J-aggregates', indicating an intact MMP, in 94.7% of the cells (Fig. 3.11 A, panel a; Fig. 3.11 B). All the copper complexes caused a loss in MMP, indicated by the absence of red/orange fluorescence, as seen in Fig. 3.11 A, panels b, c, d and e. AD3 caused 97.8 % of the cells to fluoresce green while OM, L1Cu and L6Cu caused 100.0% of the cells to shift from red to green fluorescence, indicating mitochondrial depolarization (Fig. 3.11 B). An increase in diffuse, even, green fluorescing JC-1 monomers was observed in 98 % of doxorubicin-treated cells (Fig. 3.11 A, panel f), possibly caused by the loss of structure of the mitochondria. AD3-, OM- and L1Cu-treated cells showed punctate fluorescence, indicating intact mitochondria (Figure 3.11 A, panels b, c and d), while some L1Cu-treated cells showed diffuse, even fluorescence (Fig. 3.11 A, panels d). Loss of mitochondrial structural integrity was also observed in cells treated with L6Cu, as seen by the even, green fluorescence (Figure 3.11 A, panel e). The complexes and doxorubicin showed similar efficacy in the induction of mitochondrial membrane depolarization, as determined by statistical evaluation (Fig. 3.11 B).

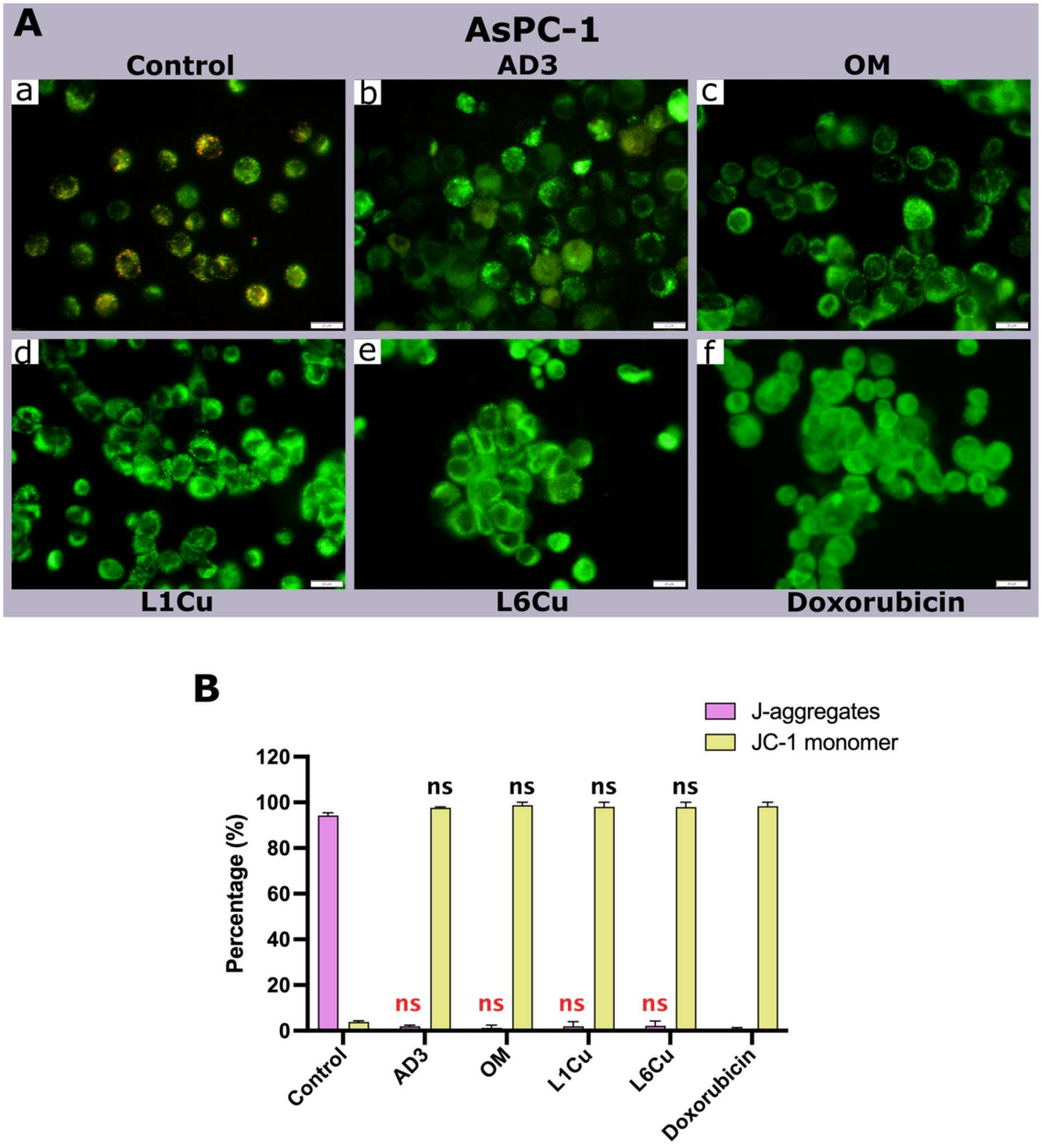


Figure 3.11 Representative photomicrographs (A) and a bar graph (B) showing the effects of the copper complexes on mitochondrial membrane potential in AsPC-1 cells after 18 h treatment. Photomicrographs show merged images of red J-aggregates and green JC-1 monomers. A, panel a: untreated cells. A, panel b: AD3 (6 µM). A, panel c: OM (4 µM). A, panel d: L1Cu (2 µM). A, panel e: L6Cu (2 µM). A, panel f: doxorubicin (5 µM). Cells viewed with Olympus BX41 microscope. Images captured with Olympus DP72 camera. Magnification: 400X, scale bar: 20 µm. Each photomicrograph is representative of three independent experiments (n = 3). Each bar represents mean from three independent experiments. Error bars represent SEM. Copper complexes compared to doxorubicin using ANOVA ($p < 0.05$) followed by Dunnett's post hoc multiple comparisons test. Fig. 3.11 B: red text represents statistical comparison of J-aggregates; black text represents statistical comparison of JC-1 monomers. P values: not significant (ns): $p > 0.05$.

3.5.2 The effect of the copper complexes on mitochondrial membrane potential in MIA PaCa-2 cells

In untreated cells, the MMP was intact in 100 % of the cells, as observed by the presence of orange/red fluorescing 'J-aggregates' (Fig. 3.12 A, panel a). The copper complexes caused a shift from red fluorescing 'J-aggregates' to green fluorescing JC-1 monomers, which indicated that all the complexes caused a loss of MMP (Fig 3.12 A, panels b-e). AD3, L1Cu, L6Cu and OM caused a loss in the MMP in close to 100 % of the cells (Fig. 3.12 B). In doxorubicin-treated cells, green-fluorescing JC-1 monomers were observed in 97 % of the cells (Fig. 3.12 A, panel f; Figure 3.12 B). In treated cells with a rounder morphology, the green fluorescence was diffuse and even, indicating a loss in the mitochondrial integrity. This was seen in cells treated with AD3, OM and L1Cu (Fig. 3.12 A, panels b, c, and d). Cells treated with L6Cu and doxorubicin showed punctate green fluorescence, suggesting that the mitochondria were structurally intact (Fig. 3.12 A, panel e and f). The complexes showed similar potency to doxorubicin, in their ability to cause a loss of MMP (Fig. 3.12 B).

3.5.3 Summary of the effects of the copper complexes on mitochondrial membrane potential

In both cells lines, the copper complexes caused a loss in the MMP after an 18 hour treatment. The observed fluorescence was either punctate or diffuse/even, indicating that some cells had a loss in their mitochondrial structural integrity while others remained intact. The copper complexes were not more active than doxorubicin in their abilities to cause a loss in the MMP. Further assays measuring caspase activity were performed in order to confirm the mechanism of cell death of the copper complexes.

3.6 The effect of the copper complexes on caspase-9 activity

The effect of the copper complexes on caspase-9 activity was evaluated as described in Section 2.5.2.3. Cells were treated with the copper complexes at concentrations equivalent to their IC_{80} concentrations for 24 and 48 hours. Doxorubicin was used as a positive control at a concentration of 5 μM and an untreated control was included. The results for AsPC-1 and MIA PaCa-2, are shown in Figures 3.13 and 3.14, respectively.

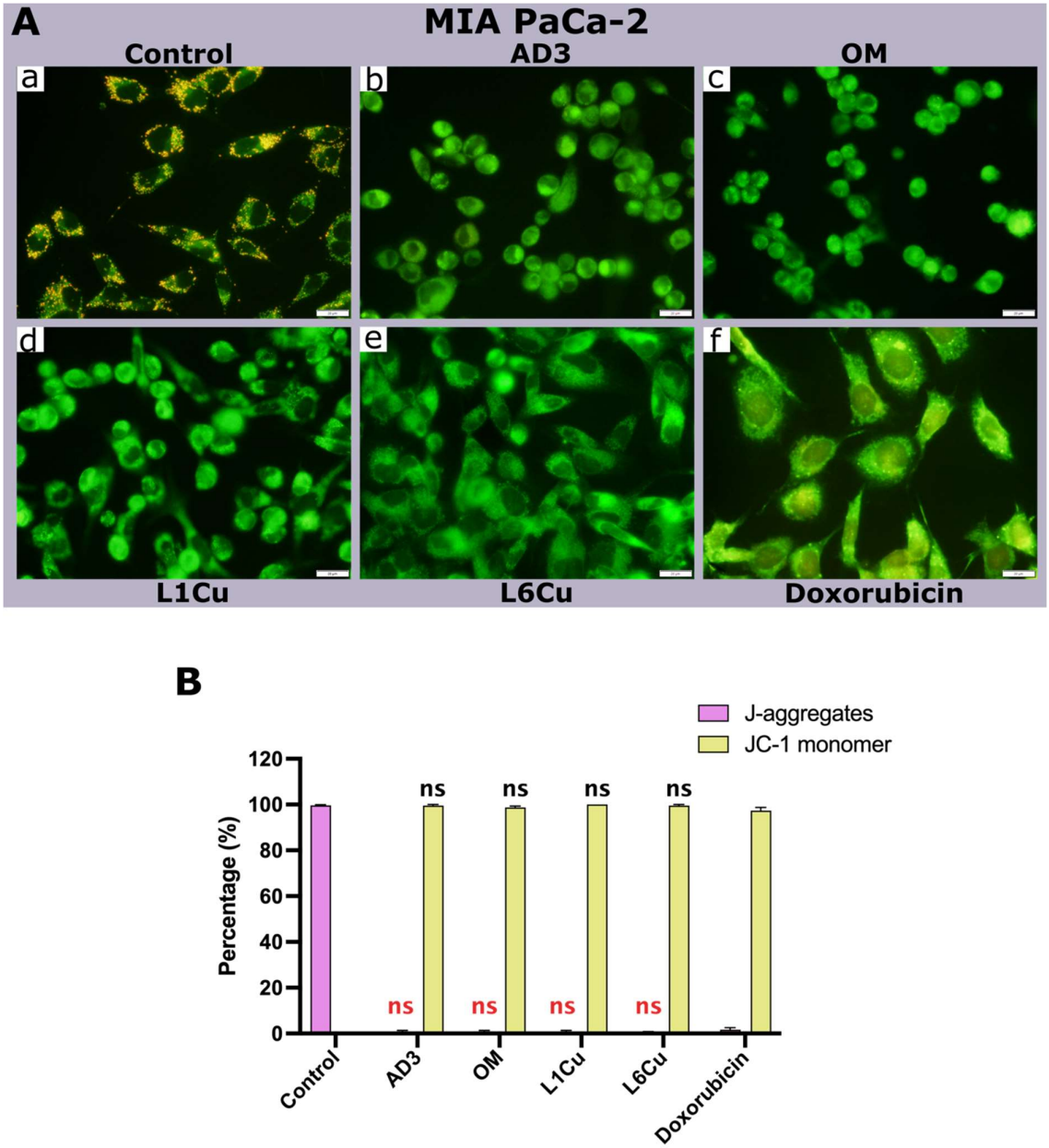


Figure 3.12 Representative photomicrographs (A) and a bar graph (B) showing the effects of the copper complexes on mitochondrial membrane potential in MIA PaCa-2 cells after 18 h treatment. Photomicrographs show merged images of red J-aggregates and green JC-1 monomers. A, panel a: untreated cells. A, panel b: AD3 (6 µM). A, panel c: OM (5 µM). A, panel d: L1Cu (2 µM). A, panel e: L6Cu (2 µM). A, panel f: doxorubicin (5 µM). Cells viewed with Olympus BX41 microscope. Images captured with Olympus DP72 camera. Magnification: 400X, scale bar: 20 µm. Each photomicrograph is representative of three independent experiments (n = 3). Each bar represents mean from three independent experiments. Error bars represent SEM. Copper complexes compared to doxorubicin using ANOVA ($p < 0.05$) followed by Dunnett's post hoc multiple comparisons test. Fig. 3.12 B: red text represents statistical comparison of J-aggregates; black text represents statistical comparison of JC-1 monomers. P values: not significant (ns): $p > 0.05$.

3.6.1 The effect of the copper complexes on caspase-9 activity in AsPC-1 cells

There was no meaningful activation by the copper complexes of caspase-9 at 24 hours (Appendix B), therefore, cells were treated for 48 hours. Caspase-9 activity was absent in untreated cells, indicated by the normal cell morphology and the absence of a green fluorescent signal and the cells had a normal morphology (Fig. 3.13 A, panels a and b). Phase contrast images of treated cells are shown in Fig. 3.13 A, panels c, e, g, i and k). All the copper complexes and doxorubicin caused the activation of caspase-9 after a 48 hour treatment (Fig. 3.13 A, panels d, f, h, j and l). OM, L1Cu and L6Cu had between 75.9 % and 84.0 % of cells with active caspase-9 (Fig. 3.12 B). AD3 was the least efficient activator of caspase-9, with 53.2 % of cells showing active caspase-9 (Fig. 3.13 B). Doxorubicin was more active than the copper complexes, with the highest percentage (93 %) of cells with active caspase-9 (Fig. 3.13 B). Doxorubicin was significantly more effective than AD3 ($p = 0.03$) in its caspase-9 activating effects, while having a similar effect as OM, L1Cu and L6Cu ($p > 0.05$) (Fig. 3.13 B).

3.6.2 The effect of the copper complexes on caspase-9 activity in MIA PaCa-2 cells

Similar to the AsPC-1 cell line, active caspase-9 was not observed after a 24 hour treatment period (Appendix B), therefore, cells were treated for 48 hours. Untreated cells had a normal morphology and lacked active caspase-9 (Figure 3.14 A, panel a and b). Phase contrast images of the copper complex-treated cells showed rounded up cells while doxorubicin-treated cells remained attached to the growth surface (Fig. 3.14 A, panels c, e, g, i and k). All the copper complexes and doxorubicin caused activation of caspase-9 (Fig. 3.14 A, panels d, f, h, j, and l). AD3 and OM were the most potent activators of caspase-9 with more than 90 % of the cells showing active caspase-9 (Fig. 3.14 A, panels c-f; Fig. 3.14 B). L1Cu showed 76 % of MIA PaCa-2 cells with active caspase-9 (Fig. 3.14 B). From the copper complexes, L6Cu was the least efficient in activating caspase 9 in MIA PaCa-2 cells with 41 % of cells showing active caspase-9 (Fig. 3.14 B). Doxorubicin activated caspase-9 in 86.0 % of the cells (Fig. 3.14 B). Doxorubicin was significantly more effective in activating caspase-9 than L1Cu ($p = 0.02$) and L6Cu ($p < 0.0001$), while AD3 and OM were similar to doxorubicin in their ability to activate caspase-9 at this treatment period (Fig. 3.14 B).

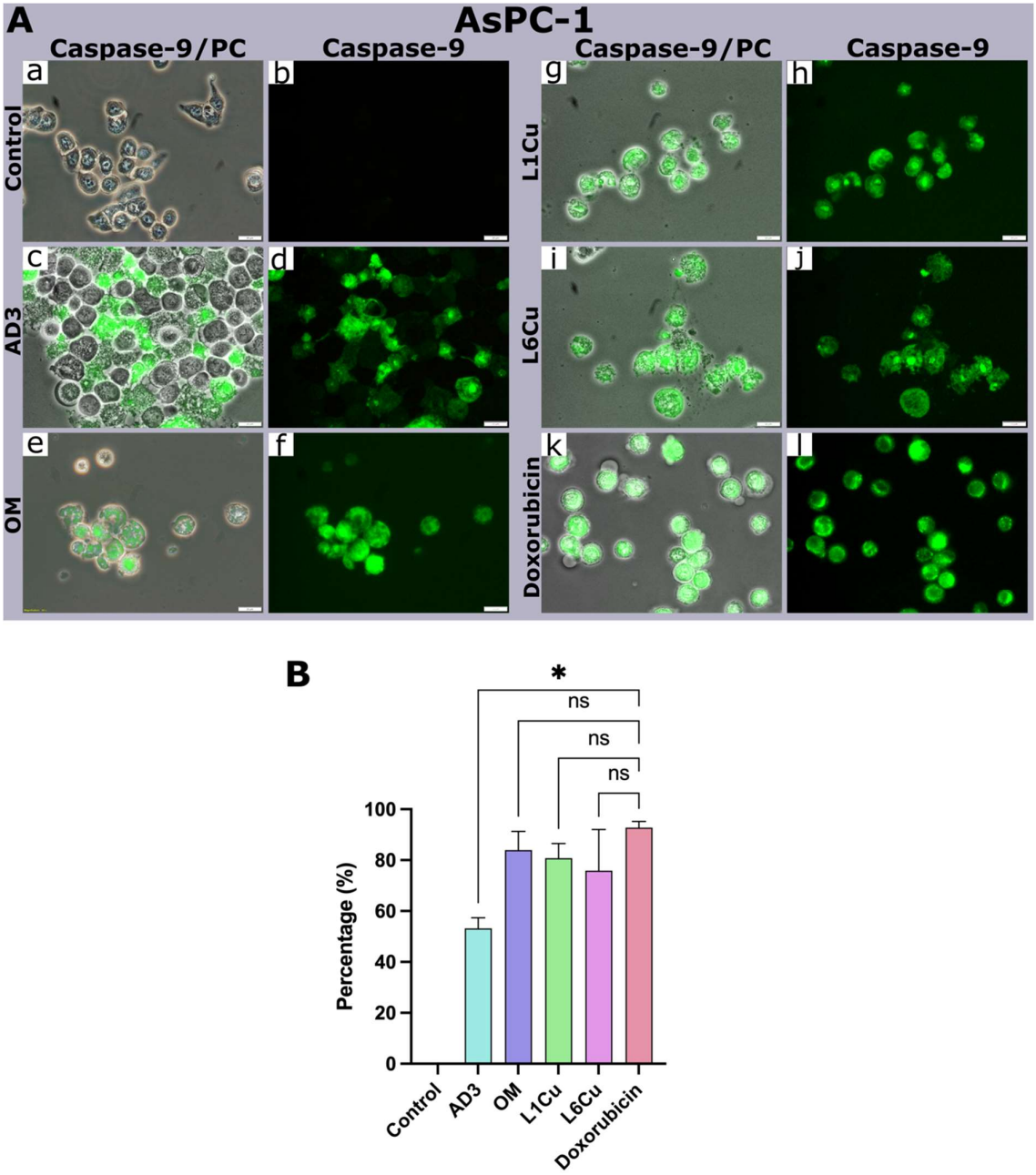


Figure 3.13 Representative photomicrographs (A) and a bar graph (B) showing the effects of the copper complexes on caspase-9 activation in AsPC-1 cells after a 48 h treatment period. A, panel a: untreated cells. A, panel b: AD3 (6 µM). A, panel c: OM (4 µM). A, panel d: L1Cu (2 µM). A, panel e: L6Cu (2 µM). A, panel f: doxorubicin (5 µM). Cells viewed with Olympus BX41 microscope. Images captured with Olympus DP72 camera. Green fluorescence= active caspase-9. Magnification: 400X, scale bar: 20 µm. Each photomicrograph is representative of three independent experiments (n = 3). Each bar represents mean from three independent experiments. Error bars represent SEM. Copper complexes compared to doxorubicin using ANOVA ($p < 0.05$) followed by Dunnett's post hoc multiple comparisons test. Legend: not significant (ns): $p > 0.05$. * = $p \leq 0.05$. PC = phase contrast.

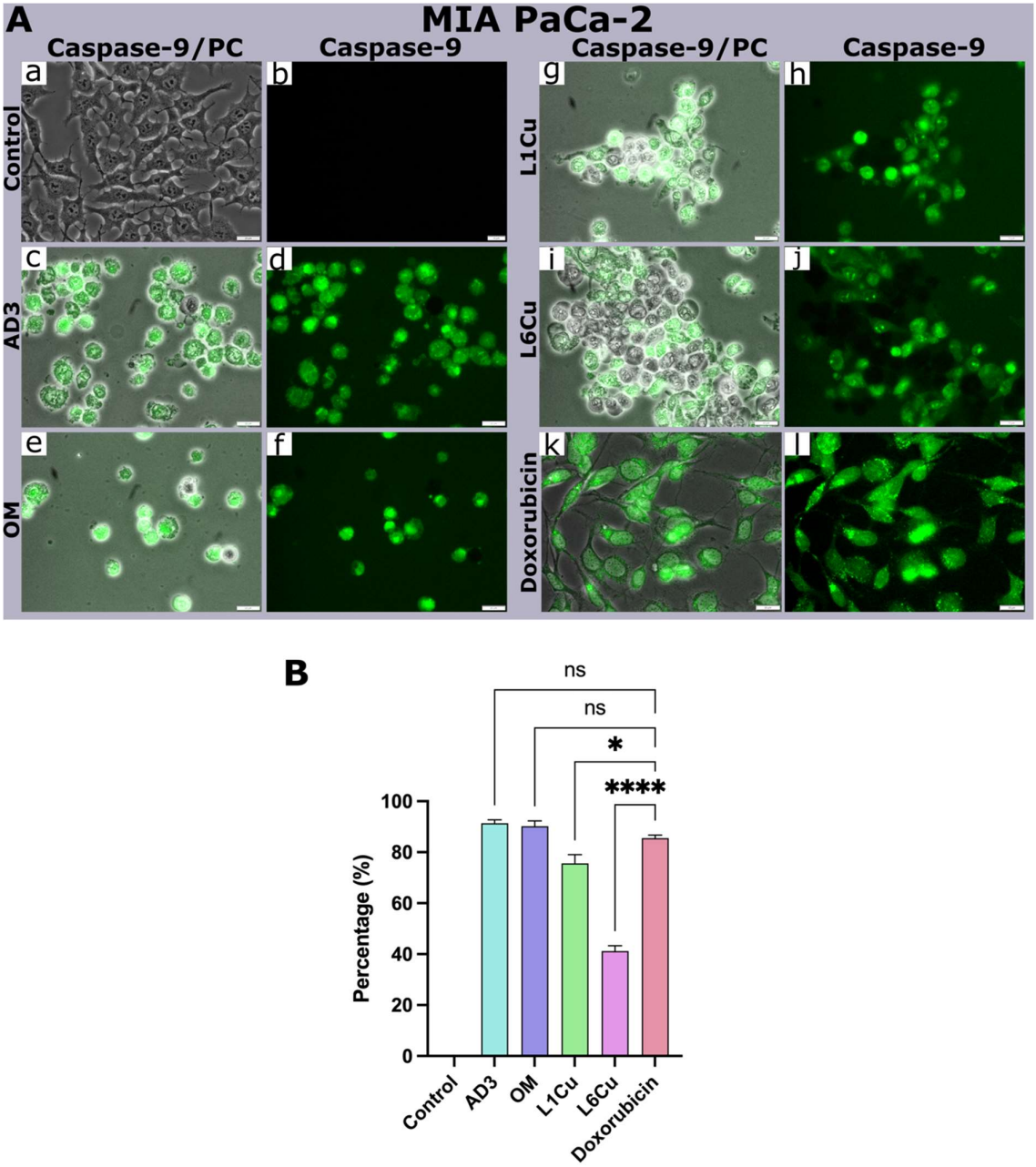


Figure 3.14 Representative photomicrographs (A) and a bar graph (B) showing the effects of the copper complexes on caspase-9 activation in MIA PaCa-2 cells after a 48 h treatment period. A, panel a: untreated cells. A, panel b: AD3 (6 µM). A, panel c: OM (5 µM). A, panel d: L1Cu (2 µM). A, panel e: L6Cu (2 µM). A, panel f: doxorubicin (5 µM). Cells viewed with Olympus BX41 microscope. Images captured with Olympus DP72 camera. Green fluorescence= active caspase-9. Magnification: 400X, scale bar: 20 µm. Each photomicrograph is representative of three independent experiments (n = 3). Each bar represents mean from three independent experiments. Error bars represent SEM. Copper complexes compared to doxorubicin using ANOVA ($p < 0.05$) followed by Dunnett's post hoc multiple comparisons test. Legend: not significant (ns): $p > 0.05$. * = $p \leq 0.05$. **** = $p \leq 0.0001$. PC = phase contrast.

3.6.3 Summary of the effects of the copper complex on caspase-9 activity

The copper complexes activated caspase-9 in both cell lines after 48 hour. Across cell lines, OM, L1Cu and doxorubicin showed similar caspase-9 activity in both the AsPC-1 and MIA PaCa-2 cell lines. However, AD3 and L6Cu were different across the two cell lines. In the AsPC-1 cell line, AD3 was the weakest activator of caspase-9 while in the MIA PaCa-2 cell line, AD3 was the strongest activator. L6Cu had a percentage activation of caspase-9 of 76 % in the AsPC-1 cell line while in the MIA PaCa-2 cell line, the percentage of cells with active caspase-9 dropped to 41 %. However, the activation of caspase-9 by all the complexes supports the activation of the intrinsic apoptotic pathway. The copper complexes were then evaluated for their effect on caspase-3/7 activity in order to confirm apoptosis.

3.7 The effect of the copper complexes on caspase-3/7 activation

Caspase-3 and caspase-7 are executioner caspases involved in the late stages of apoptotic cell death. The effect of the copper complexes on caspase-3/7 activity was determined as described in Section 2.5.2.2. AsPC-1 and MIA PaCa-2 cells were treated with the copper complexes at concentrations equivalent to their IC_{80} values. Due to the lack of caspase-9 activity at 24 hours and since caspase-3/7 activation is a late event during apoptosis, the cells were treated with the copper complexes and doxorubicin for 48 hours. Doxorubicin was used as a positive control at 5 µM. The results from the caspase-3/7 assay are shown in Figures 3.15 and 3.16 for AsPC-1 and MIA PaCa-2, respectively.

3.7.1 The effect of the copper complexes on caspase-3/7 activity in AsPC-1 cells

Caspase-3/7 activity was not observed in untreated AsPC-1 cells (Fig 3.15 A, panels a and b). All the copper complexes and doxorubicin showed the presence of a green fluorescent signal indicating the activation of caspase-3/7 (Fig. 3.15 A, panels c-l). Amongst the copper complexes, OM was the most efficient activator of caspase-3/7 with 67 % of cells showing active caspase-3/7 (Fig. 3.15 A, panels e and f; Fig. 3.15 B). This was followed by AD3 and L6Cu, where active caspase-3/7 was observed in approximately 30 % of the cells (Fig. 3.15 A, panels c, d, i and j; Fig. 3.15 B). L1Cu was the least efficient activator of caspase-3/7, with 16.2 % of the cells showing active caspase-3/7 (Fig. 3.15 A, panel g and h; Fig. 3.15 B). Doxorubicin was the most effective activator of caspase-3/7, with 89.8 % of the cells showing active caspase-3/7 (Fig. 3.15 A, panels k and l; Fig. 3.15 B). Doxorubicin was significantly more effective than the copper complexes in activating caspase-3/7 (Fig. 3.15 B).

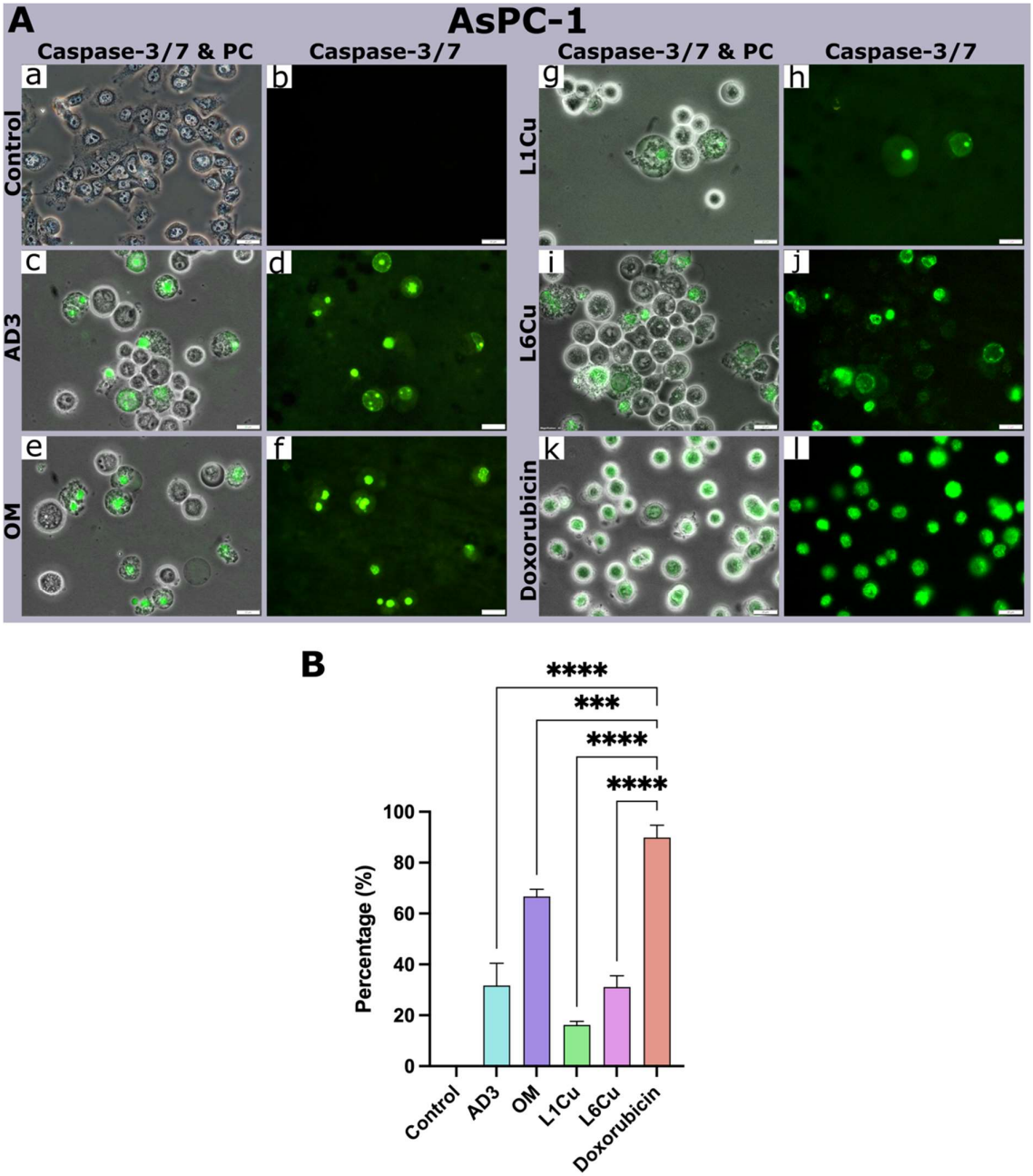


Figure 3.15 Representative photomicrographs (A) and a bar graph (B) showing the effects of the copper complexes on caspase-3/7 activation in AsPC-1 cells after a 48 h treatment period. A, panel a: untreated cells. A, panel b: AD3 (6 µM). A, panel c: OM (4 µM). A, panel d: L1Cu (2 µM). A, panel e: L6Cu (2 µM). A, panel f: doxorubicin (5 µM). Cells viewed with Olympus BX41 microscope. Images captured with Olympus DP72 camera. Green fluorescence= active caspase-3/7. Magnification: 400X, scale bar: 20 µm. Each photomicrograph is representative of three independent experiments (n = 3). Each bar represents mean from three independent experiments. Error bars represent SEM. Copper complexes compared to doxorubicin using ANOVA ($p < 0.05$) followed by Dunnett's post hoc multiple comparisons test. Legend: **** = $p \leq 0.0001$. PC = phase contrast

3.7.2 The effect of the copper complexes on caspase-3/7 activity in MIA PaCa-2 cells

Cells were treated with the copper complexes and doxorubicin for 48 hours. Caspase-3/7 activity was absent in untreated cells (Fig. 3.16 A, panels a and b). The four copper complexes were effective activators of caspase-3/7 in MIA PaCa-2 cells, with copper-complex-treated cells showing more than 88 % of cells with active caspase-3/7 (Fig. 3.16 A, panels c-j). The positive control, doxorubicin, was slightly less effective, with 85 % of cells showing active caspase-3/7 (Fig. 3.16 A, panels k and l; Fig. 3.16 B). Results from three experiments showed that AD3 and L6Cu had the highest percentage of cells (97 % and 98 % of cells, respectively) with active caspase-3/7 (Fig. 3.16 A, panels c, d, i and j; Fig. 3.16 B). This was followed by L1Cu and OM with caspase-3/7 present in 92 % and 88 % of the cells respectively (Fig. 3.16 A, panels e-h; Fig. 3.16 B). AD3 and L6Cu caused statistically significant increases in caspase-3/7 activity compared to doxorubicin (Fig. 3.16 B), while OM and L1Cu activated caspase-3/7 with a similar potency to doxorubicin (Fig. 3.16 B).

3.7.3 Summary of the effects of the copper complexes on caspase-3/7 activity

In the AsPC-1 cell line, OM was the most efficient copper complex to activate caspase-3/7, while AD3, L1Cu and L6Cu were less active with low percentages (16-31 %) of cells with active caspase-3/7. In MIA PaCa-2 cells, AD3 and L6Cu had close to 100 % of cells with active caspase-3/7, while OM and L1Cu had close to 90 % of cells showing active caspase-3/7. Similar to previous assays, the complexes were more effective at activating caspase-3/7 in the MIA PaCa-2 cell line. Doxorubicin was more effective than the copper complexes at activating caspase-3/7 in the AsPC-1 cell line, while AD3 and L6Cu were more effective than doxorubicin in the MIA PaCa-2 cell line. In conclusion, all four copper complexes caused the activation of the intrinsic apoptotic pathway, as confirmed by the induction of active caspase-9 and caspase-3/7 in all treated cells. Additionally, caspase-3/7 functions in the nucleus, and the presence of fragmented nuclei can be seen in treated cells in both cell lines.

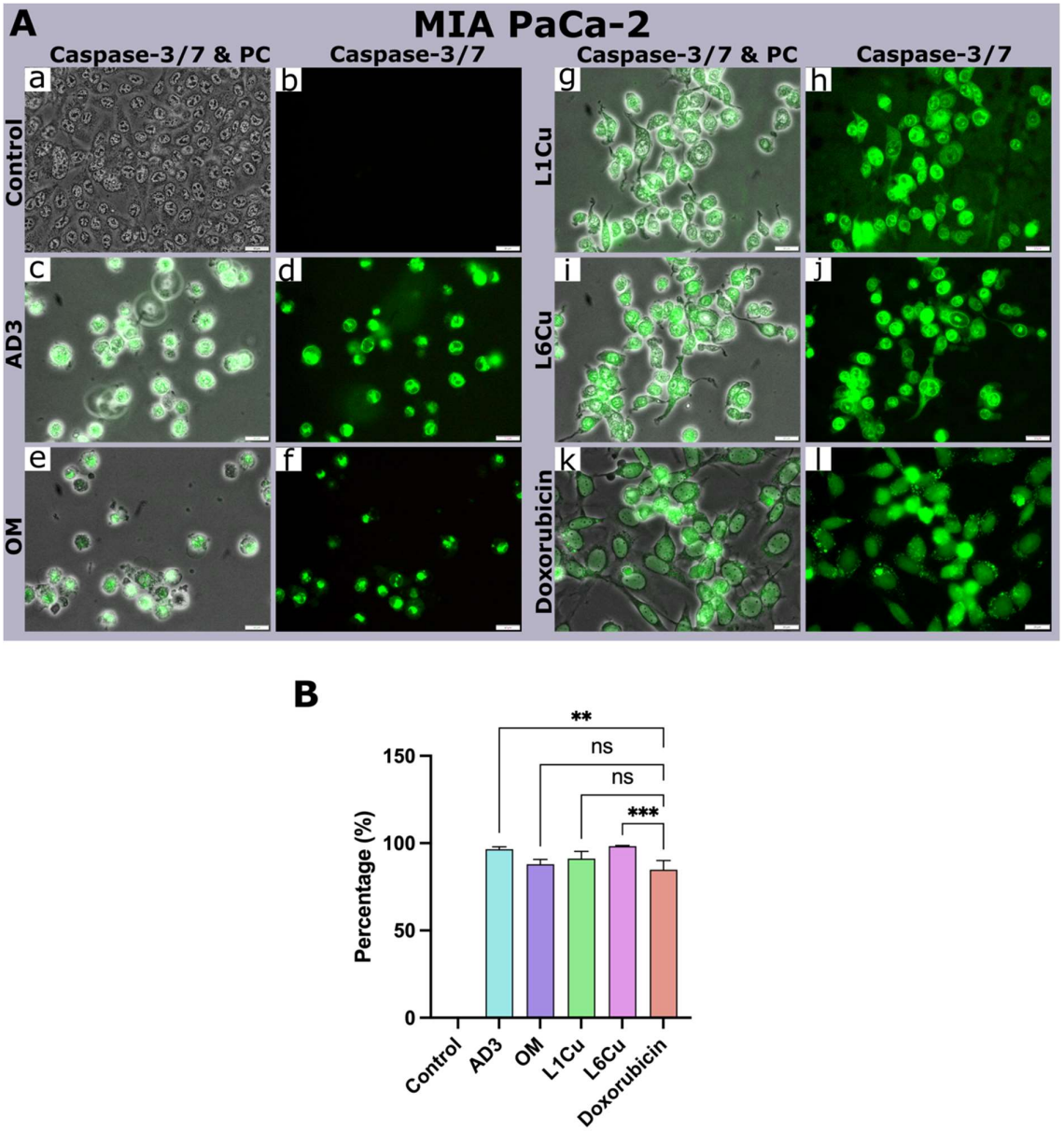


Figure 3.16 Representative photomicrographs (A) and a bar graph (B) showing the effects of the copper complexes on caspase-3/7 activation in MIA PaCa-2 cells after a 48 h treatment period. A, panel a: untreated cells. A, panel b: AD3 (6 µM). A, panel c: OM (5 µM). A, panel d: L1Cu (2 µM). A, panel e: L6Cu (2 µM). A, panel f: doxorubicin (5 µM). Cells viewed with Olympus BX41 microscope. Images captured with Olympus DP72 camera. Green fluorescence= active caspase-3/7. Magnification: 400X, scale bar: 20 µm. Each photomicrograph is representative of three independent experiments (n = 3). Each bar represents mean from three independent experiments. Error bars represent SEM. Copper complexes compared to doxorubicin using ANOVA ($p < 0.05$) followed by Dunnett's post hoc multiple comparisons test. Legend: not significant (ns): $p > 0.05$. ** = $p \leq 0.01$. *** = $p \leq 0.001$. PC = phase contrast.

3.8 The effect of the copper complexes on HMOX1 expression

HMOX1 is overexpressed in PDAC and is associated with treatment failure and poor prognosis of the disease (Ahmad *et al*., 2021). Previous studies have reported an increase in HMOX1 expression following treatment with copper complexes (Harmse *et al*., 2019). Therefore, this study evaluated the effect of the copper complexes on HMOX1 expression in pancreatic cancer cell lines using immunofluorescence and western blot studies.

3.8.1 The effect of the copper complexes on HMOX1 expression in AsPC-1 cells

3.8.1.1 Immunofluorescence studies investigating the effect of the copper complexes on HMOX1 expression in AsPC-1 cells

An immunofluorescence assay was used to evaluate the changes in HMOX1 expression induced by the copper complexes as described in Section 2.7. AsPC-1 cells were treated with the copper complexes at concentrations equivalent to their IC_{80} values, and doxorubicin was used at 5 μM, for 18 hours before incubation with the primary and secondary antibodies. An untreated negative control, where incubation with the primary antibody was omitted, was included to ensure specificity of the secondary antibody and to ensure the absence of non-specific binding. An untreated positive control was incubated with both primary and secondary antibody to show baseline expression of HMOX1 in untreated cells. The photomicrographs of AsPC-1 cells from immunofluorescence assays are shown in Figure 3.17. Fluorescent intensities of individual cells depicting changes in HMOX1 expression compared to the untreated positive control is shown in Table 3.3.

The untreated negative control lacked green fluorescence, confirming the specificity of AlexaFluor® 488 for the anti-HMOX primary antibody only (Fig. 3.17, panels a-c). The untreated positive control showed normal cell morphology and expressed low levels of HMOX1 (Fig. 3.17, panels d-f). Phase contrast images of treated cells are shown in Fig. 3.17, panels g, j, m, p and s. All the copper complexes caused an increase in HMOX1 expression compared to untreated AsPC-1 cells (Fig. 3.17, panels f, i, l, r, o and u). Fluorescence intensity measurements of individual cells showed that AD3, OM and L6Cu caused a very highly significant increase in fluorescent intensity compared to untreated cells (Table 3.3). HMOX1 in untreated cells fluoresced with an intensity of 295.5 ± 15.04 arbitrary units (AU) (Table 3.3). From amongst the copper complexes and doxorubicin, AD3 was the strongest inducer of HMOX1 with the highest average fluorescence intensity signal of 1 082.0 ± 34.1 AU (Fig. 3.17, panel i and Table 3.3). This was followed by L6Cu and OM with a fluorescence intensity

of 848.8 ± 7.1 and 747.5 ± 36.8 AU, respectively (Fig. 3.17, panels l and r; Table 3.3). L1Cu was the weakest inducer of HMOX1, with a fluorescence intensity of 381.2 ± 34.9 AU, which was non-significant compared to untreated cells (Fig. 3.17, panel o; Table 3.3). Doxorubicin-treated cells fluoresced at an intensity of 1 046 ± 18.5 AU, indicating that doxorubicin was the second most potent inducer of HMOX1 expression after AD3 (Fig. 3.17, panel u; Table 3.3).

Colocalization analysis measuring Pearson's correlation coefficient, to determine whether HMOX1 translocated to the nucleus following treatment, was performed between Hoechst 3342 staining and HMOX1 protein staining as described in Section 2.8, using CellProfiler™ Image analysis software. The results indicated a strong positive correlation between HMOX1 and Hoechst 3342 in all treated cells which confirmed the localization of HMOX1 to the nucleus after treatment (Table 3.3). Cells treated with the copper complexes showed an increase in correlation compared to untreated cells indicating that HMOX1 translocated to the nucleus following exposure to the copper complexes (Fig 3.17, panels e, h, k, n, q, t and Table 3.3). Doxorubicin-treated cells had the lowest correlation compared to the copper complexes and untreated cells (Table 3.3), indicating that doxorubicin did not induce the translocation of HMOX1 to the nucleus and there was an increase in cytoplasmic HMOX1 compare to untreated cells.

Table 3.3 The mean fluorescence intensity and nuclear localization of HMOX1 in AsPC-1 cells after treatment with copper complexes and doxorubicin for 18 hours.

Test Compound	Mean Fluorescence Intensity (AU)	p value (significance)	Nuclear localization (PCC)	% Nuclear localization
Control	295.5 ± 15.04		0.767 ± 0.030	76.7
AD3	1 082.0 ± 34.1	p = <0.0001	0.816 ± 0.013	81.6
OM	747.5 ± 36.8	p = <0.0001	0.878 ± 0.016	87.8
L1Cu	381.2 ± 34.9	p = 0.1521	0.867 ± 0.003	86.7
L6Cu	848.8 ± 7.1	p = <0.0001	0.843 ± 0.017	84.3
Doxorubicin	1 046 ± 18.5	p = <0.0001	0.578 ± 0.004	57.8

One-way ANOVA followed by Dunnett's post hoc multiple comparisons test compared fluorescence intensities of copper complexes to untreated cells.
AU = arbitrary units. PCC = Pearson's correlation coefficient

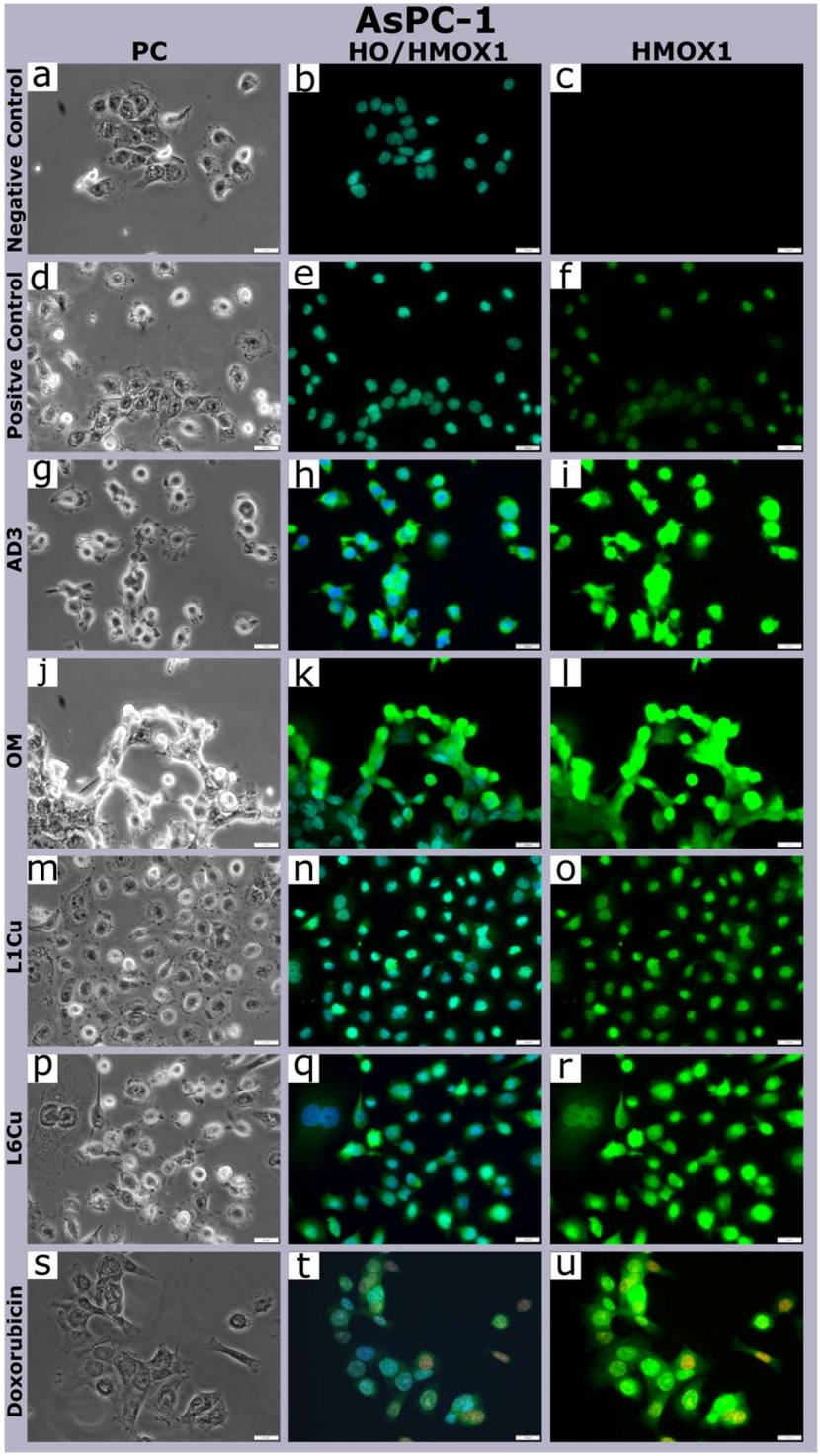


Figure 3.17 Representative photomicrographs of immunofluorescence showing the effects of the copper complexes on HMOX1 expression in AsPC-1 cells after 18 h. A, panel a: untreated cells. A, panel b: AD3 (6 µM). A, panel c: OM (4 µM). A, panel d: L1Cu (2 µM). A, panel e: L6Cu (2 µM). A, panel f: doxorubicin (5 µM). Cells viewed with Olympus BX41 microscope. Images captured with Olympus DP72 camera. Green fluorescence: HMOX1 protein. Blue fluorescence: HO/nuclear staining. Magnification: 400X, scale bar: 20 µm. Each photomicrograph is representative of three independent experiments (n = 3). Legend: PC = Phase contrast. HO = Hoechst 33342. HMOX1 = haem oxygenase-1.

3.8.1.2 Western blot studies investigating the effect of the copper complexes on HMOX1 expression in AsPC-1 cells

Western blot analysis was utilized to verify the results obtained from immunofluorescence studies. Whole cell lysates were prepared from cells treated with the copper complexes for 18 hours at concentrations equivalent to their IC_{80} values as described in Section 2.8. The 18 hour treatment period was selected to assess HMOX1 expression levels before the cells died. Doxorubicin was used as a positive control at 5 μM and an untreated control was included. The HMOX1 western blot on the AsPC-1 cell line and its analysis is shown in Figure 3.18.

A band corresponding to the molecular weight of HMOX1 of low intensity was visible in the untreated sample lane (5.7×10^5 AU) (Fig. 3.18 A and 3.18 B). All four copper complexes caused highly significant ($p < 0.0001$) increases in HMOX1 expression compared to the untreated cells (Fig. 3.18 A and 3.18 B). AD3 and L6Cu caused the highest increases in HMOX1 expression with a 16.3 fold and a 12.6 fold increase in band intensity, respectively, compared to the control (Fig. 3.18 A and 3.18 B). OM caused a 10.2 fold increase in HMOX1 expression and L1Cu was the weakest inducer of HMOX1, with a 3.0 fold increase (Fig. 3.18 A and 3.18 B). The data obtained from the western blot analysis confirmed the immunofluorescence findings on AsPC-1 cells, with AD3 being the strongest inducer of HMOX1; OM and L6Cu having similar effects on HMOX1 expression; while L1Cu was the weakest inducer of HMOX1. Doxorubicin did not induce the expression of HMOX1 as seen in western blot analysis (Fig. 3.18 A and 3.18 B). This did not correlate with doxorubicin's induction of HMOX1 expression observed in immunofluorescence studies. The effect of doxorubicin on HMOX1 is, therefore, inconclusive and requires further investigation.

3.9.2 The effect of the copper complexes on HMOX1 expression in MIA PaCa-2 cells

3.9.2.1 Immunofluorescence studies investigating the effect of the copper complexes on HMOX1 expression in MIA PaCa-2 cells

The immunofluorescence assay was used to evaluate the changes in HMOX1 expression induced by the copper complexes as described in Section 2.7. MIA PaCa-2 cells were treated with the copper complexes at concentrations equivalent to their IC_{80} values, and doxorubicin

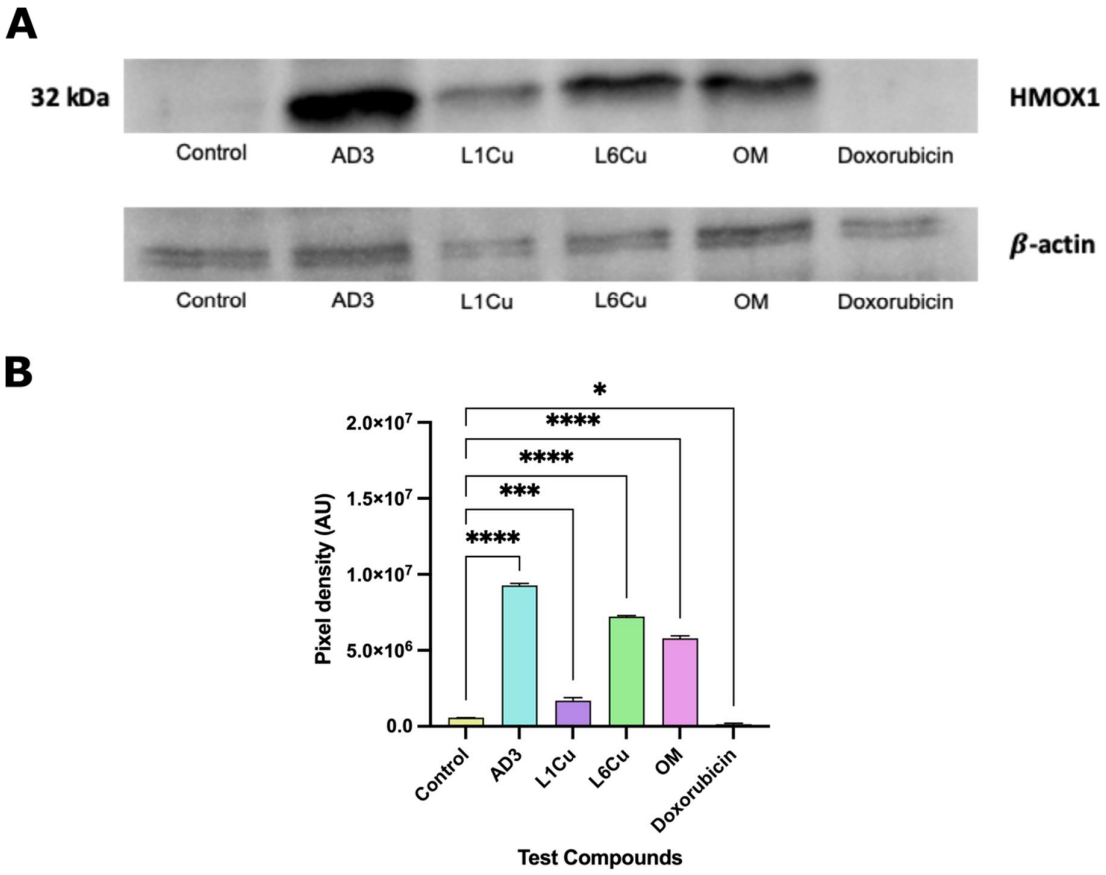


Figure 3.18 Immunoblot of HMOX1 (A) and a graph (B) of the pixel densities of HMOX1 bands in AsPC-1 cells. Cells treated with complexes at concentrations of: AD3 at 6 µM; OM at 4 µM; L1Cu at 2 µM; L6Cu at 2 µM and doxorubicin at 5 µM. Each sample lysate contained 20 µg of protein and were separated on a 12 % denaturing polyacrylamide gel. β-actin used as loading control. Bands detected by chemiluminescence with a Bio-Rad ChemiDoc™ MP Imaging system and blot analysed using Bio-Rad Image Lab software. Results representative of three independent experiments. Error bars represent SEM. Copper complexes compared to untreated sample using ANOVA ($p < 0.05$) followed by Dunnett's post hoc multiple comparisons test. Legend: * = $p \leq 0.05$. *** = $p \leq 0.001$. **** = $p \leq 0.0001$. HMOX1 = haem oxygenase-1. AU = arbitrary units.

was used at 5 µM, for 18 hours before incubation with the primary and secondary antibodies, as for AsPC-1 cells (Section 3.9.1.1 above). The photomicrographs of MIA PaCa-2 cells from immunofluorescence assays are shown in Figure 3.19. Fluorescent intensities of individual cells depicting changes in HMOX1 expression compared to the untreated positive control is shown in Table 3.4.

Green fluorescence was absent from the untreated negative control, confirming the absence of non-specific binding of AlexaFluor ® 488, and its specificity for the secondary antibody (Fig. 3.19, panels a-c). The untreated positive control fluoresced with a weak signal intensity of

173.1 ± 7.6 AU (Fig. 3.19, panels d-f; Table 3.4). Phase contrast images of treated cells are shown in Fig. 3.19, panels g, j, m, p and s. In comparison with untreated cells, all the copper complexes caused a very highly significant ($p < 0.0001$) increase in HMOX1 fluorescence intensity (Fig. 3.19, panels i, l, o, r and u; Table 3.4). Amongst the copper complexes, AD3-treated cells had the strongest fluorescence intensity of 908.4 ± 36.8 AU (Fig. 3.19, panel i and Table 3.4). This was followed by OM and L6Cu with fluorescence intensities of 733.4 ± 8.8 and 558.2 ± 17.9 AU, respectively (Fig. 3.19, panels l and r; Table 3.4). L1Cu had the lowest fluorescence intensity of 496.5 ± 2.2 AU compared to the rest of the copper complexes (Fig. 3.19, panel o; Table 3.4). Doxorubicin induced the lowest fluorescence intensity signal of 360.1 ± 13.3 AU compared to the copper complexes (Fig. 3.19, panel u; Table 3.4).

All the copper complexes and doxorubicin had a strong positive correlation (Pearson's correlation coefficient > 0.5) between Hoechst 3342 and HMOX1 for all treated cells. There was an increase in the correlation coefficient in copper-complex-treated cells compared to untreated cells, indicating that HMOX1 co-localizes with Hoechst 3342 in the nucleus following treatment with the copper complexes (Fig. 3.19, panels h, k, n and q; Table 3.4). Doxorubicin-treated cells had a lower correlation than untreated cells indicating that doxorubicin caused an increase in cytoplasmic HMOX1 compared to control (Fig. 3.19, panel t; Table 3.4).

Table 3.4 The mean fluorescence intensity and nuclear localization of HMOX1 in MIA PaCa-2 cells after treatment with copper complexes and doxorubicin for 18 hours.

Test Compound	Mean Fluorescence Intensity (AU)	p value (significance)	Nuclear localization (PCC)	% Nuclear localization
Control	173.1 ± 7.6		0.721 ± 0.043	72.1
AD3	908.4 ± 36.8	p = < 0.0001	0.899 ± 0.021	89.9
OM	733.4 ± 8.8	p = < 0.0001	0.879 ± 0.004	87.9
L1Cu	496.5 ± 2.2	p = < 0.0001	0.888 ± 0.012	88.8
L6Cu	558.2 ± 17.9	p = < 0.0001	0.869 ± 0.010	86.9
Doxorubicin	360.1 ± 13.3	p = 0.0005	0.590 ± 0.014	59.0

One-way ANOVA followed by Dunnett's post hoc multiple comparisons test was compared fluorescence intensities of copper complexes to untreated cells.
AU = arbitrary units. PCC = Pearson's correlation coefficient.

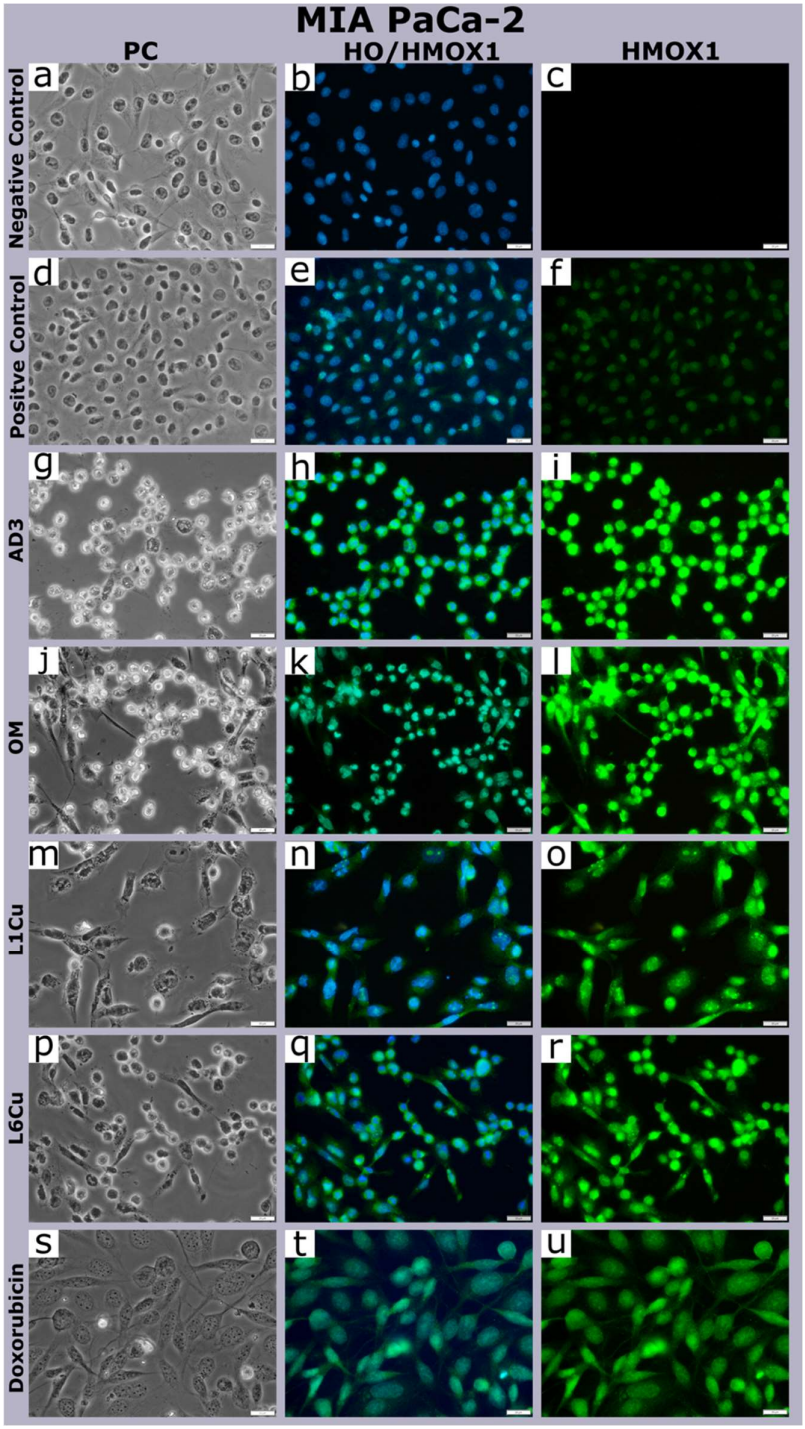


Figure 3.19 Representative photomicrographs of immunofluorescence showing the effects of the copper complexes on HMOX1 expression in MIA PaCa-2 cells after 18 h treatment. A, panel a: untreated cells. A, panel b: AD3 (6 μM). A, panel c: OM (5 μM). A, panel d: L1Cu (2 μM). A, panel e: L6Cu (2 μM). A, panel f: doxorubicin (5 μM). Cells viewed with Olympus BX41 microscope. Images captured with Olympus DP72 camera. Green fluorescence: HMOX1 protein. Blue fluorescence: HO/nuclear staining. Magnification: 400X, scale bar: 20 μm. Each photomicrograph is representative of three independent experiments (n = 3). Legend: PC = Phase contrast. HO = Hoechst 33342. HMOX1 = haem oxygenase-1.

3.9.2.2 Western blot studies investigating the effect of the copper complexes on HMOX1 expression in MIA PaCa-2 cells

Western blot studies were utilized to verify the results obtained from immunofluorescence studies, and was performed as for AsPC-1 cells (3.9.2 above). Samples were prepared from whole cell lysates of cells treated with the copper complexes for 18 hours at concentrations equivalent to their IC_{80} values as described in Section 2.8. Doxorubicin was used as a positive control at 5 μM and an untreated control was included. The HMOX1 blot obtained from western blot analysis on MIA PaCa-2 cells is presented in Figure 3.20.

A low intensity band (3.2×10^5 AU) was visible in the control lane (Fig. 3.20 A and 3.20 B). AD3, OM and L6Cu showed highly significant ($p < 0.001$) increases in HMOX1 expression compared to untreated cells (Fig. 3.20 A and 3.20 B). AD3 was the strongest inducer of HMOX1 with a significant 37.5 fold increase in HMOX1 expression (Fig. 3.20 A and 3.20 B). The second most potent inducer of HMOX1 was OM (20.9 fold increase from the control) followed by L6Cu with a significant 6.6 fold increase compared to the control. L1Cu induced a significant ($p = 0.0004$) 4.4 fold increase when compared with the control (Fig. 3.20 A and 3.20 B). Western blot analysis confirmed the immunofluorescence studies regarding the effects of the copper complexes on HMOX1 expression. The HMOX1 band for doxorubicin was absent, indicating that doxorubicin did not induce HMOX1 expression (Fig. 3.20 A). This did not correlate with immunofluorescence studies, where doxorubicin-treated cells showed an increase in HMOX1 expression. The effect of doxorubicin on HMOX1 is, therefore, inconclusive and requires further investigation.

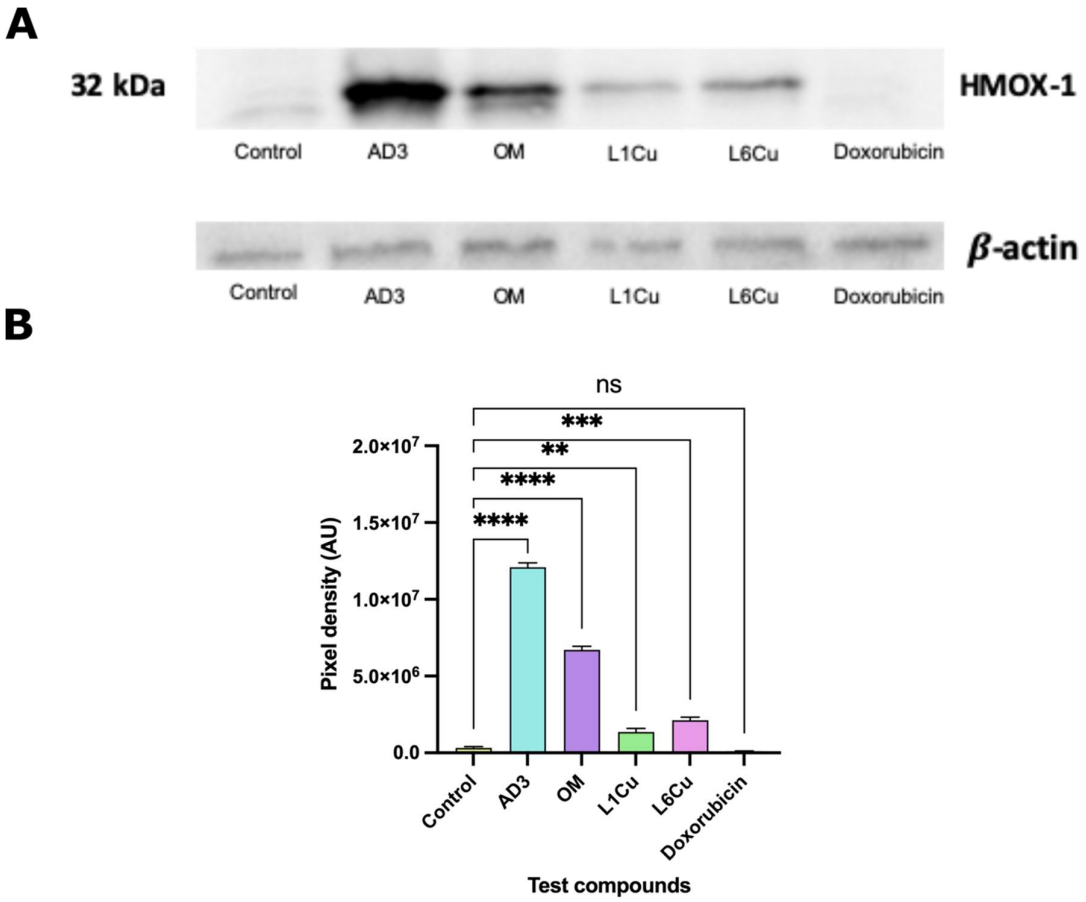


Figure 3.20 Immunoblot of HMOX1 (A) and a graph (B) of the pixel densities of HMOX1 bands in MIA PaCa-2 cells. Cells treated with complexes at concentrations of: AD3 at 6 µM; OM at 5 µM; L1Cu at 2 µM; L6Cu at 2 µM and doxorubicin at 5 µM. Each sample lysate contained 20 µg of protein and was separated on a 12 % denaturing polyacrylamide gel. β-actin used as loading control. Bands detected by chemiluminescence with Bio-Rad ChemiDoc™ MP Imaging system and blot analysed using Bio-Rad Image Lab software. Results representative of three independent experiments. Error bars represent SEM. Copper complexes compared to untreated sample using ANOVA ($p < 0.05$) followed by Dunnett's post hoc multiple comparisons test. Legend: not significant (ns): $p > 0.05$. ** = $p \leq 0.01$. *** = $p \leq 0.001$. **** = $p \leq 0.0001$. HMOX1 = haem oxygenase-1. AU = arbitrary units.

3.10 The effect of HMOX1 inhibition on the IC_{50} values of copper complexes in AsPC-1 and MIA PaCa-2 cells

Immunofluorescence and western blot studies confirmed that the copper complexes caused an increase in the expression of HMOX1. Therefore, combination cell viability experiments were done to determine the effect of HMOX1 inhibition on the IC_{50} values of the copper complexes (Table 3.4 and 3.5). OB24 hydrochloride (OB24 HCl), a selective small-molecule HMOX1 inhibitor (Alaoui-Jamali *et al*., 2009), was tested in combination with the copper complexes. Cells were exposed to the copper complexes at a range of concentrations as was done for the

determination of the IC_{50} values of the complexes, in the presence of a constant concentration of 20 µM OB24 HCl. The concentration at which OB24 HCl inhibits 50 % of HMOX1 enzyme activity is approximately 11.66 µM (6.5 µmol/L) (Alaoui-Jamali *et al*., 2009). Therefore, OB24 HCl was used at a constant concentration of 20 µM.

3.10.1 The effect of OB24 HCl on the cell viability of AsPC-1 and MIA PaCA-2 cell line

OB24 HCl was tested at concentrations of 5-, 40-, 100- and 200 µM, alone, using a 48 hour MTT as described in Section 2.4. OB24 HCl did not show significant cytotoxic activity against either cell line, and at 20 µM, OB24 HCl showed marginal effects on cytotoxicity (Fig. 3.21 A). The chemical structure of OB24-HCl is shown in Fig. 3.21 B.

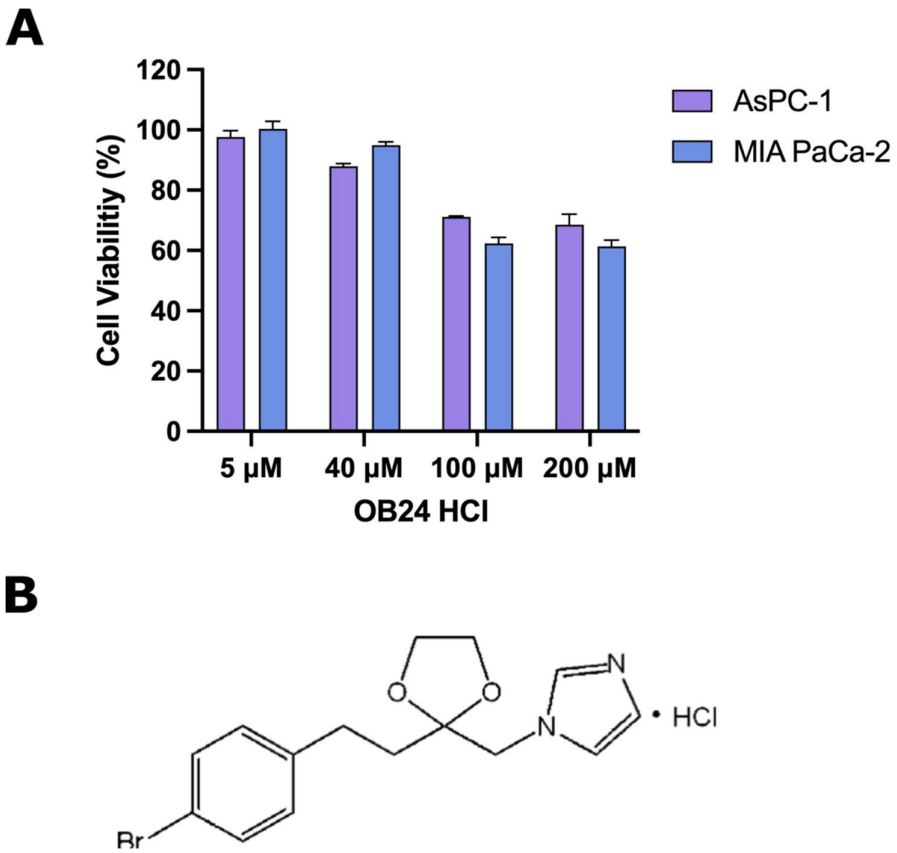


Figure 3.21 Graph (A) showing cell viability (%) of AsPC-1 and MIA PaCa-2 cells treated with OB24 HCl only and structure of OB24 HCl (B). AsPC-1 and MIA PaCa-2 cells treated with 200-, 100-, 40- and 5 µM OB24 HCl for 48 h and cell viability was measured with MTT assay. Each bar represents mean of at least four replicate values. Error bars represent SEM. Experiments were repeated three independent times. OB24 HCl chemical structure shown in B. (OB24 HCl: OB24 hydrochloride).

3.10.2 The effect of the combination of OB24 HCl and the copper complexes on the cell viability of AsPC-1 and MIA PaCa-2 cells

In both AsPC-1 and MIA PaCa-2cells, all the copper complexes displayed a statistically significant decrease in their IC_{50} values when viability was determined in the presence of 20 μM OB24 HCl (Table 3.5 and Table 3.6). In AsPC-1 cells, AD3 showed a 0.89-fold decrease in its IC_{50} value when combined with OB24 HCl, with a p value of 0.0108 (*) (Table 3.5). OM showed a very highly significant 2.72-fold decrease in its IC_{50} value with a p value of <0.0001 (****). L1Cu had a 7.8-fold decrease and L6Cu had a 6.7-fold decrease in IC_{50} values with p values of 0.0216 (*) and 0.0022 (**), respectively.

In the MIA PaCa-2 cell line, AD3 and OM showed very highly significant fold-decreases of 2.2 and 1.5-fold, respectively, with p values of <0.0001 (****) (Table 3.5). L1Cu and L6Cu both showed fold-decreases of 1.8, with p values of 0.0404 (*) and 0.0363 (*), respectively (Table 3.6).

Table 3.5 The IC_{50} values of copper complexes alone and in combination with 20 μM of a HMOX1 inhibitor, OB24 HCl, in AsPC-1 cells

Copper complex	IC_{50} concentration (μM): without OB24 HCl	IC_{50} concentration (μM): with OB24 HCl	P value (significance)
AD3	3.15 ± 0.07 μM	2.79 ± 0.04 μM	p = 0.0108
OM	2.75 ± 0.14 μM	1.01 ± 0.10 μM	p = <0.0001
L1Cu	1.41 ± 0.33 μM	0.18 ± 0.03 μM	p = 0.0216
L6Cu	1.27 ± 0.22 μM	0.19 ± 0.04 μM	p = 0.0022

Student's t test was performed comparing IC_{50} values of copper complexes with and without OB24 HCl.

Table 3.6 The IC_{50} values of copper complexes alone and in combination with 20 μM of a HMOX1 inhibitor, OB24 HCl, in MIA PaCa-2 cells

Copper complex	IC_{50} concentration (μM): without OB24 HCl	IC_{50} concentration (μM): with OB24 HCl	P value (significance)
AD3	4.04 ± 0.07 μM	1.83 ± 0.15 μM	p = < 0.0001
OM	3.62 ± 0.08 μM	2.45 ± 0.07 μM	p = < 0.0001
L1Cu	1.08 ± 0.15 μM	0.59 ± 0.05 μM	p = 0.0404
L6Cu	1.39 ± 0.16 μM	0.77 ± 0.16 μM	p = 0.0363

Student's t test was performed comparing IC_{50} values of copper complexes with and without OB24 HCl.

The observed decreases in the IC_{50} values of the copper complexes after combination with OB24 HCl were statistically significant. Given that OB24 HCl did not display cytotoxic activity on its own against the cell lines, it can be concluded that the observed decrease was not due to the cytotoxic activity of OB24 HCl, but due to its inhibition of HMOX1. The results indicate that HMOX1-inhibition sensitized the pancreatic cancer cell lines to the copper complexes.

Chapter IV: Discussion

4.1 Introduction

This study evaluated and compared three classes of copper complexes for their potential cytotoxic effects against AsPC-1 and MIA PaCa-2 pancreatic cancer cell lines. In order to progress the development of copper complexes as potential anti-cancer agents in the preclinical stage, studies on their mechanism of cell death are required. Therefore, the mechanism of cell death of the active complexes was investigated further using various cell death related assays. HMOX1 is implicated in treatment failure of chemotherapy (Bukowska-Strakova *et al*., 2021). Therefore, the effects of the complexes on HMOX1 protein expression was evaluated using immunofluorescence and western blot studies. The lastly, the effect of a HMOX1-inhibitor, OB24 HCl on the cytotoxicity of the copper complexes were investigated.

4.2 The cytotoxic effects of the copper complexes on AsPC-1 and MIA PaCa-2 cells

This study evaluated four copper complexes plus their respective copper-free ligands for their cytotoxic potential using the MTT cell viability assay. The copper complexes consisted of a copper-theophylline-phenanthroline complex (AD); a copper-8-aminoquinoline-naphthyl complex (OM); and copper-isoindoline complexes (LCu). The initial evaluation showed that complexes AD3, OM, L1Cu, and L6Cu had less than 50 % cell viability at 5 µM and less than 1 % cell viability at 50 µM. The copper-free ligands did not show efficient inhibition of cell viability and were not investigated further.

Gemcitabine and doxorubicin were evaluated for their effect on AsPC-1 and MIA PaCa-2 cell viability in order to select a positive control for this study. Gemcitabine is used clinically to treat PDAC as neoadjuvant chemotherapy, adjuvant chemotherapy and for metastatic disease. Therefore, gemcitabine was initially evaluated against AsPC-1 and MIA PaCa-2 cell lines at concentrations of 50- and 5- µM using a 48 hour MTT assay. Doxorubicin is commonly used as a positive control in in-house studies and was therefore also selected for initial evaluation at the same concentrations. Gemcitabine exhibited poor cytotoxic activity at both concentrations while doxorubicin demonstrated sufficient growth inhibition at 50 µM. Consequently, doxorubicin was selected as a positive control for this study.

Gemcitabine is a deoxycitidine analog used to treat various sold tumors. Gemcitabine is hydrophilic and does not cross the cell membrane by diffusion. Instead, gemcitabine requires

membrane nucleoside transporters to facilitate its entry into the cell. Upon entry into the cell, gemcitabine requires stepwise activation to its diphosphate and triphosphate metabolites. Active gemcitabine triphosphate incorporates into DNA, thereby disrupting DNA synthesis of cancer cells. Additionally, gemcitabine diphosphate inhibits ribonucleotide reductase, preventing the formation of deoxyribonucleotides and hence, de novo DNA synthesis. Doxorubicin is an anthracycline used to treat multiple cancers including breast, gastric and lung cancers, among others. Doxorubicin acts by intercalating into DNA; inhibiting topoisomerase-II; and generating free radicals which cause DNA damage (Wellstein and Sausville, 2023). Doxorubicin readily crosses the cell membrane and does not require activation, which is likely the reason for the differences in activity of gemcitabine and doxorubicin at the same treatment period of 48 h. Most studies employed a 72 h MTT when testing gemcitabine, indicating that gemcitabine requires more time to exert its effects (Xu *et al*., 2016; Huanwen *et al*., 2009). Therefore, doxorubicin was a more suitable choice as a positive control in this study.

Doxorubicin had an IC_{50} value of 14.6 $\pm$ 1.2 µM in the MIA PaCa-2 cell line using a 24 hour MTT (Nurcahyanti and Wink, 2016), which is similar to the IC_{50} value of 12.1 $\pm$ 0.6 µM obtained using a 48 hour MTT in this study. In contrast, doxorubicin was reported to have an IC_{50} value of 0.4 µM in the AsPC-1 cell line, obtained using a luciferase-based assay (Graeser *et al*., 2009). This was inconsistent with the value of 6.6 $\pm$ 0.1 µM obtained in this study, for the same cell line. However, due to the difference in methods used and the lack of information pertaining to the treatment period, comparisons of the IC_{50} values are not possible.

IC_{50} values were obtained for the selected copper complexes. The National Cancer Institute considers IC_{50} values below 10 µM as clinically relevant and is used as the selection criteria for novel cancer drugs to be developed further (Kumar *et al*., 2016). All four complexes had clinically relevant IC_{50} values of below 5 µM.

In both cell lines, the copper complexes had highly significantly lower IC_{50} values than the positive control, doxorubicin, indicating that the copper complexes were more active than doxorubicin. In the AsPC-1 cell line, the IC_{50} values ranged from 3.15 µM to 2.74 µM for AD3 and OM, respectively, while L1Cu and L6Cu had IC_{50} values of 1.41 µM and 1.27 µM,

respectively. In the MIA PaCa-2 cell line, AD3 and OM had IC_{50} values of 4.04 μM and 3.62 μM, respectively, while L1Cu and L6Cu had values of 1.08 μM and 1.39 μM, respectively. The IC_{50} values were obtained from sigmoidal dose-response curves of the percentage cell survival when cells were treated with a range of concentrations of the complexes. The dose-response curves enabled the calculation of the IC_{80} values of the complexes, which is the concentration at which the complexes were tested throughout this study. An IC_{80} value was selected since the aim of cancer drug treatment is to affect a 100 % cell-kill (Swinney, 2011). Therefore, the effects of the copper complexes on cell death mechanisms were studied at their IC_{80} values throughout this study.

The IC_{50} values reported in this study are comparable to published IC_{50} values of copper complexes in various cancer cell lines (summarised in Table 4.1). Using a 48 h MTT (as for this study), Dam *et al*. (2017) reported IC_{50} values of copper-imidazo[1,2-*a*]pyridines below 10 μM against breast, colorectal and leukaemic cell lines while the imidazo[1,2-*a*]pyridines and their complexes with zinc showed poor activity against the same cell lines. The copper-imidazo[1,2-*a*]pyridines had IC_{50} values ranging between 1.7- and 5.4- μM (Dam *et al*., 2017), which is higher than the IC_{50} values of the copper-phthalimide complexes (LCu) used in this study, but comparable to the IC_{50} values of the copper-phenanthroline-theophylline (AD3) and the copper-8-aminoquinoline-naphthyl (OM) complexes. Sigman *et al*., (1979) first discovered the ability of a copper-phenanthroline complex to target DNA by inducing oxidative damage and acting as an artificial nuclease. Since then, extensive studies on copper-phenanthroline complexes have been shown to possess anticancer activity with low micromolar IC_{50} values (reviewed in Masuri *et al*., 2022). In a study on the MIA PaCa-2 cell line, a 5 day exposure to a Cu-phenanthroline based complex resulted in an IC_{50} value of 2.97 μM (Fantoni *et al.,* 2021). The complex also demonstrated the ability to bind to the minor groove of DNA (Fantoni *et al.,* 2021). AD3, the same copper complex that was used in this study, was reported to have IC_{50} values of below 5 μM in lung, breast, colorectal and glioblastoma cell lines (Gordon *et al*., 2022). The IC_{50} value reported for AD3 in MIA PaCa-2 cells was 2.44 ± 0.13 μM (Gordon *et al*., 2022), compared to the 4.04 ± 0.07 μM obtained in this study. Reasons for discrepancies were possibly due to the instability of the complex upon storage, as AD3 had a tendency to precipitate when stored at 4 ºC as well as at room temperature. This may have caused its reduced efficacy. Further investigations regarding the stability of this complex are required. In a another study on MCF-7 breast adenocarcinoma cells treated with two polypyridyl-based

copper (II) complexes, IC_{50} values of 4.57 μM and 1.98 μM were reported after a 24 h MTT (Salimi *et al*., 2015). The two polypyridyl-based copper (II) complexes were more active than the positive control, cisplatin (Salimi *et al*., 2015). Numerous studies have reported low micromolar IC_{50} values of copper complexes on a variety of cancer cell lines, however, direct comparisons are not always possible due to variations in cell viability studies and exposure times employed (C. Wang *et al*., 2023). The low IC_{50} values obtained for the copper complexes in this study contribute to the expanding literature showing the potential for copper complexes as anticancer agents.

Table 4.1 IC_{50} values of copper complexes from various studies, using the MTT assay.

Copper complex	Cell line	IC_{50} concentration (μM)	Treatment period	Reference
Cu(I)/triphenylphosphine-naphthoquinone	MDA-MB-231 MCF-7 A549	5.5 ± 0.3 15 ± 3 3.6 ± 0.3	48 h	Leite *et al*. (2023)
Copper-phenanthroline triphenylphosphine	HeLa SKOV-3 HK-2	7.32 ± 1.35 6.56 ± 1.28 21.57 ± 1.26	48 h	Shi *et al*. (2018)
[{Cu(phen)$_2$}$_2$(terph)](terph) Where terph= terephthalic acid	MCF-7 DU145 HT-29	7.9 ± 0.4 5.7 ± 0.2 5.4 ± 0.3	24 h	Kellet *et a*l. (2011)
Cu(II)(L)(Cl) [Cu(II)$_2$(L)$_2$(NO$_3$)$_2$] [Cu(II)$_2$Cu(I)(L)$_2$(Br)$_3$] Where L= dithiocarbazate Schiff-base ligand	AsPC-1 PANC-1 AsPC-1 PANC-1 AsPC-1 PANC-1	4.39 ± 0.58 4.73 ± 0.48 0.46 ± 0.05 0.73 ± 0.08 0.41 ± 0.05 0.62 ± 0.05	48 h	Y. Guo *et al.* (2021)
Copper-imidazo[1,2-a]pyridines: Compound 21 Compound 29	 HT-29 MCF-7 MDA-MB-231 K562 HL-60 HT-29 MCF-7	 0.79 ± 0.02 0.62 ± 0.03 28 ± 2 1.9 ± 0.9 2.2 ± 0.5 1.6 ± 0.3 1.20 ± 0.08	48 h	Dam *et al.,* (2017)

	MDA-MB-231 K562 HL-60	2.4 ± 0.4 6.0 ± 0.4 2.1 ± 0.3		
Copper-phenanthroline-theophylline (AD3)	SF-268 SH-SY5Y MIA PaCa-2 A549 MDA-MB-231 MCF7 HT-29	3.17 ± 0.17 1.74 ± 0.26 2.44 ± 0.13 4.9 ± 0.37 1.5 ± 0.05 2.63 ± 0.18 3.1 ± 0.26	48 h	Gordon *et al*. (2022)

4.3 The effects of the copper complexes on the morphology of AsPC-1 and MIA PaCa-2 cells

Apoptosis is characterized by the condensation of nuclear material, nuclear fragmentation (karyorrhexis), rounding up of the cell, decrease in cellular volume (pyknosis), membrane blebbing and the retraction of pseudopodes (Galluzzi *et al*., 2018). HO, AO and PI were used to assess the effects of the copper complexes on the morphology of the cells. The changes observed in the morphology of treated cells are summarized in Table 4.2. HO is a membrane permeant dye that binds to the minor groove of DNA and indicates the health status of the nuclei (Chazotte, 2011). Toné *et al*. (2007) classified the nuclear changes of apoptotic cells into three stages. Stage I is called "ring condensation" and involves the condensation of the cells' chromatin along the periphery of the nuclear membrane. The nuclear membrane remains intact during this state. "Necklace condensation" defines stage II, wherein the chromatin forms irregular, discontinuous fragments that are visible as bead-like structures, throughout the nucleus. Necklace condensation is termed karyorrhexis. Stage III involves nuclear collapse or disassembly. The chromatin shrinks into a compacted structure while the structural integrity of the nuclear envelope is lost (Toné *et al*., 2007). Chromatin condensation begins at the periphery and progresses to include the entire nucleus (Galluzzi *et al*., 2015). Untreated AsPC-1 and MIA PaCa-2 cells stained homogenously blue with HO, indicating normal nuclei. Ring condensation, necklace condensation and chromatin collapse was observed in the nuclei of all treated cells, suggesting that the copper complexes caused apoptosis.

In healthy cells, PI is unable to cross the cell membrane. Necrotic cells have a compromised cell membrane which allows for the entry of PI into the cells, staining the nuclei of these cells red. Therefore, PI is used as an indicator for necrosis (Dengler *et al*., 1995). None of the

untreated AsPC-1 and MIA PaCa-2 cells, or the copper-complex-treated cells displayed red nuclei, confirming the absence of PI staining and hence, necrotic cells. AO is useful in identifying lysosomes and endosomes. AO accumulates in acidic compartments and causes lysosomes to fluoresce bright red, while endosomes fluoresce with a bright green signal (Darzynkiewicz *et al*., 1992; Pierzyńska-Mach *et al*., 2014). Lysosomes are membrane-bound acidic vesicles that contain hydrolytic enzymes involved in the degradation of proteins, lipids, polysaccharides and nucleic acids. Lysosomes are involved in endocytosis, phagocytosis and autophagy (Bonam *et al*., 2019). Lysosomes were observed most prominently in AsPC-1 cells treated with AD3, L6Cu and doxorubicin. Increased acidification and the perinuclear localization of lysosomes (as observed in AD3- and doxorubicin-treated cells) is suggestive of cellular stress and is an initial indicator for autophagy (Yim and Mizushima, 2020). Endosomes are a collection of cytoplasmic vesicles that organize the intracellular components of the cell, either for re-uptake by the plasma membrane; or for degradation by lysosomes (Mellman, 1996). Endosomes were seen in untreated and treated AsPC-1 cells, as well as in L1Cu- and L6Cu-treated MIA PaCa-2 cells.

The formation of cytoplasmic vacuoles are implicated in autophagy and paraptosis and is an indicator of cell stress (Kessel and Reiners, 2019). Cytoplasmic vacuoles were seen in MIA PaCa-2 cells treated with AD3, OM, L1Cu and L6Cu, indicating that the cells were in a stressed state. Membrane blebbing is a characteristic of apoptosis whereby protrusions form in the plasma membrane (Stillwell, 2016). This is caused by the contraction of actin-myosin filaments in the cytoskeleton (Coleman *et al*., 2001). Membrane blebbing was seen in phase contrast images of AsPC-1 cells treated with AD3, OM and doxorubicin. The blebs seen in phase contrast images stained with AO confirmed that they were extensions of the cell membrane. Membrane blebbing was not observed in MIA PaCa-2 treated cells, but the cells adopted a rounded appearance, indicating their imminent detachment from the growth surface.

4.4 The effect of the copper complexes on phosphatidylserine exposure in AsPC-1 and MIA PaCa-2 cells

Phosphatidylserine is a phospholipid normally found in the inner leaflet of the plasma membrane. During apoptosis, phosphatidylserine translocates to the outer leaflet of the plasma membrane, allowing for the recognition and subsequent engulfment of the apoptotic cell by macrophages (Logue *et al*., 2009). Annexin-V binds to exposed phosphatidylserine with high

affinity (Logue *et al*., 2009). Alexa Fluor® 488-tagged annexin-V fluoresces with a bright green signal, allowing the detection of cells with annexin-V bound to phosphatidylserine.

AsPC-1 and MIA PaCa-2 cells were treated with the copper complexes at concentrations equivalent to their IC_{80} values and doxorubicin was evaluated at 5 μM. After a 24 hour treatment period, all the cells treated with the four copper complexes showed annexin-V binding in both cell lines. In AsPC-1 cells, the binding of annexin-V only, without PI-staining suggested early apoptosis. MIA PaCa-2 cells showed annexin-V-only staining as well as staining with annexin-V and PI, indicating the presence of late apoptotic or secondary necrotic cells. Secondary necrotic cells refers to circulating dead cells that have lost their cell membrane integrity due to the length of the treatment period since phagocytes, which are responsible for the removal of apoptotic cells, are not present in cell culture (Galluzzi and Kroemer, 2017). The presence of secondary necrotic cells in MIA PaCa-2-treated cells suggested that MIA PaCa-2 cells responded faster to all four copper complexes than AsPC-1 cells. In both cell lines, L6Cu was the most effective inducer of annexin-V whilst L1Cu was the least effective. Doxorubicin was more effective in AsPC-1 cells, with 95 % of the cells showing annexin-V binding compared to the 31 % in MIA PaCa-2 cells. This correlated with the lower IC_{50} value obtained for doxorubicin in AsPC-1 cells compared with MIA PaCa-2 cells. In AsPC-1 cells, doxorubicin was significantly more efficient than the copper complexes in causing annexin-V binding in AsPC-1 cells, while in MIA PaCa-2 cells, doxorubicin was minimally more active than L6Cu in causing annexin-V binding.

Numerous studies have reported the ability of copper complexes to induce phosphatidylserine exposure to the outer cell membrane leaflet. Copper-imidazo[1,2-*a*]pyridines induced annexin-V binding in leukaemic cell lines (Ismail *et al*., 2022) as well as in colorectal cancer cell lines (Harmse *et al*., 2019). Additionally, polypyridyl based copper (II) complexes demonstrated annexin-V binding in breast cancer cells (Salimi *et al*., 2015). Ternary copper (II) complexes with reduced Schiff base ligands and heterocyclic bases, which also included a phenanthroline-based copper complex, were able to induce annexin-V binding in human lung, oesophageal and gastric cancer cell lines (Ma *et al*., 2015).

4.5 The effect of the copper complexes on the formation of reactive oxygen species in AsPC-1 and MIA PaCa-2 cells

ROS are highly reactive molecules that have an unpaired electron in their outer shell, enabling them to readily partake in chemical reactions (Liou and Storz, 2010). ROS are generated during oxidative phosphorylation and β oxidation of fatty acids (Kirtonia *et al*., 2020). At low and controlled levels, ROS play a key role in physiological processes, such as aging, activation of the immune system, inflammatory responses and maturation of sperm cells, enabling successful fertilization (Bardaweel *et al*., 2018). High levels of ROS have been implicated in pathological conditions such as infertility and cancer (Bardaweel *et al*., 2018). Under pathological conditions, ROS interacts with DNA, causing DNA damage and the formation of oncogenic mutations that drive tumorigenesis (Kirtonia *et al*., 2020). In *KRAS*-mutant murine models of pancreatic cancer, the inhibition of ROS resulted in a decrease of the initiation and progression of pre-cancerous pancreatic lesions (Liou et al., 2016). KRAS-activation induced mitochondrial ROS formation, leading to the activation of various signaling pathways that promoted the de-differentiation of pancreatic acinar cells into precancerous lesions, promoting the progression of PDAC (Liou et al., 2016).

Owing to the fact that ROS have extremely short half-lives; and added to the fact that increases in ROS levels are fleeting over time (Juan *et al*., 2021), the formation of ROS in this study was measured at different exposure periods: at four, six and 18 h treatment periods. The copper complexes showed ROS formation at 6 h, but not at 4- and 18- hour treatment periods. After a six hour treatment, ROS was observed in untreated AsPC-1 cells, indicating that the cells had high baseline levels of ROS. This is not uncommon for cancer cells given their high metabolic rate (Nakamura and Takada, 2021). The increase in ROS levels observed in treated cells indicated that the copper complexes induced the formation of ROS. In the AsPC-1 cell line, AD3, OM, L6Cu and doxorubicin caused a statistically significant increase in ROS fluorescence intensity compared to the control, with doxorubicin causing the highest increase. L1Cu showed a non-significant increase in ROS fluorescence intensity compared to untreated AsPC-1 cells. ROS were absent in untreated MIA PaCa-2 cells, while all treated cells fluoresced with a high intensity, red signal, with AD3 and L6Cu showing the most intense signal caused by the copper complexes. Doxorubicin had the highest increase in fluorescence intensity compared to the copper complexes. Formation of ROS was more prevalent in MIA PaCa-2 than in AsPC-1 cells as indicated by the increases in fluorescence intensity caused by all four complexes: AD3, OM, L1Cu and L6Cu. The innate red fluorescence of doxorubicin

made the interpretation of the data more difficult but the inclusion of a doxorubicin-only control confirmed that doxorubicin caused ROS formation in both cell lines which is consistent with the its published mechanism of action (Wellstein and Sausville, 2023). Doxorubicin was statistically significantly more effective than the copper complexes at inducing the formation of ROS in MIA PaCa-2 cells, at the treatment periods tested.

The induction of high levels of ROS in cancer cells leading to irreparable DNA and mitochondrial damage followed by the induction of apoptosis is a valuable treatment strategy in cancer treatment. ROS triggered the intrinsic apoptotic pathway by increasing the permeability of the mitochondrial membrane and by inhibiting the anti-apoptotic protein Bcl-2 in human lung epithelial cancer cells and oral squamous carcinoma cells (Luanpitpong et al., 2013; Li et al., 2004). Additionally, tyrosine kinase inhibitors caused ROS-dependent apoptosis in melanoma and non-small-cell lung cancer cell lines through the disruption of the MMP (Chang et al., 2011; Shan et al., 2016). A disulfiram-based copper complex triggered apoptosis through the ROS/JNK pathway in a human osteosarcoma cell line (W. Guo *et al*., 2021). The JNK pathway is implicated in ROS-induced apoptosis (W. Guo *et al*., 2021). An additional study evaluated synthesized 2-naphthlenol-Cu^{2+} complexes against A549 lung cancer cells (Khan *et al*., 2019). The copper complexes activated apoptosis through endoplasmic reticulum stress-mediated pathways, inhibited topoisomerase I and caused DNA damage through the formation of ROS (Khan *et al*., 2019).

The effects of HMOX1-induced chemoresistance of cancer cells is linked with its ability to protect cancer cells against chemotherapy-induced ROS. This chemoprotective effect is significant in drugs whose mechanism of action is via ROS-mediated mechanisms. In a human liver cancer cell line, HMOX1 inhibition with zinc protoporphyrin sensitized the cells to cisplatin-induced cytotoxicity, through the increased production of ROS (Liu *et al*., 2014). The number of apoptotic cells induced by cisplatin decreased after induction of HMOX1 with hemin, as did the levels of cisplatin-induced-ROS and caspase-3 (Liu *et al*., 2014). In a study on 5-FU-resistant pancreatic cancer cell lines, silencing of Nrf-2 resulted in decreased levels of its downstream target, HMOX1 as well as increased levels of intracellular ROS, compared to the unsilenced control (Kim *et al*., 2020). The Nrf-2-silenced 5-FU-resistant cells showed a decrease in cell viability after treatment with 5-FU compared to the unsilenced 5-FU-resistant control (Kim *et al*., 2020). The results indicated that the resistance to 5-FU was mediated through increased HMOX1 expression and its ROS-depleting effects (Kim *et al*., 2020). In

another study on MIA PaCa-2 cells, there was an observed increase in ROS formation and apoptosis, and a suppression of autophagy, following HMOX1-inhibition in chemotherapy-treated cells (Ahmad *et al*., 2023). The suppression of autophagy was mediated via increased levels of ROS, as the effects were deleted after treatment of the cells with the ROS scavenger, N-acetylcysteine (Ahmad *et al*., 2023).

The data from this study thus indicate that ROS formation, although transient, is an important event following treatment with the copper complexes.

4.6 The effect of the copper complexes on mitochondrial membrane potential of AsPC-1 and MIA PaCa-2 cells

The generation of ATP through oxidative phosphorylation is driven by a series of redox reactions that creates an electrochemical gradient in the mitochondria. This electrochemical gradient contributes to the MMP of the mitochondria (Sakamuru *et al*., 2016). Consequently, the status of MMP is a key indicator for mitochondrial activity. A decrease in MMP indicates a disruption in mitochondrial activity and, hence the viability of the cell (Sakamuru *et al*., 2016). A decrease in MMP results from the opening of the mitochondrial permeability transition pore, allowing the release of pro-apoptotic proteins and factors such as cytochrome c, Smac/DIABLO and HtrA2/Omi (Ly *et al*., 2003). Additionally, the release of apoptosis inducing factor (AIF) is dependent on the disruption of MMP (Ly *et al*., 2003). Thus, loss of MMP is a prerequisite and preliminary indicator of apoptosis (Redza-Dutordoir and Averill-Bates, 2016).

Epithelial cancer cell lines, such as AsPC-1 and MIA PaCa-2 cell lines, have demonstrated a notably higher MMP than normal cells (Summerhayes *et al*., 1982). Studies evaluating the effects of high MMP revealed that colon carcinoma cells with higher MMP were associated with increased secretions of VEGF and matrix metalloproteinase 7, causing augmented migration and invasiveness of the tumour cells (Heerdt *et al*., 2005).

The JC-1 reagent was used as an indicator of mitochondrial health. In healthy cells with an intact MMP, JC-1 is present as a dimer showing red fluorescent “J-aggregates”. In depolarized mitochondria, JC-1 does not form dimers, with the monomeric form showing green fluorescence (Reers *et al*., 1991). In untreated AsPC-1 and MIA PaCa-2 cells, accumulation of red J-aggregates was seen, indicating active mitochondria. All the copper complexes and

doxorubicin decreased the red fluorescence whereby the mitochondria of treated cells were visible as green fluorescence, indicating a complete loss in MMP. In AsPC-1 cells treated with OM, AD3 and L1Cu, most of the cells showed punctate green fluorescence, indicating the mitochondria were structurally intact. In contrast, L6Cu-treated cells demonstrated diffuse green fluorescence, indicating loss of mitochondrial structural integrity (Zuliani *et al*., 2003).

In MIA PaCa-2 cells, diffuse green fluorescence was observed in rounded cells while cells that were still attached to the growth surface showed a more punctate green fluorescence, indicating that longer treatment times were required to affect mitochondrial structural integrity. In MIA PaCa-2 cells, doxorubicin caused a loss of MMP, possibly induced by ROS formation. Statistical analysis comparing doxorubicin to the copper complexes indicated a similar effect in their ability to decrease the MMP.

4.7 The effect of the copper complexes on caspase-3/7 activation in AsPC-1 and MIA PaCa-2 cells

Caspase-3 is the major executioner caspase of apoptosis. The presence of active caspase-3 and -7 serves as confirmation of apoptotic cell death. Caspase-3 is responsible for the distinct nuclear changes that occur during apoptosis such as, DNA fragmentation as well as morphological changes including membrane blebbing (through the activation of ROCK I) (Jänicke *et al*., 1998; Böing *et al*., 2013). Caspase-3 activates caspase-activated-DNAse (CAD) by cleaving its inhibitor, ICAD, enabling CAD-mediated DNA degradation (Enari *et al*., 1998). Additionally, caspase-3 cleaves components of the cytoskeleton (actin, lamin, fodrin) leading to cellular collapse and disassembly (Enari *et al*., 1998). *In vitro*, caspase-3 suppresses the inflammatory response through the release of anti-inflammatory cytokines, such as TGF-β, resulting in anti-proliferative and anti-tumor effects (Martin *et al*., 2012).

Activation of caspase-3/7 is a late apoptotic event, therefore, its activation was measured after a 48 hour treatment period in both cell lines. Active caspase-3 and -7 cleave the same amino acid recognition sequence which the assay-probe binds to, labelling it with a fluorescent signal. The probe is, therefore, non-selective and labels both active caspase-3 and -7. All the copper complexes caused the activation of caspase-3/7 in both cell lines. Doxorubicin caused more than 80 % of cells to show activation of caspase-3/7 in both cell lines. In AsPC-1 cells, doxorubicin caused the highest percentage (90 %) of cells with activated caspase-3/7, followed by OM (67 %). AD3 (32 %), L6Cu (31 %) and L1Cu (17 %) showed the smallest percentage

of cells with increases in caspase-3/7 activation and were the least efficient activators. L1Cu caused caspase-9 activation in 81 % of cells while only 17 % of L1Cu-treated cells showed active caspase-3/7. Since caspase-3/7 activation occurs downstream of caspase-9 activation, it is likely that additional time was required for L1Cu to cause further activation of caspase-3/7 in the AsPC-1 cell line. In MIA PaCa-2 cells, all the copper complexes caused increases in the percentage of cells with active caspase-3/7, with a similar efficacy to one another. Doxorubicin-treated cells had the lowest percentage of cells with active caspase-3/7 (85 %). AD3 and L6Cu were more efficient activators of caspase-3/7 than doxorubicin, with highly significant increases compared to doxorubicin.

Copper complexes have demonstrated the ability to activate caspase-3 in numerous cancer cell lines. In a study on synthesized copper-isoquinoline compounds, selective toxicity was shown in A549 lung cancer cells and the activation of caspase-3 was also observed in these cells (Gul *et al*., 2020). In human cervical cancer (HeLa) cells, a copper-pyrazalone complex caused activation of caspase-3 and caspase-9 after a 24 hour treatment, indicating the induction of the intrinsic apoptotic pathway (Reheman *et al*., 2020). Additionally, copper-imidazo[1,2-*a*]pyridines caused caspase-3/7 activation in colorectal and leukaemic cancer cell lines (Harmse *et al*., 2019; Ismail *et al*., 2021).

4.8 The effect of the copper complexes on caspase-9 activation in AsPC-1 and MIA PaCa-2 cells

Caspase-9 is the initiator caspase of the intrinsic/mitochondrial apoptotic pathway (Wong, 2011). After a 48 hour treatment with the test compounds, all the copper complexes caused a statistically significant activation of caspase-9 in both cell lines. In AsPC-1 cells, OM and L1Cu were the strongest inducers of active caspase-9, followed by L6Cu, while AD3 was the weakest activator. In MIA PaCa-2 cells, AD3 and OM were the strongest activators of caspase-9, followed by L1Cu. Doxorubicin activated caspase-9 in both cell lines with a high potency. In AsPC-1 cells, doxorubicin was more effective at activating caspase-9 than the copper complexes. In MIA PaCa-2 cells, the complexes AD3 and OM activated caspase-9 with greater potency than doxorubicin.

PDAC cells are known for their resistance to death-receptor mediated apoptosis (Hamacher *et al*., 2008). Fas-associated phosphatase-1 is overexpressed in PDAC cells and renders pancreatic carcinoma cells resistant to Fas-initiated apoptosis by inhibiting the activation of

caspase-8 and preventing the formation of DISC (Hamacher *et al*., 2008). PDAC cells are classified as type II cells, meaning they require mitochondrial amplification pathways to induce apoptosis (Westphal and Kalthoff, 2003). The data obtained in this study suggested that the copper complexes initiated apoptosis through the mitochondrial/intrinsic apoptotic pathway in both cell lines.

In contrast to its caspase-9 activity, L6Cu was the strongest activator of caspase-3/7 in MIA PaCa-2 cells. In L6Cu-treated MIA PaCa-2 cells, caspase-3/7 activation was observed in 98.3 % of cells, while only 41.2 % of cells demonstrated active caspase-9 at the same treatment time period. Reasons for this could be due to increased expression/availability of XIAP which is a member of the anti-apoptotic family of proteins, the inhibitor of apoptosis proteins (IAPs). XIAP expression has been shown to be overexpressed in PDAC, and MIA PaCa-2 cells show high levels of XIAP (Rückert *et al*., 2010). XIAP utilizes different binding sites to inhibit caspase-9 and -3 thus, caspase-9 may have been inhibited in a manner that is independent of caspase-3 inhibition (Shiozaki *et al*., 2003). In non-small cell lung cancer cell lines, caspase-9 inhibition by XIAP did not block apoptosis induced by gemcitabine, cisplatin and topotecan (Stewart, 2010). The results were similar to the current study in which L6Cu showed low levels of caspase-9 activation but high levels of caspase-3/7 activation. However, previous studies with different copper complexes indicate a suppression of XIAP (Harmse *et al*., 2019; Ismail *et al*., 2022). The direct effect of the copper complexes tested in this study on XIAP expression requires further investigation. Additionally, the effects of the copper complexes on SMAC/DIABLO, a caspase-9 activating protein also requires further investigation.

The percentage activation of caspase-3/7 and caspase-9 in both cell lines is summarized in Table 4.2. The differences in caspase activation across cell lines demonstrates the varied responses of different cell types to the same complex, highlighting the need for personalized medicine in clinical practice.

Table 4.2 Summary of the effect of the copper complexes on caspase-3/7 and caspase-9 activation (%) in AsPC-1 and MIA PaCa-2 cells

	AD3		OM		L1Cu		L6Cu	
	AsPC-1	MIA PaCa-2	AsPC-1	MIA PaCa-2	AsPC-1	MIA PaCa-2	AsPC-1	MIA PaCa-2
Caspase-3/7	**	***	***	***	*	***	*	***
Caspase-9	**	***	***	***	***	***	***	**

Percentage cells with active enzyme: ***: high. **: medium. *: low

4.9 The effect of the copper complexes on HMOX1 expression as evaluated by immunofluorescence and western blot studies

HMOX1 is a highly inducible enzyme that is increased in response to cellular stresses such as ROS, UV irradiation, pro-inflammatory cytokines, hypoxia, ischemia, heavy metals and nitric oxide as well as other stimuli such as the presence of its substrate heme (Muchaa *et al*., 2019; Jun *et al*., 2018). The dual role of HMOX1 in cancer has been studied extensively and remains inconclusive, due to its pro- and anti-tumour effects in different cancer types (Mascaro *et al*., 2021). In PDAC, HMOX1 expression has been reported to increase in response to chemotherapy and is associated with treatment failure (Ahmad *et al*., 2021). Previous studies have reported the ability of copper complexes to induce HMOX1 expression. A copper diethyldithiocarbamate complex induced HMOX1 through activation of Nrf2 in vascular endothelial cells in culture (Fujie *et al*., 2016). Additionally, copper-imidazo[1,2-*a*]pyridines induced HMOX1 expression in HT-29 colorectal cells, which potentially decreased the cytotoxicity of the copper complexes (Harmse *et al*., 2019). Consequently, this study investigated the effect of the copper complexes on HMOX1 expression in PC cell lines.

Immunofluorescence and western bot studies confirmed that all four copper complexes increased the expression of HMOX1 in both the AsPC-1 and MIA PaCa-2 cell lines. AD3 was the strongest inducer of HMOX1 as shown by immunofluorescence as well as western blot studies. L1Cu was the weakest inducer of HMOX1 while OM was similar to L6Cu in its HMOX1-inducing ability. The trends observed in HMOX1 expression was the same in both cell lines, and was confirmed in both immunofluorescence and western blot assays. The induction of HMOX1 expression by all the complexes may be associated with their ability to stimulate ROS formation (Ahmad *et al*., 2023). Immunofluorescence studies on doxorubicin indicated an increase in HMOX-1 expression following treatment. However, this could not be confirmed with western blot studies. In a study conducted by Tan *et al.* (2015), treatment of MDA-MB-231 breast cancer cells with doxorubicin resulted in the induction of HMOX1 which subsequently conferred resistance to MDA-MB-231 cells to doxorubicin treatment. The effect of doxorubicin on HMOX1 expression in PC cell lines in this study was inconclusive and requires further investigation.

Increased HMOX1 expression protects tumour cells against oxidative stress, inflammatory mediators and apoptosis and promotes angiogenesis in the tumour cells (Nowis *et al*., 2006; Banerjee *et al*., 2012; Cheng *et al*., 2016). High levels of HMOX1 mRNA expression is associated with a significantly worse prognosis for lung, brain, breast, colorectal and blood cancers, as predicted by a meta-analysis database (Wang *et al*., 2023). In ovarian cancer cells, SIRT-5 (a mitochondrial enzyme) confers cisplatin-resistance to the cells via upregulation of the Nrf2/HMOX1 pathway, which protects against ROS-mediated DNA damage caused by cisplatin (Sun *et al*., 2019). Another study on acute myeloid leukaemia compared HMOX1 expression in tyrosine-kinase-inhibitor-resistant cells vs tyrosine-kinase-inhibitor-sensitive cells (Kannan *et al*., 2022). There was an up-regulation of HMOX1 in the tyrosine-kinase-inhibitor-resistant cell line. Following HMOX1 knockdown in the resistant cell line, a 25 % suppression in cell proliferation was observed. Additionally, after a 48 hour treatment of the cells with the HMOX1 inhibitor, zinc protoporphyrin, in combination with the tyrosine-kinase-inhibitor, quizartinib, a synergistic two to three-fold increase in apoptosis was observed compared to treatment with the individual drugs alone (Kannan *et al*., 2022).

Under normal conditions HMOX1 is found in the cytoplasm, anchored to the smooth endoplasmic reticulum membrane. Certain disease states induce HMOX1 translocation to the mitochondria, plasma membrane and the nucleus. Its enzymatic activity is preserved in all compartments except in the nucleus (Chiang *et al*., 2021). In this study, the strong positive correlation between the Hoechst fluorescent signal and the HMOX1 immunofluorescent signal in immunofluorescence studies (measured by Pearson's correlation coefficient) indicated that HMOX1 was predominantly in the nucleus. The copper complexes caused an increase in the correlation coefficient compared to the untreated cells, indicating that a fraction of HMOX1 likely translocated to the nucleus. Doxorubicin showed a decrease in Pearson's correlation coefficient compared to the untreated cells, indicating an increase in cytoplasmic HMOX1 following treatment with doxorubicin.

In mouse embryonic fibroblasts, HMOX1 translocated to the nucleus in response to hypoxia and promoted the up-regulation of transcription factors involved in oxidative stress (Lin *et al*., 2007). The transcription factors included AP-1, AP-2, Brn-3 and Core Binding Factor which play a role in cell proliferation and differentiation, and possibly caused an increase in cell proliferation (Lin *et al*., 2007). Additionally, the nuclear translocation of HMOX1 resulted in decreased binding of nuclear factor kappa B (NF-κB) to DNA (Lin *et al*., 2007). Western blot

studies that isolated cytoplasmic and nuclear fractions of the cell demonstrated an increase in nuclear HMOX1 following treatment of MIA PaCa-2 cells with nab-paclitaxel/gemcitabine, indicating nuclear translocation of HMOX1 (Ahmad *et al*., 2021). The nuclear HMOX1 contributed to the cells' resistance to chemotherapy treatment (Ahmad *et al*., 2021). In another study on chronic myeloid leukaemic cell lines, HMOX1 induction following hemin treatment protected the cells against imatinib-induced apoptosis (Tibullo *et al*., 2013). Furthermore, exposure of the cells to CO and biliverdin was unable to protect the cells against imatinib, indicating that the anti-apoptotic effects were conferred to the cells independent of the enzymatic activity of HMOX1 (Tibullo *et al*., 2013). In the same study, inhibition of the nuclear translocation of HMOX1 was achieved after treatment of the cells with E64d, a cysteine protease inhibitor that prevents the proteolytic cleavage necessary for nuclear translocation. This resulted in the restoration of imatinib-induced apoptosis, further suggesting that resistance to chemotherapy treatment is provided by the action of nuclear HMOX1 (Tibullo *et al*., 2013). In a different study by the same group, inhibition of nuclear translocation of HMOX1 using E64d resulted in increased sensitization of multiple myeloma cells to bortezomib treatment (Tibullo *et al*., 2016).

4.10 The effect of HMOX1 inhibition on the cytotoxicity of the copper complexes in AsPC-1 and MIA PaCa-2 cells

Following the detection of increased HMOX1 expression in treated cells, the effects of HMOX1 inhibition on the IC_{50} values of the complexes were evaluated. Experiments using the MTT assay evaluated the cytotoxic effects of the complexes in combination with an imidazole HMOX1-inhibitor, OB24 HCl. Dose response curves were constructed using the same concentration range that was used to determine the IC_{50} values of the individual complexes. The HMOX1 inhibitor, OB24 HCl, was used at a constant concentration of 20 μM. IC_{50} values of the combinations were calculated and a statistically significant decrease in the IC_{50} values of all the complexes was observed in both cell lines. On its own, OB24 HCl did not affect the viability of the cells. The results indicated that HMOX1-inhibition, which was not detrimental to the cells on its own, sensitized the cell lines to the treatment with the copper complexes. The use of OB24 HCl on prostate cancer cell lines resulted in a synergistic effect when combined with paclitaxel, showing a reduction in cell viability of the prostate cancer cells (Alaoui-Jamali *et al*., 2009). In the prostate cancer cells, OB24 HCl showed an inhibitory effect on cell proliferation on its own, *in vivo* and *in vitro* (Alaoui-Jamali *et al*., 2009), which is in contrast to the findings of the current study.

Numerous studies have reported the chemosensitization of cancer cells to treatment following HMOX1-inhibition (Mucha *et al*., 2019; Kongpetch *et al*., 2012; Miyake *et al*., 2010; Furfaro *et al*., 2016; Furfaro *et al*., 2022). In a PDAC mice model, a significant reduction in tumor size was observed in mice treated with gemcitabine and the HMOX1 inhibitor, zinc protoporphyrin, compared to gemcitabine alone (Nuhn *et al*., 2009). MIA PaCa-2 cells showed increased sensitivity to nab/paclitaxel and gemcitabine treatment when used in conjunction with the HMOX1 inhibitor, zinc protoporphyrin (Ahmad *et al*., 2021). Following HMOX1 gene silencing in patient-derived pancreatic cancer cell lines, the cells were exposed to radiation and gemcitabine chemotherapy. The results revealed a significant reduction in cell viability in HMOX1-silenced-cells, confirming that HMOX1 depletion sensitizes cancer cells to radiation and chemotherapy (Berberat *et al*., 2005). In MIA PaCa-2 cells, chemotherapy treatment with arsenic trioxide (ATO) induced apoptosis, measured by annexin-V flow cytometry (Ahmad *et al*., 2023). Inhibition of HMOX1 with zinc protoporphyrin in these cells caused a 2.9-fold increase in apoptotic cells compared to cells treated with ATO alone. The same study highlighted the role of autophagy in ATO-resistance – whereby inhibiting the antioxidant role of HMOX1 deleted the protective role of autophagy, combatting ATO-resistance (Ahmad *et al*., 2023). The tumour microenvironment is another avenue where HMOX1 exerts its effects, contributing to tumor resistance to treatment. Tumour associated macrophages express HMOX1 in high levels following differentiation and infiltration of monocytes into the TME of thymus cancer cells (Alaluf *et al*., 2020). Tumour regression was observed in a lymphoma mice model where HMOX1 was deleted in myeloid cells (Alaluf *et al*., 2020). The $HMOX1^{-}$ mice demonstrated an increase in the proliferation and cytotoxic functions of $CD8^{+}$ T cells following treatment with cyclophosphamide as well as an antitumor vaccine, resulting in tumour regression (Alaluf *et al*., 2020).

4.11 Comparisons of the effects of the copper complexes on cell-death-assay-findings and HMOX1-expression between cell lines

At the same treatment period, the copper complexes demonstrated higher caspase-3/7 activation in MIA PaCa-2 cells than in AsPC-1 cells. This was in line with annexin-V findings and cell morphology evaluation that demonstrated a higher frequency of late apoptotic cells in which detached/floating cells were observed more often in MIA PaCa-2 cells than in AsPC-1 cells. Additionally, the copper complexes induced ROS more potently in MIA PaCa-2 cells than in AsPC-1 cells. The data suggested that MIA PaCa-2 cells appeared to be more sensitive

to the complexes than AsPC-1 cells. However, in both cell lines, the copper complexes caused a complete loss of MMP in 100 % of the cells. Additionally, the complexes had similar percentages of cells with active caspase-9 in both cell lines.

The effect of HMOX1 expression in both cell lines were aligned. The data from immunofluorescence and western blot studies showed AD3 to be the strongest inducer of HMOX1, while L1Cu was the least potent. In both cell lines, truncated HMOX1 was absent in the doxorubicin-treated sample. Taken together, the results indicated that the copper complexes caused the activation of the intrinsic apoptotic pathway in both cell lines and induced the expression of nuclear HMOX1. In addition, cytotoxicity studies indicated that HMOX-1 inhibition sensitized the cancer cells to the copper complexes. In conclusion, together with the literature, the results obtained in this study support the potential for HMOX1-inhibition as a viable strategy to combat chemotherapy-resistance in different tumour types.

Chapter V: Conclusions

This study aimed to evaluate the cytotoxicity of novel copper complexes of different classes on AsPC-1 and MIA PaCa-2 pancreatic cancer cell lines. Their mechanism of cell death was elucidated using various cell death assays and their effect on the expression of HMOX1 was evaluated using immunofluorescence and western blots. The effect of HMOX1-inhibition on the cytotoxicity of the copper complexes was investigated with an imidazole-based HMOX1-inhibitor, OB24 HCl.

5.1 The copper complexes inhibited the growth of AsPC-1 and MIA PaCa-2 cell lines at low micromolar IC_{50} values

Using the MTT cell viability assays, this study aimed to evaluate the cytotoxic effects of the copper complexes on AsPC-1 and MIA PaCa-2 cells. In both cell lines, all four copper complexes were significantly more active than the positive control, doxorubicin. AD3, OM, L1Cu and L6Cu all had IC_{50} values of below 5 μM in both cell lines. The LCu complexes were the most effective inhibitors of proliferation in both cell lines. In the AsPC-1 cell line, L6Cu had the lowest IC_{50} value (1.27 μM), while in the MIA PaCa-2 cell line, L1Cu had the lowest IC_{50} value (1.08 μM). In the AsPC-1 cell line, doxorubicin's IC_{50} value was approximately half its value in the MIA PaCa-2 cell line, with IC_{50} values of 6.64 and 12.07 μM in AsPC-1 and MIA PaCa-2 cells, respectively.

5.2 The copper complexes caused the formation of ROS

After a 6 hour treatment period, the copper complexes caused the formation of ROS in both the AsPC-1 and MIA PaCa-2 cell lines. Doxorubicin caused the highest increase in ROS formation, with a statistically significant increase compared to the copper complexes. The formation of ROS by the copper complexes indicate that, although, transient, ROS formation is an important event following treatment and is possibly responsible for the copper complex-induced increase in HMOX1.

5.3 The copper complexes activate the intrinsic apoptotic pathway

No evidence of necrosis was observed in cell morphology studies while apoptotic features such as chromatin condensation and membrane blebbing were seen in treated cells. The copper complexes caused the binding of annexin-V to translocated phosphatidylserine. The presence

of annexin-V-only binding showed the presence of early apoptotic cells in AsPC-1 cells, while late apoptotic/secondary necrotic cells were indicated by the presence of annexin-V and propidium iodide binding in treated MIA PaCa-2 cells. This suggested that the copper complexes exerted their action faster in the MIA PaCa-2 cell line than in AsPC-1 cells. In both cell lines, L6Cu was the strongest effector of annexin-V binding while L1Cu was the least potent effector. The loss of mitochondrial membrane potential was observed in close to 100 % of copper-complex-treated cells in both cell lines, indicating a disruption in mitochondrial functioning. The copper complexes activated caspases -3/7 and -9 in both cell lines in varying amounts. Caspase-3/7 activation was most frequently seen in OM-treated cells, in the AsPC-1 cell line. In MIA PaCa-2, caspase-3/7 activation was seen in more than 85 % of all copper-complex- and doxorubicin- treated cells. In AsPC-1 cells, OM was the strongest activator of caspase-9 while in MIA PaCa-2 cells, AD3 and OM were both more effective activators than the other complexes. Caspase-3/7 activation was the highest in MIA PaCa-2 cells compared to AsPC-1 cells. Caspase-9 activation was seen in 53-92 % of AsPC-1 cells while MIA PaCa-2 showed caspase-9 activation in 41-91 % of the cells, indicating a similar caspase-9 activating effect.

Annexin-V-binding and caspase-3/7-activation confirmed that the complexes activated apoptosis in both cell lines. The loss of MMP and the activation of caspase-9 indicated that the copper complexes activated the intrinsic apoptotic pathway.

5.4 The copper complexes induce the expression of HMOX1

The copper complexes caused an increase in HMOX1 expression, confirmed by immunofluorescence and western blot studies. AD3 was the strongest inducer while L1Cu was the least potent inducer of HMOX1, in both cell lines. The results correlate with other studies showing an increase in HMOX1 expression following treatment with chemotherapeutic agents (Ahmad et al., 2021; Han et al., 2018). Additionally, colocalization analysis showed a strong positive correlation between the Hoechst nuclear signal and HMOX1 immunofluorescence signal, indicating that hMOX1 was predominantly in the nucleus. The increase in correlation in treated cells compared to untreated cells suggested that HMOX1 translocated to the nucleus following treatment with the copper complexes.

5.5 The effect of HMOX1-inhibition on the cytotoxicity of the copper complexes

Following HMOX1-inhibition using an inhibitor of HMOX1 activity (OB24 HCl), the IC_{50} values of the copper complexes against the AsPC-1 and MIA PaCa-2 cell lines were decreased with statistical significance. Alone, OB24 HCl had no effect on the viability of the cells, indicating that HMOX1 sensitizes the cancer cells to cell death induced by the copper complexes and HMOX1-inhibition on its own has no effect on cell survival. The results affirm the role of HMOX1 in treatment failure and resistance of cancer cells to chemotherapy and demonstrate how HMOX1-inhibition can be targeted in clinical settings to sensitize cancer cells to chemo- and radiation-therapy.

5.6 Limitations

One of the limitations of this study is that the assays were performed in a cell culture model, therefore, the results of this study cannot be extrapolated beyond this setting. In order to be developed further, the copper complexes need to be evaluated in pre-clinical animal models. Additionally, information on the pharmacokinetics, pharmacodynamics and safety profile of the copper complexes are absent.

Another limitation involves the use of OB24 HCl as the method for HMOX1 inhibition. There is limited data available on the pharmacokinetics, pharmacodynamics and safety of OB24 HCl. This study did not evaluate the effect of the complexes on the activity of HMOX1, and its levels were only investigated in the context of gene expression. The evaluation of the extent of nuclear translocation of HMOX1 was limited to colocalization analysis of immunofluorescence images. Additionally, the function of nuclear HMOX1 remains unclear. Further, the effect of HMOX1-inhibition was investigated only on the cytotoxicity of the copper complexes and their IC_{50} values. None of the cell death assays were evaluated with the copper complexes in combination with OB24 HCl. Therefore, future studies should investigate the role of HMOX1-inhibition on the activation of the various apoptotic parameters.

5.7 Future considerations

Since the copper complexes have been confirmed to induce apoptosis, the effect of the copper complexes on the apoptotic protein profile in the pancreatic cancer cell lines should be investigated to gain a more global understanding on the expression levels of IAPs and pro-apoptotic proteins. Cuproptosis should be investigated as a possible mode of cell death by the copper complexes. Additionally, the role of HMOX1-inhibition on the effect of the copper

complexes on apoptotic parameters in cell culture should be tested. Future studies utilising HMOX1 gene knockout using CRISPR and ChIP (Chromatin Immunoprecipitation) assays would provide more information regarding the function of nuclear HMOX1. Nuclear translocation should be inhibited using the cysteine protease inhibitor, E64d, preceding treatment with the copper complexes, to determine whether or not the protection conferred to cancer cells is due to nuclear HMOX1.

The novel copper complexes used in this study likely display different bioavailability, reactivity and stability compared to other copper-based compounds. Future studies should aim to elucidate these differences. A nude mouse model can be used to evaluate the pharmacokinetics, pharmacodynamics and safety of the copper complexes, *in vitro*. This study evaluated the effects of the copper complexes after short-term exposure to the complexes. As such, the effect of chronic exposure to the copper complexes and long-term efficacy and toxicity studies are needed. Further, the role of HMOX1 in the tumour microenvironment should be investigated using a mouse model whereby HMOX1 is deleted. Mice models that can be used for this purpose include genetically-engineered mouse models and xenograft mouse models using athymic nude mice as well as severe combined immune deficiency mice (Jung, 2014). Lastly, formulation studies aiming to increase delivery of the drug through the dense stroma and limited blood supply of the pancreatic tumour microenvironment may be studied, exploring the potential of a nano-particle formulation.

5.8 Conclusion

To conclude, this study has identified four copper complexes of three different ligand-classes as promising lead compounds for pre-clinical studies in the treatment of pancreatic ductal adenocarcinoma. The copper complexes include AD3, a copper-phenanthroline-theophylline complex; OM, a copper 8-aminoquinolone naphthyl complex; and L1Cu and L6Cu, copper iso-indoline complexes. The complexes activated the intrinsic apoptotic pathway – as seen by by the formation of ROS, the binding of annexin-V, the loss in MMP and the activation of caspases -3/7 and -9. Additionally, the complexes induced the expression of HMOX1. Inhibition of HMOX1 resulted in a decrease in the IC_{50} values of the copper complexes, indicating that HMOX1-inhibition sensitizes AsPC-1 and MIA PaCa-2 cells to the copper complexes. This study affirms the use of HMOX1-inhibition as a promising and viable strategy to combat treatment resistance in pancreatic ductal adenocarcinoma.

References

Abdalla, M. Y., Ahmad, I. M., Rachagani, S., Banerjee, K., Thompson, C. M., Maurer, C. H., Olive, K. P., Bailey, K. L., Britigan, B. E., Kumar, S. (2019). Enhancing responsiveness of pancreatic cancer cells to gemcitabine treatment under hypoxia by heme oxygenase-1 inhibition. *Translational Reasearch* 207, 56-69.

Ahmad, I. M., Dafferner, A. J., O'Connell, K. A., Mehla, K., Britigan, B. E., Hollingsworth, M. A., and Abdalla, M. Y. (2021). Heme Oxygenase-1 Inhibition Potentiates the Effects of Nab-Paclitaxel-Gemcitabine and Modulates the Tumor Microenvironment in Pancreatic Ductal Adenocarcinoma. *Cancers*, *13*(9), 2264. https://doi.org/10.3390/cancers13092264

Ahmad, I. M., Dafferner, A. J., Salloom, R. J., and Abdalla, M. Y. (2023). Heme Oxygenase-1 Inhibition Modulates Autophagy and Augments Arsenic Trioxide Cytotoxicity in Pancreatic Cancer Cells. *Biomedicines*, *11*(9), 2580. https://doi.org/10.3390/biomedicines11092580

Alaluf, E., Vokaer, B., Detavernier, A., Azouz, A., Splittgerber, M., Carrette, A., Boon, L., Libert, F., Soares, M., Moine, A. L., and Goriely, S. (2020). Heme oxygenase-1 orchestrates the immunosuppressive program of tumor-associated macrophages. *JCI Insight*, *5*(11). https://doi.org/10.1172/jci.insight.133929

Alaoui-Jamali, M. A., Bismar, T. A., Gupta, A., Szarek, W. A., Su, J., Song, W., Xu, Y., Xu, B., Liu, G., Vlahakis, J. Z., Roman, G., Jiao, J., and Schipper, H. M. (2009). A novel experimental heme oxygenase-1-targeted therapy for hormone-refractory prostate cancer. *Cancer research*, *69*(20), 8017–8024. https://doi.org/10.1158/0008-5472.CAN-09-0419

American Cancer Society. (2023). *Survival Rates for Pancreatic Neuroendocrine Tumor*. https://www.cancer.org/cancer/types/pancreatic-neuroendocrine-tumor/detection-diagnosis-staging/survival-rates.html. Accessed February 2024.

American Cancer Society. (2024). *Cancer Facts & Figures 2024*. Atlanta: American Cancer Society. https://www.cancer.org/content/dam/cancer-org/research/cancer-facts-and-statistics/annual-cancer-facts-and-figures/2024/2024-cancer-facts-and-figures-acs.pdf. Accessed February 2024.

An, B., Goldfarb, R. H., Siman, R., & Dou, Q. P. (1998). Novel dipeptidyl proteasome inhibitors overcome Bcl-2 protective function and selectively accumulate the cyclin-dependent kinase inhibitor p27 and induce apoptosis in transformed, but not normal, human fibroblasts. *Cell death and differentiation*, *5*(12), 1062–1075. https://doi.org/10.1038/sj.cdd.4400436

Andrés, N. C., Fermento, M. E., Gandini, N. A., Romero, A. L., Ferro, A., Donna, L. G., Curino, A. C., and Facchinetti, M. M. (2014). Heme oxygenase-1 has antitumoral effects in colorectal cancer: Involvement of p53. *Experimental and Molecular Pathology*, *97*(3), 321–331. https://doi.org/10.1016/j.yexmp.2014.09.012

Arnold, J. N., Magiera, L., Kraman, M., & Fearon, D. T. (2014). Tumoral immune suppression by macrophages expressing fibroblast activation protein-α and heme oxygenase-1. *Cancer immunology research*, *2*(2), 121–126. https://doi.org/10.1158/2326-6066.CIR-13-0150

Banerjee, P., Basu, A., Wegiel, B., Otterbein, L. E., Mizumura, K., Gasser, M., Waaga-Gasser, A. M., Choi, A. M., and Pal, S. (2012). Heme Oxygenase-1 Promotes Survival of Renal Cancer Cells through Modulation of Apoptosis- and Autophagy-regulating Molecules*. *Journal of Biological Chemistry*, *287*(38), 32113–32123. https://doi.org/10.1074/jbc.M112.393140

Bank, H. L. (1988). Rapid assessment of islet viability with acridine orange and propidium iodide. *In Vitro Cell Dev Biol*, *24*(4), 266-273. doi:10.1007/BF02628826

Bardaweel, S. K., Gul, M., Alzweiri, M., Ishaqat, A., ALSalamat, H. A., & Bashatwah, R. M. (2018). Reactive Oxygen Species: The Dual Role in Physiological and Pathological Conditions of the Human Body. *The Eurasian Journal of Medicine*, *50*(3), 193–201. https://doi.org/10.5152/eurasianjmed.2018.17397

Berberat, P. O., Dambrauskas, Z., Gulbinas, A., Giese, T., Giese, N., Künzli, B., Autschbach, F., Meuer, S., Büchler, M. W., and Friess, H. (2005). Inhibition of heme oxygenase-1 increases responsiveness of pancreatic cancer cells to anticancer treatment. *Clinical Cancer Research: An Official Journal of the American Association for Cancer Research*, *11*(10), 3790–3798. https://doi.org/10.1158/1078-0432.CCR-04-2159

Böing, A. N., Stap, J., Hau, C. M., Afink, G. B., Ris-Stalpers, C., Reits, E. A., Sturk, A., van Noorden, C. J. F., & Nieuwland, R. (2013). Active caspase-3 is removed from cells by release of caspase-3-enriched vesicles. *Biochimica et Biophysica Acta (BBA) - Molecular Cell Research*, *1833*(8), 1844–1852. https://doi.org/10.1016/j.bbamcr.2013.03.013

Bonam, S. R., Wang, F., and Muller, S. (2019). Lysosomes as a therapeutic target. *Nature reviews. Drug discovery*, *18*(12), 923–948. https://doi.org/10.1038/s41573-019-0036-1

Bouaoun, L., Sonkin, D., Ardin, M., Hollstein, M., Byrnes, G., Zavadil, J., and Olivier, M. (2016). TP53 Variations in Human Cancers: New Lessons from the IARC TP53 Database and Genomics Data. *Human Mutation*, *37*(9), 865–876. https://doi.org/10.1002/humu.23035

Bukowska-Strakova, K., Włodek, J., Pitera, E., Kozakowska, M., Konturek-Cieśla, A., Cieśla, M., Gońka, M., Nowak, W., Wieczorek, A., Pawińska-Wąsikowska, K., Józkowicz, A., and Siedlar, M. (2021). Role of *HMOX1* Promoter Genetic Variants in Chemoresistance and Chemotherapy Induced Neutropenia in Children with Acute Lymphoblastic Leukemia. *International journal of molecular sciences*, *22*(3), 988. https://doi.org/10.3390/ijms22030988

Carapuça, E. F., Gemenetzidis, E., Feig, C., Bapiro, T. E., Williams, M. D., Wilson, A. S., Delvecchio, F. R., Arumugam, P., Grose, R. P., Lemoine, N. R., Richards, F. M., and Kocher, H. M. (2016). Anti-stromal treatment together with chemotherapy targets multiple signalling pathways in pancreatic adenocarcinoma. *The Journal of Pathology*, *239*(3), 286–296. https://doi.org/10.1002/path.4727

Castillo-Rodríguez, R. A., Palencia, G., Anaya-Rubio, I., Pérez, J. C. G., Jiménez-Farfán, D., Escamilla-Ramírez, Á., Zavala-Vega, S., Cruz-Salgado, A., Cervantes-Rebolledo, C., Gracia-Mora, I., Ruiz-Azuara, L., & Trejo-Solis, C. (2021). Anti-proliferative, pro-apoptotic and anti-invasive effect of the copper coordination compound Cas III-La through the induction of reactive oxygen species and regulation of Wnt/β-catenin pathway in glioma. *Journal of Cancer*, *12*(19), 5693–5711. https://doi.org/10.7150/jca.59769

Census, Stats SA. (2022). Stats by Theme. https://census.statssa.gov.za/#/statsbytheme. Accessed March 2024.

Chang, S. P., Shen, S. C., Lee, W. R., Yang, L. L., & Chen, Y. C. (2011). Imatinib mesylate induction of ROS-dependent apoptosis in melanoma B16F0 cells. *Journal of dermatological science*, *62*(3), 183–191. https://doi.org/10.1016/j.jdermsci.2011.03.001

Chau, L. Y. (2015). Heme oxygenase-1: emerging target of cancer therapy. *Journal of Biomedical Science* 22 (22). Doi: 10.1186/s12929-015-0128-0

Chavez-Gonzalez, A., Centeno-Llanos, S., Moreno-Lorenzana, D., Sandoval-Esquivel, M. A., Aviles-Vazquez, S., Bravo-Gomez, M. E., Ruiz-Azuara, L., Ayala-Sanchez, M., Torres-Martinez, H., & Mayani, H. (2017). Casiopeina III-Ea, a copper-containing small molecule, inhibits the in vitro growth of primitive hematopoietic cells from chronic myeloid leukemia. *Leukemia research*, *52*, 8–19. https://doi.org/10.1016/j.leukres.2016.11.001

Chazotte B. (2011). Labeling nuclear DNA with hoechst 33342. *Cold Spring Harbor protocols*, *2011*(1), pdb.prot5557. https://doi.org/10.1101/pdb.prot5557

Chen, N.-T., Wu, C.-Y., Chung, C.-Y., Hwu, Y., Cheng, S.-H., Mou, C.-Y., and Lo, L.-W. (2012). Probing the Dynamics of Doxorubicin-DNA Intercalation during the Initial Activation of Apoptosis by Fluorescence Lifetime Imaging Microscopy (FLIM). *PLoS ONE*, *7*(9), e44947. https://doi.org/10.1371/journal.pone.0044947

Chen, W. H., Horoszewicz, J. S., Leong, S. S., Shimano, T., Penetrante, R., Sanders, W. H., Berjian, R., Douglass, H. O., Martin, E. W., and Chu, T. M. (1982). Human pancreatic adenocarcinoma: In vitro and in vivo morphology of a new tumor line established from ascites. *In Vitro*, *18*(1), 24–34. https://doi.org/10.1007/BF02796382

Cheng, C. C., Guan, S. S., Yang, H. J., Chang, C. C., Luo, T. Y., Chang, J., and Ho, A. S. (2016). Blocking heme oxygenase-1 by zinc protoporphyrin reduces tumor hypoxia-mediated VEGF release and inhibits tumor angiogenesis as a potential therapeutic agent against colorectal cancer. *Journal of biomedical science*, *23*, 18. https://doi.org/10.1186/s12929-016-0219-6

Chiang, S.-K., Chen, S.-E., and Chang, L.-C. (2021). The Role of HO-1 and Its Crosstalk with Oxidative Stress in Cancer Cell Survival. *Cells*, *10*(9), 2401. https://doi.org/10.3390/cells10092401

Coleman, M. L., Sahai, E. A., Yeo, M., Bosch, M., Dewar, A., and Olson, M. F. (2001). Membrane blebbing during apoptosis results from caspase-mediated activation of ROCK I. *Nature Cell Biology*, *3*(4), 339–345. https://doi.org/10.1038/35070009

Conroy, T., Castan, F., Lopez, A., Turpin, A., Ben Abdelghani, M., Wei, A. C., Mitry, E., Biagi, J. J., Evesque, L., Artru, P., Lecomte, T., Assenat, E., Bauguion, L., Ychou, M., Bouché, O., Monard, L., Lambert, A., Hammel, P., & Canadian Cancer Trials Group and the Unicancer-GI–PRODIGE Group. (2022). Five-Year Outcomes of FOLFIRINOX vs Gemcitabine as Adjuvant Therapy for Pancreatic Cancer: A Randomized Clinical Trial. *JAMA Oncology*, *8*(11), 1571–1578. https://doi.org/10.1001/jamaoncol.2022.3829

Conroy, T., Desseigne, F., Ychou, M., Bouché, O., Guimbaud, R., Bécouarn, Y., Adenis, A., Raoul, J.-L., Gourgou-Bourgade, S., de la Fouchardière, C., Bennouna, J., Bachet, J.-B., Khemissa-Akouz, F., Péré-Vergé, D., Delbaldo, C., Assenat, E., Chauffert, B., Michel, P., Montoto-Grillot, C., and Ducreux, M. (2011). FOLFIRINOX versus Gemcitabine for Metastatic Pancreatic Cancer. *New England Journal of Medicine*, *364*(19), 1817–1825. https://doi.org/10.1056/NEJMoa1011923

Consonni, F. M., Bleve, A., Totaro, M. G., Storto, M., Kunderfranco, P., Termanini, A., Pasqualini, F., Alì, C., Pandolfo, C., Sgambelluri, F., Grazia, G., Santinami, M., Maurichi, A., Milione, M., Erreni, M., Doni, A., Fabbri, M., Gribaldo, L., Rulli, E., Soares, M. P., … Sica, A. (2021). Heme catabolism by tumor-associated macrophages controls metastasis formation. *Nature immunology*, *22*(5), 595–606. https://doi.org/10.1038/s41590-021-00921-5

D'Arcy, M. S. (2019). Cell death: A review of the major forms of apoptosis, necrosis and autophagy. *Cell Biology International*, *43*(6), 582–592. https://doi.org/10.1002/cbin.11137

Dam, J., Ismail, Z., Kurebwa, T., Gangat, N., Harmse, L., Marques, H. M., Lemmerer, A., Bode, M. L., and de Koning, C. B. (2017). Synthesis of copper and zinc 2-(pyridin-2-yl)imidazo[1,2-*a*]pyridine complexes and their potential anticancer activity. *European Journal of Medicinal Chemistry*, *126*, 353–368. https://doi.org/10.1016/j.ejmech.2016.10.041

Darzynkiewicz, Z., Bruno, S., Del Bino, G., Gorczyca, W., Hotz, M. A., Lassota, P., and Traganos, F. (1992). Features of apoptotic cells measured by flow cytometry. *Cytometry*, *13*(8), 795–808. doi: https://doi.org/10.1002/cyto.990130802

Das, S., and Batra, S. K. (2015). Pancreatic Cancer Metastasis: Are we being Pre-EMTed? *Current Pharmaceutical Design*, 21(10), 1249–1255.

De La Cruz, M. S. D., Young, A. P., and Ruffin, M. T. (2014). Diagnosis and management of pancreatic cancer. *American Family Physician*, 89(8), 626–632.

Dengler, W. A., Schulte, J., Berger, D. P., Mertelsmann, R., and Fiebig, H. H. (1995). Development of a propidium iodide fluorescence assay for proliferation and cytotoxicity assays. *Anti-cancer drugs*, *6*(4), 522–532. https://doi.org/10.1097/00001813-199508000-00005

Dixon, S. J., Lemberg, K. M., Lamprecht, M. R., Skouta, R., Zaitsev, E. M., Gleason, C. E., Patel, D. N., Bauer, A. J., Cantley, A. M., Yang, W. S., Morrison, B., 3rd, and Stockwell, B. R. (2012). Ferroptosis: an iron-dependent form of nonapoptotic cell death. *Cell*, *149*(5), 1060–1072. https://doi.org/10.1016/j.cell.2012.03.042

diSibio, G., French, S. W. (2008). Metastatic patterns of cancers: Results from a large autopsy study. *Arch Pathol Lab Med* 132, 931–939.

Enari, M., Sakahira, H., Yokoyama, H., Okawa, K., Iwamatsu, A., & Nagata, S. (1998). A caspase-activated DNase that degrades DNA during apoptosis, and its inhibitor ICAD. *Nature*, *391*(6662), 43–50. https://doi.org/10.1038/34112

Ene-Obong, A., Clear, A. J., Watt, J., Wang, J., Fatah, R., Riches, J. C., Marshall, J. F., Chin-Aleong, J., Chelala, C., Gribben, J. G., Ramsay, A. G., & Kocher, H. M. (2013). Activated

pancreatic stellate cells sequester CD8+ T cells to reduce their infiltration of the juxtatumoral compartment of pancreatic ductal adenocarcinoma. *Gastroenterology*, *145*(5), 1121–1132. https://doi.org/10.1053/j.gastro.2013.07.025

Esposito, I., Kleeff, J., Abiatari, I., Shi, X., Giese, N., Bergmann, F., Roth, W., Friess, H., and Schirmacher, P. (2007). Overexpression of cellular inhibitor of apoptosis protein 2 is an early event in the progression of pancreatic cancer. *Journal of clinical pathology*, *60*(8), 885–895. https://doi.org/10.1136/jcp.2006.038257

Fantoni, N. Z., Molphy, Z., O'Carroll, S., Menounou, G., Mitrikas, G., Krokidis, M. G., Chatgilialoglu, C., Colleran, J., Banasiak, A., Clynes, M., Roche, S., Kelly, S., Mckee, V., and Kellett, A. (2021). Polypyridyl-Based Copper Phenanthrene Complexes: Combining Stability with Enhanced DNA Recognition. *Chem.-A Eur. J.*, *27*, 971–983. https://doi.org/10.1002/chem.202001996

Fujie, T., Murakami, M., Yoshida, E., Tachinami, T., Shinkai, Y., Fujiwara, Y., Yamamoto, C., Kumagai, Y., Naka, H., and Kaji, T. (2016). Copper diethyldithiocarbamate as an activator of Nrf2 in cultured vascular endothelial cells. *JBIC Journal of Biological Inorganic Chemistry*, *21*(2), 263–273. https://doi.org/10.1007/s00775-016-1337-z

Furfaro, A. L., Loi, G., Ivaldo, C., Passalacqua, M., Pietra, G., Mann, G. E., & Nitti, M. (2022). HO-1 Limits the Efficacy of Vemurafenib/PLX4032 in BRAFV600E Mutated Melanoma Cells Adapted to Physiological Normoxia or Hypoxia. *Antioxidants*, *11*(6), Article 6. https://doi.org/10.3390/antiox11061171

Furfaro, A. L., Piras, S., Domenicotti, C., Fenoglio, D., Luigi, A. D., Salmona, M., Moretta, L., Marinari, U. M., Pronzato, M. A., Traverso, N., and Nitti, M. (2016). Role of Nrf2, HO-1 and GSH in Neuroblastoma Cell Resistance to Bortezomib. *PLoS ONE*, *11*(3), e0152465. https://doi.org/10.1371/journal.pone.0152465

Galluzzi, L., & Myint, M. (2023). Cell death and senescence. *Journal of Translational Medicine*, *21*(1), 425. https://doi.org/10.1186/s12967-023-04297-y

Galluzzi, L., and Kroemer, G. (2017). Secondary Necrosis: Accidental No More. *Trends in Cancer*, *3*(1), 1–2. https://doi.org/10.1016/j.trecan.2016.12.001

Galluzzi, L., Bravo-San Pedro, J. M., Vitale, I., Aaronson, S. A., Abrams, J. M., Adam, D., Alnemri, E. S., Altucci, L., Andrews, D., Annicchiarico-Petruzzelli, M., Baehrecke, E. H., Bazan, N. G., Bertrand, M. J., Bianchi, K., Blagosklonny, M. V., Blomgren, K., Borner, C., Bredesen, D. E., Brenner, C., … Kroemer, G. (2015). Essential versus accessory aspects of cell death: Recommendations of the NCCD 2015. *Cell Death & Differentiation*, *22*(1), Article 1. https://doi.org/10.1038/cdd.2014.137

Galluzzi, L., Kepp, O., and Kroemer, G. (2012). Mitochondria: master regulators of danger signalling. *Nature reviews. Molecular cell biology*, *13*(12), 780–788. doi: https://doi.org/10.1038/nrm3479

Galluzzi, L., Vitale, I., Aaronson, S. A., Abrams, J. M., Adam, D., Agostinis, P., Alnemri, E. S., Altucci, L., Amelio, I., Andrews, D. W., Annicchiarico-Petruzzelli, M., Antonov, A. V., Arama, E., Baehrecke, E. H., Barlev, N. A., Bazan, N. G., Bernassola, F., Bertrand, M. J. M.,

Bianchi, K., … Kroemer, G. (2018). Molecular mechanisms of cell death: Recommendations of the Nomenclature Committee on Cell Death 2018. *Cell Death & Differentiation*, *25*(3), 486–541. https://doi.org/10.1038/s41418-017-0012-4

Garajová, I., Peroni, M., Gelsomino, F., & Leonardi, F. (2023). A Simple Overview of Pancreatic Cancer Treatment for Clinical Oncologists. *Current Oncology*, *30*(11), Article 11. https://doi.org/10.3390/curroncol30110694

García-Ramos, J. C., Gutiérrez, A. G., Vázquez-Aguirre, A., Toledano-Magaña, Y., Alonso-Sáenz, A. L., Gómez-Vidales, V., Flores-Alamo, M., Mejía, C., AND Ruiz-Azuara, L. (2017). The mitochondrial apoptotic pathway is induced by Cu(II) antineoplastic compounds (Casiopeínas®) in SK-N-SH neuroblastoma cells after short exposure times. *Biometals : an international journal on the role of metal ions in biology, biochemistry, and medicine*, *30*(1), 43–58. https://doi.org/10.1007/s10534-016-9983-8

Geng, M., Wang, L., and Li, P. (2013). Correlation between chemosensitivity to anticancer drugs and Bcl-2 expression in gastric cancer. *International journal of clinical and experimental pathology*, *6*(11), 2554–2559

Gordon, A., Abosede, O., Ntsimango, S., Hosten, E., Myeza, N., Eyk, A., Harmse, L., and Ogunlaja, A. (2022). Synthesis and anticancer evaluation of copper(II)- and manganese(II)-theophylline mixed ligand complexes. *Polyhedron, 214*: 115649. 10.1016/j.poly.2022.115649.

Gou, Y., Chen, M., Li, S., Deng, J., Li, J., Fang, G., Yang, F., & Huang, G. (2021). Dithiocarbazate-Copper Complexes for Bioimaging and Treatment of Pancreatic Cancer. *Journal of Medicinal Chemistry*, *64*(9), 5485–5499. https://doi.org/10.1021/acs.jmedchem.0c01936

Graeser, R., Esser, N., Unger, H., Fichtner, I., Zhu, A., Unger, C., and Kratz, F. (2009). INNO-206, the (6-maleimidocaproyl hydrazone derivative of doxorubicin), shows superior antitumor efficacy compared to doxorubicin in different tumor xenograft models and in an orthotopic pancreas carcinoma model. *Investigational New Drugs*, *28*, 14–19. https://doi.org/10.1007/s10637-008-9208-2

Gul, N. S., Khan, T.-M., Chen, M., Huang, K.-B., Hou, C., Choudhary, M. I., Liang, H., and Chen, Z.-F. (2020). New copper complexes inducing bimodal death through apoptosis and autophagy in A549 cancer cells. *Journal of Inorganic Biochemistry*, *213*, 111260. https://doi.org/10.1016/j.jinorgbio.2020.111260

Guo, W., Zhang, X., Lin, L., Wang, H., He, E., Wang, G., and Zhao, Q. (2021). The disulfiram/copper complex induces apoptosis and inhibits tumour growth in human osteosarcoma by activating the ROS/JNK signalling pathway. *The Journal of Biochemistry*, *170*(2), 275–287. https://doi.org/10.1093/jb/mvab045

Hamacher, R., Schmid, R. M., Saur, D., and Schneider, G. (2008). Apoptotic pathways in pancreatic ductal adenocarcinoma. *Molecular Cancer*, *7*, 64. https://doi.org/10.1186/1476-4598-7-64

Harmse, L., Gangat, N., Martins-Furness, C., Dam, J., and de Koning, C. B. (2019). Copper-imidazo[1,2-a]pyridines induce intrinsic apoptosis and modulate the expression of mutated

p53, haem-oxygenase-1 and apoptotic inhibitory proteins in HT-29 colorectal cancer cells. *Apoptosis: An International Journal on Programmed Cell Death*, *24*(7–8), 623–643. https://doi.org/10.1007/s10495-019-01547-7

Haynes, B. F., Soderberg, K. A., and Fauci, A. S. Introduction to the immune system. Loscalzo, J., Fauci, A., Kasper, D., Hauser, S., Longo, D., and Jameson, J. (Eds.), (publicationyear2). *Harrison's Principles of Internal Medicine, 21e*. McGraw-Hill Education. https://0-accesspharmacy-mhmedical-com.innopac.wits.ac.za/content.aspx?bookid=3095&sectionid=265430581

Hecht, J. R., Lonardi, S., Bendell, J., Sim, H. W., Macarulla, T., Lopez, C. D., Van Cutsem, E., Muñoz Martin, A. J., Park, J. O., Greil, R., Wang, H., Hozak, R. R., Gueorguieva, I., Lin, Y., Rao, S., & Ryoo, B. Y. (2021). Randomized Phase III Study of FOLFOX Alone or With Pegilodecakin as Second-Line Therapy in Patients With Metastatic Pancreatic Cancer That Progressed After Gemcitabine (SEQUOIA). *Journal of clinical oncology : official journal of the American Society of Clinical Oncology*, *39*(10), 1108–1118. https://doi.org/10.1200/JCO.20.02232

Heerdt, B. G., Houston, M. A., and Augenlicht, L. H. (2005). The Intrinsic Mitochondrial Membrane Potential of Colonic Carcinoma Cells Is Linked to the Probability of Tumor Progression. *Cancer Research*, *65*(21), 9861–9867. https://doi.org/10.1158/0008-5472.CAN-05-2444

Hill, M., Pereira, V., Chauveau, C., Zagani, R., Remy, S., Tesson, L., Mazal, D., Ubillos, L., Brion, R., Ashgar, K., Mashreghi, M. F., Kotsch, K., Moffett, J., Doebis, C., Seifert, M., Boczkowski, J., Osinaga, E., and Anegon, I. (2005). Heme oxygenase-1 inhibits rat and human breast cancer cell proliferation: Mutual cross inhibition with indoleamine 2,3-dioxygenase. *The FASEB Journal*, *19*(14), 1957–1968. https://doi.org/10.1096/fj.05-3875com

Hu, G. F. (1998). Copper stimulates proliferation of human endothelial cells under culture. *Journal of cellular biochemistry*, *69*(3), 326–335. https://doi.org/10.1002/(sici)10974644(19980601)69:3<326::aid-jcb10>3.0.co;2-a

Hu, H., Ye, Z., Qin, Y., Xu, X., Yu, X., Zhuo, Q., and Ji, S. (2021). Mutations in key driver genes of pancreatic cancer: Molecularly targeted therapies and other clinical implications. *Acta Pharmacologica Sinica*, *42*(11), Article 11. https://doi.org/10.1038/s41401-020-00584-2

Huanwen, W., Zhiyong, L., Xiaohua, S., Xinyu, R., Kai, W., & Tonghua, L. (2009). Intrinsic chemoresistance to gemcitabine is associated with constitutive and laminin-induced phosphorylation of FAK in pancreatic cancer cell lines. *Molecular Cancer*, *8*(1), 125. https://doi.org/10.1186/1476-4598-8-125

Iacobuzio-Donahue, C. A., Fu, B., Yachida, S., Luo, M., Abe, H., Henderson, C. M., Vilardell, F., Wang, Z., Keller, J. W., Banerjee, P., Herman, J. M., Cameron, J. L., Yeo, C. J., Halushka, M. K., Eshleman, J. R., Raben, M., Klein, A. P., Hruban, R. H., Hidalgo, M., and Laheru, D. (2009). DPC4 Gene Status of the Primary Carcinoma Correlates With Patterns of Failure in Patients With Pancreatic Cancer. *Journal of Clinical Oncology*, 27(11), 1806–1813. https://doi.org/10.1200/JCO.2008.17.7188

Iacobuzio-Donahue, C. A., Velculescu, V. E., Wolfgang, C. L., and Hruban, R. H. (2012). Genetic basis of pancreas cancer development and progression: insights from whole-exome and whole-genome sequencing. *Clinical cancer research : an official journal of the American Association for Cancer Research*, *18*(16), 4257–4265. https://doi.org/10.1158/1078-0432.CCR-12-0315

Iacobuzio-Donahue, C.A. (2011). Genetic evolution of pancreatic cancer: lessons learnt from the pancreatic cancer genome sequencing project. *Gut, 61*, 1085 - 1094.

Ijäs, H., Shen, B., Heuer-Jungemann, A., Keller, A., Kostiainen, M. A., Liedl, T., Ihalainen, J. A., and Linko, V. (2021). Unraveling the interaction between doxorubicin and DNA origami nanostructures for customizable chemotherapeutic drug release. *Nucleic Acids Research*, *49*(6), 3048–3062. https://doi.org/10.1093/nar/gkab097

Im, K., Mareninov, S., Diaz, M. F. P., and Yong, W. H. (2019). An Introduction to Performing Immunofluorescence Staining. *Methods in molecular biology (Clifton, N.J.)*, *1897*, 299–311. doi: https://doi.org/10.1007/978-1-4939-8935-5_26

Ismail, Z., Dam, J., Penny, C., de Koning, C. B., and Harmse, L. (2022). Copper-imidazo[1,2-a]pyridines differentially modulate pro- and anti-apoptotic protein and gene expression in HL-60 and K562 leukaemic cells to cause apoptotic cell death. *Biochimica et biophysica acta. Molecular cell research*, *1869*(1), 119160. https://doi.org/10.1016/j.bbamcr.2021.119160

Jänicke, R. U., Sprengart, M. L., Wati, M. R., and Porter, A. G. (1998). Caspase-3 is required for DNA fragmentation and morphological changes associated with apoptosis. *Journal of Biological Chemistry*, *273*(16), 9357–9360. https://doi.org/10.1074/jbc.273.16.9357

Ji, P., Wang, P., Chen, H., Xu, Y., Ge, J., Tian, Z., & Yan, Z. (2023). Potential of Copper and Copper Compounds for Anticancer Applications. *Pharmaceuticals (Basel, Switzerland)*, *16*(2), 234. https://doi.org/10.3390/ph16020234

Juan, C. A., Pérez de la Lastra, J. M., Plou, F. J., and Pérez-Lebeña, E. (2021). The Chemistry of Reactive Oxygen Species (ROS) Revisited: Outlining Their Role in Biological Macromolecules (DNA, Lipids and Proteins) and Induced Pathologies. *International journal of molecular sciences*, *22*(9), 4642. https://doi.org/10.3390/ijms22094642

Jun, S. Y., Hong, S. M., Bae, Y. K., Kim, H. K., Jang, K, Y., Eom, D. W. (2018). Clinicopathological and prognostic significance of heme oxygenase-1 expression in small intestinal adenocarcinoma. *Pathology International* 68, 294-300.

Jung J. (2014). Human tumor xenograft models for preclinical assessment of anticancer drug development. *Toxicological research*, *30*(1), 1–5. https://doi.org/10.5487/TR.2014.30.1.001

Kachadourian, R., Brechbuhl, H. M., Ruiz-Azuara, L., Gracia-Mora, I., & Day, B. J. (2010). Casiopeína IIgly-induced oxidative stress and mitochondrial dysfunction in human lung cancer A549 and H157 cells. *Toxicology*, *268*(3), 176–183. https://doi.org/10.1016/j.tox.2009.12.010

Kanda, M., Matthaei, H., Wu, J., Hong, S.-M., Yu, J., Borges, M., Hruban, R. H., Maitra, A., Kinzler, K., Vogelstein, B., and Goggins, M. (2012). Presence of Somatic Mutations in Most

Early-Stage Pancreatic Intraepithelial Neoplasia. *Gastroenterology*, *142*(4), 730-733.e9. https://doi.org/10.1053/j.gastro.2011.12.042

Kannan, S., Irwin, M. E., Herbrich, S. M., Cheng, T., Patterson, L. L., Aitken, M. J. L., Bhalla, K., You, M. J., Konopleva, M., Zweidler-McKay, P. A., and Chandra, J. (2022). Targeting the NRF2/HO-1 Antioxidant Pathway in FLT3-ITD-Positive AML Enhances Therapy Efficacy. *Antioxidants*, *11*(4), Article 4. https://doi.org/10.3390/antiox11040717

Kauffman, M. K., Kauffman, M. E., Zhu, H., Jia, Z., & Li, Y. R. (2016). Fluorescence-Based Assays for Measuring Doxorubicin in Biological Systems. Reactive Oxygen Species (Apex, N.C.), 2(6), 432–439. https://doi.org/10.20455/ros.2016.873

Keleg, S., Büchler, P., Ludwig, R., Büchler, M. W., and Friess, H. (2003). Invasion and metastasis in pancreatic cancer. *Molecular Cancer*, 2, 14. https://doi.org/10.1186/1476-4598-2-14

Kellett, A., O'Connor, M., McCann, M., McNamara, M., Lynch, P., Rosair, G., McKee, V., Creaven, B., Walsh, M., McClean, S., Foltyn, A., O'Shea, D., Howe, O., and Devereux, M. (2011). Bis-phenanthroline copper(II) phthalate complexes are potent in vitro antitumour agents with 'self-activating' metallo-nuclease and DNA binding properties. *Dalton Transactions (Cambridge, England: 2003)*, *40*(5), 1024–1027. https://doi.org/10.1039/c0dt01607a

Kennelly, P. J. The biochemical roles of transition metals. Kennelly, P. J., Botham, K. M., McGuinness, O. P., Rodwell, V. W., and Weil, P. (Eds.). (2023). *Harper's Illustrated Biochemistry, 32nd Edition*. McGraw Hill Education. https://0accesspharmacymhmedicalcom.innopac.wits.ac.za/content.aspx?bookid=3220&sectionid=268300912

Kessel, D., and Reiners, J. J. (2020). Photodynamic therapy: Autophagy and mitophagy, apoptosis and paraptosis. *Autophagy*, *16*(11), 2098–2101. https://doi.org/10.1080/15548627.2020.1783823

Khan, M. H., Cai, M., Deng, J., Yu, P., Liang, H., and Yang, F. (2019). Anticancer Function and ROS-Mediated Multi-Targeting Anticancer Mechanisms of Copper (II) 2-hydroxy-1-naphthaldehyde Complexes. *Molecules*, *24*(14), 2544. https://doi.org/10.3390/molecules24142544

Kim, E. J., Kim, Y. J., Lee, H. I., Jeong, S. H., Nam, H. J., and Cho, J. H. (2020). NRF2 Knockdown Resensitizes 5-Fluorouracil-Resistant Pancreatic Cancer Cells by Suppressing HO-1 and ABCG2 Expression. *International journal of molecular sciences*, *21*(13), 4646. https://doi.org/10.3390/ijms21134646

Kim, H. R., Kim, S., Kim, E. J., Park, J. H., Yang, S. H., Jeong, E. T., Park, C., Youn, M. J., So, H. S., & Park, R. (2008). Suppression of Nrf2-driven heme oxygenase-1 enhances the chemosensitivity of lung cancer A549 cells toward cisplatin. *Lung cancer (Amsterdam, Netherlands)*, *60*(1), 47–56. https://doi.org/10.1016/j.lungcan.2007.09.021

Kim, S. H., Kim, S. J., Park, J., Joe, Y., Lee, S. E., Saeidi, S., Zhong, X., Kim, S. H., Park, S. A., Na, H. K., Chung, H. T., & Surh, Y. J. (2021). Reprograming of Tumor-Associated

Macrophages in Breast Tumor-Bearing Mice under Chemotherapy by Targeting Heme Oxygenase-1. *Antioxidants (Basel, Switzerland)*, *10*(3), 470. https://doi.org/10.3390/antiox10030470

Kim, S., Park, B. K., Seo, J. H., Choi, J., Choi, J. W., Lee, C. K., Chung, J. B., Park, Y., and Kim, D. W. (2020). Carbohydrate antigen 19-9 elevation without evidence of malignant or pancreatobiliary diseases. *Scientific Reports*, *10*(1), Article 1. https://doi.org/10.1038/s41598-020-65720-8

Kim, Y.-M., Pae, H.-O., Park, J. E., Lee, Y. C., Woo, J. M., Kim, N.-H., Choi, Y. K., Lee, B.-S., Kim, S. R., and Chung, H.-T. (2011). Heme Oxygenase in the Regulation of Vascular Biology: From Molecular Mechanisms to Therapeutic Opportunities. *Antioxidants & Redox Signaling*, *14*(1), 137–167. https://doi.org/10.1089/ars.2010.3153

Kirtonia, A., Sethi, G., and Garg, M. (2020). The multifaceted role of reactive oxygen species in tumorigenesis. *Cellular and Molecular Life Sciences*, *77*(22), 4459–4483. https://doi.org/10.1007/s00018-020-03536-5

Klein-Brill, A., Amar-Farkash, S., Lawrence, G., Collisson, E. A., & Aran, D. (2022). Comparison of FOLFIRINOX vs Gemcitabine Plus Nab-Paclitaxel as First-Line Chemotherapy for Metastatic Pancreatic Ductal Adenocarcinoma. *JAMA network open*, *5*(6), e2216199. https://doi.org/10.1001/jamanetworkopen.2022.16199

Kongpetch, S., Kukongviriyapan, V., Prawan, A., Senggunprai, L., Kukongviriyapan, U., and Buranrat, B. (2012). Crucial Role of Heme Oxygenase-1 on the Sensitivity of Cholangiocarcinoma Cells to Chemotherapeutic Agents. *PL0S ONE*, *7*(4), e34994. https://doi.org/10.1371/journal.pone.0034994

Knipper, K., Lyu, S. I., Goebel, H., Damanakis, A. I., Zhao, Y., Bruns, C. J., Schmidt, T., Kashkar, H., Quaas, A., Schiffmann, L. M., Popp, F. C., & PANCALYZE Study Group (2023). X-linked inhibitor of apoptosis protein is a prognostic marker for a favorable outcome in three identified subsets in resectable adenocarcinoma of the pancreas. *Journal of cancer research and clinical oncology*, *149*(9), 5531–5538. https://doi.org/10.1007/s00432-022-04476-2

Kroemer, G., Galluzzi, L., and Brenner, C. (2007). Mitochondrial membrane permeabilization in cell death. *Physiological reviews*, *87*(1), 99–163. https://doi.org/10.1152/physrev.00013.2006

Kruger, N. J. (1994). The Bradford Method for Protein Quantitation. In J. M. Walker, *Basic Protein and Peptide Protocols* (Vol. 32, pp. 9–16). Humana Press. https://doi.org/10.1385/0-89603-268-X:9

Kumar, S., Bajaj, S., and Bodla, R. B. (2016). Preclinical screening methods in cancer. *Indian journal of pharmacology*, *48*(5), 481–486. https://doi.org/10.4103/0253-7613.190716

Kwaśniewska, D., Fudalej, M., Nurzyński, P., Badowska-Kozakiewicz, A., Czerw, A., Cipora, E., Sygit, K., Bandurska, E., & Deptała, A. (2023). How A Patient with Resectable or Borderline Resectable Pancreatic Cancer should Be Treated-A Comprehensive Review. *Cancers*, *15*(17), 4275. https://doi.org/10.3390/cancers15174275

Lee, W. Y., Chen, Y. C., Shih, C. M., Lin, C. M., Cheng, C. H., Chen, K. C., and Lin, C. W. (2014). The induction of heme oxygenase-1 suppresses heat shock protein 90 and the proliferation of human breast cancer cells through its byproduct carbon monoxide. *Toxicology and applied pharmacology*, *274*(1), 55–62. https://doi.org/10.1016/j.taap.2013.10.027

Leite, C. M., Araujo-Neto, J. H., Guedes, A. P. M., Costa, A. R., Demidoff, F. C., Netto, C. D., Castellano, E. E., Nascimento, O. R., and Batista, A. A. (2023). Copper(I)/Triphenylphosphine Complexes Containing Naphthoquinone Ligands as Potential Anticancer Agents. *Inorganics*, *11*(9), Article 9. https://doi.org/10.3390/inorganics11090367

Levine, B., & Kroemer, G. (2019). Biological Functions of Autophagy Genes: A Disease Perspective. *Cell*, *176*(1-2), 11–42. https://doi.org/10.1016/j.cell.2018.09.048

Li, D., Ueta, E., Kimura, T., Yamamoto, T., & Osaki, T. (2004). Reactive oxygen species (ROS) control the expression of Bcl-2 family proteins by regulating their phosphorylation and ubiquitination. *Cancer science*, *95*(8), 644–650. https://doi.org/10.1111/j.1349-7006.2004.tb03323.x

Li, J., Hu, Z., Zhu, J., Lin, X., Gao, X., and Lv, G. (2023). Antitumor Effects of Pegylated Zinc Protoporphyrin-Mediated Sonodynamic Therapy in Ovarian Cancer. *Pharmaceutics*, *15*(9), Article 9. https://doi.org/10.3390/pharmaceutics15092275

Li, Q., Feng, Z., Miao, R., Liu, X., Liu, C., and Liu, Z. (2022). Prognosis and survival analysis of patients with pancreatic cancer: Retrospective experience of a single institution. *World Journal of Surgical Oncology*, *20*(1), 11. https://doi.org/10.1186/s12957-021-02478-x

Lin, C.-W., Shen, S.-C., Hou, W.-C., Yang, L.-Y., and Chen, Y.-C. (2008). Heme oxygenase-1 inhibits breast cancer invasion via suppressing the expression of matrix metalloproteinase-9. *Molecular Cancer Therapeutics*, *7*(5), 1195–1206. https://doi.org/10.1158/1535-7163.MCT-07-2199

Lin, Q., Weis, S., Yang, G., Weng, Y. H., Helston, R., Rish, K., Smith, A., Bordner, J., Polte, T., Gaunitz, F., Dennery, P. A. (2007). Heme Oxygenase-1 protein localizes to the nucleus and activates transcription factors important in oxidative stress. *The Journal of Biological Chemistry* 282(28), 20621–20633.

Linkermann, A., Hackl, M. J., Kunzendorf, U., Walczak, H., Krautwald, S., and Jevnikar, A. M. (2013). Necroptosis in Immunity and Ischemia-Reperfusion Injury. *American Journal of Transplantation*, *13*(11), 2797–2804. https://doi.org/10.1111/ajt.12448

Liou, G.-Y., and Storz, P. (2010). Reactive oxygen species in cancer. *Free Radical Research*, *44*(5), 10.3109/10715761003667554. https://doi.org/10.3109/10715761003667554

Liu, X., Xia, S., Zhang, Z., Wu, H., and Lieberman, J. (2021). Channelling inflammation: Gasdermins in physiology and disease. *Nature Reviews Drug Discovery*, *20*(5), 384–405. https://doi.org/10.1038/s41573-021-00154-z

Liu, Y. S., Li, H. S., Qi, D. F., Zhang, J., Jiang, X. C., Shi, K., Zhang, X. J., and Zhang, X. H. (2014). Zinc protoporphyrin IX enhances chemotherapeutic response of hepatoma cells to

cisplatin. *World journal of gastroenterology*, *20*(26), 8572–8582. https://doi.org/10.3748/wjg.v20.i26.8572

Logue, S. E., Elgendy, M., and Martin, S. J. (2009). Expression, purification and use of recombinant annexin V for the detection of apoptotic cells. *Nature Protocols*, *4*(9), Article 9. https://doi.org/10.1038/nprot.2009.143

Luanpitpong, S., Chanvorachote, P., Stehlik, C., Tse, W., Callery, P. S., Wang, L., & Rojanasakul, Y. (2013). Regulation of apoptosis by Bcl-2 cysteine oxidation in human lung epithelial cells. *Molecular biology of the cell*, *24*(6), 858–869. https://doi.org/10.1091/mbc.E12-10-0747

Luchini, C., Grillo, F., Fassan, M., Vanoli, A., Capelli, P., Paolino, G., Ingravallo, G., Renzulli, G., Doglioni, C., D'Amuri, A., Mattiolo, P., Pecori, S., Parente, P., Florena, A. M., Zamboni, G., and Scarpa, A. (2020). Malignant epithelial/exocrine tumors of the pancreas. *Pathologica*, *112*(3), 210–226. https://doi.org/10.32074/1591-951X-167

Ly, J. D., Grubb, D. R., and Lawen, A. (2003). The mitochondrial membrane potential (Δψm) in apoptosis; an update. *Apoptosis*, *8*(2), 115–128. https://doi.org/10.1023/A:1022945107762

Ma, T., Xu, J., Wang, Y., Yu, H., Yang, Y., Liu, Y., Ding, W., Zhu, W., Chen, R., Ge, Z., Tan, Y., Jia, L., and Zhu, T. (2015). Ternary copper(II) complexes with amino acid chains and heterocyclic bases: DNA binding, cytotoxic and cell apoptosis induction properties. *Journal of inorganic biochemistry*, *144*, 38–46. https://doi.org/10.1016/j.jinorgbio.2014.12.011

Maddalena, M., Mallel, G., Nataraj, N. B., Shreberk-Shaked, M., Hassin, O., Mukherjee, S., Arandkar, S., Rotkopf, R., Kapsack, A., Lambiase, G., Pellegrino, B., Ben-Isaac, E., Golani, O., Addadi, Y., Hajaj, E., Eilam, R., Straussman, R., Yarden, Y., Lotem, M., & Oren, M. (2021). *TP53* missense mutations in PDAC are associated with enhanced fibrosis and an immunosuppressive microenvironment. *Proceedings of the National Academy of Sciences of the United States of America*, *118*(23), e2025631118. https://doi.org/10.1073/pnas.2025631118

Mahmood, T., & Yang, P.-C. (2012). Western Blot: Technique, Theory, and Trouble Shooting. *North American Journal of Medical Sciences*, *4*(9), 429–434. https://doi.org/10.4103/1947-2714.100998

Manrai, M., Tilak, T. V. S. V. G. K., Dawra, S., Srivastava, S., and Singh, A. (2021). Current and emerging therapeutic strategies in pancreatic cancer: Challenges and opportunities. *World journal of gastroenterology*, *27*(39), 6572–6589. https://doi.org/10.3748/wjg.v27.i39.6572

Martin, S. J., Henry, C. M., and Cullen, S. P. (2012). A Perspective on Mammalian Caspases as Positive and Negative Regulators of Inflammation. *Molecular Cell*, *46*(4), 387–397. https://doi.org/10.1016/j.molcel.2012.04.026

Mascaró, M., Alonso, E. N., Alonso, E. G., Lacunza, E., Curino, A. C., & Facchinetti, M. M. (2021). Nuclear Localization of Heme Oxygenase-1 in Pathophysiological Conditions: Does It Explain the Dual Role in Cancer?. *Antioxidants (Basel, Switzerland)*, *10*(1), 87. https://doi.org/10.3390/antiox10010087

Masuri, S., Vaňhara, P., Cabiddu, M. G., Moráň, L., Havel, J., Cadoni, E., and Pivetta, T. (2022). Copper(II) Phenanthroline-Based Complexes as Potential AntiCancer Drugs: A Walkthrough on the Mechanisms of Action. *Molecules*, *27*(1), Article 1. https://doi.org/10.3390/molecules27010049

Mazur, P. K., and Siveke, J. T. (2012). Genetically engineered mouse models of pancreatic cancer: Unravelling tumour biology and progressing translational oncology. Gut, 61(10), 1488–1500. https://doi.org/10.1136/gutjnl-2011-300756

McAuslan, B. R., & Reilly, W. (1980). Endothelial cell phagokinesis in response to specific metal ions. *Experimental cell research*, *130*(1), 147–157. https://doi.org/10.1016/0014-4827(80)90051-8

McCarthy, A. J., and Chetty, R. (2018). Smad4/DPC4. *Journal of Clinical Pathology*, *71*(8), 661–664. https://doi.org/10.1136/jclinpath-2018-205095

McCarthy, D. M., Brat, D. J., Wilentz, R. E., Yeo, C. J., Cameron, J. L., Kern, S. E., and Hruban, R. H. (2001). Pancreatic intraepithelial neoplasia and infiltrating adenocarcinoma: Analysis of progression and recurrence by DPC4 immunohistochemical labeling. *Human Pathology*, 32(6), 638–642. https://doi.org/10.1053/hupa.2001.24991

McGuigan, A., Kelly, P., Turkington, R. C., Jones, C., Coleman, H. G., & McCain, R. S. (2018). Pancreatic cancer: A review of clinical diagnosis, epidemiology, treatment and outcomes. *World journal of gastroenterology*, *24*(43), 4846–4861. https://doi.org/10.3748/wjg.v24.i43.4846

Mellman, I. (1996). Endocytosis and molecular sorting. *Annual Review of Cell and Developmental Biology*, *12*, 575–625. https://doi.org/10.1146/annurev.cellbio.12.1.575

Miyake, M., Fujimoto, K., Anai, S., Ohnishi, S., Nakai, Y., Inoue, T., Matsumura, Y., Tomioka, A., Ikeda, T., Okajima, E., Tanaka, N., and Hirao, Y. (2010). Inhibition of Heme Oxygenase-1 Enhances the Cytotoxic Effect of Gemcitabine in Urothelial Cancer Cells. *Anticancer Research*, *30*(6), 2145–2152.

Molinaro, C., Wambang, N., Pellegrini, S., Henry, N., Lensink, M. F., Germain, E., Bousquet, T., de Ruyck, J., Cailliau, K., Pélinski, L., and Martoriati, A. (2023). Synthesis and Biological Activity of a New Indenoisoquinoline Copper Derivative as a Topoisomerase I Inhibitor. *International Journal of Molecular Sciences*, *24*(19), 14590. https://doi.org/10.3390/ijms241914590

Moore, P. S., Sipos, B., Orlandini, S., Sorio, C., Real, F. X., Lemoine, N. R., Gress, T., Bassi, C., Klöppel, G., Kalthoff, H., Ungefroren, H., Löhr, M., and Scarpa, A. (2001). Genetic profile of 22 pancreatic carcinoma cell lines: Analysis of K-ras, p53, p16 and DPC4/Smad4. *Virchows Archiv*, *439*(6), 798–802. https://doi.org/10.1007/s004280100474

Mosmann, T. (1983). Rapid colorimetric assay for cellular growth and survival: application to proliferation and cytotoxicity assays. *Journal of immunological methods*, *65*(1-2), 55–63. doi: https://doi.org/10.1016/0022-1759(83)90303-4

Moussata, D., Amara, S., Siddeek, B., Decaussin, M., Hehlgans, S., Paul-Bellon, R., Mornex, F., Gerard, J. P., Romestaing, P., Rödel, F., Flourie, B., Benahmed, M., and Mauduit, C. (2012). XIAP as a radioresistance factor and prognostic marker for radiotherapy in human rectal adenocarcinoma. *The American Journal of Pathology*, *181*(4), 1271–1278. https://doi.org/10.1016/j.ajpath.2012.06.029

Mucha, O., Podkalicka, P., Mikulski, M., Barwacz, S., Andrysiak, K., Biela, A., Mieczkowski, M., Kachamakova-Trojanowska, N., Ryszawy, D., Białas, A., Szelążek, B., Grudnik, P., Majewska, E., Michalik, K., Jakubiec, K., Bień, M., Witkowska, N., Gluza, K., Ekonomiuk, D., … Łoboda, A. (2019). Development and characterization of a new inhibitor of heme oxygenase activity for cancer treatment. *Archives of Biochemistry and Biophysics*, *671*, 130–142. https://doi.org/10.1016/j.abb.2019.07.002

Muchaa, O., Podkalickaa, P., Mikulskib, M., Barwacza, S., Andrysiaka, K., Bielaa, A., Mieczkowskia, M., Kachamakova-Trojanowskaa, N., Ryszawye, D., Białasb, A., Szelążekc, B., Grudnikg, P., Majewskab, E., Michalikb, K., Jakubiecb, K., Bieńb, M., Witkowskab, N., Gluzab, K., Ekonomiukb, D., Sitarzb, K., Gałęzowskib, M., Brzózkab, K., Dubinc, G., Józkowicza, A., Dulaka, J., Łobodaa, A. (2019). Development and characterization of a new inhibitor of heme oxygenase activity for cancer treatment. *Archives of Biochemistry and Biophysics* 671, 130-142. https://doi.org/10.1016/j.abb.2019.07.002

Muller, P. A. J., and Vousden, K. H. (2014). Mutant p53 in Cancer: New Functions and Therapeutic Opportunities. Cancer Cell, 25(3), 304–317. https://doi.org/10.1016/j.ccr.2014.01.021

Nakamura, H., and Takada, K. (2021). Reactive oxygen species in cancer: Current findings and future directions. *Cancer science*, *112*(10), 3945–3952. https://doi.org/10.1111/cas.15068

National Cancer Institute, Surveillance, Epidemiology and End Results Program. (2023). *Cancer of the Pancreas—Cancer Stat Facts*. https://seer.cancer.gov/statfacts/html/pancreas.html. Accessed February 2024

National Cancer Institute. (2022). *Pancreatic Neuroendocrine Tumors (Islet Cell Tumors) Treatment (PDQ®)*. https://www.cancer.gov/types/pancreatic/hp/pnet-treatment-pdq. Accessed February 2024.

National Health Laboratory Services., National Cancer Registry. (2020). National cancer incidence report. https://www.nicd.ac.za/wp-content/uploads/2023/04/The-National-Pathology-Cancer-Incidence-Report-2020.pdf Accessed February 2024

Neophytou, C. M., Trougakos, I. P., Erin, N., and Papageorgis, P. (2021). Apoptosis Deregulation and the Development of Cancer Multi-Drug Resistance. *Cancers*, *13*(17), Article 17. https://doi.org/10.3390/cancers13174363

Neoptolemos, J. P., Palmer, D. H., Ghaneh, P., Psarelli, E. E., Valle, J. W., Halloran, C. M., Faluyi, O., O'Reilly, D. A., Cunningham, D., Wadsley, J., Darby, S., Meyer, T., Gillmore, R., Anthoney, A., Lind, P., Glimelius, B., Falk, S., Izbicki, J. R., Middleton, G. W., … Büchler, M. W. (2017). Comparison of adjuvant gemcitabine and capecitabine with gemcitabine monotherapy in patients with resected pancreatic cancer (ESPAC-4): A multicentre, open-

label, randomised, phase 3 trial. *The Lancet*, *389*(10073), 1011–1024. https://doi.org/10.1016/S0140-6736(16)32409-6

Nitti, M., Ortolan, J., and Furfaro, A. L. (2023). Role of heme oxygenase-1 in tumor immune escape. *Redox Experimental Medicine*, *2023*(1). https://doi.org/10.1530/REM-23-0006

Nowis, D., Legat, M., Grzela, T., Niderla, J., Wilczek, E., Wilczynski, G. M., Głodkowska, E., Mrówka, P., Issat, T., Dulak, J., Józkowicz, A., Waś, H., Adamek, M., Wrzosek, A., Nazarewski, S., Makowski, M., Stokłosa, T., Jakóbisiak, M., & Gołab, J. (2006). Heme oxygenase-1 protects tumor cells against photodynamic therapy-mediated cytotoxicity. *Oncogene*, *25*(24), 3365–3374. https://doi.org/10.1038/sj.onc.1209378

Nuhn, P., Künzli, B. M., Hennig, R., Mitkus, T., Ramanauskas, T., Nobiling, R., Meuer, S. C., Friess, H., & Berberat, P. O. (2009). Heme oxygenase-1 and its metabolites affect pancreatic tumor growth in vivo. *Molecular Cancer* 8(37). Doi: https://doi.org/10.1186/1476- 4598-8-37

Nurcahyanti, A. D., and Wink, M. (2016). L-Canavanine potentiates the cytotoxicity of doxorubicin and cisplatin in arginine deprived human cancer cells. *PeerJ*, *4*, e1542. https://doi.org/10.7717/peerj.1542

O'Reilly, E. M., and Hechtman, J. F. (2019). Tumour response to TRK inhibition in a patient with pancreatic adenocarcinoma harbouring an NTRK gene fusion. *Annals of Oncology*, *30*(Suppl 8), viii36–viii40. https://doi.org/10.1093/annonc/mdz385

Olive, K. P., Jacobetz, M. A., Davidson, C. J., Gopinathan, A., McIntyre, D., Honess, D., Madhu, B., Goldgraben, M. A., Caldwell, M. E., Allard, D., Frese, K. K., Denicola, G., Feig, C., Combs, C., Winter, S. P., Ireland-Zecchini, H., Reichelt, S., Howat, W. J., Chang, A., Dhara, M., … Tuveson, D. A. (2009). Inhibition of Hedgehog signaling enhances delivery of chemotherapy in a mouse model of pancreatic cancer. *Science (New York, N.Y.)*, *324*(5933), 1457–1461. https://doi.org/10.1126/science.1171362

Pai, M., Spalding, D. (2015). Pancreatic cancer. *Medicine* 43(6), 329-333.

Pellei, M., Santini, C., Bagnarelli, L., Battocchio, C., Iucci, G., Venditti, I., Meneghini, C., Amatori, S., Sgarbossa, P., Marzano, C., De Franco, M., & Gandin, V. (2022). Exploring the Antitumor Potential of Copper Complexes Based on Ester Derivatives of Bis(pyrazol-1-yl)acetate Ligands. *International Journal of Molecular Sciences*, *23*(16), 9397. https://doi.org/10.3390/ijms23169397

Peters, J.-M., Cejka, Z., Harris, J. R., Kleinschmidt, J. A., & Baumeister, W. (1993). Structural Features of the 26 S Proteasome Complex. *Journal of Molecular Biology*, *234*(4), 932–937. https://doi.org/10.1006/jmbi.1993.1646

Petrelli, F., Parisi, A., Tomasello, G., Mini, E., Arru, M., Russo, A., Garrone, O., Khakoo, S., Ardito, R., & Ghidini, M. (2023). Comparison of different second line treatments for metastatic pancreatic cancer: A systematic review and network meta-analysis. *BMC Gastroenterology*, *23*(1), 212. https://doi.org/10.1186/s12876-023-02853-w

Pierzyńska-Mach, A., Janowski, P. A., and Dobrucki, J. W. (2014). Evaluation of acridine orange, LysoTracker Red, and quinacrine as fluorescent probes for long-term tracking of acidic vesicles. *Cytometry Part A*, *85*(8), 729–737. https://doi.org/10.1002/cyto.a.22495

Pittman, M. E., Rao, R., and Hruban, R. H. (2017). Classification, Morphology, Molecular Pathogenesis, and Outcome of Premalignant Lesions of the Pancreas. *Archives of pathology & laboratory medicine*, 141(12), 1606–1614. https://doi.org/10.5858/arpa.2016-0426-RA

Podkalicka, P., Mucha, O., Józkowicz, A., Dulak, J., & Łoboda, A. (2018). Heme oxygenase inhibition in cancers: Possible tools and targets. *Contemporary Oncology*, *22*(1A), 23–32. https://doi.org/10.5114/wo.2018.73879

Podolsky, D. K., Camilleri, M., Fitz, J. G., Kalloo, A. N., Shanahan, F., Wang, T. C. (2016). Chapter 31: Neoplasia of the gastrointestinal tract. In: *Yamada's Textbook of Gastroenterology.* West Sussex: John Wiley and Sons Ltd.

Porporato, P. E., Filigheddu, N., Pedro, J. M. B.-S., Kroemer, G., & Galluzzi, L. (2018). Mitochondrial metabolism and cancer. *Cell Research*, 28(3), 265–280. https://doi.org/10.1038/cr.2017.155

Principe, D. R., Underwood, P. W., Korc, M., Trevino, J. G., Munshi, H. G., and Rana, A. (2021). The Current Treatment Paradigm for Pancreatic Ductal Adenocarcinoma and Barriers to Therapeutic Efficacy. *Frontiers in Oncology*, 11. https://www.frontiersin.org/articles/10.3389/fonc.2021.688377

Qiu, W., Sahin, F., Iacobuzio-Donahue, C., Garcia-Carracedo, D., Wang, W., Kuo, C.-Y., Chen, D., Arking, D., Lowy, A., Hruban, R., Remotti, H., and Su, G. H. (2011). Disruption of p16 and Activation of Kras in Pancreas Increase Ductal Adenocarcinoma Formation and Metastasis in vivo. *Oncotarget*, 2(11), 862–873. https://doi.org/10.18632/oncotarget.357

Rawla, P., Sunkara, T., Gaduputic, V. (2019). Epidemiology of Pancreatic Cancer: Global Trends, Etiology and Risk Factors. *World Journal of Oncology* 10(1), 10-27. doi: 10.14740/wjon1166

Redza-Dutordoir, M., and Averill-Bates, D. A. (2016). Activation of apoptosis signalling pathways by reactive oxygen species. *Biochimica et biophysica acta*, *1863*(12), 2977–2992. https://doi.org/10.1016/j.bbamcr.2016.09.012

Reers, M., Smith, T. W., & Chen, L. B. (1991). J-aggregate formation of a carbocyanine as a quantitative fluorescent indicator of membrane potential. *Biochemistry*, *30*(18), 4480–4486. https://doi.org/10.1021/bi00232a015

Reheman, D., Zhao, J., Guan, S., Xu, G.-C., Li, Y.-J., and Sun, S.-R. (2020). Apoptotic effect of novel pyrazolone-based derivative [Cu(PMPP-SAL)(EtOH)] on HeLa cells and its mechanism. *Scientific Reports*, *10*(1), 18235. https://doi.org/10.1038/s41598-020-75173-8

Reilly, B., Tan, C., Murao, A., Nofi, C., Jha, A., Aziz, M., and Wang, P. (2022). Necroptosis-Mediated eCIRP Release in Sepsis. *Journal of Inflammation Research*, *15*, 4047–4059. https://doi.org/10.2147/JIR.S370615

Rodrigues, J. H. V., De Carvalho, A. B., Silva, V. R., De S. Santos, L., Soares, M. B. P., Bezerra, D. P., Oliveira, K. M., & Corrêa, R. S. (2023). Copper(II)/diiminic complexes based on 2-hydroxybenzophenones: DNA- and BSA-binding studies and antitumor activity against HCT116 and HepG2 tumor cells. *Polyhedron*, *239*, 116431. https://doi.org/10.1016/j.poly.2023.116431

Rooplal, N. J. (2023). An evaluation of the anticancer effects of metal complexes on glioblastoma cell lines. (M.Sc. Thesis). University of the Witwatersrand, Johannesburg.

Ryter, S. W., Alam, J., and Choi, A. M. K. (2006). Heme Oxygenase-1/Carbon Monoxide: From Basic Science to Therapeutic Applications. *Physiological Reviews*, *86*(2), 583–650. https://doi.org/10.1152/physrev.00011.2005

Sacca, P., Meiss, R., Casas, G., Mazza, O., Calvo, J. C., Navone, N., and Vazquez, E. (2007). Nuclear translocation of haeme oxygenase-1 is associated to prostate cancer. *British Journal of Cancer*, *97*(12), 1683–1689. https://doi.org/10.1038/sj.bjc.6604081

Sakamuru, S., Attene-Ramos, M. S., and Xia, M. (2016). Mitochondrial Membrane Potential Assay. *Methods in Molecular Biology (Clifton, N.J.)*, *1473*, 17–22. https://doi.org/10.1007/978-1-4939-6346-1_2

Salimi, M., Abdi, K., Kandelous, H. M., Hadadzadeh, H., Azadmanesh, K., Amanzadeh, A., and Sanati, H. (2015). Antiproliferative effects of copper(II)–polypyridyl complexes in breast cancer cells through inducing apoptosis. *BioMetals*, *28*(2), 267–278. https://doi.org/10.1007/s10534-015-9820-5

Sass, G., Leukel, P., Schmitz, V., Raskopf, E., Ocker, M., Neureiter, D., Meissnitzer, M., Tasika, E., Tannapfel, A., and Tiegs, G. (2008). Inhibition of heme oxygenase 1 expression by small interfering RNA decreases orthotopic tumor growth in livers of mice. *International journal of cancer*, *123*(6), 1269–1277. https://doi.org/10.1002/ijc.23695

Schawkat, K., Manning, M. A., Glickman, J. N., and Mortele, K. J. (2020). Pancreatic Ductal Adenocarcinoma and Its Variants: Pearls and Perils. *RadioGraphics*, *40*(5), 1219–1239. https://doi.org/10.1148/rg.2020190184

Schulz, S., Wong, R. J., Vreman, H. J., & Stevenson, D. K. (2012). Metalloporphyrins - an update. *Frontiers in pharmacology*, *3*, 68. https://doi.org/10.3389/fphar.2012.00068

Schutte, M., Hruban, R. H., Geradts, J., Maynard, R., Hilgers, W., Rabindran, S. K., Moskaluk, C. A., Hahn, S. A., Schwarte-Waldhoff, I., Schmiegel, W., Baylin, S. B., Kern, S. E., and Herman, J. G. (1997). Abrogation of the Rb/p16 tumor-suppressive pathway in virtually all pancreatic carcinomas. *Cancer Research*, *57*(15), 3126–3130.

Serrano, M., Hannon, G. J., and Beach, D. (1993). A new regulatory motif in cell-cycle control causing specific inhibition of cyclin D/CDK4. *Nature*, *366*(6456), 704–707. https://doi.org/10.1038/366704a0

Shan, F., Shao, Z., Jiang, S., & Cheng, Z. (2016). Erlotinib induces the human non-small-cell lung cancer cells apoptosis via activating ROS-dependent JNK pathways. *Cancer medicine*, *5*(11), 3166–3175. https://doi.org/10.1002/cam4.881

Shi, X., Chen, Z., Wang, Y., Guo, Z., and Wang, X. (2018). Hypotoxic copper complexes with potent anti-metastatic and anti-angiogenic activities against cancer cells. *Dalton Transactions*, *47*(14), 5049–5054. https://doi.org/10.1039/C8DT00794B

Shiozaki, E. N., Chai, J., Rigotti, D. J., Riedl, S. J., Li, P., Srinivasula, S. M., Alnemri, E. S., Fairman, R., and Shi, Y. (2003). Mechanism of XIAP-mediated inhibition of caspase-9. *Molecular cell*, *11*(2), 519–527. https://doi.org/10.1016/s1097-2765(03)00054-6

Sigman, D. S., Graham, D. R., D'Aurora, V., and Stern, A. M. (1979). Oxygen-dependent cleavage of DNA by the 1,10-phenanthroline. Cuprous complex. Inhibition of Escherichia coli DNA polymerase I. *Journal of Biological Chemistry*, *254*(24), 12269–12272. https://doi.org/10.1016/S0021-9258(19)86305-6

Smaglo, B. G. (2023). Role for Neoadjuvant Systemic Therapy for Potentially Resectable Pancreatic Cancer. *Cancers*, *15*(8), 2377. https://doi.org/10.3390/cancers15082377

Sofuni, A., Iijima, H., Moriyasu, F., Nakayama, D., Shimizu, M., Nakamura, K., Itokawa, F., & Itoi, T. (2005). Differential diagnosis of pancreatic tumors using ultrasound contrast imaging. *Journal of gastroenterology*, *40*(5), 518–525. https://doi.org/10.1007/s00535-005-1578-z

Springfeld, C., Ferrone, C. R., Katz, M. H. G., Philip, P. A., Hong, T. S., Hackert, T., Büchler, M. W., & Neoptolemos, J. (2023). Neoadjuvant therapy for pancreatic cancer. *Nature Reviews Clinical Oncology*, *20*(5), 318–337. https://doi.org/10.1038/s41571-023-00746-1

Stahnke, K., Fulda, S., Friesen, C., Strauß, G., and Debatin, K.-M. (2001). Activation of apoptosis pathways in peripheral blood lymphocytes by in vivo chemotherapy. *Blood*, *98*(10), 3066–3073. https://doi.org/10.1182/blood.V98.10.3066

Stewart, D. J. (2010). Tumor and host factors that may limit efficacy of chemotherapy in non-small cell and small cell lung cancer. *Critical Reviews in Oncology/Hematology*, *75*(3), 173–234. https://doi.org/10.1016/j.critrevonc.2009.11.006

Stillwell, W. (2016). Chapter 19: Membrane Transport. In: *An Introduction To Biological Membranes*, Second Edition. Elsevier. 423-451.

Strober, W. (2015). Trypan Blue Exclusion Test of Cell Viability. *Current protocols in immunology*, *111*, A3.B.1–A3.B.3. doi: https://doi.org/10.1002/0471142735.ima03bs111

Summerhayes, I. C., Lampidis, T. J., Bernal, S. D., Nadakavukaren, J. J., Nadakavukaren, K. K., Shepherd, E. L., & Chen, L. B. (1982). Unusual retention of rhodamine 123 by mitochondria in muscle and carcinoma cells. *Proceedings of the National Academy of Sciences of the United States of America*, *79*(17), 5292–5296. https://doi.org/10.1073/pnas.79.17.5292

Sun, X., Wang, S., Gai, J., Guan, J., Li, J., Li, Y., Zhao, J., Zhao, C., Fu, L., and Li, Q. (2019). SIRT5 Promotes Cisplatin Resistance in Ovarian Cancer by Suppressing DNA Damage in a ROS-Dependent Manner via Regulation of the Nrf2/HO-1 Pathway. *Frontiers in Oncology*, *9*. https://www.frontiersin.org/journals/oncology/articles/10.3389/fonc.2019.00754

Sunamura, M., Duda, D. G., Ghattas, M. H., Lozonschi, L., Motoi, F., Yamauchi, J., Matsuno, S., Shibahara, S., and Abraham, N.G. (2003). Heme oxygenase-1 accelerates tumor angiogenesis of human pancreatic cancer. *Angiogenesis* 6(1), 15–24.

Swinney, D.C. (2011). Molecular Mechanism of Action (MMoA) in Drug Discovery. *Annual Reports in Medicinal Chemistry, 46*, 301-317. https://doi.org/10.1016/B978-0-12-386009-5.00009-6

Tamm, I., Richter, S., Scholz, F., Schmelz, K., Oltersdorf, D., Karawajew, L., Schoch, C., Haferlach, T., Ludwig, W. D., and Wuchter, C. (2004). XIAP expression correlates with monocytic differentiation in adult de novo AML: impact on prognosis. *The hematology journal : the official journal of the European Haematology Association*, *5*(6), 489–495. https://doi.org/10.1038/sj.thj.6200549

Tan, Q., Wang, H., Hu, Y., Hu, M., Li, X., Aodengqimuge, Ma, Y., Wei, C., and Song, L. (2015). Src/STAT3-dependent heme oxygenase-1 induction mediates chemoresistance of breast cancer cells to doxorubicin by promoting autophagy. *Cancer Science*, *106*(8), 1023–1032. https://doi.org/10.1111/cas.12712

Thati, B., Noble, A., Creaven, B. S., Walsh, M., Kavanagh, K., & Egan, D. A. (2007). Apoptotic cell death: a possible key event in mediating the in vitro anti-proliferative effect of a novel copper(II) complex, [Cu(4-Mecdoa)(phen)(2)] (phen=phenanthroline, 4-Mecdoa=4-methylcoumarin-6,7-dioxactetate), in human malignant cancer cells. *European journal of pharmacology*, *569*(1-2), 16–28. https://doi.org/10.1016/j.ejphar.2007.04.064

Tibullo, D., Barbagallo, I., Giallongo, C., La Cava, P., Parrinello, N., Vanella, L., Stagno, F., A. Palumbo, G., Li Volti, G., and Di Raimondo, F. (2013). Nuclear Translocation of Heme Oxygenase-1 Confers Resistance to Imatinib in Chronic Myeloid Leukemia Cells. *Current Pharmaceutical Design*, *19*(15), 2765–2770. https://doi.org/10.2174/1381612811319150012

Tibullo, D., Barbagallo, I., Giallongo, C., Vanella, L., Conticello, C., Romano, A., Saccone, S., Godos, J., Raimondo, F. D., and Volti, G. L. (2016). Heme oxygenase-1 nuclear translocation regulates bortezomib-induced cytotoxicity and mediates genomic instability in myeloma cells. *Oncotarget*, *7*(20), 28868–28880. https://doi.org/10.18632/oncotarget.7563

Toesca, D. A. S., Koong, A. J., Poultsides, G. A., Visser, B. C., Haraldsdottir, S., Koong, A. C., and Chang, D. T. (2018). Management of Borderline Resectable Pancreatic Cancer. *International Journal of Radiation Oncology*Biology*Physics*, *100*(5), 1155–1174. https://doi.org/10.1016/j.ijrobp.2017.12.287

Toné, S., Sugimoto, K., Tanda, K., Suda, T., Uehira, K., Kanouchi, H., Samejima, K., Minatogawa, Y., and Earnshaw, W. C. (2007). Three distinct stages of apoptotic nuclear condensation revealed by time-lapse imaging, biochemical and electron microscopy analysis of cell-free apoptosis. *Experimental cell research*, *313*(16), 3635–3644. https://doi.org/10.1016/j.yexcr.2007.06.018

Toufektchan, E., and Toledo, F. (2018). The Guardian of the Genome Revisited: P53 Downregulates Genes Required for Telomere Maintenance, DNA Repair, and Centromere Structure. *Cancers*, *10*(5), 135. https://doi.org/10.3390/cancers10050135

Tsvetkov, P., Coy, S., Petrova, B., Dreishpoon, M., Verma, A., Abdusamad, M., Rossen, J., Joesch-Cohen, L., Humeidi, R., Spangler, R. D., Eaton, J. K., Frenkel, E., Kocak, M., Corsello, S. M., Lutsenko, S., Kanarek, N., Santagata, S., and Golub, T. R. (2022). Copper induces cell death by targeting lipoylated TCA cycle proteins. *Science (New York, N.Y.)*, *375*(6586), 1254–1261. https://doi.org/10.1126/science.abf0529

Tuveson, D. A., and Neoptolemos, J. P. (2012). Understanding Metastasis in Pancreatic Cancer: A Call for New Clinical Approaches. *Cell*, 148(1), 21–23. https://doi.org/10.1016/j.cell.2011.12.021

Valdez-Camacho, J. R., Pérez-Salgado, Y., Espinoza-Guillén, A., Gómez-Vidales, V., Alberto Tavira-Montalvan, C., Meneses-Acosta, A., Leyva, M. A., Vázquez-Ríos, M. G., Juaristi, E., Höpfl, H., Ruiz-Azuara, L., & Escalante, J. (2020). Synthesis, structural characterization and antiproliferative activity on MCF-7 and A549 tumor cell lines of [Cu(*N*-*N*)(*β*3-aminoacidate)]NO3 complexes (Casiopeínas®). *Inorganica Chimica Acta*, *506*, 119542. https://doi.org/10.1016/j.ica.2020.119542

Van Cutsem, E., Tempero, M. A., Sigal, D., Oh, D. Y., Fazio, N., Macarulla, T., Hitre, E., Hammel, P., Hendifar, A. E., Bates, S. E., Li, C. P., Hingorani, S. R., de la Fouchardiere, C., Kasi, A., Heinemann, V., Maraveyas, A., Bahary, N., Layos, L., Sahai, V., Zheng, L., … HALO 109-301 Investigators (2020). Randomized Phase III Trial of Pegvorhyaluronidase Alfa With Nab-Paclitaxel Plus Gemcitabine for Patients With Hyaluronan-High Metastatic Pancreatic Adenocarcinoma. *Journal of clinical oncology : official journal of the American Society of Clinical Oncology*, *38*(27), 3185–3194. https://doi.org/10.1200/JCO.20.00590

van Oosten, A. F., Daamen, L. A., Groot, V. P., Biesma, N. C., Habib, J. R., van Goor, I. W. J. M., Kinny-Köster, B., Burkhart, R. A., Wolfgang, C. L., van Santvoort, H. C., He, J., and Molenaar, I. Q. (2023). Predicting post-recurrence survival for patients with pancreatic cancer recurrence after primary resection: A Bi-institutional validated risk classification. *European Journal of Surgical Oncology*, *49*(9), 106910. https://doi.org/10.1016/j.ejso.2023.04.009

Vermes, I., Haanen, C., Steffens-Nakken, H., and Reutelingsperger, C. (1995). A novel assay for apoptosis. Flow cytometric detection of phosphatidylserine expression on early apoptotic cells using fluorescein labelled Annexin V. *Journal of immunological methods*, *184*(1), 39–51. https://doi.org/10.1016/0022-1759(95)00072-i

Voutsadakis, I. A. (2021). Mutations of p53 associated with pancreatic cancer and therapeutic implications. *Annals of Hepato-Biliary-Pancreatic Surgery*, *25*(3), 315–327. https://doi.org/10.14701/ahbps.2021.25.3.315

Wang-Gillam, A., Hubner, R. A., Siveke, J. T., Hoff, D. D. V., Belanger, B., Jong, F. A. de, Mirakhur, B., & Chen, L.-T. (2019). NAPOLI-1 phase 3 study of liposomal irinotecan in metastatic pancreatic cancer: Final overall survival analysis and characteristics of long-term survivors. *European Journal of Cancer*, *108*, 78–87. https://doi.org/10.1016/j.ejca.2018.12.007

Wang, C., Yang, X., Dong, C., Chai, K., Ruan, J., and Shi, S. (2023). Cu-related agents for cancer therapies. *Coordination Chemistry Reviews*, *487*, 215156. https://doi.org/10.1016/j.ccr.2023.215156

Wang, H., Cheng, Q., Bao, L., Li, M., Chang, K., and Yi, X. (2023). Cytoprotective Role of Heme Oxygenase-1 in Cancer Chemoresistance: Focus on Antioxidant, Antiapoptotic, and Pro-Autophagy Properties. *Antioxidants*, *12*(6), Article 6. https://doi.org/10.3390/antiox12061217

Was, H., Cichon, T., Smolarczyk, R., Rudnicka, D., Stopa, M., Chevalier, C., Leger, J. J., Lackowska, B., Grochot, A., Bojkowska, K., Ratajska, A., Kieda, C., Szala, S., Dulak, J., and Jozkowicz, A. (2006). Overexpression of Heme Oxygenase-1 in Murine Melanoma. *The American Journal of Pathology*, *169*(6), 2181–2198. https://doi.org/10.2353/ajpath.2006.051365

Waters, A. M., and Der, C. J. (2018). KRAS: The Critical Driver and Therapeutic Target for Pancreatic Cancer. *Cold Spring Harbor Perspectives in Medicine*, 8(9), a031435. https://doi.org/10.1101/cshperspect.a031435

Wegiel, B., Gallo, D., Csizmadia, E., Harris, C., Belcher, J., Vercellotti, G. M., Penacho, N., Seth, P., Sukhatme, V., Ahmed, A., Pandolfi, P. P., Helczynski, L., Bjartell, A., Persson, J. L., & Otterbein, L. E. (2013). Carbon Monoxide Expedites Metabolic Exhaustion to Inhibit Tumor Growth. *Cancer Research*, *73*(23), 10.1158/0008-5472.CAN-13–1075. https://doi.org/10.1158/0008-5472.CAN-13-1075

Wei, S., Wang, Y., Chai, Q., Fang, Q., Zhang, Y., and Wang, J. (2014). Potential crosstalk of Ca2+-ROS-dependent mechanism involved in apoptosis of Kasumi-1 cells mediated by heme oxygenase-1 small interfering RNA. *International journal of oncology*, *45*(6), 2373–2384. https://doi.org/10.3892/ijo.2014.2661

Weller, M., Malipiero, U., Aguzzi, A., Reed, J. C., and Fontana, A. (1995). Protooncogene bcl-2 gene transfer abrogates Fas/APO-1 antibody-mediated apoptosis of human malignant glioma cells and confers resistance to chemotherapeutic drugs and therapeutic irradiation. *The Journal of clinical investigation*, *95*(6), 2633–2643. https://doi.org/10.1172/JCI117965

Wellstein, A., and Atkins, M. B. Antibodies, car t cells, and proteins to treat cancer. Brunton, L. L., and Knollmann, B. C.(Eds.), (2023). *Goodman & Gilman's: The Pharmacological Basis of Therapeutics, 14th Edition*. McGraw-Hill Education. https://0-accesspharmacy-mhmedical-com.innopac.wits.ac.za/content.aspx?bookid=3191&sectionid=269731564

Wellstein, A., and Giaccone, G. Protein kinase inhibitors and pathway-targeted small molecules. Brunton, L. L., and Knollmann, B. C.(Eds.), (2023). *Goodman & Gilman's: The Pharmacological Basis of Therapeutics, 14th Edition*. McGraw-Hill Education. https://0-accesspharmacy-mhmedical-com.innopac.wits.ac.za/content.aspx?bookid=3191&sectionid=269309724

Wellstein, A., and Sausville, E. A. Cytotoxics and antimetabolites. Brunton, L. L., and Knollmann, B. C. (Eds.). (2023). Goodman and Gilman's: The Pharmacological Basis of Therpeutics, 14th Edition. McGraw-Hill Education.

Westphal, S., and Kalthoff, H. (2003). Apoptosis: Targets in Pancreatic Cancer. *Molecular Cancer*, *2*, 6. https://doi.org/10.1186/1476-4598-2-6

WHO., International Agency for Research on Cancer. (2022). Pancreas cancer facts sheet. https://gco.iarc.fr/today/data/factsheets/cancers/13-Pancreas-fact-sheet.pdf. Accessed February 2024.

Wilson, J. H., and Hunt, T. (2002). Molecular biology of the cell, 4th edition: a problems approach. New York: Garland Science.

Woo, Y., Lee, H. J., Jung, Y. M., & Jung, Y. J. (2020). Regulated Necrotic Cell Death in Alternative Tumor Therapeutic Strategies. *Cells*, 9(12), 2709. https://doi.org/10.3390/cells9122709

Wu, H., Ou, S., Zhang, H., Huang, R., Yu, S., Zhao, M., and Tai, S. (2022). Advances in biomarkers and techniques for pancreatic cancer diagnosis. *Cancer Cell International*, *22*(1), 220. https://doi.org/10.1186/s12935-022-02640-9

Xie, H., & Kang, Y. J. (2009). Role of copper in angiogenesis and its medicinal implications. *Current Medicinal Chemistry*, *16*(10), 1304–1314. https://doi.org/10.2174/092986709787846622

Xie, J., Yang, Y., Gao, Y., & He, J. (2023). Cuproptosis: Mechanisms and links with cancers. *Molecular Cancer*, *22*(1), 46. https://doi.org/10.1186/s12943-023-01732-y

Xu, B.-Q., Fu, Z.-G., Meng, Y., Wu, X.-Q., Wu, B., Xu, L., Jiang, J.-L., Li, L., and Chen, Z.-N. (2016). Gemcitabine enhances cell invasion via activating HAb18G/CD147-EGFR-pSTAT3 signaling. *Oncotarget*, *7*(38), 62177–62193. https://doi.org/10.18632/oncotarget.11405

Xu, Y., Liu, S. Y., Zeng, L., Ma, H., Zhang, Y., Yang, H., Liu, Y., Fang, S., Zhao, J., Xu, Y., Ashby, C. R., Jr, He, Y., Dai, Z., & Pan, Y. (2022). An Enzyme-Engineered Nonporous Copper(I) Coordination Polymer Nanoplatform for Cuproptosis-Based Synergistic Cancer Therapy. *Advanced Materials (Deerfield Beach, Fla.)*, *34*(43), e2204733. https://doi.org/10.1002/adma.202204733

Yadav, D.,W and Lowenfels, A. B. (2013). The Epidemiology of Pancreatitis and Pancreatic Cancer. *Gastroenterology*, *144*(6), 1252–1261. https://doi.org/10.1053/j.gastro.2013.01.068

Yang, P. S., Hsu, Y. C., Lee, J. J., Chen, M. J., Huang, S. Y., Cheng, S. P. (2018). Heme Oxygenase-1 inhibitors induce cell cycle arrest and suppress tumor growth in thyroid cancer cells. *International Journal of Molecular Sciences* 19 (2502). Doi: doi:10.3390/ijms19092502

Yang, W. S., SriRamaratnam, R., Welsch, M. E., Shimada, K., Skouta, R., Viswanathan, V. S., Cheah, J. H., Clemons, P. A., Shamji, A. F., Clish, C. B., Brown, L. M., Girotti, A. W., Cornish, V. W., Schreiber, S. L., and Stockwell, B. R. (2014). Regulation of ferroptotic cancer cell death by GPX4. *Cell*, *156*(1-2), 317–331. https://doi.org/10.1016/j.cell.2013.12.010

Ye, K., Chen, Z., & Xu, Y. (2023). The double-edged functions of necroptosis. *Cell Death & Disease*, *14*(2), 1–12. https://doi.org/10.1038/s41419-023-05691-6

Yim, W.WY., and Mizushima, N. (2020). Lysosome biology in autophagy. *Cell Discovery 6*: 6. https://doi.org/10.1038/s41421-020-0141-7

Yoshida, T., Sato, M. (1989). Posttranslational and direct integration of heme oxygenase into microsomes. *Biochemical and Biophysical Research Communications* 163(2), 1086–1092. https://doi.org/10.1016/0006-291x(89)92332-2

Yuan, J., Amin, P., and Ofengeim, D. (2019). Necroptosis and RIPK1-mediated neuroinflammation in CNS diseases. *Nature reviews. Neuroscience*, *20*(1), 19–33. https://doi.org/10.1038/s41583-018-0093-1

Yunis, A. A., Arimura, G. K., and Russin, D. J. (1977). Human pancreatic carcinoma (MIA PaCa-2) in continuous culture: sensitivity to asparaginase. *International Journal of Cancer*, *19*(1), 128–135. https://doi.org/10.1002/ijc.2910190118

Zhang, Z., Wang, H., Wang, Q., Yan, M., Wang, H., Bi, C., Sun, S., & Fan, Y. (2016). Anticancer activity and computational modeling of ternary copper (II) complexes with 3-indolecarboxylic acid and 1,10-phenanthroline. *International Journal of Oncology*, *49*(2), 691–699. https://doi.org/10.3892/ijo.2016.3542

Zhou, P., Qin, J., Zhou, C., Wan, G., Liu, Y., Zhang, M., Yang, X., Zhang, N., & Wang, Y. (2019). Multifunctional nanoparticles based on a polymeric copper chelator for combination treatment of metastatic breast cancer. *Biomaterials*, *195*, 86–99. https://doi.org/10.1016/j.biomaterials.2019.01.007

Zuliani, T., Duval, R., Jayat, C., Schnébert, S., André, P., Dumas, M., and Ratinaud, M.-H. (2003). Sensitive and reliable JC-1 and TOTO-3 double staining to assess mitochondrial transmembrane potential and plasma membrane integrity: Interest for cell death investigations. *Cytometry Part A*, *54A*(2), 100–108. https://doi.org/10.1002/cyto.a.10059

Appendix

Appendix A: Standard protein curve

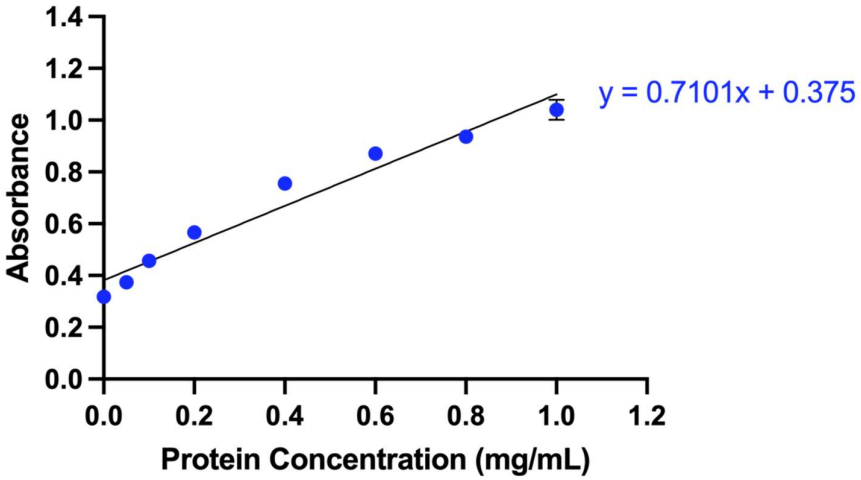


Figure A1 Standard curve for protein concentration obtained from Bradford assay for western blots.

Appendix B: The effect of the copper complexes on caspase-9 activation in AsPC-1 cells.

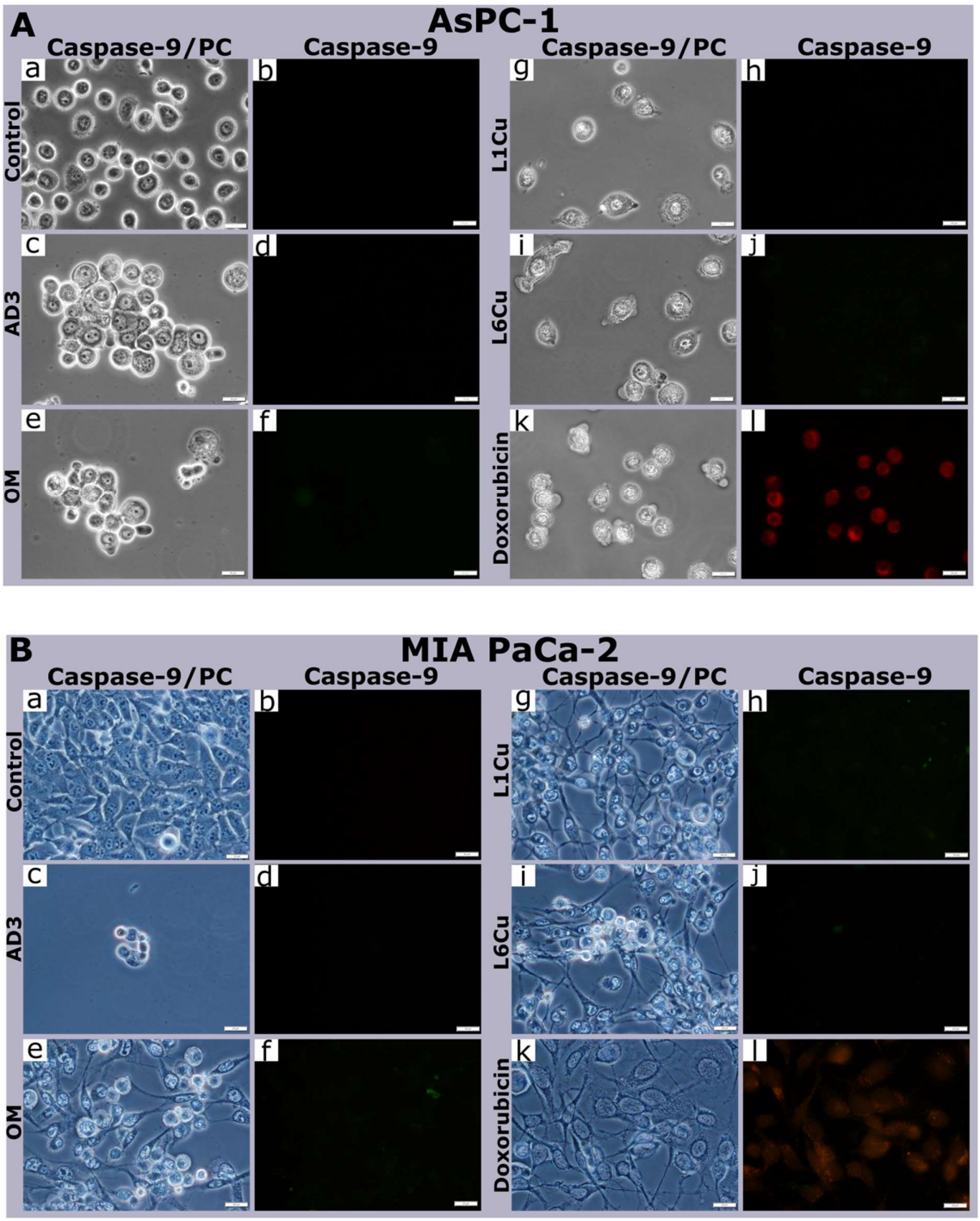


Figure B1 Representative photomicrographs showing the effects of the copper complexes on caspase-9 activation in AsPC-1 (A) and MIA PaCa-2 (B) cells after a 24 h treatment period. AsPC-1 cells were treated with AD3 at 6 µM; OM at 4 µM; and L1Cu and L6Cu at 2 µM; and doxorubicin at 5 µM. MIA PaCa-2 cells were treated with AD3 at 6 µM; OM at 5 µM; and L1Cu and L6Cu at 2 µM; and doxorubicin at 5 µM. Cells viewed with Olympus BX41 microscope. Images captured with Olympus DP72 camera. Green fluorescence= active caspase-9. Magnification: 400X, scale bar: 20 µm. Legend: PC = phase contrast.

Appendix C: Ethics waiver

UNIVERSITY OF THE WITWATERSRAND, JOHANNESBURG

HUMAN RESEARCH ETHICS COMMITTEE (MEDICAL)

12/10/2020

Ref: W-CBP-201012-01

TO WHOM IT MAY CONCERN:

Waiver: This certifies that the following research does not require clearance from the Human Research Ethics Committee (Medical).

Investigator: Ms Z Jhetam
Student No. (if appropriate): 1434073
Staff No. (if appropriate): A0068489

Supervisor: Dr L Harmse

School: Therapeutic Sciences
Department: Pharmancy and Pharmacology
Medical School
University

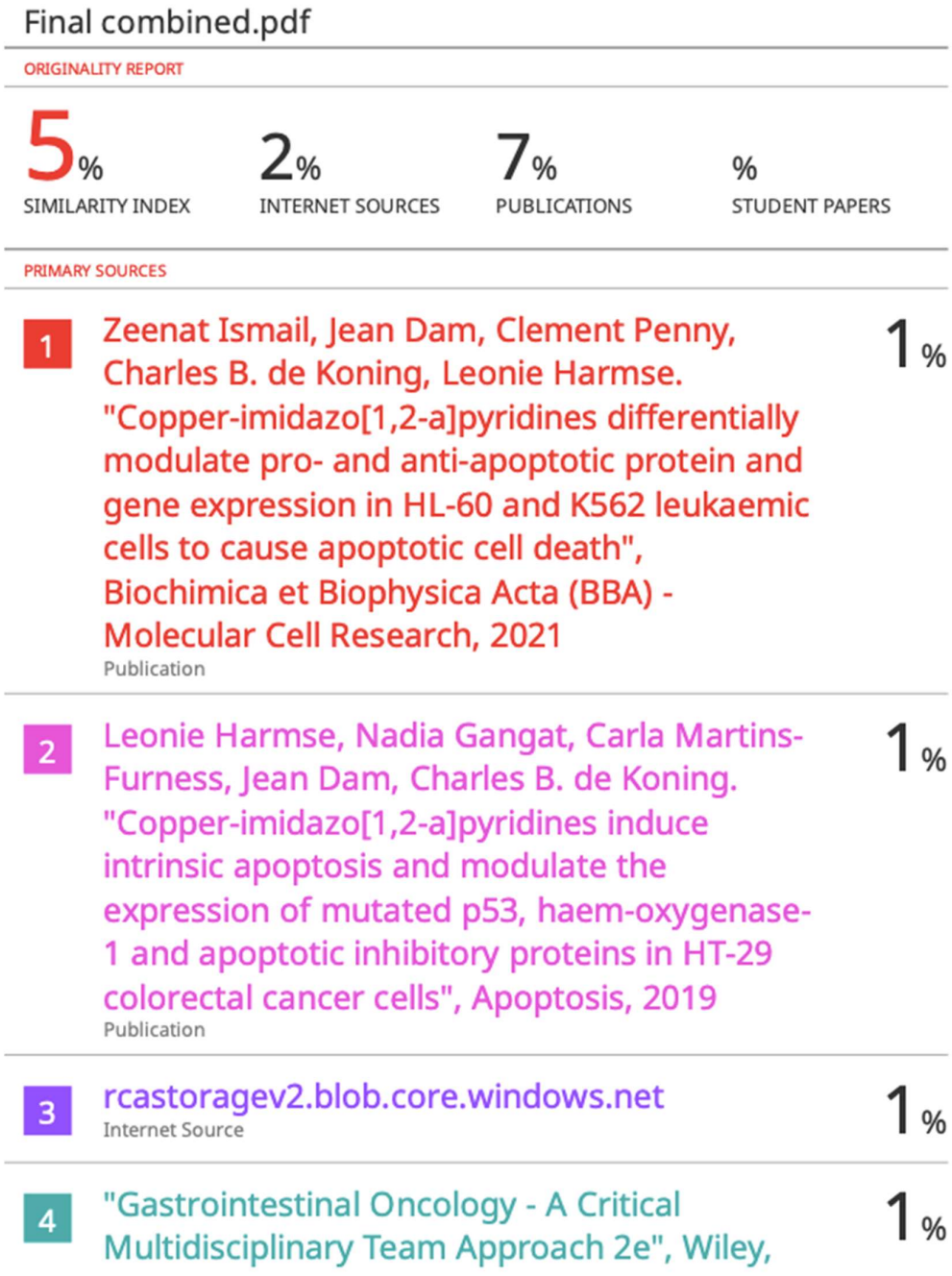
Project title: *The effects of cancer drugs and copper complexes on pancreatic cancer haem-oxygenase-1 and cell survival*

Reason: In vitro laboratory study.
No human participants will be involved in the study.

Dr CB Penny
Co-Chairperson: Human Research Ethics Committee (Medical)

Research Office Secretariat:
Physical address: Phillip Tobias Building, 3rd Floor, Office 302, Corner York Road and Princess of Wales Terrace, Parktown, Johannesburg 2193.
Postal address: Private Bag 3, Wits 2050
Tel Nos. +27 (0)11-717-1234/2656/2700/1252
Office E-mail: HREC-Medical.ResearchOffice@wits.ac.za
Website:http://www.wits.ac.za/research/about-our-research/ethics-and-research-integrity/

Appendix D: Turnitin score



Final combined.pdf

ORIGINALITY REPORT

5%	2%	7%	%
SIMILARITY INDEX	INTERNET SOURCES	PUBLICATIONS	STUDENT PAPERS

PRIMARY SOURCES

1	Zeenat Ismail, Jean Dam, Clement Penny, Charles B. de Koning, Leonie Harmse. "Copper-imidazo[1,2-a]pyridines differentially modulate pro- and anti-apoptotic protein and gene expression in HL-60 and K562 leukaemic cells to cause apoptotic cell death", Biochimica et Biophysica Acta (BBA) - Molecular Cell Research, 2021 Publication	1%
2	Leonie Harmse, Nadia Gangat, Carla Martins-Furness, Jean Dam, Charles B. de Koning. "Copper-imidazo[1,2-a]pyridines induce intrinsic apoptosis and modulate the expression of mutated p53, haem-oxygenase-1 and apoptotic inhibitory proteins in HT-29 colorectal cancer cells", Apoptosis, 2019 Publication	1%
3	rcastoragev2.blob.core.windows.net Internet Source	1%
4	"Gastrointestinal Oncology - A Critical Multidisciplinary Team Approach 2e", Wiley,	1%